

From Positive Charges to Protein-Templated Synthesis: Exploring Strategies in Anti- Infective Hit-Discovery

Dissertation

Zur Erlangung des Grades des Doktors der Naturwissenschaften
der Naturwissenschaftlich-Technischen Fakultät
der Universität des Saarlandes

von

M. Sc. Maria Braun Cornejo

Saarbrücken

2024

Tag des Kolloquiums: 11.10.2024

Dekan: N.N.

Berichterstatter: Prof. Dr. Anna K. H. Hirsch
Prof. Dr. Andreas Speicher
Priv.-Doz. Dr. Matthias Engel

Akad. Mitglied: Dr. Angelika Ullrich

Vorsitz: Prof. Dr. Claus-Michael Lehr

Die vorliegende Arbeit wurde von Dezember 2020 bis Mai 2024 unter Anleitung von Peter Maas in der Firma Specs in der Abteilung *Specs Research Laboratory* (SRL), und Prof. Dr. Anna K. H. Hirsch in der Fachrichtung Pharmazeutische und Fachrichtung Medizinische Chemie der Naturwissenschaftlich-Technischen Fakultät der Universität des Saarlandes sowie am Helmholtz-Institut für Pharmazeutische Forschung Saarland (HIPS) in der Abteilung *Drug Design and Optimisation* (DDOP) angefertigt.

Amama eta Aititeren oroimenez

Short Summary

With antimicrobial resistance (AMR) on the rise, once-effective treatments are failing and contributing to a critical global health crisis. The development of new drugs with unprecedented mechanisms of action is crucial to control this threat. This thesis aims at discovering new anti-infective starting points *via* a multifaceted approach.

The introduction gives an overview of typical strategies employed in the early stages of drug discovery and specific hurdles faced in anti-infective research.

Chapters 2 and 3 explore the use of positively charged groups in small molecules to target bacteria. Notably, the addition of *N*-alkyl guanidiniums to an antimalarial compound gave rise to a pyrazole-amide class with broad-spectrum activity. These compounds are active against a range of pathogens including *Plasmodium falciparum*, *Mycobacterium tuberculosis*, Gram-positive (GPB), and Gram-negative bacteria (GNB). A similar approach was applied by developing synthetic routes to access derivatives of α -aryl β -aza reverse fosmidomycin containing *N*-alkyl guanidiniums.

Chapters 4 and 5 present innovative protein-templated (PT) synthesis methods utilising the anti-infective target 4-diphosphocytidyl-2-C-methyl-D-erythritol kinase (IspE). In particular, the target-directed dynamic combinatorial chemistry (tdDCC) approach identified privileged scaffolds, leveraging a library of acylhydrazones formed *in situ* from aldehyde and hydrazide fragments. The alkyne fragment library designed for the kinetic target-guided synthesis (KTGS) was successfully repurposed in a fragment-based hit-identification, resulting in several IspE inhibitors of *Pseudomonas aeruginosa*.

Overall, this work led to the discovery of chemical entities with biological interest and gave valuable insights into structure–uptake relationships in various pathogens.

Kurze Zusammenfassung

Mit der zunehmenden antimikrobiellen Resistenz (AMR) versagen einst wirksame Therapeutika und tragen zu einer kritischen globalen Gesundheitskrise bei. Die Entwicklung neuer Medikamente mit neuen Wirkmechanismen ist entscheidend, um diese Bedrohung zu kontrollieren. Ziel dieser Arbeit ist es, durch ein vielfältiges Vorgehen neue Ansatzpunkte für Antiinfektiva zu entdecken.

Die Einleitung gibt einen Einblick in typische Strategien, die in den frühen Phasen der Arzneimittel-Entwicklung angewandt werden, sowie über die spezifischen Hürden mit denen die Infektionsforschung konfrontiert ist.

In den Kapiteln 1 und 2 wird die Verwendung positiv geladener Gruppen in kleinen Molekülen zur Bekämpfung von Bakterien untersucht. Insbesondere wurde durch das Integrieren von *N*-Alkyl-Guanidinen in eine Antimalaria-Verbindung eine Pyrazol-Amid-Klasse mit breitem Wirkungsspektrum entwickelt. Diese Verbindungen sind gegen eine Reihe von Krankheitserregern wie *Plasmodium falciparum*, *Mycobacterium tuberculosis*, Gram-positive (GPB) und Gram-negative Bakterien (GNB) wirksam. Ein ähnlicher Ansatz wurde bei der Synthese von α -Aryl β -aza revers fosmidomycin Derivaten mit *N*-Alkyl-Guanidinen angewandt.

In den Kapiteln 3 und 4 werden innovative Protein-vermittelte (PT) Synthesemethoden vorgestellt, die das antiinfektive Target 4-Diphosphocytidyl-2-C-methyl-D-erythritol-Kinase (IspE) nutzen. Insbesondere der Ansatz der *target-directed dynamic combinatorial chemistry* (tdDCC) identifizierte privilegierte Strukturen, indem eine Reihe von Acylhydrazonen genutzt wurde, die *in situ* aus Aldehyd- und Hydrazid-Fragmenten gebildet wurden. Die Auswahl von Alkin-Fragmenten für die *kinetic target-guided synthesis* (KTGS) wurde erfolgreich in einer fragmentbasierten Hit-Identifizierung verwendet, die zu mehreren IspE-Inhibitoren von *Pseudomonas aeruginosa* führte.

Insgesamt führte diese Arbeit zur Entdeckung chemischer Strukturen von biologischem Interesse und lieferte wertvolle Einblicke in die *structure–uptake relationships* bei verschiedenen Krankheitserregern.

Abbreviations

Aa	<i>Aquifex aeolicus</i>
AA	amino acid
Ab	<i>Acinetobacter baumannii</i>
ACN, MeCN	acetonitrile
AcOH	acetic acid
ADME	absorption, distribution, metabolism, excretion
AMR	antimicrobial resistance
ATP	adenosine triphosphate
aq.	aqueous
Boc	<i>tert</i> -butyloxycarbonyl
CC	cytotoxic concentration
CFU	colony forming units
CuAAC	copper(I)-catalysed azide-alkyne cycloaddition
DCM	dichloromethane
DCL	dynamic combinatorial library
DIPEA	<i>N,N</i> -diisopropylethylamine
DMAP	4-dimethylaminopyridine
DMF	dimethylformamide
DMSO	dimethyl sulfoxide
DNA	deoxyribonucleic acid
DXR	deoxy-d-xylulose-5-phosphate reductoisomerase
Ec	<i>Escherichia coli</i>
EtOAc	ethyl acetate
EtOH	ethanol
eNTRY	N = ionisable nitrogen, T = low three-dimensionality, R = rigidity
eq.	equivalents
ESI	electrospray ionisation
GP	general procedure
GPB	Gram-positive bacteria
GNB	Gram-negative bacteria
HATU	2-(3 <i>H</i> -[1,2,3]triazolo[4,5- <i>b</i>]pyridin-3-yl)-1,1,3,3-tetramethylisouronium
HEPES	4-(2-hydroxyethyl)-1-piperazineethanesulfonic acid
HRMS	high-resolution mass spectrometry
HPLC	high-performance liquid chromatography
HTS	high-throughput screening
Hz	hertz
IC₅₀	half maximal inhibitory concentration
IspE	4-diphosphocytidyl-2-C-methyl-D-erythritol kinase

J	coupling constant
KTGS	kinetic target-guided synthesis
LCMS	liquid chromatography-mass spectrometry
LBDD	ligand-based drug design
MeOH	methanol
MEP	2-C-methyl-d-erythritol 4-phosphate
MIC	minimum inhibitory concentration
MST	microscale thermophoresis
<i>Mtb</i>	<i>mycobacterium tuberculosis</i>
MTT	3-(4,5-dimethylthiazol-2-yl)-2,5-diphenyltetrazolium bromide
NaAsc	sodium ascorbate
NAD	nicotinamide adenine dinucleotide
NMR	nuclear magnetic resonance
OD	optical density
o.n.	overnight
<i>Pa</i>	<i>pseudomonas aeruginosa</i>
PBS	phosphate-buffered saline
PE	petroleum ether
<i>Pf</i>	<i>Plasmodium falciparum</i>
PK/LDH	pyruvate kinase/lactate dehydrogenase
PT	protein-templated
q	quartet
r.t.	room temperature
rpm	revolutions per minute
s	singlet
SAR	structure–activity relationship
SBDD	structure-based drug design
<i>Sa</i>	<i>staphylococcus aureus</i>
<i>Sp</i>	<i>streptococcus pneumoniae</i>
tdDCC	target-directed dynamic combinatorial chemistry
TFA	trifluoroacetic acid
THF	tetrahydrofuran
TLC	thin-layer chromatography
T_m	melting temperature
TSA	thermal shift assay
TTIP	titanium(IV) isopropoxide
UPLC	ultra-performance liquid chromatography
WHO	World Health Organization
XTT	2,3-bis-(2-methoxy-4-nitro-5-sulfohenyl)-2 <i>h</i> -tetrazolium-5-carboxanilide

Table of Contents

Short Summary	IV
Kurze Zusammenfassung.....	V
Abbreviations	VI
Table of Contents	IX
1. Introduction	1
1.1. The Early Stages of Drug Discovery.....	1
1.1.1. Common biological assays	2
1.1.2. Protein-templated synthesis	4
1.2. Antimicrobial resistance: a global health threat.....	5
1.2.1. Gram-negative bacteria	5
1.2.2. Tuberculosis	6
1.2.3. Malaria.....	7
1.3. The MEP pathway as source of anti-infective drug targets.....	7
1.3.1. Deoxy-D-xylulose-5-phosphate reductoisomerase (DXR).....	8
1.3.2. 4-Diphosphocytidyl-2-C-methyl-D-erythritol kinase (IspE)	8
References.....	9
Aims of the thesis	13
2. Chapter: A Positive Charge in an Antimalarial Compound Unlocks broad-spectrum antibacterial activity	15
2.1. Supporting Information	31
3. Chapter: Guanylated α / γ-Substituted Aza-Fosmidomycin Derivatives	61
4. Chapter: Target-Directed Dynamic Combinatorial Chemistry Affords Binders of <i>Mycobacterium tuberculosis</i> IspE	69
4.1. Supporting Information	81
5. Chapter: Exploring Protein-Templated and Biophysical Approaches for Fragment Discovery using IspE from Gram-Negative Bacteria	99
5.1. Supporting Information	111
Conclusions and Outlook	181
Acknowledgements	185

1. Introduction

1.1. The Early Stages of Drug Discovery

In the search for new drugs against a specific disease, drug discovery campaigns are crucial for the development of compounds with therapeutic potential, but they are lengthy and complex with many unique factors and nuances influencing each project.¹ The first step in this process is to find chemical starting points, called "hits", able to modulate the target activity (e.g., inhibition). In brief, the hit-discovery steps typically involve compound selection, the screening against the biological target(s), and the analysis of the results. This cycle is iterative, with previous results used to refine the selection, design, and synthesis of compounds (Figure 1). Ultimately, this should lead to more potent and drug-like compounds, transitioning through the drug discovery stages from hit-identification, over -expansion, and -optimisation (or hit-to-lead optimisation). Additionally, the knowledge gained on the biological activity of compounds gives a (quantitative) structure–activity relationship, in short (Q)SAR, that is crucial in guiding rational drug design.² The culmination of medicinal chemistry efforts is lead-optimisation, where the focus shifts towards improving the hits' specificity, and drug-like properties; absorption, distribution, metabolism, excretion (ADME), and reduction of toxicity. These characteristics are essential for a successful progression into preclinical development, the last phase aimed at obtaining candidates for clinical trials.³ At this stage disciplines like pharmacology and process chemistry take over.

Preclinical Phase:

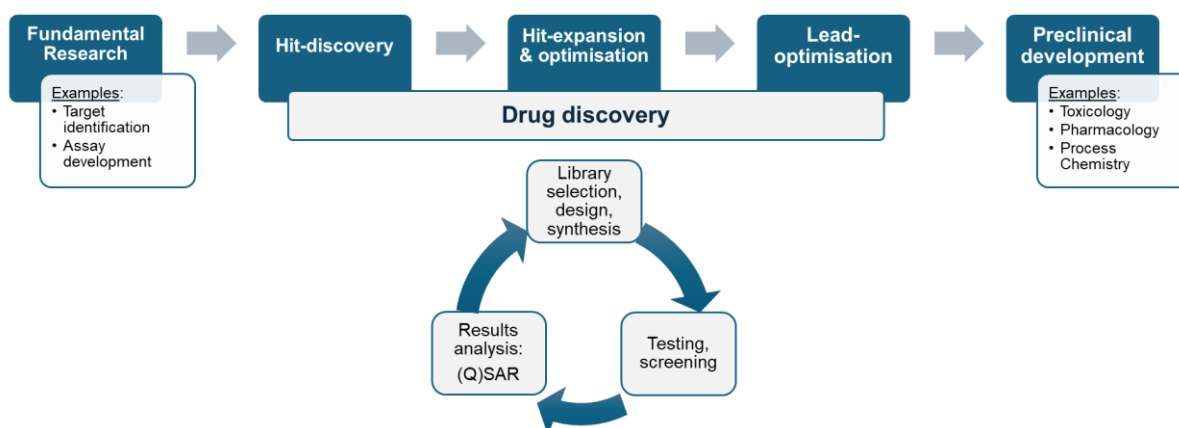


Figure 1. Overview of the different stages in the preclinical phase of drug discovery and development.

The early stages of drug discovery play a critical role in setting the foundation for a successful drug-discovery project. Every project is unique, with distinct needs, capabilities, and resources that must be carefully considered when selecting hit-discovery and-optimisation approaches. When initiating a hit-discovery process random screenings might be one among the many possible options. Especially, when neither structural knowledge about the target nor ligands are available, or to find structurally novel starting points. In these cases, the widest possible chemical space should be covered in the compound selection.⁴ In the pharmaceutical industry, complex automated laboratories allow for high-throughput screening (HTS) campaigns of their huge compound libraries, covering a big structural diversity to obtain novel hits.⁵ Conversely, in academic research, HTS is usually scarce, compound library sizes are modest and biological assays are not established to run at such high throughput. Fragment-based screening is a more efficient way to explore chemical diversity using small compounds (<300 Da) as starting points. The total number of possible drug-like molecules is estimated around 10^{60} ,⁶ by using much smaller molecules this chemical space is vastly reduced and easier to cover.⁷ However, due to their size, fragments have lower

1. Introduction

binding affinities and a rational design strategy often supported by crystallography is necessary to grow fragment-hits into drug-like compounds.⁸

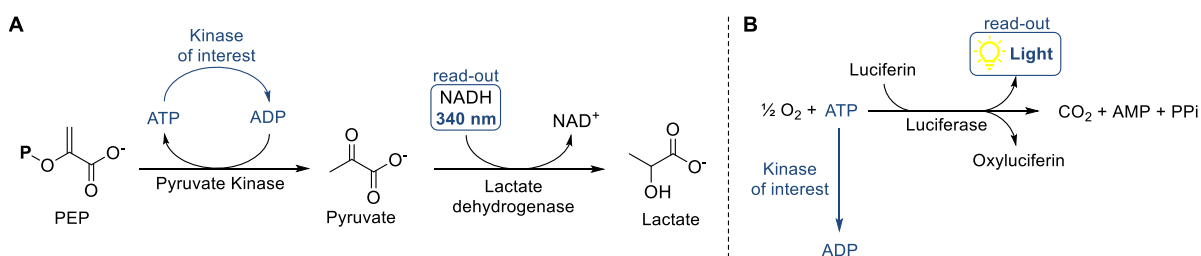
Established biological targets likely have structural information of the protein and its ligands available. This information is very valuable and opens the door to structure-based drug design (SBDD) and ligand-based drug design (LBDD). The former relies on structural information about the protein and the latter uses input from its natural ligands or known hits.⁹ For the drug-discovery process, both drug design approaches are widely used. In hit-discovery, SBDD methods are common, for example virtual screening computationally assesses the binding potential of compounds by leveraging X-ray structures of biological targets.¹⁰ These compounds are "docked" into a pre-defined binding pocket in various conformations. Different scoring functions, specific to the software used, then evaluate the possible interactions between the compound and the target. Biological testing cannot be replaced with this method, however, it can filter out the most promising compounds from big libraries, resulting in a manageable selection for testing. Similarly, LBDD methods can also aid in filtering compound libraries for a more effective hit-discovery. These approaches rely on extracting information from known ligands and inhibitors to identify structural features and properties that are necessary for binding. This knowledge is used to build pharmacophore- or descriptor-based models to search for compounds with compatible geometries, and pharmacophore points or descriptor space.⁴ These computer-aided approaches can significantly reduce time and cost in hit-discovery and can help rationalise binding modes, which is increasingly important as the drug discovery process advances.

1.1.1. Common biological assays

The selection of compounds and their method of evaluation is interdependent since there are many different assays available for biological testing, each with its own strengths and limitations. The choice ultimately depends on the nature and number of compounds to test, as well as cost and time considerations. The following section gives an overview of the most relevant assays for this thesis, hence focusing on enzymes. Notably, most of these assays are compatible with a range of biological targets beyond enzymes such as receptors, ion channels or DNA/RNA.¹¹

Enzymatic Assays:

Enzymatic assays offer a valuable tool for evaluating the activity of compounds by measuring their impact on a target enzyme's activity. These assays are typically better suited for larger, drug-like compounds compared to fragments due to their lower affinity.⁸ A diverse range of methods exist for detecting the concentration of substrates, products, or cofactors during the enzymatic reaction. For enzymes lacking a directly measurable variable, coupled enzymatic assays provide a solution. In these assays, the target enzyme activity is linked to a secondary enzyme reaction that generates a detectable product. A common example is the use of coupled assays to determine the activity of kinases. Kinases use ATP to phosphorylate substrates, resulting in ADP. Both ATP and ADP can be interconverted further by secondary enzymes to indirectly monitor their concentration. The tandem pyruvate kinase/lactate dehydrogenase



Scheme 1. Examples of coupled assays to determine activities of kinases. A) Absorption at 340 nm indirectly monitors the concentration of ADP produced by the kinase of interest, adapted from McFarlane *et al.*¹² B) Consumption of ATP by the kinase of interest is monitored by detection of light.

(PK/LDH), for instance, consumes ADP to produce pyruvate, which is further converted to lactate. This last conversion transforms NADH to NAD⁺, leading to a decrease in absorbance at 340 nm detectable by a spectrophotometer.¹² Alternatively, ATP levels can be quantified through a luminescence assay employing luciferase, which produces a detectable light signal by catalysing luciferin into oxyluciferin using ATP.¹³

Biophysical assays:

Biophysical techniques offer a complementary approach to enzymatic assays for evaluating potential drug candidates. These methods measure various properties of enzymes to determine binding of compounds or fragments. Biophysical assay protocols are generally compatible with any enzyme, although some techniques require special handles to immobilise the proteins. These methods use small amounts of protein and measurements tend to be fast and often (semi-) automated allowing for mid-to-high throughput screenings, making them very useful in the early stages of drug discovery. Examples include surface plasmon resonance, mass spectrometry, microscale thermophoresis, nuclear magnetic resonance (NMR), and thermal shift assays (TSA).^{3,14} NMR-based techniques can give information on the binding site even for weak binders, making it a powerful approach for fragments, as they require a rational design approach to develop them into bigger compounds.¹⁵

TSA determine the stability of a protein by steadily elevating the temperature while measuring the level of unfolding. The temperature at which 50% of protein is unfolded and 50% remains intact is called melting temperature (T_m). The stability of a protein can be related to its T_m , the higher the T_m the more stable it is. TSA are a quick, cheap and easy tool to evaluate the stability of an enzyme under certain conditions. For instance, TSA are commonly used to screen buffer compatibility or protein stability over time.¹⁶ In the context of hit-discovery, TSA can be employed since bound compounds or fragments (de)stabilise proteins, leading to a shift in T_m . A stabilising compound will increase the T_m , while a destabilising compound will decrease it.

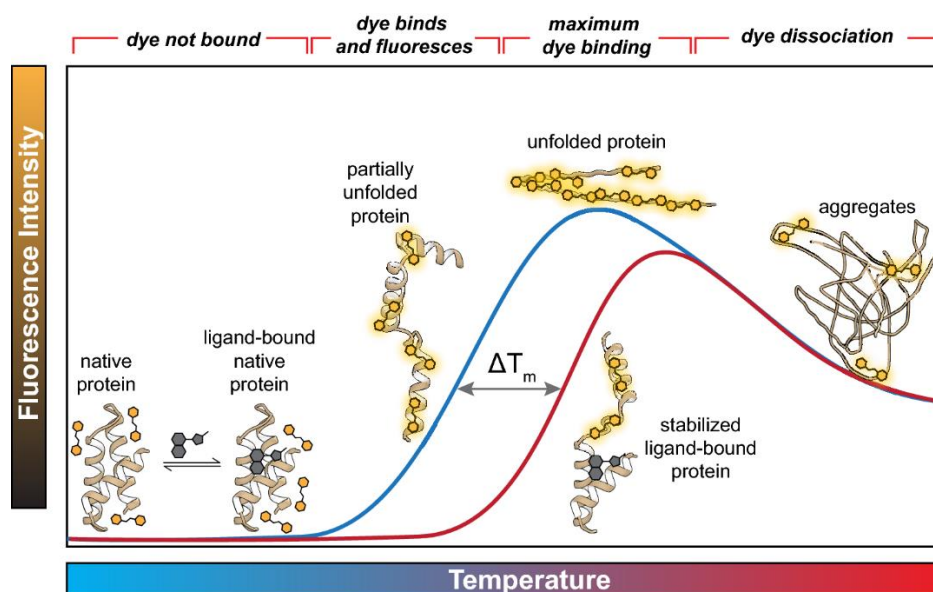


Figure 2. Two melting curves representing the unfolding of proteins with (red) and without (blue) a bound ligand. The melting temperature (T_m) corresponds to the inflection point of the curve and increases when a ligand stabilises the protein structure. Reprinted from Samuel *et al.*,¹⁴ CC BY 4.0.

Phenotypic or cell-based assays:

Phenotypic assays directly measure the overall effect of a compound on living cells making them crucial for lead-optimisation prior to *in vivo* studies.¹¹ Nevertheless, phenotypic assays are exploited throughout the whole drug-discovery and -optimisation process. Notably, these assays offer unique advantages in the hit-discovery stage and can be employed when no specific target is known. As mentioned above, in antibacterial drug development, a major challenge involves identifying compounds that can permeate the

1. Introduction

bacterial cell wall. Phenotypic assays that directly screen compounds against bacterial pathogens can effectively identify high-quality hits possessing the desired cell permeability. However, to effectively optimise the identified hits, subsequent target-identification studies are required. Similarly, human cell lines are used in phenotypic assays to evaluate membrane permeability and potential toxicity.

To summarise, there is a big array of assays available and ultimately a combination of many are necessary throughout the drug-discovery process to effectively identify hits and optimise them. As noted before, the choice of assay will depend on the compounds that need to be tested and on the purpose of the screening. In hit-discovery, quick, cheap techniques are generally preferred and complementary assays are used to validate and optimise them. Depending on the properties that need to be improved upon, target-based or cell-based assays can be used. In the case of fragments, target-based techniques that give structural information should be incorporated as early as possible for a successful and efficient drug design.

1.1.2. Protein-templated synthesis

Protein-templated (PT) synthesis offers an effective shortcut around traditional laborious hit-discovery efforts by combining synthesis and screening in one step. This innovative approach takes advantage of the inherent catalytic potential of a target enzyme and uses building blocks that can be linked together. The protein selectively influences the covalent bond formation guided by favourable binding interactions of fragments with complementary reactivities.^{17,18} PT approaches can be broadly categorised based on the underlying reaction type: target-directed dynamic combinatorial chemistry (tdDCC) for reversible reactions,^{19,20} and kinetic target-guided synthesis (KTGS) for irreversible reactions.^{21,22}

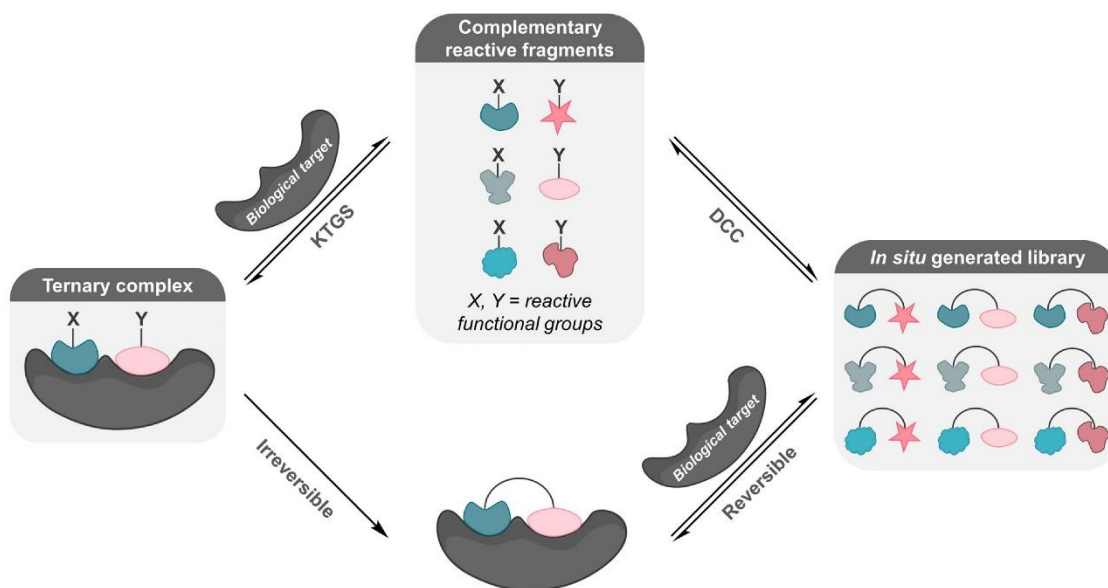


Figure 3. Representation of reversible target-directed dynamic combinatorial chemistry (tdDCC), and irreversible kinetic target-guided synthesis (KTGS). Reprinted from Parvatkar *et al.*,²² Copyright (2024), with permission from Elsevier.

Huc and Lehn set the groundwork for PT synthesis in 1997, pioneering the use of tdDCC by reacting a mixture of aldehydes and amines giving imines that were reduced to obtain amine products.²³ They quantified the products by HPLC analysis and compared the PT experiment with a blank sample to identify compounds amplified by the protein. However, not all reversible reactions are suitable for tdDCC. The fragments' reactivities need to be compatible with the protein and its buffer, and the equilibrium must be reached before the protein degrades. In 2001, the Lehn group introduced the formation of acylhydrazones from aldehydes and hydrazides to tdDCC in acidic conditions.²⁴ In 2010, Bhat *et al.* further expanded the applicability of the reaction by accelerating the equilibration of acylhydrazones at neutral pH using a nucleophilic catalyst, making the reaction useable for a wider range of proteins.²⁵ On the contrary, since KTGS reactions are irreversible, equilibration is not an issue, however, the reactions do need to be

biocompatible. The importance of bioorthogonal chemistry, and click chemistry, crucial tools in KTGS, was recently recognised with the 2022 Nobel Prize in Chemistry. One of the winners, Sharpless, published the first “*in situ* click chemistry” using acetylcholinesterase to synthesize a highly potent inhibitor from alkynes and azides.²⁶ This was among the first examples of KTGS and to this day, this alkyne-azide cycloaddition click chemistry is the most widely used reaction in KTGS, constituting over 70% of reported studies.²¹

Since the emergence of PT synthesis, many successes have been achieved using a range of different proteins, reactions and analytical methods.^{19,22} While complementary hit-verification using biological assays remains necessary, the PT approach significantly reduces the number of compounds to be synthesised and tested. Leveraging the dynamic nature of proteins in solution, PT methods are applicable without structural information on the target protein, thereby establishing them as an effective hit-identification approach. Specifically, in the context of hit-discovery numerous success stories applying tdDCC have been published.^{20,27,28} However, the first example using KTGS for random hit-finding was reported only last year by Kassu *et al.* They obtained 12 bioactive hits by combining 45 thio acids and 38 sulfonyl azides, resulting in a total of 1710 possible *N*-acylsulfonamide products in their KTGS experiment.²⁹ Applications of hit-optimisation and -expansion in KTGS have been more common, typically one of the fragment types is rationally designed based on a verified hit and a random library of the complementary building blocks is used to combine the two.³⁰⁻³² In the case of tdDCC, the first application of hit-optimisation was only published in 2021 by the Hirsch group.³³ In this work an initial hit-identification tdDCC experiment was performed, and the hits’ structures were used to select and design new building blocks for a new tdDCC experiment. This concept was applied again for two more tdDCC rounds and ultimately yielded hits with improved bioactivities and gained insight on SAR. These recent successes provide strong evidence for the emergence of PT synthesis as a robust, efficient, and versatile approach for hit-discovery and -optimisation.

1.2. Antimicrobial resistance: a global health threat

The rise of antimicrobial resistance (AMR) is one of the most pressing global health crises of our time, as treating infectious diseases is becoming an increasingly complex challenge.^{34,35} Pathogens naturally evolve mechanisms of resistance continuously, diminishing the efficacy of once-reliable treatments. The development of new anti-infective drugs effective against resistant strains lags behind the pace of resistance evolution.³⁶ This growing resistance leaves healthcare systems vulnerable to untreatable infections and jeopardises decades of progress in public health. The World Health Organization (WHO) classifies numerous diseases impacted by AMR as critical public health concerns, including malaria,³⁷ tuberculosis,³⁸ and various other bacterial infections.³⁹ Combating AMR necessitates a multifaceted approach encompassing responsible antimicrobial use in humans and animals, the development of novel drugs, and the implementation of robust infection-control measures.^{35,40}

1.2.1. Gram-negative bacteria

Antibiotics have dramatically reduced bacterial infections, saving countless lives since the discovery of penicillin. However, the effectiveness of antibiotics is threatened by the spread of multidrug-resistant bacteria with nearly 5 million deaths annually associated to bacterial AMR.^{34,36} Projections suggest this number could double by 2050, returning to a pre-antibiotic era as infections are increasingly untreatable.⁴⁰ The WHO urges for the search and development of novel antibiotics. In 2017, they released a list of resistant bacterial strains to prioritize, highlighting especially Gram-negative bacteria (GNB) as critical.³⁹ This categorisation aligns with estimates of the deadliest resistant pathogens in 2019; *Escherichia coli* (*Ec*), *Staphylococcus aureus* (*Sa*), *Klebsiella pneumoniae* (*Kp*), *Streptococcus pneumoniae* (*Sp*), *Acinetobacter baumannii* (*Ab*) and *Pseudomonas aeruginosa* (*Pa*). With the exception of the Gram-positive *Sa*, and *Sp*, the remaining four pathogens are GNB. Compared to Gram-positive bacteria, GNB have an additional outer membrane with lipopolysaccharides that makes them even more difficult to target.⁴¹⁻⁴³

1. Introduction

Therefore, current antibiotic drug candidates effective against GNB are vastly underrepresented. Very few new antibiotic classes have been approved in the past 50 years, in contrast, the "golden age" (1940s–1960s) of antibiotics introduced 16 new classes.⁴⁴ Traditional screening libraries are often biased towards compounds with favourable properties for human bioavailability, which does not translate effectively to bacterial bioavailability.³⁶ Therefore, high-throughput screening campaigns by big pharmaceutical companies have largely failed to identify novel antibiotics.⁴⁵

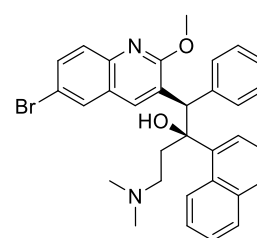
1.2.1.1. Design of small molecules to overcome the Gram-negative barrier

Since 1968, statistical studies have sought to elucidate the physicochemical properties conducive to compound uptake in GNB.⁴⁶ However, the correlation between molecular properties and bacterial activity has presented challenges.⁴⁷ The limited number of antibiotic compound classes results in a lack of diverse structures to study, leaving out a big chemical space with potentially promising structural motifs. In addition, it is difficult to distinguish properties that influence antibacterial activity directly by killing bacteria from those impacting bacterial bioavailability. The concept of bioavailability is important because it includes the permeation of compounds into cells and also their accumulation in them. Bacteria have various efflux pumps that can expel potential antibacterial compounds before they have time to act.^{41,43,48} Drug efflux pumps are a major defence mechanism and contributor to the growing problem of antibiotic resistance in Gram-negative bacteria.⁴⁹

A breakthrough was made in 2017 when the Hergenrother group measured the concentration of a diverse set of compounds inside *E. coli* cells, assessing their bioavailability.⁵⁰ Computational analysis was used to study the physicochemical properties related to compound accumulation. A set of guidelines called "eNTRY-rules" was established, suggesting that compounds containing an ionisable nitrogen, with low three-dimensionality, and high rigidity, demonstrate a greater likelihood of accumulating within *E. coli* cells.⁵¹ These findings have been widely applied, mostly by introducing a primary amine to already flat, and rigid Gram-positive active compounds.^{52–55} A FabI inhibitor is among the most successful examples, given that it shows *in vivo* efficacy in drug resistant GNB infections.⁵⁶ Further research, employing alternative structural motifs and pathogens followed,^{57,58} but these studies only mark the beginning.⁵⁹ The bacterial membrane make-up differs widely among pathogens and even strains. Therefore, beneficial and unbeneficial properties of compounds for accumulation need to be assessed specifically for each species before broad conclusions can be made.^{58–60} Hopefully, leading to a deeper understanding to aid narrow- and broad-spectrum antibiotic development.

1.2.2. Tuberculosis

Tuberculosis, caused by bacteria belonging to the *Mycobacterium tuberculosis* (*Mtb*) complex, is one of the deadliest infectious diseases. It is estimated that tuberculosis claims 1.5 million lives and infects around 10 million people annually.³⁸ The infection usually affects the lungs but can also spread to other parts of the body, causing persistent cough, exhaustion, weight loss and more. The treatment of tuberculosis typically involves a combination of antibiotics taken for many months. Infections with multidrug-resistant strains pose a significant challenge, requiring more complex treatment regimens that can last up to two years, have increased risk of side effects, and patient compliance. This highlights the urgent need for novel therapies with improved efficacy and reduced side effects. In addition, the WHO set an ambitious goal to eliminate tuberculosis as a public health threat by 2050.³⁸ This target requires an unprecedented decline in infections, putting novel and innovative research in the spotlight. Research into novel diagnostic tools, potential vaccines, and drug candidates for tuberculosis are critical to control this disease. The development of the diarylquinoline bedaquiline (Figure 4) for the treatment of



Bedaquiline

Figure 4. Structure of antitubercular compound bedaquiline.

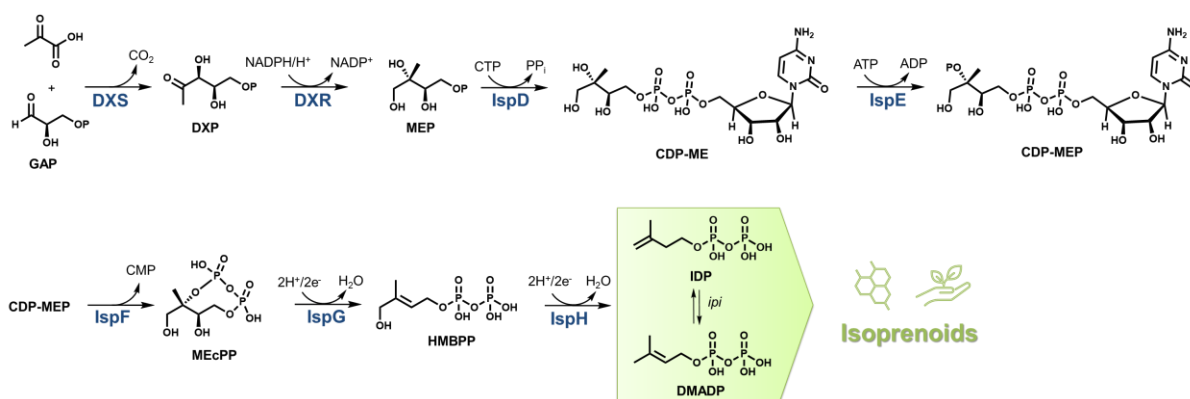
multidrug-resistant tuberculosis was a significant breakthrough, as no drugs targeting resistant strains had been approved in decades.⁶¹ The target of bedaquiline is a novel cellular mechanism, highlighting the importance of exploring new pathways in the fight against multidrug-resistance.⁶² Nevertheless, bedaquiline-resistant *Mtb* strains are already emerging, showcasing how fast new resistance mechanisms can evolve and emphasising the need of a constant supply of new antibiotic drug candidates.⁶³

1.2.3. Malaria

Malaria is an example of how an infectious disease can re-emerge due to drug resistance.⁶⁴ In fact, malaria was eradicated and controlled in many different regions of the world in the 1950s. However, incidences started to rise again some decades after, spreading to regions that had been malaria free.⁶⁵ Currently, around 250 million people are infected annually causing over 600,000 deaths primarily concentrated in Africa and Southeast Asia.³⁷ Malaria is transmitted by the bite of *Plasmodium* parasite-infected mosquitos, these parasites invade the liver causing flu-like symptoms and disrupt the function of red blood cells. Several species of *Plasmodium* are known to cause human malaria, yet the vast majority of cases are due to *Plasmodium falciparum* (*Pf*). The increasing spread of resistant *Pf* strains is one of the major hurdles for the eradication of malaria, highlighting the need for novel antimalarial drug development. Besides strategies to reduce mosquito bites, the main ways to combat malaria are artemisinin-based combination therapy to minimise the risk of resistance development, and chemoprophylaxis for vulnerable groups and travellers to endemic regions. Antimalarial drug discovery has traditionally relied on phenotypic screening approaches. However, the identification of novel drug targets through *Pf* genome sequencing has pushed the use of target-based methods.⁶⁶ Given the importance of minimising increasing resistance issues, targeting new biochemical pathways is essential to ensure promising drug candidates in the antimalarial pipeline. In parallel, the optimisation of current treatments through the development of new analogues, as well as the continuous refinement of combination therapies is vital. In 2021, the first vaccine against malaria was approved, an unprecedented achievement combating parasitic infections.⁶⁷ This breakthrough hopefully strengthens the prevention of malaria but does not make the investigation of new treatments any less important.

1.3. The MEP pathway as source of anti-infective drug targets

As elucidated above, combating the ever-growing threat of AMR demands the discovery of anti-infective drugs with entirely new mechanisms of action.^{36,68} The 2-C-methyl-D-erythritol 4-phosphate (MEP) pathway is a promising source of targets for such novel therapeutics.⁶⁹ This cascade of seven enzymes (Scheme 2) is essential for the biosynthesis of isopentenyl diphosphate (IDP) and dimethylallyl diphosphate (DMADP), the vital precursors of isoprenoids. The MEP pathway is an important cellular mechanism in many pathogens such as *M. tuberculosis*, *P. falciparum*, Gram-negative bacteria, and some critical Gram-positive bacteria.⁷⁰ Notably, humans and other mammals acquire these essential building



Scheme 2. Biosynthesis of isoprenoid precursors isopentenyl diphosphate (IDP) and dimethylallyl diphosphate (DMADP) via the MEP pathway.

1. Introduction

blocks through the alternative mevalonate pathway. This crucial difference offers a good opportunity to target an essential pathogenic mechanism, without adding risks of target-related toxicity in humans. The MEP-pathway has been studied since the 1990s, despite decades of research, targeting the enzymes of this pathway for the development of drugs has proven challenging.⁷¹ While some promising leads have emerged, with only one compound, fosmidomycin, being studied in clinical trials for malaria treatment, significant hurdles remain.⁷²

1.3.1. Deoxy-D-xylulose-5-phosphate reductoisomerase (DXR)

Deoxy-D-xylulose-5-phosphate reductoisomerase (DXR), also known as IspC, is the second enzyme in the MEP-pathway and the rate-limiting step.⁷³ It is one of the most well studied enzymes of the pathway with several crystal structures from pathogenic homologues available.⁶⁹ Fosmidomycin is a competitive inhibitor of DXR and shows potent antimalarial efficacy.⁷² However, its poor pharmacokinetic properties limit its clinical use. Nevertheless, this natural product undergoes active transport to permeate *P. falciparum* and has been studied in clinical trials, for instance as combination therapy with other potent antimalarials.⁶⁶ While numerous fosmidomycin derivative classes have been synthesised in the past 40 years, especially focusing on improving pharmacokinetic and pharmacodynamic properties, no significant bacterial whole-cell activity has been achieved.⁷²

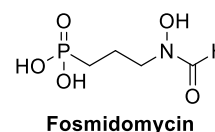


Figure 5. Structure of DXR inhibitor fosmidomycin.

1.3.2. 4-Diphosphocytidyl-2-C-methyl-D-erythritol kinase (IspE)

4-Diphosphocytidyl-2-C-methyl-D-erythritol kinase (IspE), is the fourth enzyme of the MEP pathway and the only kinase.⁶⁹ The enzyme phosphorylates its substrate to form 4-diphosphocytidyl-2-C-methyl-D-erythritol-2-phosphate (CDP-MEP) consuming ATP. IspE's catalytic binding site was assessed as a druggable pocket, and is located deep inside the structure.⁷¹ Considering the relatively small size of CDP-ME compared to substrates of human kinases (macromolecules e.g., proteins, and sugars), toxicity concerns are minimal, especially when targeting the substrate binding site. Many X-ray crystal structures of IspE are deposited in the protein databank (PDB), however structures of some key pathogens like *P. aeruginosa* or *P. falciparum* are missing. Most published structures are apo structures or co-crystals with IspE's natural ligands. Nevertheless, the most potent IspE inhibitor to date, **1** (Figure 6), mimics the cytidine of CDP-ME and is the only co-crystallised inhibitor class, dating back to 2007.⁷⁴ Unsurprisingly, it binds in the cytidine pocket and is a competitive inhibitor. Despite its single digit micromolar inhibitory potency on *E. coli* IspE (*EclspE*), no whole-cell activity has been achieved by this class. As discussed above, this is a persistent problem when targeting Gram-negative bacteria. Further research efforts by various groups identified more IspE inhibitors, but limited advances in GNB efficacy was made.⁷¹ An example of a potent structurally diverse *EclspE* inhibitor is compound **2** (Figure 6).⁷⁵ Recently, the Hirsch group aimed to overcome this issue by filtering the Specs library for compounds with improved properties for accumulation in *E. coli*, inspired by the eNTRY rules, and performed virtual screening of this selection against *EclspE*.⁷⁶ This approach was successful, resulting in promising hit starting points, however optimisation attempts of IspE inhibition proved to be difficult and seemed to be counterproductive to whole-cell activity. Another recent virtual screening study yielded the first confirmed hit on *MtblspE*; a great achievement, however, it took huge computational effort docking 15 million compounds and optimisation attempts of the hit have failed so far.⁷⁷ These ongoing efforts highlight the need for innovative research to expand the chemical diversity and potency of IspE inhibitors, with a particular focus on improving activity against pathogens, and aiming to target other homologues besides *E. coli*.

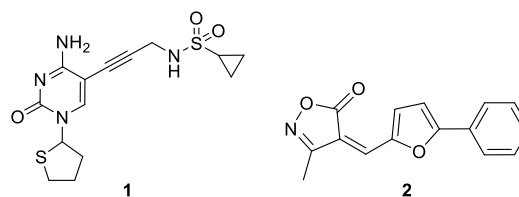


Figure 6. Potent *Escherichia coli* IspE inhibitors.

References

- (1) Hughes, J. P.; Rees, S. S.; Kalindjian, S. B.; Philpott, K. L. Principles of Early Drug Discovery. *Br J Pharmacol* **2011**, *162* (6), 1239–1249. <https://doi.org/10.1111/j.1476-5381.2010.01127.x>.
- (2) Verma, J.; Khedkar, V.; Coutinho, E. 3D-QSAR in Drug Design - A Review. *Curr Top Med Chem* **2010**, *10* (1), 95–115. <https://doi.org/10.2174/156802610790232260>.
- (3) Noe, M. C. The Modern Drug Discovery Process. In *The Handbook of Medicinal Chemistry: Principles and Practice*; Davis, A., Ward, S. E., Eds.; The Royal Society of Chemistry, 2014; pp 456–485. <https://doi.org/10.1039/9781782621836-00456>.
- (4) Reymond, J. L. The Chemical Space Project. *Acc Chem Res* **2015**, *48* (3), 722–730. <https://doi.org/10.1021/ar500432k>.
- (5) Frearson, J. A.; Collie, I. T. HTS and Hit Finding in Academia - from Chemical Genomics to Drug Discovery. *Drug Discov Today* **2009**, *14* (23–24), 1150–1158. <https://doi.org/10.1016/j.drudis.2009.09.004>.
- (6) Hall, R. J.; Mortenson, P. N.; Murray, C. W. Efficient Exploration of Chemical Space by Fragment-Based Screening. *Prog Biophys Mol Biol* **2014**, *116* (2–3), 82–91. <https://doi.org/10.1016/j.pbiomolbio.2014.09.007>.
- (7) Ettmayer, P.; Schnitzer, R.; Bergner, A.; Nar, H. Hit and Lead Generation Strategies. In *Comprehensive Medicinal Chemistry III*; Elsevier, 2017; pp 33–63. <https://doi.org/10.1016/B978-0-12-409547-2.12313-3>.
- (8) Hubbard, R. E. Fragment Based Lead Discovery. In *The Handbook of Medicinal Chemistry: Principles and Practice*; Davis, A., Ward, S. E., Eds.; The Royal Society of Chemistry, 2014; pp 122–153. <https://doi.org/10.1039/9781782621836-00122>.
- (9) Sharma, V.; Wakode, S.; Kumar, H. Structure- and Ligand-Based Drug Design. In *Chemoinformatics and Bioinformatics in the Pharmaceutical Sciences*; Elsevier, 2021; pp 27–53. <https://doi.org/10.1016/B978-0-12-821748-1.00004-X>.
- (10) Buckley, M. E.; Ndukwe, A. R. N.; Nair, P. C.; Rana, S.; Fairfull-Smith, K. E.; Gandhi, N. S. Comparative Assessment of Docking Programs for Docking and Virtual Screening of Ribosomal Oxazolidinone Antibacterial Agents. *Antibiotics* **2023**, *12* (3), 463. <https://doi.org/10.3390/antibiotics12030463>.
- (11) Hammonds, T.; Simpson, P. B. Assays. In *The Handbook of Medicinal Chemistry: Principles and Practice*; Davis, A., Ward, S. E., Eds.; The Royal Society of Chemistry, 2014; pp 266–291. <https://doi.org/10.1039/9781782621836-00266>.
- (12) McFarlane, C. R.; Murray, J. W. A Sensitive Coupled Enzyme Assay for Measuring Kinase and ATPase Kinetics Using ADP-Specific Hexokinase. *Bio Protoc* **2020**, *10* (9). <https://doi.org/10.21769/BioProtoc.3599>.
- (13) Worzella, T.; Gallagher, A. Optimizing Kinase Assays for Ultrahigh-Throughput Profiling Using the Kinase-Glo plus Assay. *J Lab Autom* **2007**, *12* (2), 99–103. <https://doi.org/10.1016/j.jala.2006.07.001>.
- (14) Samuel, E. L. G.; Holmes, S. L.; Young, D. W. Processing Binding Data Using an Open-Source Workflow. *J Cheminform* **2021**, *13* (1), 99. <https://doi.org/10.1186/s13321-021-00577-1>.
- (15) Jahnke, W.; Widmer, H. Protein NMR in Biomedical Research. *Cellular and Molecular Life Sciences* **2004**, *61* (5), 580–599. <https://doi.org/10.1007/s00018-003-3382-3>.
- (16) Niesen, F. H.; Berglund, H.; Vedadi, M. The Use of Differential Scanning Fluorimetry to Detect Ligand Interactions That Promote Protein Stability. *Nat Protoc* **2007**, *2* (9), 2212–2221. <https://doi.org/10.1038/nprot.2007.321>.
- (17) Bedwell, E. V.; McCarthy, W. J.; Coyne, A. G.; Abell, C. Development of Potent Inhibitors by Fragment-Linking Strategies. *Chem Biol Drug Des* **2022**, *100* (4), 469–486. <https://doi.org/10.1111/cbdd.14120>.
- (18) Jaegle, M.; Wong, E. L.; Tauber, C.; Nawrotzky, E.; Arkona, C.; Rademann, J. Protein-Templated Fragment Ligations—From Molecular Recognition to Drug Discovery. *Angew Chem Int Ed* **2017**, *129* (26), 7464–7485. <https://doi.org/10.1002/ange.201610372>.
- (19) Frei, P.; Hevey, R.; Ernst, B. Dynamic Combinatorial Chemistry: A New Methodology Comes of Age. *Chem. Eur. J.* **2019**, *25*, 60–73. <https://doi.org/10.1002/chem.201803365>.
- (20) Mondal, M.; Hirsch, A. K. H. Dynamic Combinatorial Chemistry: A Tool to Facilitate the Identification of Inhibitors for Protein Targets. *Chem Soc Rev* **2015**, *44* (8), 2455–2488. <https://doi.org/10.1039/c4cs00493k>.
- (21) Bosc, D.; Camberlein, V.; Gealageas, R.; Castillo-Aguilera, O.; Deprez, B.; Deprez-Poulain, R. Kinetic Target-Guided Synthesis: Reaching the Age of Maturity. *J Med Chem* **2020**, *63* (8), 3817–3833. <https://doi.org/10.1021/acs.jmedchem.9b01183>.
- (22) Parvatkar, P. T.; Wagner, A.; Manetsch, R. Biocompatible Reactions: Advances in Kinetic Target-Guided Synthesis. *Trends Chem* **2023**, *5* (9), 657–671. <https://doi.org/10.1016/j.trechm.2023.06.002>.
- (23) Huc, I.; Lehn, J. Virtual Combinatorial Libraries: Dynamic Generation of Molecular and Supramolecular Diversity by Self-Assembly. *Proc Natl Acad Sci* **1997**, *94* (6), 2106–2110.
- (24) Bunyapaiboonsri, T.; Ramström, O.; Lohmann, S.; Lehn, J.-M.; Peng, L.; Goeldner, M. Dynamic Deconvolution of a Pre-Equilibrated Dynamic Combinatorial Library of Acetylcholinesterase Inhibitors. *ChemBioChem* **2001**, *2* (6), 438–444. [https://doi.org/10.1002/1439-7633\(20010601\)2:6<438::AID-CBIC438>3.0.CO;2-J](https://doi.org/10.1002/1439-7633(20010601)2:6<438::AID-CBIC438>3.0.CO;2-J).

1. Introduction

- (25) Bhat, V. T.; Caniard, A. M.; Luksch, T.; Brenk, R.; Campopiano, D. J.; Greaney, M. F. Nucleophilic Catalysis of Acylhydrazone Equilibration for Protein-Directed Dynamic Covalent Chemistry. *Nat Chem* **2010**, *2* (6), 490–497. <https://doi.org/10.1038/nchem.658>.
- (26) Lewis, W. G.; Green, L. G.; Grynszpan, F.; Radić, Z.; Carlier, P. R.; Taylor, P.; Finn, M. G.; Sharpless, K. B. Click Chemistry in Situ: Acetylcholinesterase as a Reaction Vessel for the Selective Assembly of a Femtomolar Inhibitor from an Array of Building Blocks. *Angew Chem Int Ed* **2002**, *41* (6), 1053–1057. [https://doi.org/10.1002/1521-3773\(20020315\)41:6<1053::AID-ANIE1053>3.0.CO;2-4](https://doi.org/10.1002/1521-3773(20020315)41:6<1053::AID-ANIE1053>3.0.CO;2-4).
- (27) Hartman, A. M.; Elgaher, W. A. M.; Hertrich, N.; Andrei, S. A.; Ottmann, C.; Hirsch, A. K. H. Discovery of Small-Molecule Stabilizers of 14-3-3 Protein – Protein Interactions via Dynamic Combinatorial Chemistry. *ACS Med Chem Lett* **2020**. <https://doi.org/10.1021/acsmchemlett.9b00541>.
- (28) Ekström, A. G.; Wang, J. T.; Bella, J.; Campopiano, D. J. Non-Invasive ¹⁹F NMR Analysis of a Protein-Templated N-Acylhydrazone Dynamic Combinatorial Library. *Org Biomol Chem* **2018**, *16* (43), 8144–8149. <https://doi.org/10.1039/c8ob01918e>.
- (29) Kassu, M.; Parvatkar, P. T.; Milanes, J.; Monaghan, N. P.; Kim, C.; Dowgiallo, M.; Zhao, Y.; Asakawa, A. H.; Huang, L.; Wagner, A. *et al.* Shotgun Kinetic Target-Guided Synthesis Approach Enables the Discovery of Small-Molecule Inhibitors against Pathogenic Free-Living Amoeba Glucokinases. *ACS Infect Dis* **2023**, *9* (11), 2190–2201. <https://doi.org/10.1021/acsinfectdis.3c00284>.
- (30) Camberlein, V.; Fléau, C.; Sierocki, P.; Li, L.; Gealageas, R.; Bosc, D.; Guillaume, V.; Warenghem, S.; Leroux, F.; Rosell, M. *et al.* Discovery of the First Selective Nanomolar Inhibitors of ERAP2 by Kinetic Target-Guided Synthesis. *Angew Chem Int Ed* **2022**, *61* (39). <https://doi.org/10.1002/anie.202203560>.
- (31) Unver, M. Y.; Gierse, R. M.; Ritchie, H.; Hirsch, A. K. H. Druggability Assessment of Targets Used in Kinetic Target-Guided Synthesis. *J Med Chem* **2018**, *61* (21), 9395–9409. <https://doi.org/10.1021/acs.jmedchem.8b00266>.
- (32) Peruzzotti, C.; Borrelli, S.; Ventura, M.; Pantano, R.; Fumagalli, G.; Christodoulou, M. S.; Monticelli, D.; Luzzani, M.; Fallacara, A. L.; Tintori, C. *et al.* Probing the Binding Site of Abl Tyrosine Kinase Using in Situ Click Chemistry. *ACS Med Chem Lett* **2013**, *4* (2), 274–277. <https://doi.org/10.1021/ml300394w>.
- (33) Jumde, R. P.; Guardigni, M.; Gierse, R. M.; Alhayek, A.; Zhu, D.; Hamid, Z.; Johannsen, S.; Elgaher, W. A. M.; Neusens, P. J.; Nehls, C. *et al.* Hit-Optimization Using Target-Directed Dynamic Combinatorial Chemistry: Development of Inhibitors of the Anti-Infective Target 1-Deoxy-D-Xylulose-5-Phosphate Synthase. *Chem Sci* **2021**, *12* (22), 7775–7785. <https://doi.org/10.1039/D1SC00330E>.
- (34) Murray, C. J.; Ikuta, K. S.; Sharara, F.; Swetschinski, L.; Robles Aguilar, G.; Gray, A.; Han, C.; Bisignano, C.; Rao, P.; Wool, E. *et al.* Global Burden of Bacterial Antimicrobial Resistance in 2019: A Systematic Analysis. *The Lancet* **2022**, *399* (10325), 629–655. [https://doi.org/10.1016/S0140-6736\(21\)02724-0](https://doi.org/10.1016/S0140-6736(21)02724-0).
- (35) World Health Organization. *Global Antimicrobial Resistance and Use Surveillance System (GLASS) Report 2022*; Geneva, 2022.
- (36) Walesch, S.; Birkelbach, J.; Jézéquel, G.; Haeckl, F. P. J.; Hegemann, J. D.; Hestekamp, T.; Hirsch, A. K. H.; Hammann, P.; Müller, R. Fighting Antibiotic Resistance—Strategies and (Pre)Clinical Developments to Find New Antibacterials. *EMBO Rep* **2023**, *24* (1). <https://doi.org/10.15252/embr.202256033>.
- (37) World Health Organization. *World Malaria Report 2022*; Geneva, 2022.
- (38) World Health Organization. *Implementing the End TB Strategy: The Essentials*; Geneva, 2022.
- (39) World Health Organization. *Global Priority List of Antibiotic-Resistant Bacteria to Guide Research, Discovery, and Development of New Antibiotics - 2017*; Geneva, 2017.
- (40) O’Neill, J. *Tackling Drug-Resistant Infections Globally: Final Report and Recommendations*; London, 2016.
- (41) Pérez, A.; Poza, M.; Fernández, A.; Del Carmen Fernández, M.; Mallo, S.; Merino, M.; Rumbo-Feal, S.; Cabral, M. P.; Bou, G. Involvement of the AcrAB-TolC Efflux Pump in the Resistance, Fitness, and Virulence of Enterobacter Cloacae. *Antimicrob Agents Chemother* **2012**, *56* (4), 2084–2090. <https://doi.org/10.1128/AAC.05509-11>.
- (42) Tamae, C.; Liu, A.; Kim, K.; Sitz, D.; Hong, J.; Becket, E.; Bui, A.; Solaimani, P.; Tran, K. P.; Yang, H.; Miller, J. H. Determination of Antibiotic Hypersensitivity among 4,000 Single-Gene-Knockout Mutants of Escherichia Coli. *J Bacteriol* **2008**, *190* (17), 5981–5988. <https://doi.org/10.1128/JB.01982-07>.
- (43) Sulavik, M. C.; Houseweart, C.; Cramer, C.; Jiwani, N.; Murgolo, N.; Greene, J.; Didomenico, B.; Shaw, K. J.; Miller, G. H.; Hare, R.; Shimer, G. Antibiotic Susceptibility Profiles of Escherichia Coli Strains Lacking Multidrug Efflux Pump Genes. *Antimicrob Agents Chemother* **2001**, *45* (4), 1126–1136. <https://doi.org/10.1128/AAC.45.4.1126-1136.2001>.
- (44) Hutchings, M.; Truman, A.; Wilkinson, B. Antibiotics: Past, Present and Future. *Curr Opin Microbiol* **2019**, *51*, 72–80. <https://doi.org/10.1016/j.mib.2019.10.008>.
- (45) Payne, D. J.; Gwynn, M. N.; Holmes, D. J.; Pompliano, D. L. Drugs for Bad Bugs: Confronting the Challenges of Antibacterial Discovery. *Nat Rev Drug Discov* **2007**, *6* (1), 29–40. <https://doi.org/10.1038/nrd2201>.

- (46) Lien, E. J.; Hansch, C.; Anderson, S. M. Structure-Activity Correlations for Antibacterial Agents on Gram-Positive and Gram-Negative Cells. *J Med Chem* **1968**, *11* (3), 430–441. https://doi.org/10.1021/JM00309A004/ASSET/JM00309A004.FP.PNG_V03.
- (47) Ropponen, H. K.; Richter, R.; Hirsch, A. K. H.; Lehr, C. M. Mastering the Gram-Negative Bacterial Barrier – Chemical Approaches to Increase Bacterial Bioavailability of Antibiotics. *Adv Drug Deliv Rev* **2021**, *172*, 339–360. <https://doi.org/10.1016/j.addr.2021.02.014>.
- (48) Mehla, J.; Mallocci, G.; Mansbach, R.; López, C. A.; Tsivkovski, R.; Haynes, K.; Leus, I. V.; Grindstaff, S. B.; Cascella, R. H.; D’cunha, N. *et al.* Predictive Rules of Efflux Inhibition and Avoidance in *Pseudomonas Aeruginosa*. *mBio* **2021**, *12* (1), 1–19. <https://doi.org/10.1128/mBio.02785-20>.
- (49) Soto, S. M. Role of Efflux Pumps in the Antibiotic Resistance of Bacteria Embedded in a Biofilm. *Virulence* **2013**, *4* (3), 223–229. <https://doi.org/10.4161/viru.23724>.
- (50) Richter, M. F.; Drown, B. S.; Riley, A. P.; Garcia, A.; Shirai, T.; Svec, R. L.; Hergenrother, P. J. Predictive Compound Accumulation Rules Yield a Broad-Spectrum Antibiotic. *Nature* **2017** *545*:7654 **2017**, *545* (7654), 299–304. <https://doi.org/10.1038/nature22308>.
- (51) Richter, M. F.; Hergenrother, P. J. The Challenge of Converting Gram-Positive-Only Compounds into Broad-Spectrum Antibiotics. *Ann N Y Acad Sci* **2019**, *1435* (1), 18–38. <https://doi.org/10.1111/nyas.13598>.
- (52) Smith, P. A.; Koehler, M. F. T.; Girgis, H. S.; Yan, D.; Chen, Y.; Chen, Y.; Crawford, J. J.; Durk, M. R.; Higuchi, R. I.; Kang, J. *et al.* Optimized Arylomycins Are a New Class of Gram-Negative Antibiotics. *Nature* **2018**, *561* (7722), 189–194. <https://doi.org/10.1038/s41586-018-0483-6>.
- (53) Hu, Y.; Shi, H.; Zhou, M.; Ren, Q.; Zhu, W.; Zhang, W.; Zhang, Z.; Zhou, C.; Liu, Y.; Ding, X. *et al.* Discovery of Pyrido[2,3- b]Indole Derivatives with Gram-Negative Activity Targeting Both DNA Gyrase and Topoisomerase IV. *J Med Chem* **2020**, *63* (17), 9623–9649. <https://doi.org/10.1021/acs.jmedchem.0c00768>.
- (54) Liu, B.; Trout, R. E. L.; Chu, G. H.; McGarry, D.; Jackson, R. W.; Hamrick, J. C.; Daigle, D. M.; Cusick, S. M.; Pozzi, C.; De Luca, F. *et al.* Discovery of Taniborbactam (VNRX-5133): A Broad-Spectrum Serine- And Metallo- β -Lactamase Inhibitor for Carbapenem-Resistant Bacterial Infections. *J Med Chem* **2020**, *63* (6), 2789–2801. <https://doi.org/10.1021/acs.jmedchem.9b01518>.
- (55) Schumacher, C. E.; Rausch, M.; Greven, T.; Neudörfel, J. M.; Schneider, T.; Schmalz, H. G. Total Synthesis and Antibiotic Properties of Amino-Functionalized Aromatic Terpenoids Related to Erogorgiaene and the Pseudopterosins. *European J Org Chem* **2022**, *2022* (26). <https://doi.org/10.1002/ejoc.202200058>.
- (56) Parker, E. N.; Cain, B. N.; Hajian, B.; Ulrich, R. J.; Geddes, E. J.; Barkho, S.; Lee, H. Y.; Williams, J. D.; Raynor, M.; Caridha, D. *et al.* An Iterative Approach Guides Discovery of the FabI Inhibitor Fabimycin, a Late-Stage Antibiotic Candidate with In Vivo Efficacy against Drug-Resistant Gram-Negative Infections. *ACS Cent Sci* **2022**, *8* (8), 1145–1158. <https://doi.org/10.1021/acscentsci.2c00598>.
- (57) Perlmutter, S. J.; Geddes, E. J.; Drown, B. S.; Motika, S. E.; Lee, M. R.; Hergenrother, P. J. Compound Uptake into *E. Coli* Can Be Facilitated by *N*-Alkyl Guanidiniums and Pyridiniums. *ACS Infect Dis* **2021**, *7* (1), 162–173. <https://doi.org/10.1021/acsinfectdis.0c00715>.
- (58) Hu, Z.; Leus, I. V.; Chandar, B.; Sherborne, B. S.; Avila, Q. P.; Rybenkov, V. V.; Zgurskaya, H. I.; Duerfeldt, A. S. Structure-Uptake Relationship Studies of Oxazolidinones in Gram-Negative ESKAPE Pathogens. *J Med Chem* **2022**, *65* (20), 14144–14179. <https://doi.org/10.1021/acs.jmedchem.2c01349>.
- (59) Stoorza, A. M.; Duerfeldt, A. S. Guiding the Way: Traditional Medicinal Chemistry Inspiration for Rational Gram-Negative Drug Design. *J Med Chem* **2024**, *67* (1), 65–80. <https://doi.org/10.1021/acs.jmedchem.3c01831>.
- (60) Andrews, L. D.; Kane, T. R.; Dozzo, P.; Haglund, C. M.; Hilderbrandt, D. J.; Linsell, M. S.; Machajewski, T.; McEnroe, G.; Serio, A. W.; Wlasichuk, K. B. *et al.* Optimization and Mechanistic Characterization of Pyridopyrimidine Inhibitors of Bacterial Biotin Carboxylase. *J Med Chem* **2019**, *62* (16), 7489–7505. <https://doi.org/10.1021/acs.jmedchem.9b00625>.
- (61) He, Y.; Fan, A.; Han, M.; Zhang, Y.; Tong, Y.; Zheng, G.; Zhu, S. New Perspectives on the Treatment of Mycobacterial Infections Using Antibiotics. *Appl Microbiol Biotechnol* **2020**, *104* (10), 4197–4209. <https://doi.org/10.1007/s00253-020-10513-2>.
- (62) Ciprich, J. F.; Buckhalt, A. J. E.; Carroll, L. L.; Chen, D.; Defiglia, S. A.; McConnell, R. S.; Parmar, D. J.; Pistor, O. L.; Rao, A. B. *et al.* Synthesis and Evaluation of *Pseudomonas Aeruginosa* ATP Synthase Inhibitors. *ACS Omega* **2022**, *7* (32), 28434–28444. <https://doi.org/10.1021/acsomega.2c03127>.
- (63) Mi, J.; Gong, W.; Wu, X. Advances in Key Drug Target Identification and New Drug Development for Tuberculosis. *Biomed Res Int* **2022**, *2022*, 1–23. <https://doi.org/10.1155/2022/5099312>.
- (64) Krostad, D. J. Malaria as a Reemerging Disease. *Epidemiol Rev* **1996**, *18* (1), 77–89. <https://doi.org/10.1093/oxfordjournals.epirev.a017918>.
- (65) Baird, J. K. Resurgent Malaria at the Millennium. *Drugs* **2000**, *59* (4), 719–743. <https://doi.org/10.2165/00003495-200059040-00001>.
- (66) Ashley, E. A.; Phyo, A. P. Drugs in Development for Malaria. *Drugs* **2018**, *78* (9), 861–879. <https://doi.org/10.1007/s40265-018-0911-9>.

1. Introduction

- (67) El-Moamly, A. A.; El-Sweify, M. A. Malaria Vaccines: The 60-Year Journey of Hope and Final Success—Lessons Learned and Future Prospects. *Trop Med Health* **2023**, *51* (1). <https://doi.org/10.1186/s41182-023-00516-w>.
- (68) Lewis, K. The Science of Antibiotic Discovery. *Cell* **2020**, *181* (1), 29–45. <https://doi.org/10.1016/j.cell.2020.02.056>.
- (69) Allamand, A.; Piechowiak, T.; Lièvreumont, D.; Rohmer, M.; Grosdemange-Billiard, C. The Multifaceted MEP Pathway: Towards New Therapeutic Perspectives. *Molecules* **2023**, *28* (1403). <https://doi.org/10.3390/molecules28031403>.
- (70) Hunter, W. N. The Non-Mevalonate Pathway of Isoprenoid Precursor Biosynthesis. *J. Biol. Chem.* **2007**, *282* (30), 21573–21577. <https://doi.org/10.1074/jbc.R700005200>.
- (71) Masini, T.; Hirsch, A. K. H. Development of Inhibitors of the 2C-Methyl-D-Erythritol 4-Phosphate (MEP) Pathway Enzymes as Potential Anti-Infective Agents. *J Med Chem* **2014**, *57* (23), 9740–9763. <https://doi.org/10.1021/jm5010978>.
- (72) Knak, T.; Abdullaziz, M. A.; Höfmann, S.; Alves Avelar, L. A.; Klein, S.; Martin, M.; Fischer, M.; Tanaka, N.; Kurz, T. Over 40 Years of Fosmidomycin Drug Research: A Comprehensive Review and Future Opportunities. *Pharmaceuticals* **2022**, *15* (12). <https://doi.org/10.3390/ph15121553>.
- (73) Jomaa, H.; Wiesner, J.; Sanderbrand, S.; Altincicek, B.; Weidemeyer, C.; Hintz, M.; Türbachova, I.; Eberl, M.; Zeidler, J.; Lichtenthaler, H. K. *et al.* Inhibitors of the Nonmevalonate Pathway of Isoprenoid Biosynthesis as Antimalarial Drugs. *Science* (1979) **1999**, *285* (5433), 1573–1576. <https://doi.org/10.1126/science.285.5433.1573>.
- (74) Hirsch, A. K. H.; Lauw, S.; Gersbach, P.; Schweizer, W. B.; Rohdich, F.; Eisenreich, W.; Bacher, A.; Diederich, F. Nonphosphate Inhibitors of IspE Protein, a Kinase in the Non-Mevalonate Pathway for Isoprenoid Biosynthesis and a Potential Target for Antimalarial Therapy. *ChemMedChem* **2007**, *2* (6), 806–810. <https://doi.org/10.1002/cmdc.200700014>.
- (75) Tang, M.; Odejinmi, S. I.; Allette, Y. M.; Vankayalapati, H.; Lai, K. Identification of Novel Small Molecule Inhibitors of 4-Diphosphocytidyl-2- C-Methyl-d-Erythritol (CDP-ME) Kinase of Gram-Negative Bacteria. *Bioorg Med Chem* **2011**, *19* (19), 5886–5895. <https://doi.org/10.1016/j.bmc.2011.08.012>.
- (76) Ropponen, H.; Diamanti, E.; Johannsen, S.; Illarionov, B.; Hamid, R.; Jaki, M.; Sass, P.; Fischer, M. Exploring the Translational Gap of a Novel Class of Escherichia Coli IspE Inhibitors. *ChemMedChem* **2023**, *e202300346* (18). <https://doi.org/10.1002/cmdc.202300346>.
- (77) Choi, S.; Narayanasamy, P. Investigating Novel IspE Inhibitors of the MEP Pathway in Mycobacterium. *Microorganism* **2024**, *12* (18). <https://doi.org/https://doi.org/10.3390/microorganisms12010018>.

Aims of the thesis

The double membrane of GNB makes them especially hard to target by small molecules. There is little knowledge on structural motifs and properties that facilitate or hinder GNB uptake. As a result, the development of anti-Gram-negative antibiotics is extremely challenging and the number of approved drugs is inadequate given the critical state and rise of GNB infections. The eNTRY rules address this knowledge gap, indicating that flat, rigid compounds containing an ionisable nitrogen are more likely to accumulate in *E. coli*. The objective of the first part of this thesis was to design and synthesise eNTRY-compliant compounds to gain activity against GNB.

In previous unpublished work of the consortium, a promising antimalarial class had been discovered, however, these pyrazole-amides lacked antibacterial activity. One suitable starting point of this class was selected to be modified by introducing a variety of ionisable nitrogen-containing functional groups. The aim was to test this eNTRY-compliant library in phenotypic screenings, not only against GNB but also GPB, *M. tuberculosis*, and *P. falciparum* to establish their anti-infective profile, while simultaneously assessing the applicability and limitations of the eNTRY guidelines (2. Chapter). The results of this work inspired a small collaborative project within an ongoing study of the consortium involving the design and synthesis of fosmidomycin derivatives guided by the eNTRY rules. The goal was to develop new analogues containing *N*-alkyl guanidine substituents with the hope to improve the potency against *E. coli* (3. Chapter).

Drug discovery typically involves laborious synthesis and biological evaluations of many compounds, one approach to minimise these efforts is PT synthesis. The aim of the second part of this thesis was to establish the use of the anti-infective target IspE in PT synthesis, taking advantage of the catalytic potential of the enzyme itself to obtain selective binders. Following a typical tdDCC method, aldehydes and hydrazides were selected to generate *N*-acylhydrazone libraries *in situ* and allow IspE to amplify potential binders. Given the lack of *M. tuberculosis* IspE hits, the aim was to discover specific starting points targeting this pathogenic homologue (4. Chapter). In addition, KTGS was pursued using *in situ* click chemistry with the goal of obtaining triazole products catalysed by IspE. Previous target-identification studies of the pyrazole-amide class indicated IspE as a possible target. Therefore, the aim was to synthesise tailored azide derivatives for hit-expansion of this class by combining them with a diverse library of alkynes in presence of IspE (5. Chapter).

2. Chapter:

A Positive Charge in an Antimalarial Compound Unlocks broad-spectrum antibacterial activity

Maria Braun-Cornejo, Mitchell Platteschorre, Vincent de Vries, Patricia Bravo, Vidhisha Sonawane, Mostafa M. Hamed, Jörg Haupenthal, Norbert Reiling, Matthias Rottmann, Dennis Piet, Peter Maas, Eleonora Diamanti, and Anna K. H. Hirsch.

Manuscript submitted on June 5th 2024 to ACS Journal of Medicinal Chemistry and is available on the preprint server ChemRxiv ([10.26434/chemrxiv-2024-rs2v8-v2](https://doi.org/10.26434/chemrxiv-2024-rs2v8-v2)).

Author Contributions

M. Braun-Cornejo was involved in designing the project, synthesising compounds, and writing of the manuscript. M. Platteschorre and V. de Vries were involved in synthesising compounds. P. Bravo performed and evaluated the *Pf*NF54 activity tests. V. Sonawane performed and evaluated the *Mtb*H37Rv activity tests. M. M. Hamed was involved in purification of compounds. J. Haupenthal coordinated and evaluated the bacterial and HepG2 activity tests. N. Reiling, M. Rottmann, and D. Piet were involved in supervising the project. P. Maas, E. Diamanti, and A.K. H. Hirsch were involved in designing and supervising the project. All authors edited or approved the submitted manuscript.

Note: Please refer to ChemRxiv for full Supporting Information including NMR, HRSM, and LCMS spectra not included in this thesis.

A Positive Charge in an Antimalarial Compound Unlocks Broad-spectrum Antibacterial Activity

Maria Braun-Cornejo,^{1,2,3} Mitchell Platteschorre,¹ Vincent de Vries,¹ Patricia Bravo,^{4,5} Vidhisha Sonawane,⁶ Mostafa M. Hamed,³ Jörg Haupenthal,³ Norbert Reiling,^{6,7} Matthias Rottmann,⁴ Dennis Piet,¹ Peter Maas,¹ Eleonora Diamanti,³ and Anna K. Hirsch.^{2,3*}

¹ Specs Research Laboratory, Specs Compound Handling, B.V., Bleiswijkseweg 55, 2712 PB Zoetermeer, The Netherlands.

² Department of Pharmacy, Saarland University, Campus Building E8.1, 66123 Saarbrücken, Germany.

³ Helmholtz Institute for Pharmaceutical Research Saarland (HIPS) – Helmholtz Centre for Infection Research (HZI), Campus Building E8.1, 66123 Saarbrücken, Germany.

⁴ Swiss Tropical and Public Health Institute Kreuzstrasse 2, 4123 Allschwil, Switzerland.

⁵ Universität Basel, Petersplatz 1, 4003 Basel, Switzerland.

⁶ Microbial Interface Biology, Research Center Borstel, Leibniz Lung Center, 23845 Borstel, Germany.

⁷ German Center for Infection Research (DZIF), Partner Site Hamburg-Lübeck-Borstel-Riems, 23845 Borstel, Germany.

*Corresponding author: Anna.Hirsch@helmholtz-hips.de

Abstract

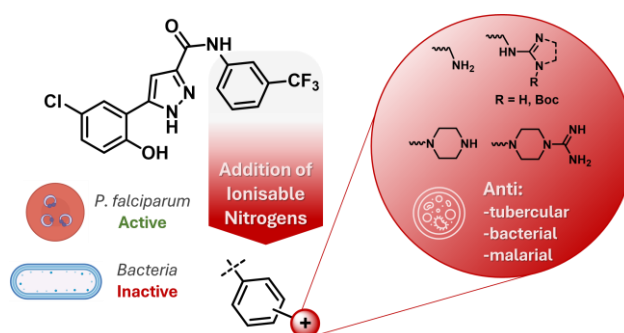
In this study, we synthesised a library of eNTRY-rule-complying compounds by introducing ionisable nitrogens to an antimalarial compound. These positively-charged derivatives gained activity against both Gram-negative and -positive bacteria, *Mycobacterium tuberculosis* and boosted *Plasmodium falciparum* inhibition to the double-digit nanomolar range. Overcoming and remaining inside the cell

envelope of Gram-negative bacteria is one of the major difficulties in antibacterial drug development. The eNTRY rules (N = ionisable nitrogen, T = low three-dimensionality, R = rigidity) can be a useful structural guideline to improve accumulation of small molecules in Gram-negative bacteria. With the aim of unlocking Gram-negative activity, we added amines and (cyclic) *N*-alkyl guanidines to an already flat and rigid pyrazole-amide class. To test their performance, we compared these eNTRY-rule-complying compounds to closely related non-complying ones through phenotypic assay screenings of various pathogens (*P. falciparum*, *Escherichia coli*, *Acinetobacter baumannii*, *Pseudomonas aeruginosa*, *Staphylococcus aureus*, *Streptococcus pneumoniae*, and *M. tuberculosis*) obtaining a handful of broad-spectrum hits. The results support the working hypothesis and even extend its applicability, the studied pyrazole-amide class adheres to the eNTRY rules; non-compliant compounds do not kill any of the bacteria tested, while compliant compounds largely showed inhibition of Gram-negative, -positive, and *M. tuberculosis* bacteria in the single-digit micromolar range.

Keywords: antimicrobial resistance, eNTRY rules, antimalarial, broad-spectrum antibiotic, antitubercular, Gram-negative accumulation.

Introduction

Antimicrobial resistance is increasing rapidly and has become a major global health threat.¹ The World Health Organisation (WHO) highlights the urgency for novel treatments against Gram-negative bacteria



(GNB).² Over the past five decades, few new antibiotic classes have been approved, with Gram-negative active ones being vastly underrepresented.³ Therefore, research and development of antibacterial drug candidates should focus more on targeting GNB, ideally designing novel chemical classes with unprecedented modes of action.⁴

The difficulty of small compounds to permeate and remain inside GNB's cell is the main reason why many antibiotics are active only against Gram-positive bacteria (GPB).⁵⁻⁷ Many statistical studies to understand the physicochemical properties that promote compound uptake in GNB have been completed since 1968.⁸ However, correlation of molecular properties and their bacterial activity give skewed results for two main reasons: (1) limited number of antibiotic compound classes causes lack of structural diversity; (2) in general it is not possible to separate the properties of a molecule that affect its antibacterial activity from the ones that affect its bacterial bioavailability.⁹ A fundamentally different approach was taken in 2017 by developing a biological assay that quantifies compound concentration inside *Escherichia coli* cells, effectively measuring compound bioavailability.¹⁰ Applying this assay to a diverse set of nearly 200 compounds and using computational methods to analyse the results, the Hergenrother group developed the so-called "eNTRY rules" (N = ionisable nitrogen, T = low three-dimensionality, R = rigidity).^{10,11} According to these guidelines, compounds containing an ionisable nitrogen, with low globularity and high rigidity are more likely to accumulate inside *E. coli* cells. The group's initial work identified primary amines as the most effective ionisable nitrogen-containing functional group, outperforming secondary and tertiary amines. Since these rules were introduced, many successes of their application to Gram-positive-only starting points to achieve GNB inhibition have been published.¹²⁻¹⁵ The most advanced compounds show *in vivo* efficacy, and inhibition of critical GNB pathogens like *Klebsiella pneumoniae* and *Acinetobacter baumannii*, indicating that eNTRY rules have a promising broad applicability.¹⁶⁻¹⁸ In 2021, Hergenrother's team broadened their investigation to other functional groups and revealed that *N*-alkyl guanidiniums perform similarly to primary amines, regarding enhanced accumulation in *E. coli*.¹⁹ This finding aligns with previous work of Masci *et al.*, who observed that the inclusion of an amine or guanidine, into their new antibiotic class was essential to overcome the GNB outer membrane, obtaining enhanced activity against *E. coli*, *K. pneumoniae* and *A. baumannii*.²⁰ Given that GNB's membrane composition differs between species and individual strains, with *E. coli*'s membrane generally being easier to cross, applying the eNTRY rules to other Gram-negative species needs caution.²¹⁻²³ For instance, Andrews *et al.* enhanced the polarity of a hit compound to overcome efflux problems in *E. coli* by introducing various ionisable groups, achieving a significant improvement with primary amine derivatives.²⁴ However, this approach did not translate to *A. baumannii* or *Pseudomonas aeruginosa*. Recently, an extensive investigation across different strains of *E. coli*, *A. baumannii*, and *P. aeruginosa* using a carefully designed library of 80 oxazolidinones, revealed that small structural changes can heavily influence the accumulation and efflux of this class in different GNB.²⁵ This study suggests that *E. coli* and *A. baumannii* have a more comparable membrane composition than *P. aeruginosa*, which generally proved to be more difficult to target.

These important findings on structural features and properties of small molecules and their relationship with GNB uptake, mark a crucial starting point for the rational design of anti Gram-negative antibiotics. The relevance of these rules for compounds that do not show previous antibiotic activity needs to be assessed, as it would be especially useful and important for accessing novel antibacterial classes and thereby delay the emergence of cross-resistance.³ Recently, we filtered a screening library for an *in silico* hit-identification study according to the eNTRY guidelines with the aim of increasing *E. coli*

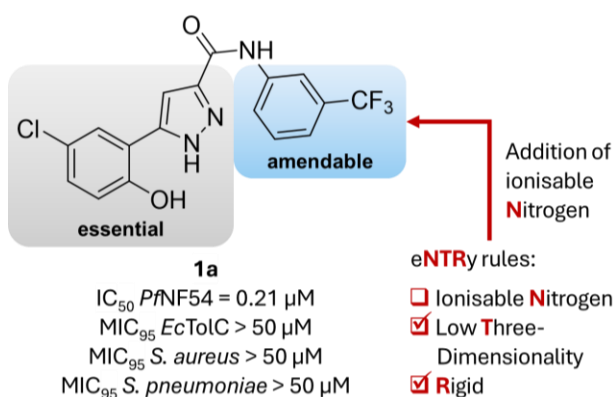


Figure 1: Illustration of our design strategy: use of compound **1a** as antimalarial starting point to incorporate ionisable nitrogen functionalities.

bioavailability.²⁶ This approach led to the identification of several *E. coli* inhibitors indicating that eNTRY rules are beneficial for the selection of antibacterial compound libraries. Optimisation of the hits, however, demonstrated the challenges of balancing antibacterial activity with target engagement whilst minimising toxicity. In a previous study, we introduced primary amine moieties through amino acid based residues to an antimalarial chemical class, obtaining compounds compliant with the eNTRY rules.²⁷ These derivatives, however, did not show significant efficacy against *E. coli*, showcasing that the addition of an ionisable nitrogen is not always enough to gain GNB uptake.

In this study, we further investigate the applicability of Hergenrother's guidelines to antimalarial compounds to expand their anti-infective scope. We achieved this by introducing a variety of ionisable nitrogen functionalities to a flat and rigid antimalarial structure (Figure 1). The functional groups comprise various amine motifs, and *N*-alkyl guanidines including novel cyclised forms not previously explored in this context. A concise synthesis yielded 48 derivatives, including neutral controls. The compounds with ionisable nitrogen atoms display broad-spectrum activity against a wide variety of pathogens. In addition to boosting activity against the parasite *Plasmodium falciparum*, many compounds demonstrate antibacterial activity against *E. coli*, *A. baumannii*, *P. aeruginosa*, *Staphylococcus aureus*, *Streptococcus pneumoniae*, and *Mycobacterium tuberculosis*.

Results and Discussion

Molecular Design. Our antimalarial starting point **1a** originates from previous unpublished work, its structure comprises three aromatic ring systems: a phenol directly connected to a pyrazole with an amide linking to a trifluoromethyl-substituted phenyl ring (Figure 1). The analysis of our hit molecule with the eNTRY rules revealed that it already complies with two out of the three structural properties from Hergenrother's findings. Specifically, it is rigid (less than five rotatable bonds), and the scaffold of three connected aromatic rings is extremely flat (low globularity), but it does not contain an ionisable

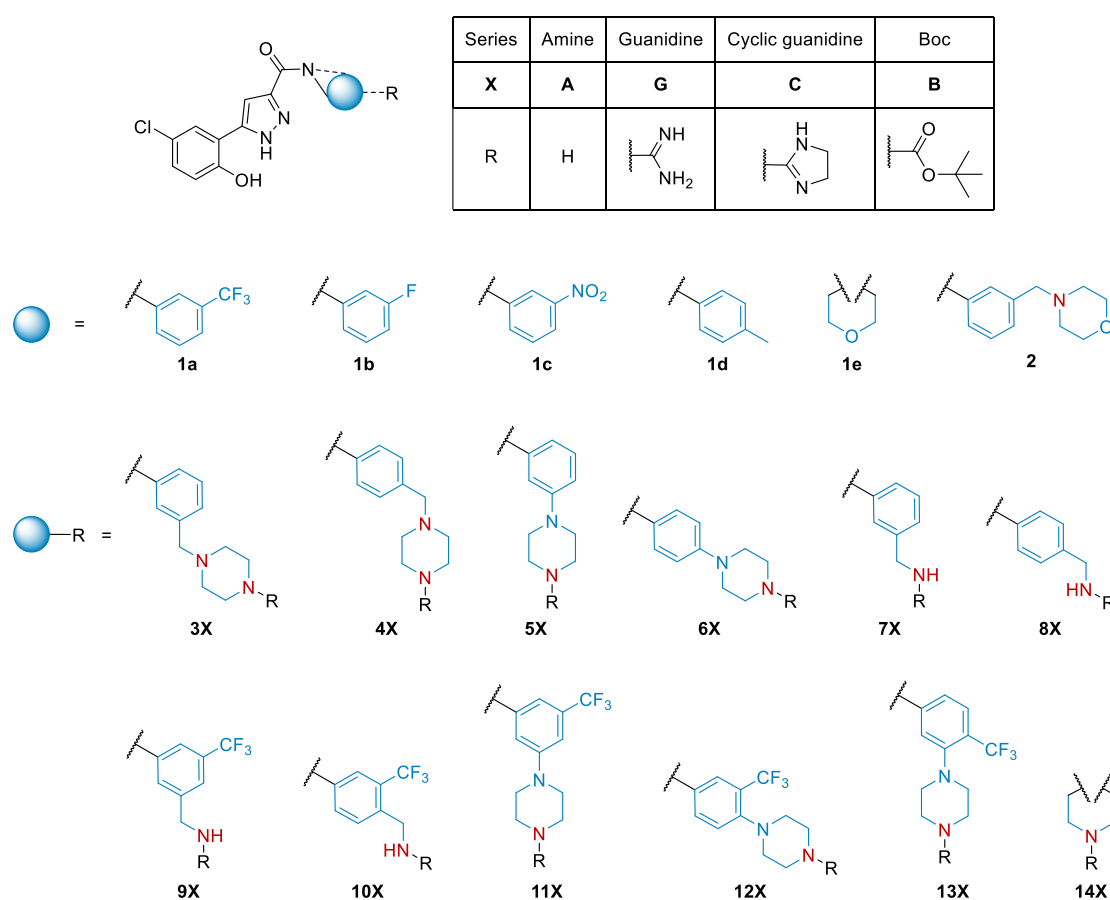
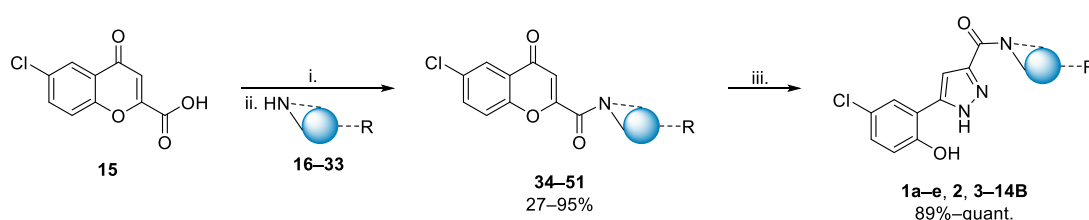


Figure 2: Focused library of pyrazole-amide class, including control compounds (**1a–e** and **3–14B**), amine (**2**, **3–14A**), Guanidine (**5–14G**), and Cyclic-guanidine (**7–11C**) derivatives. Potential ionisable nitrogens in red.

nitrogen.^{10,11} Compound **1a** presents antimalarial activity by inhibiting *P. falciparum* in the moderate nanomolar range but shows no antibacterial activity. Previous work suggests that the phenol and pyrazole moieties are crucial for antimalarial efficacy, whereas the amide-linked phenyl is amenable to changes. Modifications on this part of the molecule are easily accessible synthetically via amide couplings. Therefore, we rationally designed a focused library (Figure 2) of 32 compounds containing ionisable nitrogen atoms while preserving the essential phenol and pyrazole moieties, with the aim of obtaining anti-Gram-negative activity. The introduced positively charged nitrogen-containing functional groups are amines (**A-series**), and *N*-alkyl guanidines (**G-series**). More specifically, amine moieties include methylamines, piperazines, and morpholine. We derived the guanidines from the primary and secondary amines for a direct comparison of the anti-infective profile, with some analogues featuring cyclised guanidines (**C-series**) for added lipophilicity (Figure 2). Additionally, to gain further insights, we included *N*-Boc (**B-series**) protected analogues of the amines as uncharged controls. As additional controls, we also included some alternative electron-withdrawing substituents to the trifluoromethyl of **1a**, namely fluorine **1b** and nitro **1c**. To assess the influence of an electron-donating substituent, we included methyl-derivative **1d** and to evaluate the influence of the aromatic ring we removed it in structures **1e** and **14**.

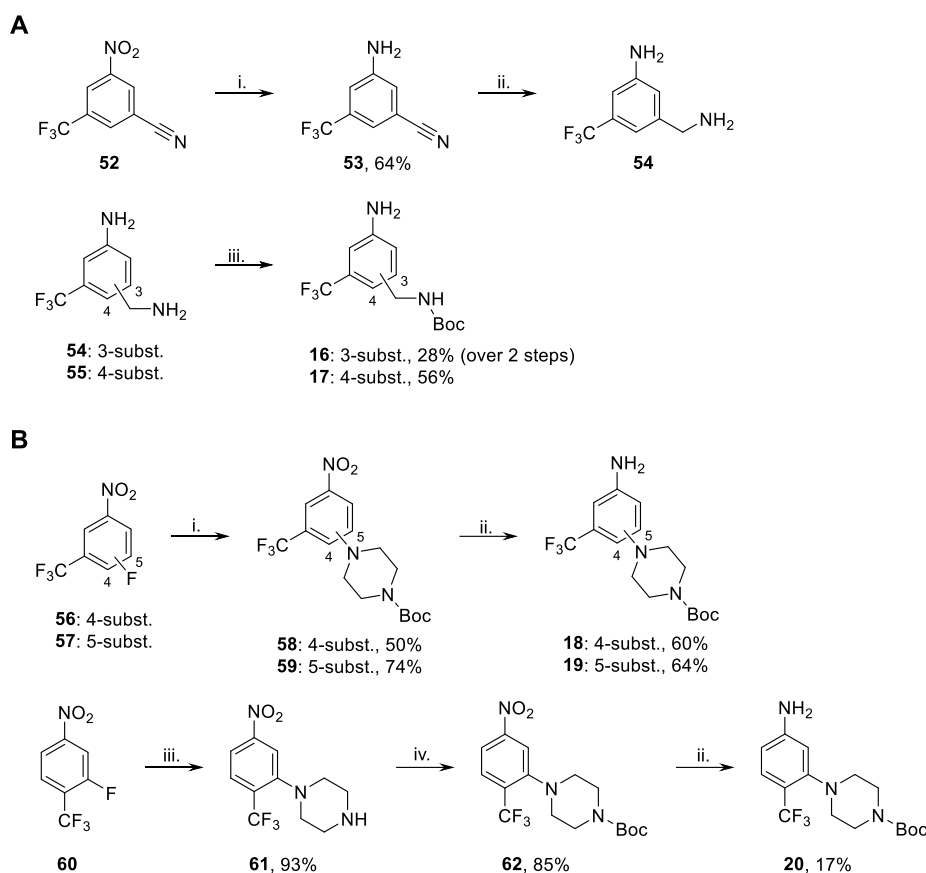
Synthesis. We optimised the synthesis of the designed library using key chromene amide intermediates **34–51**. Initially, we investigated amide couplings of pyrazole-carboxylic acid derivatives with anilines. This procedure was hampered by low yields, and purification and isolation of the products proved difficult. Alternatively, we used commercially available 6-chlorochromene-2-carboxylic acid (**15**) for the amide coupling. Subsequent reaction with hydrazine hydrate formed pyrazole-amide products **1a–e**, **2** and **3–14B** in quantitative yield (Scheme 1). The amines **16–33** used in the amide coupling were largely commercially available, however, maintaining the trifluoromethyl substituent of parent compound **1a** in addition to the ionisable nitrogen functionality, required synthesis of **16–20** (Scheme 2).



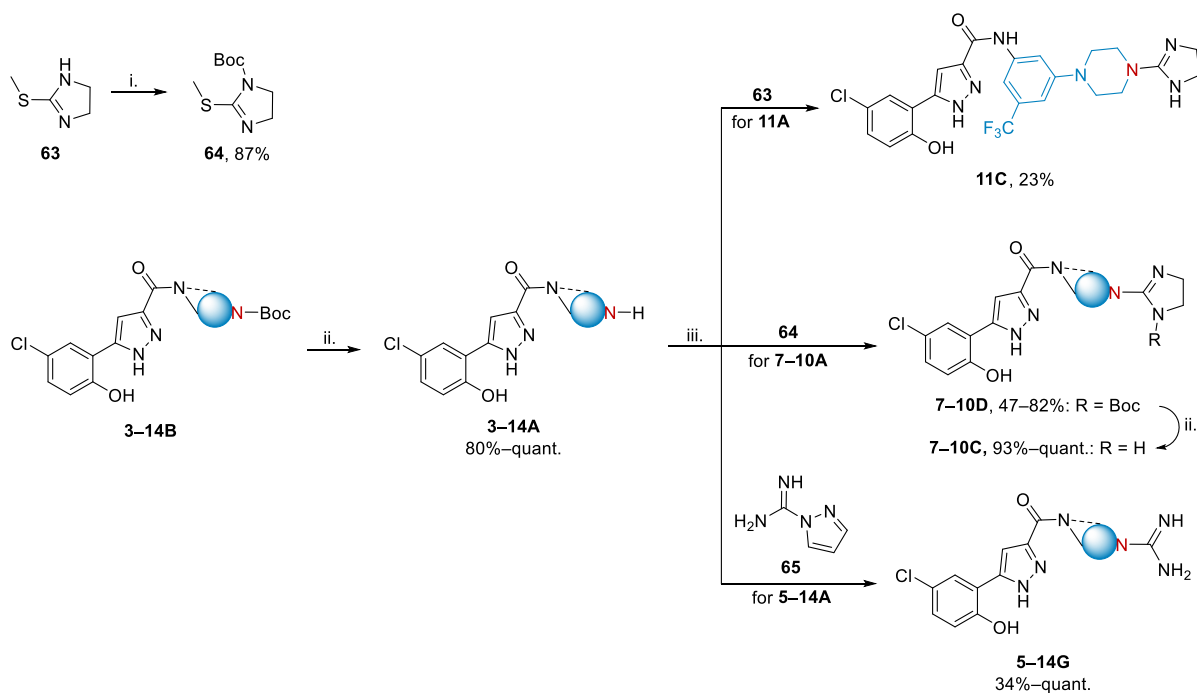
Scheme 1: General synthetic scheme of pyrazole-amides compounds **1a–e**, **2** and **3–14B**, reagents and conditions: i) DIPEA, HATU, DMF, 0 °C, 30 min; ii.) r.t., 2–24 h;²⁸ iii.) hydrazine hydrate, EtOH, reflux, 2–18 h.²⁹

To minimise the formation of by-products in the amide coupling, the methylamine- and piperazine-substituted anilines needed *N*-Boc protection, which, at the same time allowed to obtain the **B-series** (**3–14B**) as control compounds. To obtain aniline **16** and **17**, we selectively *N*-Boc protected methylamine analogues **54** and **55**. Analogue **54** was prepared by reducing the nitro and nitrile groups of **52**, and **55** was commercially available (Scheme 2A). We obtained piperazine-substituted anilines **18** and **19** in a two step synthesis starting with fluorine displacement of derivatives **56** and **57** using 1-Boc piperazine. Subsequent reduction of the nitro group using sodium dithionite gave anilines **18** and **19** in good to moderate yields. The synthesis of aniline **20** required an additional step, because the direct fluorine displacement of **60** using 1-Boc piperazine was unsuccessful. Using an excess of unsubstituted piperazine, however, followed by *N*-Boc protection afforded **62** in a good yield. Lastly, reduction of the nitro group afforded aniline **20** in a modest yield (Scheme 2B).

The obtained compounds of the Boc-series (**3–14B**) served as intermediates providing the desired amine series as TFA salts in excellent yields (**3–14A**). Following a similar approach, the **A-series** was used to obtain both guanidine series **C** and **G**. The initial guanidinylation strategy for the five-membered ring guanidine series **C** yielded undesired double-guanylated products. Controlling the reaction rate for selective guanidinylation using reagent **63** proved challenging, leading to difficult purifications and low yield of product **11C** (Scheme 3). To address this issue, we *N*-Boc protected **63**, obtaining the



Scheme 2. Synthesis of anilines **16–20**. A) Methylamine-substituted anilines, *reagents and conditions*: i) Fe, NH₄Cl, EtOH:H₂O (2:1), reflux, 24 h; ii.) LiAlH₄, THF, reflux, 4 h; iii.) Boc₂O, NEt₃, DCM, 0 °C–r.t., 6–24 h.³⁰ B) Piperazine-substituted anilines, *reagents and conditions*: i.) 1-Boc piperazine, K₂CO₃, DMSO, 100 °C, 18–20 h;³¹ ii.) Na₂S₂O₄, EtOH, reflux, 6 h; iii.) piperazine, K₂CO₃, 100 °C, DMSO, 24 h;³¹ iv.) Boc₂O, DMAP, DCM, r.t., 72 h.³²



Scheme 3. General synthetic scheme of pyrazole-amides containing ionisable nitrogens: amine (**A**), guanidine (**G**), cyclic-guanidine (**C**) and *N*-Boc cyclic-guanidine (**D**). *Reagents and conditions*: i.) Boc₂O, NEt₃, DCM, r.t., 24 h;³⁰ ii.) TFA, DCM, r.t., o.n.;³³ iii.) DIPEA, DMF, r.t., o.n.^{34–36}

alternative guanidinylation agent **64**. This modification facilitated the synthesis of the remaining cyclic guanidines (**5–10C**) via their corresponding Boc analogues (**7–10D**) in good yields. As piperazines are more lipophilic than methylamines, we opted to exclude piperazine derivatives from the **C** and **D**-series. The *N*-alkyl guanidine series **G** was accessed by employing guanidinylation agent **65**, resulting in moderate to excellent yields (Scheme 3).

Overview of anti-infective activity. We assessed the anti-infective profile of our newly synthesised library against the parasite *P. falciparum*, and various bacterial strains both Gram-negative, and -positive, as well as *M. tuberculosis*. The vast majority of compounds largely retained antimalarial activity (strain *PfNF54*) compared to the parent compound **1a**, indicating that anti-infective properties were not affected by the addition of a positive charge (Table 1). This finding gave a good foundation to determine antibacterial efficacy of the library and evaluate the applicability of the eNTRY rules. In the case of Gram-negative bacteria, firstly we tested all compounds against the efflux-pump deficient *E. coli* strain *EcΔtolC*. As the majority of positively charged compounds showed at least moderate *EcΔtolC* inhibition, we extended the panel and included the *E. coli* wild type *EcK12*, *A. baumannii* and *P. aeruginosa* strain PA14. Approximately half of the compounds are active against *EcK12*, however, with significant loss in potency compared to *EcΔtolC*, indicating efflux liabilities. Many of the *E. coli* inhibitors were also active against *A. baumannii* and PA14. Interestingly, the addition of ionisable nitrogens to this class also yielded excellent activities against *M. tuberculosis* strain *MtbH37Rv* and GPB. None of our neutral control compounds presented antibacterial activity. These findings confirm that the eNTRY rules are applicable to our pyrazole-amide class. In addition to gaining activity against GNB by introducing ionisable nitrogens, for the first time, we showed that this effect can expand to GPB and *M. tuberculosis*. Excitingly, this approach yielded a new broad-spectrum anti-infective class, with many compounds being active across species. We illustrated the big overlap of active compounds across *PfNF54*, *EcΔtolC*, *MtbH37Rv* and GPB (*S. pneumoniae* or *S. aureus*) in a Venn diagram (Figure 3). In addition, two examples (**7D**, **10G**) inhibit all eight tested pathogens, and an additional eleven compounds (**3G**, **5A**, **6G**, **9–11C**, **9G**, **10–11A**, **11G**, **13G**) inhibit all pathogens except for *P. aeruginosa*, which is known to be particularly challenging pathogen (Table 1).

Structure–activity relationships. Our library was designed to investigate various functional groups, mostly containing nitrogens, and their effect on anti-infective properties. In total, we synthesised 48 compounds, 28 of which contain ionisable nitrogen atoms, consisting of thirteen amines (**2**, **3–14A**), ten *N*-alkyl guanidines (**5–14G**), and five cyclic guanidines (**7–11C**). In addition, we tested four Boc protected analogues (**7–10D**) of the cyclic guanidines (**7–10C**), these functionalities are likely not ionisable in physiological conditions based on computational evaluation (pK_a : ~5.1, Figure S1). The Boc protected analogues (**3–14B**) of the amines (**3–14A**) serve as more reliable neutral control compounds, as well as compounds **1a–d**, which lack ionisable nitrogen atoms altogether. Besides the nature of the functional groups, the main differences between these compounds are the motifs that contain said groups, consisting of piperazines, methylamines, and morpholine. Additionally, the substitution pattern of the motifs changes, with some examples (**9–13**) including the trifluoromethyl substituent present in parent compound **1a**.

P. falciparum. Our antimalarial starting point **1a** has an inhibitory concentration in the submicromolar range (*PfNF54* IC_{50} = 0.21 μ M) which was largely retained in the dedicated library (Table 1). Fourteen compounds (**5–6A**, **9–13A**, **9–11B**, **9–10D**, **9G**, **12G**) showed an increase in activity against *PfNF54*, all of them except for **5A** and **6A** retain the *meta*-CF₃ substitution on the aromatic ring of **1a**. The two most active compounds **11A** and **12A** (IC_{50} ≤ 0.06 μ M) contain a piperazine substituent, respectively on *meta* and *para*

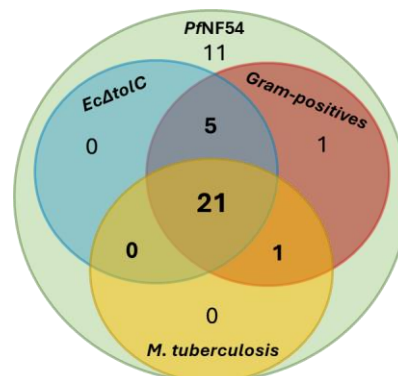


Figure 3: Venn diagram of the active compounds in *PfNF54*, *EcΔtolC*, Gram-positive bacteria and *M. tuberculosis*, indicating the broad-spectrum anti-infective nature of our pyrazole-amide class.

Table 1. Biological activity of pyrazole-amide class in *Plasmodium falciparum* (PfnF54), *Escherichia coli* (*EcΔtolC* and *EcK12*), *Acinetobacter baumannii* (*Ab*), *Pseudomonas aeruginosa* (PA14), *Streptococcus pneumoniae* (*Sp*), *Staphylococcus aureus* (*Sa*), *Mycobacterium tuberculosis* (*MtbH37Rv*), and human liver cells (HepG2).

Cmp	PfnF54 IC ₅₀	Gram-negative				Gram-positive		<i>MtbH37Rv</i> MIC ₉₀	HepG2 CC ₅₀
		<i>EcΔtolC</i> MIC ₉₅	<i>EcK12 inh.</i> at 50 μM	<i>Ab inh.</i> at 50 μM	PA14 inh. at 50 μM	<i>Sp</i> MIC ₉₅	<i>Sa</i> MIC ₉₅		
1a	0.21	>50	<10%	<10%	<10%	>50	>50	n.d.	>50
1b	0.7	>50	n.d.	n.d.	n.d.	>50	>50	n.d.	n.d.
1c	0.51	>50	n.d.	n.d.	n.d.	>50	>50	>32a	n.d.
1d	2.40	>50	n.d.	n.d.	n.d.	>50	>50	n.d.	>50
1e	>5	>50	n.d.	n.d.	n.d.	>50	>50	>16	>50
2	1.1	>50	n.d.	n.d.	n.d.	>50	>50	>16a	~50
3A	0.62	45	28%	21%	50%	40	>50	>64	12
3B	1.0	>50	n.d.	n.d.	n.d.	>50	>50	n.d.	25
4A	0.27	40	34%	24%	62%	40	>50	64	13
4B	0.2	>50	n.d.	n.d.	n.d.	>50	>50	n.d.	7
5A	0.13	21	83%	34%	60%	26	37	64	9
5B	0.9	>50	n.d.	n.d.	n.d.	>50	>50	n.d.	>50
5G	0.93	11	32%	<10%	31%	48	23.1	64	>50
6A	0.14	22.5	49%	37%	63%	45	>50	>16a	11.8
6B	1.61	>50	n.d.	n.d.	n.d.	>50	>50	n.d.	>50
6G	0.44	9	45%	32%	55%	25	26	64	>50
7A	0.30	47	27%	15%	44%	43	>50	>64	28.4
7B	1.1	>50	n.d.	n.d.	n.d.	>50	>50	n.d.	>50
7C	0.39	13	29%	33%	41%	48.2	22.3	32	>50
7D	0.36	14	56%	77%	55%	31	24.0	64	19
7G	0.21	13	61%	24%	56%	49.0	22	64	>50
8A	1.8	>50	n.d.	n.d.	n.d.	>50	>50	>16a	30
8B	1.7	>50	n.d.	n.d.	n.d.	>50	>50	n.d.	>50
8C	0.67	21.5	<10%	12%	10%	>50	49	>64	>50
8D	>5	>50	n.d.	n.d.	n.d.	>50	>50	>64	>50
8G	0.42	47.5	29%	19.9%	41%	>50	22	>64	>50
9A	0.082	8	<10%	MIC ₉₅ = 49	<10%	11	12.1	32	7
9B	0.2033	>50	n.d.	n.d.	n.d.	30	>50	>64	5.0
9C	0.517	7	<10%	47%	18%	15	9	16	>50
9D	0.15	24.0	<10%	82%	21%	21	12	16	14
9G	0.078	5	MIC ₉₅ = 46	59%	50%	>50	8	32	>50
10A	0.15	22.9	61%	86%	<10%	23	29	64	13
10B	0.19	>50	n.d.	n.d.	n.d.	>50	>50	n.d.	>50
10C	0.404	5.5	77%	47%	29%	14	8	16	>50
10D	0.14	18	17%	<10%	<10%	>50	11.6	16	11
10G	0.25	3.5	86%	49%	55%	16	5	8	>50
11A	0.05	7	72%	MIC ₉₅ = 22	<10%	5	6	32	9
11B	0.13	>50	n.d.	n.d.	n.d.	>50	>50	n.d.	4.0
11C	0.59	7	63%	53%	<10%	7	8	8	>50
11G	0.5	4	MIC ₉₅ = 48	MIC ₉₅ = 17	25%	28	3.2	8	>25
12A	0.06	18.9	12%	29%	<10%	8	14	16	6
12B	0.56	>50	n.d.	n.d.	n.d.	>50	>50	n.d.	>50
12G	0.2	2.8	51%	33%	<10%	31	2.4	4	30
13A	0.160	>50	n.d.	n.d.	n.d.	29	>50	32	8
13B	0.3418	>50	n.d.	n.d.	n.d.	>50	>50	n.d.	2.8
13G	0.5	5	59%	46%	17%	16	2.5	8	>25
14A	3.3	>50	n.d.	n.d.	n.d.	>50	>50	>16	>50
14G	>5	>50	n.d.	n.d.	n.d.	>50	>50	>64	>50

^a Not active at maximum solubility; n.d.: not determined. IC₅₀, MIC, and CC₅₀ values are in μM.

positions. In contrast, the compounds without an aromatic ring linked to the nitrogen of the amide (**1e**, **14A**, **14G**) are inactive, suggesting that the aromatic moiety is essential. When it comes to the aromatic ring, *para*-methylene substitution seems detrimental, methyl derivative **1d**, methylamine **8A** and Boc-protected cyclic guanidine **8D** have a tenfold decrease in activity compared to **1a** ($IC_{50} > 2 \mu M$). Similarly, Boc-protected amine derivatives without an additional CF_3 substituent suffer from a significant loss in activity (**5–8B**: $IC_{50} = 0.9–1.7 \mu M$). Exchanging the trifluoromethyl substituent of **1a** with other electron-withdrawing groups led to a loss in activity (**1b–c**: $IC_{50} = 0.5–0.7 \mu M$). These findings reveal that the combination of trifluoromethyl substitution and ionisable nitrogen atom can be highly favourable for activity in *PfNF54* and that bigger substituents such as piperazine and *N*-Boc piperazine are well-tolerated.

Gram-negative bacteria. The *E. coli* inhibition of all 48 compounds was investigated using the efflux-pump deficient *EcΔtolC* strain. We obtained 26 hits with a wide range of activities (MIC_{95} : 2.8–47.5 μM , Table 1). None of the neutral control compounds significantly affected the growth of *EcΔtolC* (Table S1), indicating that these structures were not permeable and that a positive charge is essential for *E. coli* activity. The eleven most potent hits have a single-digit micromolar minimum inhibitory concentration (MIC) and consist of nine (cyclic) guanidines (**6G**, **9–13G**, **9–11C**,) and two amine derivatives (**9A**, **11A**). Similarly to *PfNF54*, only one of the top hits does not contain a *m*- CF_3 substituent (**6G**). In addition, the compounds with no antimalarial activity also lack activity against *E. coli*. Only two positively charged antimalarial hits are inactive against *EcΔtolC* (**2**, **13A**). These findings suggest that the engagement with the anti-infective target is largely consistent across these two species. In the case of *EcΔtolC* inhibition there is a clear trend indicating that guanidine-type groups enhance potency. When comparing the different positively charged groups of identical scaffolds, the amine derivatives (**A**-series) have the lowest potencies, with one exception (MIC_{95} : **9A** = 8 μM vs **9D** = 24 μM). Within the various types of guanidine functionalities (**C**-, **D**-, **G**-series), the *N*-Boc protected cyclic guanidine derivatives (**D**-series) are less active, with the most significant difference observed for scaffold **10** (MIC_{95} : **10D** = 18 μM vs **10C** = 5.5 μM vs **10G** = 3.5 μM).

To further investigate the antibacterial profile and assess the eNTRY rules' applicability, the 26 *EcΔtolC* hits ($MIC_{95} < 50 \mu M$) were tested against the *E. coli* wild type K12, *A. baumannii* and *P. aeruginosa*. As expected these pathogenic strains were harder to target, nevertheless, fifteen hits (**5–6A**, **10–11A**, **6G**, **7G**, **9–11G**, **13G**, **7D**, **9D**, **9–11C**) were identified with moderate inhibition ($\geq 45\%$) at 50 μM compound concentration against *EcK12*. Structurally, we confirm once again that the guanidine functionality is beneficial for *E. coli* activity, with the two most active compounds being **9G** and **11G**. These structures have *EcK12* MIC_{95} values just below 50 μM (**9G** = 46 μM ; **11G** = 48 μM), which indicates a tenfold decrease in activity compared to *EcΔtolC* (**9G** = 5 μM ; **11G** = 4 μM), making efflux a main concern for the activity of this class. Noteworthy, the most significant loss of activity is observed for methylamine **9A**, one of the top *EcΔtolC* inhibitors that did not show any effect on *EcK12* growth (**9A** *ΔtolC* MIC_{95} = 8 μM vs **9A** K12 < 10% inh. at 50 μM). A similar trend also applies to compound **9D** where the good activity against *EcΔtolC* did not translate to *EcK12* (**9D** *ΔtolC* MIC_{95} = 24 μM vs **9D** K12 < 10% inh. at 50 μM). These findings led us to speculate that the structural makeup of compounds **9** seems to be especially prone to *tolC* efflux. In the case of *A. baumannii*, eleven compounds (**7D**, **9D**, **9–11C**, **9–11G**, **13G**, **10–11A**) showed a moderate ($\geq 45\%$ inh. at 50 μM) to good ($MIC_{95} < 25 \mu M$) activity, with **11A** and **11G** as the best hits having an MIC_{95} of 22 μM and 17 μM , respectively. Interestingly, these doubly *meta*-substituted structures are also among the best *E. coli* hits. The remaining nine *A. baumannii* inhibitors also largely contain a CF_3 substituent and (cyclic) guanidines, with all of them except for **9D** being active against *EcK12*. This big overlap in their inhibitory profile suggest that the bioavailability and target engagement of our pyrazole-amide class is similar in *A. baumannii* and *EcK12*. When comparing to *P. aeruginosa*, however, the species have less hits in common as illustrated in the Venn diagram (Figure 4). We identified nine compounds (**3–6A**, **6–7G**, **9–10G**, **7D**) with a moderate effect ($\geq 45\%$ inh. at 50 μM) on the growth of *P. aeruginosa* strain PA14. Three of the PA14 hits (**7D**, **9–10G**) are also active against the other two GNB wild-types *EcK12* and *A. baumannii*, and an additional four compounds (**5–6A**, **6–7G**,) share activity with *EcK12* (Figure 4). Methylamine derived guanidines seem to be a privileged

scaffold for targeting GNB, they appear in the three common hits across all tested GNB and in several other shared hit scaffolds of *E. coli* and *A. baumannii* (**9–10C**) or PA14 (**3G**). Overall, the potencies of the PA14 hits are the lowest we obtained across all pathogens (Table 1). The CF₃ substituent and the guanidine moieties seem to be significantly less effective in targeting PA14 compared to the other GNB. In contrast, amines with (methyl-) piperazine motifs yielded better results. These findings align with the structure–uptake study on Oxazolidinones where they identified a CF₃-substituted phenyl motif as a liability to *P. aeruginosa* outer membrane permeation and also concluded that *P. aeruginosa* is more divergent compared to *E. coli* and *A. baumannii*.²⁵

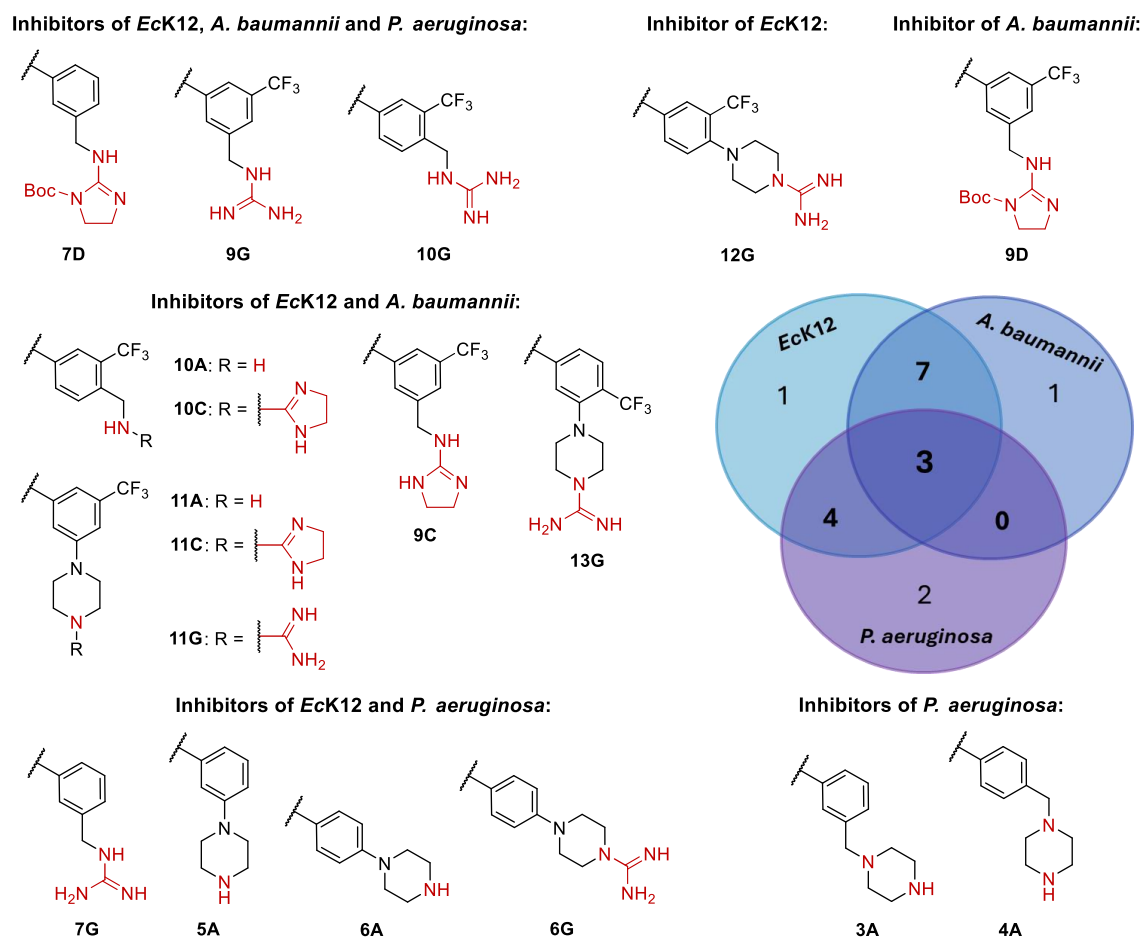


Figure 4. Chemical structures and Venn diagram of the active compounds in *Escherichia coli* K12 (EckK12), *Acinetobacter baumannii*, and *Pseudomonas aeruginosa* ($\geq 45\%$ inhibition at 50 μM). Ionisable nitrogen moieties in red.

Gram-positive bacteria. The use of Hergenrother’s eNTRY rules has been mostly reported by modifying a Gram-positive antibacterial class to comply with the three structural indications and thereby obtaining GNB activity. Therefore, we wanted to assess the GPB inhibition of our pyrazole-amide class and tested all 48 compounds against *S. aureus* and *S. pneumoniae*. Half of the compounds were active against at least one of the species but only one example of a neutral control compound (**9B**) inhibits *S. pneumoniae* (**9B**: MIC₉₅ = 30 μM , Table 1). This finding suggests that the bacterial permeability of our neutral compounds is very low. However, our methodology was set up for the assessment of antibacterial activity of the chemical class, we did not quantify bioavailability of our compounds, therefore we cannot rule out that the ionisable nitrogen atoms are contributing significantly to the on-target activity. Eighteen of the 24 Gram-positive hits inhibit both *S. aureus* and *S. pneumoniae*, with potencies against *S. aureus* being generally higher and guanidines being particularly favourable. Guanidines **9–10C** and **9–13G** have excellent single digit micromolar MIC₉₅ values against *S. aureus*. In addition, **11A** and **11C** are among the best hits in both species and amine **12A** in *S. pneumoniae*. These findings align with previous trends and highlight the

favourable combination of trifluoromethyl and positively charged motifs for antibacterial activity. In the case of *S. pneumoniae*, piperazine substituents are especially advantageous.

Mycobacterium tuberculosis. To obtain an even wider scope of the anti-infective profile of our chemical class, we assessed its antitubercular activity using the *M. tuberculosis* strain *MtbH37Rv* and obtained 22 hits. The five best *MtbH37Rv* inhibitors (**10–13G**, **11C**) have comparable potencies to the best Gram-positive and *EcΔtolC* hits, with an MIC₉₀ value of 4 μM **12G** is the most potent *MtbH37Rv* inhibitor (Table 1). The tendency of CF₃ and guanidine-containing structures to be especially active persists, and overall there is a big overlap in hit compounds shared between *MtbH37Rv*, GPB and *EcΔtolC* (Figure 3). Our neutral control compounds were not sufficiently soluble in the *M. tuberculosis* growth medium and could not be evaluated (Table S2). Similarly, four amines had low solubilities (16–32 μM: **2**, **4A**, **6A**, **12A**) and did not show an effect on the growth of *MtbH37Rv* at the testable concentrations (Table 1). To the best of our knowledge, this is the first record of applying the eNTRY rules to gain antitubercular activity, and was encouraged in a review on the hurdles of anti tubercular drug development from 2020.³⁷ However, similarly to the other tested pathogens, we cannot rule out that the ionisable nitrogen functionalities give rise to the antibacterial effect and not only to the bacterial uptake. Especially considering that the membrane of *M. tuberculosis* is particularly lipophilic and hard to permeate for drug-like compounds.³⁸

Cytotoxicity. To get an insight into the toxicity of the class, the impact on the viability of the human liver cell line HepG2 was evaluated for all compounds. Generally, our most potent hits were nontoxic with cytotoxic concentrations (CC₅₀) >50 μM (Table 1). However, we did identify a major cytotoxic liability. All amine derivatives had a toxic effect on the liver cells, in the worst cases the CC₅₀ values reached the single-digit micromolar range. Interestingly, the majority of Boc and guanidine analogues were not toxic, suggesting that the liability stems directly from the amine functional groups. This is exemplified when comparing the toxicities of structures **5–8**. Compounds **5** and **6** contain a piperazine-substituted phenyl, in *meta* and *para*. In the closely-related structures **7** and **8**, a methylene linker separates the piperazine from the aromatic ring, which results in both piperazine nitrogen atoms being aliphatic amines. In this case, both the amine (**7–8A**) and the Boc (**7–8B**) derivatives are toxic. In contrast, Boc and guanidine derivatives **5–6B** and **5–6G** are nontoxic, whereas amine analogues **5–6A** are, indicating that aniline-like nitrogen atoms devoid of hepatotoxicity.

We investigated the toxicity of our best *MtbH37Rv* inhibitors further by testing their effect on human monocyte-derived macrophages (**10–13G**, Table S2). None of the tested compounds were of major concern, solely **12G** exhibits a CC₉₀ of 32 μM, which is manageable given that it is an eightfold difference in activity compared to *MtbH37Rv*.

Conclusions

We report the design, synthesis, and evaluation of a small library of pyrazole-amides against *P. falciparum*, *E. coli*, *A. baumannii*, *P. aeruginosa*, *S. pneumoniae*, *S. aureus*, and *M. tuberculosis*. Through phenotypic screenings, we identified broad-spectrum anti-infective activity of the new pyrazole-amide class. We successfully applied the eNTRY rules to an antimalarial compound extending its activity not only to GNB but also GPB and *M. tuberculosis*. The best ionisable nitrogen-containing functional group for our chemical class were *N*-alkyl guanidines. For the first time, we showed that cyclised guanidines can also aid in bacterial uptake. We identified three compounds (**3D**, **9–10G**) with activity in all tested GNB. **12G** is the most potent *MtbH37Rv*, *EcΔtolC* and *S. aureus* hit with low single-digit micromolar activities in all three species, while maintaining the antimalarial potency of the parent compound **1a**. We observed the biggest SAR variations in *P. aeruginosa*, where guanidines or trifluoromethyl substitution seemed detrimental to activity opposed to the rest of the pathogens. Further evaluation of molecular properties that dictate compounds' bioavailabilities across different pathogens is needed to better understand the applicability and limitations of existing guidelines and expand them. At the same time, the target identification of the pyrazole-amide class is necessary for future hit-optimisation and better rationalisation of the SAR.

Author Contributions

M. Braun-Cornejo was involved in designing the project, synthesising compounds, and writing of the manuscript. M. Platteschorre and V. de Vries were involved in synthesising compounds. P. Bravo performed and evaluated the PfnF54 activity tests. V. Sonawane performed and evaluated the MtbH37Rv activity tests. M. M. Hamed was involved in purification of compounds. J. Hauptenthal coordinated and evaluated the bacterial and HepG2 activity tests. N. Reiling, M. Rottmann, and D. Piet were involved in supervising the project. P. Maas, E. Diamanti, and A.K. H. Hirsch were involved in designing and supervising the project. All authors edited or approved the submitted manuscript.

Acknowledgements

This project has received funding from the European Union's Horizon 2020 research and innovation programme under the Marie Skłodowska-Curie grant agreement No. 860816 (A. K. H. Hirsch, P. Maas, M. Rottmann, & N. Reiling). The authors thank Nanda de Klerk-Sprenkels for expert support in NMR.

Notes

The authors declare no competing financial interest.

References

- (1) Murray, C. J.; Ikuta, K. S.; Sharara, F.; Swetschinski, L.; Robles Aguilar, G.; Gray, A.; Han, C.; Bisignano, C.; Rao, P.; Wool, E.; Johnson, S. C.; Browne, A. J.; Chipeta, M. G.; Fell, F.; Hackett, S.; Haines-Woodhouse, G.; Kashef Hamadani, B. H.; Kumaran, E. A. P.; McManigal, B.; Agarwal, R.; Akech, S.; Albertson, S.; Amuasi, J.; Andrews, J.; Aravkin, A.; Ashley, E.; Bailey, F.; Baker, S.; Basnyat, B.; Bekker, A.; Bender, R.; Bethou, A.; Bielicki, J.; Boonkasidecha, S.; Bukosia, J.; Carvalheiro, C.; Castañeda-Orjuela, C.; Chansamouth, V.; Chaurasia, S.; Chiurchiù, S.; Chowdhury, F.; Cook, A. J.; Cooper, B.; Cressey, T. R.; Criollo-Mora, E.; Cunningham, M.; Darboe, S.; Day, N. P. J.; De Luca, M.; Dokova, K.; Dramowski, A.; Dunachie, S. J.; Eckmanns, T.; Eibach, D.; Emami, A.; Feasey, N.; Fisher-Pearson, N.; Forrest, K.; Garrett, D.; Gastmeier, P.; Giref, A. Z.; Greer, R. C.; Gupta, V.; Haller, S.; Haselbeck, A.; Hay, S. I.; Holm, M.; Hopkins, S.; Iregbu, K. C.; Jacobs, J.; Jarovsky, D.; Javanmardi, F.; Khorana, M.; Kissoon, N.; Kobeissi, E.; Kostyanov, T.; Krapp, F.; Krumkamp, R.; Kumar, A.; Kyu, H. H.; Lim, C.; Limmathurotsakul, D.; Loftus, M. J.; Lunn, M.; Ma, J.; Mturi, N.; Munera-Huertas, T.; Musicha, P.; Mussi-Pinhata, M. M.; Nakamura, T.; Navavati, R.; Nangia, S.; Newton, P.; Ngoun, C.; Novotney, A.; Nwakanma, D.; Obiero, C. W.; Olivas-Martinez, A.; Olliaro, P.; Ooko, E.; Ortiz-Brizuela, E.; Peleg, A. Y.; Perrone, C.; Plakkal, N.; Ponce-de-Leon, A.; Raad, M.; Ramdin, T.; Riddell, A.; Roberts, T.; Robotham, J. V.; Roca, A.; Rudd, K. E.; Russell, N.; Schnall, J.; Scott, J. A. G.; Shivamallappa, M.; Sifuentes-Osornio, J.; Steenkeste, N.; Stewardson, A. J.; Stoeva, T.; Tasak, N.; Thaiprakong, A.; Thwaites, G.; Turner, C.; Turner, P.; van Doorn, H. R.; Velaphi, S.; Vongpradith, A.; Vu, H.; Walsh, T.; Waner, S.; Wangrangsimaikul, T.; Wozniak, T.; Zheng, P.; Sartorius, B.; Lopez, A. D.; Stergachis, A.; Moore, C.; Dolecek, C.; Naghavi, M. Global Burden of Bacterial Antimicrobial Resistance in 2019: A Systematic Analysis. *The Lancet* **2022**, 399 (10325), 629–655. [https://doi.org/10.1016/S0140-6736\(21\)02724-0](https://doi.org/10.1016/S0140-6736(21)02724-0).
- (2) World Health Organization. *Global Priority List of Antibiotic-Resistant Bacteria to Guide Research, Discovery, and Development of New Antibiotics - 2017*; Geneva, 2017.
- (3) Walesch, S.; Birkelbach, J.; Jézéquel, G.; Haeckl, F. P. J.; Hegemann, J. D.; Hesterkamp, T.; Hirsch, A. K. H.; Hammann, P.; Müller, R. Fighting Antibiotic Resistance—Strategies and (Pre)Clinical Developments to Find New Antibacterials. *EMBO Rep* **2023**, 24 (1). <https://doi.org/10.15252/embr.202256033>.
- (4) Lewis, K. The Science of Antibiotic Discovery. *Cell* **2020**, 181 (1), 29–45. <https://doi.org/10.1016/j.cell.2020.02.056>.
- (5) Pérez, A.; Poza, M.; Fernández, A.; Del Carmen Fernández, M.; Mallo, S.; Merino, M.; Rumbo-Feal, S.; Cabral, M. P.; Bou, G. Involvement of the AcrAB-TolC Efflux Pump in the Resistance, Fitness, and Virulence of Enterobacter Cloacae. *Antimicrob Agents Chemother* **2012**, 56 (4), 2084–2090. <https://doi.org/10.1128/AAC.05509-11>.
- (6) Tamae, C.; Liu, A.; Kim, K.; Sitz, D.; Hong, J.; Becket, E.; Bui, A.; Solaimani, P.; Tran, K. P.; Yang, H.; Miller, J. H. Determination of Antibiotic Hypersensitivity among 4,000 Single-Gene-Knockout Mutants of Escherichia Coli. *J Bacteriol* **2008**, 190 (17), 5981–5988. <https://doi.org/10.1128/JB.01982-07>.
- (7) Sulavik, M. C.; Houseweart, C.; Cramer, C.; Jiwani, N.; Murgolo, N.; Greene, J.; Didomenico, B.; Shaw, K. J.; Miller, G. H.; Hare, R.; Shimer, G. Antibiotic Susceptibility Profiles of Escherichia Coli Strains Lacking Multidrug Efflux Pump Genes. *Antimicrob Agents Chemother* **2001**, 45 (4), 1126–1136. <https://doi.org/10.1128/AAC.45.4.1126-1136.2001>.
- (8) Lien, E. J.; Hansch, C.; Anderson, S. M. Structure-Activity Correlations for Antibacterial Agents on Gram-Positive and Gram-Negative Cells. *J Med Chem* **1968**, 11 (3), 430–441. https://doi.org/10.1021/JM00309A004/ASSET/JM00309A004.FP.PNG_V03.

2. Chapter

- (9) Ropponen, H. K.; Richter, R.; Hirsch, A. K. H.; Lehr, C. M. Mastering the Gram-Negative Bacterial Barrier – Chemical Approaches to Increase Bacterial Bioavailability of Antibiotics. *Adv Drug Deliv Rev* **2021**, *172*, 339–360. <https://doi.org/10.1016/j.addr.2021.02.014>.
- (10) Richter, M. F.; Drown, B. S.; Riley, A. P.; Garcia, A.; Shirai, T.; Svec, R. L.; Hergenrother, P. J. Predictive Compound Accumulation Rules Yield a Broad-Spectrum Antibiotic. *Nature* **2017** *545*:7654 **2017**, *545* (7654), 299–304. <https://doi.org/10.1038/nature22308>.
- (11) Richter, M. F.; Hergenrother, P. J. The Challenge of Converting Gram-Positive-Only Compounds into Broad-Spectrum Antibiotics. *Ann N Y Acad Sci* **2019**, *1435* (1), 18–38. <https://doi.org/10.1111/nyas.13598>.
- (12) Smith, P. A.; Koehler, M. F. T.; Girgis, H. S.; Yan, D.; Chen, Y.; Chen, Y.; Crawford, J. J.; Durk, M. R.; Higuchi, R. I.; Kang, J.; Murray, J.; Paraselli, P.; Park, S.; Phung, W.; Quinn, J. G.; Roberts, T. C.; Rougé, L.; Schwarz, J. B.; Skippington, E.; Wai, J.; Xu, M.; Yu, Z.; Zhang, H.; Tan, M.-W.; Heise, C. E. Optimized Arylomycins Are a New Class of Gram-Negative Antibiotics. *Nature* **2018**, *561* (7722), 189–194. <https://doi.org/10.1038/s41586-018-0483-6>.
- (13) Hu, Y.; Shi, H.; Zhou, M.; Ren, Q.; Zhu, W.; Zhang, W.; Zhang, Z.; Zhou, C.; Liu, Y.; Ding, X.; Shen, H. C.; Yan, S. F.; Dey, F.; Wu, W.; Zhai, G.; Zhou, Z.; Xu, Z.; Ji, Y.; Lv, H.; Jiang, T.; Wang, W.; Xu, Y.; Vercruyse, M.; Yao, X.; Mao, Y.; Yu, X.; Bradley, K.; Tan, X. Discovery of Pyrido[2,3- b]Indole Derivatives with Gram-Negative Activity Targeting Both DNA Gyrase and Topoisomerase IV. *J Med Chem* **2020**, *63* (17), 9623–9649. <https://doi.org/10.1021/acs.jmedchem.0c00768>.
- (14) Liu, B.; Trout, R. E. L.; Chu, G. H.; MCGarry, D.; Jackson, R. W.; Hamrick, J. C.; Daigle, D. M.; Cusick, S. M.; Pozzi, C.; De Luca, F.; Benvenuti, M.; Mangani, S.; Docquier, J. D.; Weiss, W. J.; Pevear, D. C.; Xerri, L.; Burns, C. J. Discovery of Taniborbactam (VNRX-5133): A Broad-Spectrum Serine- And Metallo-β-Lactamase Inhibitor for Carbapenem-Resistant Bacterial Infections. *J Med Chem* **2020**, *63* (6), 2789–2801. <https://doi.org/10.1021/acs.jmedchem.9b01518>.
- (15) Schumacher, C. E.; Rausch, M.; Greven, T.; Neudörfel, J. M.; Schneider, T.; Schmalz, H. G. Total Synthesis and Antibiotic Properties of Amino-Functionalized Aromatic Terpenoids Related to Erogorgiaene and the Pseudopteropsins. *Eur J Org Chem* **2022**, *2022* (26). <https://doi.org/10.1002/ejoc.202200058>.
- (16) Parker, E. N.; Cain, B. N.; Hajian, B.; Ulrich, R. J.; Geddes, E. J.; Barkho, S.; Lee, H. Y.; Williams, J. D.; Raynor, M.; Caridha, D.; Zaino, A.; Shekhar, M.; Muñoz, K. A.; Rzasca, K. M.; Temple, E. R.; Hunt, D.; Jin, X.; Vuong, C.; Pannone, K.; Kelly, A. M.; Mulligan, M. P.; Lee, K. K.; Lau, G. W.; Hung, D. T.; Hergenrother, P. J. An Iterative Approach Guides Discovery of the FabI Inhibitor Fabimycin, a Late-Stage Antibiotic Candidate with In Vivo Efficacy against Drug-Resistant Gram-Negative Infections. *ACS Cent Sci* **2022**, *8* (8), 1145–1158. <https://doi.org/10.1021/acscentsci.2c00598>.
- (17) Motika, S. E.; Ulrich, R. J.; Geddes, E. J.; Lee, H. Y.; Lau, G. W.; Hergenrother, P. J. Gram-Negative Antibiotic Active through Inhibition of an Essential Riboswitch. *J Am Chem Soc* **2020**, *142* (24), 10856–10862. <https://doi.org/10.1021/jacs.0c04427>.
- (18) Fortney, K. R.; Smith, S. N.; van Rensburg, J. J.; Brothwell, J. A.; Gardner, J. J.; Katz, B. P.; Ahsan, N.; Duerfeldt, A. S.; Mobley, H. L. T.; Spinola, S. M. CpxA Phosphatase Inhibitor Activates CpxRA and Is a Potential Treatment for Uropathogenic Escherichia Coli in a Murine Model of Infection. *Microbiol Spectr* **2022**, *10* (2). <https://doi.org/10.1128/spectrum.02430-21>.
- (19) Perlmutter, S. J.; Geddes, E. J.; Drown, B. S.; Motika, S. E.; Lee, M. R.; Hergenrother, P. J. Compound Uptake into *E. Coli* Can Be Facilitated by *N*-Alkyl Guanidiniums and Pyridiniums. *ACS Infect Dis* **2021**, *7* (1), 162–173. <https://doi.org/10.1021/acsinfecdis.0c00715>.
- (20) Masci, D.; Hind, C.; Islam, M. K.; Toscani, A.; Clifford, M.; Coluccia, A.; Conforti, I.; Touitou, M.; Memdouh, S.; Wei, X.; La Regina, G.; Silvestri, R.; Sutton, J. M.; Castagnolo, D. Switching on the Activity of 1,5-Diaryl-Pyrrole Derivatives against Drug-Resistant ESKAPE Bacteria: Structure-Activity Relationships and Mode of Action Studies. *Eur J Med Chem* **2019**, *178*, 500–514. <https://doi.org/10.1016/j.ejmech.2019.05.087>.
- (21) Stoorza, A. M.; Duerfeldt, A. S. Guiding the Way: Traditional Medicinal Chemistry Inspiration for Rational Gram-Negative Drug Design. *J Med Chem* **2024**, *67* (1), 65–80. <https://doi.org/10.1021/acs.jmedchem.3c01831>.
- (22) Zgurskaya, H. I.; López, C. A.; Gnanakaran, S. Permeability Barrier of Gram-Negative Cell Envelopes and Approaches to Bypass It. *ACS Infect Dis* **2016**, *1* (11), 512–522. <https://doi.org/10.1021/acsinfecdis.5b00097>.
- (23) Sohlenkamp, C.; Geiger, O. Bacterial Membrane Lipids: Diversity in Structures and Pathways. *FEMS Microbiol Rev* **2016**, *40* (1), 133–159. <https://doi.org/10.1093/femsre/fuv008>.
- (24) Andrews, L. D.; Kane, T. R.; Dozzo, P.; Haglund, C. M.; Hilderbrandt, D. J.; Linsell, M. S.; Machajewski, T.; McEnroe, G.; Serio, A. W.; Wlasichuk, K. B.; Neau, D. B.; Pakhomova, S.; Waldrop, G. L.; Sharp, M.; Pogliano, J.; Cirz, R. T.; Cohen, F. Optimization and Mechanistic Characterization of Pyridopyrimidine Inhibitors of Bacterial Biotin Carboxylase. *J Med Chem* **2019**, *62* (16), 7489–7505. <https://doi.org/10.1021/acs.jmedchem.9b00625>.
- (25) Hu, Z.; Leus, I. V.; Chandar, B.; Sherborne, B. S.; Avila, Q. P.; Rybenkov, V. V.; Zgurskaya, H. I.; Duerfeldt, A. S. Structure-Uptake Relationship Studies of Oxazolidinones in Gram-Negative ESKAPE Pathogens. *J Med Chem* **2022**, *65* (20), 14144–14179. <https://doi.org/10.1021/acs.jmedchem.2c01349>.

- (26) Ropponen, H.; Diamanti, E.; Johannsen, S.; Illarionov, B.; Hamid, R.; Jaki, M.; Sass, P.; Fischer, M. Exploring the Translational Gap of a Novel Class of Escherichia Coli IspE Inhibitors. *ChemMedChem* **2023**, e202300346 (18). <https://doi.org/10.1002/cmdc.202300346>.
- (27) Ropponen, H. K.; Diamanti, E.; Siemens, A.; Illarionov, B.; Hauptenthal, J.; Fischer, M.; Rottmann, M.; Witschel, M.; Hirsch, A. K. H. Assessment of the Rules Related to Gaining Activity against Gram-Negative Bacteria. *RSC Med Chem* **2021**, 12 (4), 593–601. <https://doi.org/10.1039/d0md00409j>.
- (28) Gaspar, A.; Reis, J.; Matos, M. J.; Uriarte, E.; Borges, F. In Search for New Chemical Entities as Adenosine Receptor Ligands: Development of Agents Based on Benzo- γ -Pyrone Skeleton. *Eur J Med Chem* **2012**, 54, 914–918. <https://doi.org/10.1016/j.ejmech.2012.05.033>.
- (29) Santos, C. M. M.; Silva, V. L. M.; Silva, A. M. S. Synthesis of Chromone-Related Pyrazole Compounds. *Molecules* **2017**, 22 (10). <https://doi.org/10.3390/molecules22101665>.
- (30) Rodríguez-Soacha, D. A.; Fender, J.; Ramírez, Y. A.; Collado, J. A.; Muñoz, E.; Maitra, R.; Sotriffer, C.; Lorenz, K.; Decker, M. “Photo-Rimonabant”: Synthesis and Biological Evaluation of Novel Photoswitchable Molecules Derived from Rimonabant Lead to a Highly Selective and Nanomolar “Cis-On” CB₁R Antagonist. *ACS Chem Neurosci* **2021**, 12 (9), 1632–1647. <https://doi.org/10.1021/acscchemneuro.1c00086>.
- (31) Hermann, T.; Hochegger, P.; Dolensky, J.; Seebacher, W.; Pferschy-Wenzig, E.-M.; Saf, R.; Kaiser, M.; Mäser, P.; Weis, R. Synthesis and Structure-Activity Relationships of New 2-Phenoxybenzamides with Antiplasmodial Activity. *Pharmaceuticals* **2021**, 14 (11), 1109. <https://doi.org/10.3390/ph14111109>.
- (32) Chen, D.; Sun, X.; Shan, Y.; You, J. One-Pot Synthesis of Polyfunctionalized Quinolines via a Copper-Catalyzed Tandem Cyclization. *Org Biomol Chem* **2018**, 16 (41), 7657–7662. <https://doi.org/10.1039/C8OB02078G>.
- (33) Svenningsen, S. W.; Frederiksen, R. F.; Counil, C.; Ficker, M.; Leisner, J. J.; Christensen, J. B. Synthesis and Antimicrobial Properties of a Ciprofloxacin and PAMAM-Dendrimer Conjugate. *Molecules* **2020**, 25 (6). <https://doi.org/10.3390/molecules25061389>.
- (34) Dardonville, C.; Caine, B. A.; Navarro De La Fuente, M.; Martín Herranz, G.; Corrales Mariblanca, B.; Popelier, P. L. A. Substituent Effects on the Basicity (pK_a) of Aryl Guanidines and 2-(Arylimino)imidazolidines: Correlations of PH-Metric and UV-Metric Values with Predictions from Gas-Phase Ab Initio Bond Lengths. *New J Chem* **2017**, 41 (19), 11016–11028. <https://doi.org/10.1039/c7nj02497e>.
- (35) Ueno, H.; Yokota, K.; Hoshi, J. I.; Yasue, K.; Hayashi, M.; Hase, Y.; Uchida, I.; Aisaka, K.; Katoh, S.; Cho, H. Synthesis and Structure-Activity Relationships of Novel Selective Factor Xa Inhibitors with a Tetrahydroisoquinoline Ring. *J Med Chem* **2005**, 48 (10), 3586–3604. <https://doi.org/10.1021/jm058160e>.
- (36) Aoyagi, N.; Endo, T. Synthesis of Five- and Six-Membered Cyclic Guanidines by Guanylation with Isothiouonium Iodides and Amines under Mild Conditions. *Synth Commun* **2017**, 47 (5), 442–448. <https://doi.org/10.1080/00397911.2016.1269927>.
- (37) Dalberto, P. F.; de Souza, E. V.; Abbadi, B. L.; Neves, C. E.; Rambo, R. S.; Ramos, A. S.; Macchi, F. S.; Machado, P.; Bizarro, C. V.; Basso, L. A. Handling the Hurdles on the Way to Anti-Tuberculosis Drug Development. *Front Chem* **2020**, 8 (586294). <https://doi.org/10.3389/fchem.2020.586294>.
- (38) Batt, S. M.; Minnikin, D. E.; Besra, G. S. The Thick Waxy Coat of Mycobacteria, a Protective Layer against Antibiotics and the Host’s Immune System. *Biochem J* **2020**, 477 (10), 1983–2006. <https://doi.org/10.1042/BCJ20200194>.

Supporting Information

A Positive Charge in an Antimalarial Compound Unlocks Broad-spectrum Antibacterial Activity

Maria Braun-Cornejo,^{1,2,3} Mitchell Platteschorre,¹ Vincent de Vries,¹ Patricia Bravo,^{4,5} Vidhisha Sonawane,⁶ Mostafa M. Hamed,³ Jörg Haupenthal,³ Norbert Reiling,^{6,7} Matthias Rottmann,⁴ Dennis Piet,¹ Peter Maas,¹ Eleonora Diamanti,³ and Anna K. Hirsch.^{2,3*}

¹ Specs Research Laboratory, Specs Compound Handling, B.V., Bleiswijkseweg 55, 2712 PB Zoetermeer, The Netherlands.

² Department of Pharmacy, Saarland University, Campus Building E8.1, 66123 Saarbrücken, Germany.

³ Helmholtz Institute for Pharmaceutical Research Saarland (HIPS) – Helmholtz Centre for Infection Research (HZI), Campus Building E8.1, 66123 Saarbrücken, Germany.

⁴ Swiss Tropical and Public Health Institute Kreuzstrasse 2, 4123 Allschwil, Switzerland.

⁵ Universität Basel, Petersplatz 1, 4003 Basel, Switzerland.

⁶ Microbial Interface Biology, Research Center Borstel, Leibniz Lung Center, 23845 Borstel, Germany.

⁷ German Center for Infection Research (DZIF), Partner Site Hamburg-Lübeck-Borstel-Riems, 23845 Borstel, Germany.

*Corresponding author: Anna.Hirsch@helmholtz-hips.de

Table of Contents

Supplementary Methods.....	32
General information	32
Chemicals	32
General procedure for Synthesis	32
Characterisation of products	33
Final Products 1–14	33
Intermediates 16–62	47
<i>P. falciparum</i> culturing and <i>in vitro</i> drug sensitivity assay on asexual blood stage parasites	55
Determination of <i>in vitro</i> antibacterial activity	55
Determination of <i>in vitro</i> anti-tubercular activity and solubility in 7H9 medium	55
Cytotoxicity assay	55
Measurement of <i>in vitro</i> cytotoxicity by XTT assay.....	56
Supplementary Tables and Figures	56
Computational evaluation of pKa	56
Biological evaluation of compounds.....	57
Supplementary References	59

Supplementary Methods

General information

All reactions were conducted under nitrogen atmosphere using oven-dried glassware. The reaction progress was monitored on thin layer chromatography (TLC) on silica gel-coated aluminum (silica gel F254, SiliCycle). Purification of the final products, when necessary, was performed by flash column chromatography using silica gel (Screening Devices 60-200 μm) or by preparative HPLC (Dionex UltiMate 3000 UHPLC+ focused, Thermo Scientific) on a reversed-phase column (C18 column, 5 μM , Macherey-Nagel, Germany). The solvents used for the chromatography were water (0.1% formic acid) and MeCN (0.1% formic acid). High-resolution mass (HRMS) of final products was determined by HPLC-MS/MS using a Thermo Scientific Q Exactive Focus Orbitrap LC-MS/MS system. All compounds were analysed for purity by LCMS on Acquity UPLC-SQD system from Waters with a gradient elution of Water (Formic acid 0.1%)/Acetonitrile on an HSS-T3 column (2.1 x 50 mm, Waters), 1.8 μm , at 30 $^{\circ}\text{C}$, PDA detection between 240-320 nm, and MS detection by simultaneous ES+/ES- ionization in a mass range of 150-800. The flow was set to 0.9 ml/min, and the gradient time is 1.5 min. NMR spectra were recorded on an Agilent 400 MHz or a Bruker Avance Neo 500 MHz. Chemical shifts (δ) are reported in ppm relative to residual solvent signals. The following abbreviations are used to describe peak patterns when appropriate: s (singlet), d (doublet), t (triplet), q (quartet), quint (quintet), sex (sextet), sept (septuplet), m (multiplet), br (broad). Coupling constants (J) are reported in Hertz (Hz). Reactions were monitored with thin layer chromatography (TLC) on silica gel-coated aluminum (silica gel F254, SiliCycle).

Chemicals

All reagents and solvents were purchased from Sigma-Aldrich, Specs, Fluorochem, or Acros Organics, were reagent grade, and used without purification unless indicated otherwise. Reagents and substrates were purchased from commercial sources and used as received. Solvents not required to be dry were purchased as technical grade and used as received. Dry solvents were purchased from commercial sources in Sure/SealTM bottles and used as received and stored under a dry inert gas (N_2 or Ar). All new compounds were fully characterised by ^1H and ^{13}C NMR and HRMS techniques. The purity of the final products was determined by HPLC-MS and found to be >95%.

General procedure for Synthesis

General procedure for pyrazole formation (GP-1)

The synthesis of the pyrazoles was prepared following a similar procedure reported in the literature.¹ The respective chromene amide (1 eq.) was suspended in EtOH (0.1 M), and hydrazine hydrate (8 eq.) was added dropwise. The reaction mixture was heated to reflux, after the reaction was completed the mixture was allowed to cool to room temperature (r.t.). The solvent was removed under reduced pressure to obtain the pure product, without purification unless stated otherwise, in excellent yields (>95%).

General procedure for Boc deprotection (GP-2)

The *N*-Boc deprotections were completed following a similar procedure reported in the literature.² The respective *N*-Boc protected product (1 eq.) was dissolved in a mixture of trifluoroacetic acid (TFA) and dichloromethane (DCM) (1:4, 0.1 M) and cooled to 0 $^{\circ}\text{C}$ in an ice-water bath. The reaction mixture stirred while allowing to reach r.t. After the reaction was completed, the solvents were removed under reduced pressure to obtain the pure products as TFA salts in excellent yields (>95%).

General procedure for guanidinylation (GP-3)

The guanidinylation of amines were completed following similar procedures reported in the literature.³⁻⁵ The respective amine TFA salt (1 eq.) was stirred in DMF (0.1 M), DIPEA (1.5-8.1 eq) and the respective guanidinylation agent (1.4-3.0 eq.) was added. The reaction mixture was heated to 50 $^{\circ}\text{C}$ and after completion allowed to cool to r.t. The excess solvent was removed under reduced pressure and ice-cold water (5-20 mL) was added to the mixture. The resulting precipitate was filtered to obtain the pure product as TFA salt, without purification unless stated otherwise, in good to excellent yields (46%-quantitative).

General procedure for amide coupling (GP-4)

The synthesis of the chromene amides was prepared following a similar procedure reported in the literature.⁶

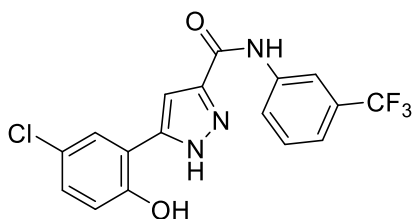
6-Chloro-4-oxo-4*H*-chromene-2-carboxylic acid **15** (1.05 eq.) was suspended in DMF (0.1 M) and DIPEA was added (1.2 eq.). The mixture was cooled to 0 $^{\circ}\text{C}$ in an ice-water bath, and 2-(3*H*-[1,2,3]triazolo[4,5-*b*]pyridin-3-yl)-1,1,3,3-tetramethylisouronium (HATU, 1.2 eq.) was added. The yellow solution stirred for 30 min and the corresponding aniline (1 eq.) was added. The reaction mixture stirred while allowing to reach

r.t. After the reaction was completed, the mixture was added to water (25–100 mL), and the resulting precipitate was filtered and washed with solvent. When necessary, the crude was purified by flash column chromatography. The respective chromene amides were obtained in low to excellent yields (27–95%).

Characterisation of products

Final Products 1–14

5-(5-Chloro-2-hydroxyphenyl)-*N*-(3-(trifluoromethyl)phenyl)-1*H*-pyrazole-3-carboxamide (**1a**):



Compound **1a** was prepared following GP-1, chromene amide **34** (76 mg, 0.21 mmol) was reacted with hydrazine hydrate (83 mg, 1.7 mmol) and the reaction mixture stirred for 1.5 h at reflux. The solvent was removed under reduced pressure to obtain **1a** as white solid in quantitative yield (80 mg, 0.21 mmol).

^1H NMR (400 MHz, DMSO- d_6) δ = 10.50 (br s, 1H), 8.30 (br s, 1H), 8.11 (br d, J = 7.8 Hz, 1H), 7.81 (d, J = 2.0 Hz, 1H), 7.59 (br t, J = 7.8 Hz, 1H), 7.44 (br d, J = 7.8 Hz, 1H), 7.41 (br s, 1H), 7.25 (br dd, J = 8.6,

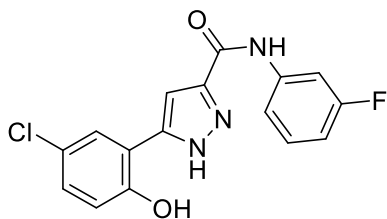
2.0 Hz, 1H), 7.02 (br d, J = 8.6 Hz, 1H) ppm.

^{13}C NMR (101 MHz, DMSO- d_6) δ = 160.9, 153.2, 146.8, 139.7, 129.8, 129.5, 129.2, 128.2, 126.6, 125.5, 123.7, 122.9, 119.6, 118.1, 117.1, 116.3, 106.2 ppm.

^{19}F NMR (470 MHz, DMSO- d_6) δ = -61.25 ppm.

HRMS (ESI $^+$): m/z calcd. for $\text{C}_{17}\text{H}_{12}\text{ClF}_3\text{N}_3\text{O}_2^+$ ($[\text{M}+\text{H}]^+$) 382.0565, measured 382.0553.

5-(5-Chloro-2-hydroxyphenyl)-*N*-(3-fluorophenyl)-1*H*-pyrazole-3-carboxamide (**1b**):



Compound **1b** was prepared following GP-1, chromene amide **35** (335 mg, 1.05 mmol) was reacted with hydrazine hydrate (588 mg, 8.5 mmol) and the reaction mixture stirred for 2 h at reflux. The solvent was removed under reduced pressure to obtain **1b** as off-white solid (345 mg, 1.04 mmol, 99%).

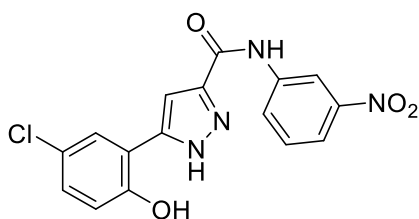
^1H NMR (500 MHz, DMSO- d_6) δ = 10.36 (br s, 1H), 7.81 (d, J = 2.4 Hz, 1H), 7.79 (s, 1H), 7.64 (br d, J = 7.8 Hz, 1H), 7.41 (br s, 1H), 7.38 (q, J = 7.8 Hz, 1H), 7.25 (dd, J = 8.7, 2.4 Hz, 1H), 7.01 (d, J = 8.7 Hz, 1H), 6.92 (br t, J = 7.8 Hz, 1H) ppm.

^{13}C NMR (101 MHz, DMSO- d_6) δ = 163.2, 160.8, 153.3, 140.6, 140.5, 130.2, 130.1, 128.9, 126.5, 122.9, 118.1, 115.9, 109.9, 107.0, 106.8, 106.0 ppm.

^{19}F NMR (470 MHz, DMSO- d_6) δ = -112.27 ppm.

HRMS (ESI $^+$): m/z calcd. for $\text{C}_{16}\text{H}_{12}\text{ClFN}_3\text{O}_2^+$ ($[\text{M}+\text{H}]^+$) 332.0597, measured 332.0580.

5-(5-Chloro-2-hydroxyphenyl)-*N*-(3-nitrophenyl)-1*H*-pyrazole-3-carboxamide (**1c**):



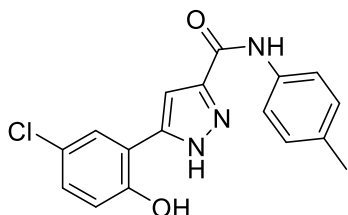
Compound **1c** was prepared following GP-1, chromene amide **36** (74 mg, 0.21 mmol) was reacted with hydrazine hydrate (86 mg, 1.72 mmol). The reaction mixture stirred for 1.5 h at reflux. The solvent was removed under reduced pressure obtaining **1c** as yellow powder (76 mg, 0.21 mmol, 99%).

^1H NMR (400 MHz, DMSO- d_6) δ = 10.64 (br s, 1H), 8.88 (br s, 1H), 8.25 (br s, 1H), 7.93 (br s, 1H), 7.80 (br s, 1H), 7.64 (br s, 1H), 7.42 (br s, 1H), 7.22 (br s, 1H), 7.01 (br s, 1H) ppm.

^{13}C NMR (101 MHz, DMSO- d_6) δ = 160.3, 153.7, 147.9, 144.2, 142.4, 140.1, 130.0, 128.7, 126.4, 126.2, 122.6, 118.13, 118.06, 117.9, 114.3, 105.8 ppm.

HRMS (ESI $^+$): m/z calcd. for $\text{C}_{16}\text{H}_{12}\text{ClN}_4\text{O}_4^+$ ($[\text{M}+\text{H}]^+$) 359.0542, measured 359.0532.

5-(5-Chloro-2-hydroxyphenyl)-*N*-(*p*-tolyl)-1*H*-pyrazole-3-carboxamide (**1d**):



Compound **1d** was prepared following GP-1 with adaptations, chromene amide **37** (218 mg, 0.70 mmol) was reacted with hydrazine hydrate (278 mg, 3.48 mmol), and the reaction mixture stirred for 1 h at reflux. A precipitate appeared, which was filtered and washed with ice-cold water (1.5 mL) to obtain **1d** as white powder (203 mg, 0.62 mmol, 89%).

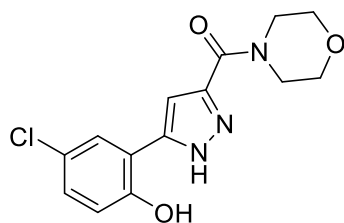
2. Chapter

^1H NMR (400 MHz, DMSO- d_6) δ = 10.05 (br s, 1H), 7.80 (d, J = 2.3 Hz, 1H), 7.69 (br d, J = 8.2 Hz, 2H), 7.44 (br s, 1H), 7.24 (dd, J = 8.6, 2.3 Hz, 1H), 7.15 (br d, J = 8.2 Hz, 2H), 7.01 (d, J = 8.6 Hz, 1H), 2.28 (s, 3H) ppm.

^{13}C NMR (101 MHz, DMSO- d_6) δ = 153.8, 136.6, 133.0, 129.5, 129.2, 126.9, 123.4, 123.3, 120.7, 118.5, 106.1, 20.9 ppm. Quaternary carbon peaks missing.

HRMS (ESI $^+$): m/z calcd. for $\text{C}_{17}\text{H}_{15}\text{ClN}_3\text{O}_2^+$ ($[M+H]^+$) 328.0847, measured 328.0830.

(5-(5-Chloro-2-hydroxyphenyl)-1H-pyrazol-3-yl)(morpholino)methanone (**1e**):



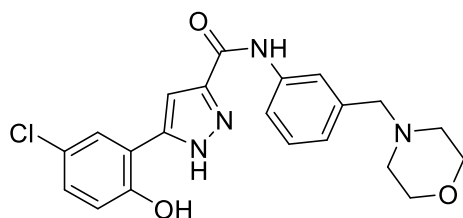
Compound **1e** was prepared following GP-1 with adaptations, chromene amide **38** (64 mg, 0.22 mmol) was reacted with hydrazine hydrate (95 mg, 1.9 mmol), and the reaction mixture stirred for 2 h at reflux. A precipitate appeared, which was filtered and washed with ice-cold water (1 mL) to obtain **1e** as white powder (65 mg, 0.21 mmol, 97%).

^1H NMR (400 MHz, DMSO- d_6) δ = 7.78 (s, 1H), 7.22 (br d, J = 8.6 Hz, 1H), 7.14 (s, 1H), 6.98 (d, J = 8.6 Hz, 1H), 3.92 (br s, 4H), 3.34 (br s, 4H) ppm.

^{13}C NMR (151 MHz, DMSO- d_6) δ = 161.4, 153.3, 146.1, 139.4, 128.8, 126.5, 122.9, 118.0, 117.8, 106.6, 66.4, 66.2, 47.1, 42.3 ppm.

HRMS (ESI $^+$): m/z calcd. for $\text{C}_{14}\text{H}_{15}\text{ClN}_3\text{O}_3^+$ ($[M+H]^+$) 308.0796, measured 308.0776.

5-(5-Chloro-2-hydroxyphenyl)-N-(3-(morpholinomethyl)phenyl)-1H-pyrazole-3-carboxamide (**2**):



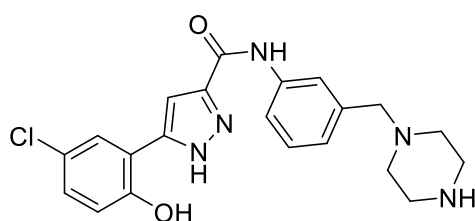
Compound **2** was prepared following GP-1, chromene amide **39** (277 mg, 0.69 mmol) was reacted with hydrazine hydrate (275 mg, 5.5 mmol) and the reaction mixture stirred at reflux overnight. The solvent was removed under reduced pressure to obtain **2** as light pink solid in quantitative yield (284 mg, 0.69 mmol).

^1H NMR (400 MHz, DMSO- d_6) δ = 10.22 (br s, 1H), 7.79 (br s, 1H), 7.76 (br s, 1H), 7.70 (d, J = 7.6 Hz, 1H), 7.44 (br s, 1H), 7.25 (t, J = 7.6 Hz, 1H), 7.18 (br d, J = 8.2 Hz, 1H), 7.10 (br d, J = 8.2 Hz, 1H), 6.99 (d, J = 7.6 Hz, 1H), 3.54 (br s, 4H), 3.42 (br s, 2H), 2.34 (br s, 4H) ppm.

^{13}C NMR (101 MHz, DMSO- d_6): δ = 161.5, 154.0, 139.1, 138.6, 129.0, 128.8, 126.8, 124.7, 123.2, 121.2, 119.4, 118.6, 106.5, 66.6, 62.9, 53.6 ppm. Quaternary carbon peaks missing.

HRMS (ESI $^+$): m/z calcd. for $\text{C}_{21}\text{H}_{22}\text{ClN}_4\text{O}_3^+$ ($[M+H]^+$) 413.1375, measured 413.1359.

5-(5-Chloro-2-hydroxyphenyl)-N-(3-(piperazin-1-ylmethyl)phenyl)-1H-pyrazole-3-carboxamide (**3A**):



Compound **3A** was prepared following GP-2, *N*-Boc amine **3B** (214 mg, 0.42 mmol) was reacted with TFA (6.3 mmol) and the reaction mixture stirred for 2 h. Compound **3A** was obtained as white powder in form of a TFA salt (257 mg, 0.40 mmol, 96%).

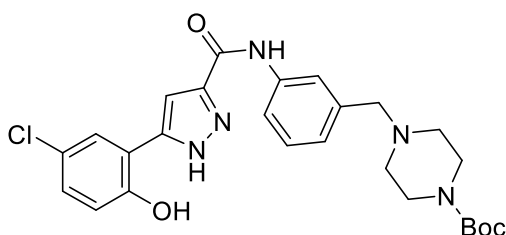
^1H NMR (400 MHz, DMSO- d_6) δ = 10.64 (br s, 1H), 10.26 (s, 1H), 8.95 (br s, 1H), 7.98 (br s, 1H), 7.81 (d, J = 2.3 Hz, 1H), 7.78 (s, 1H), 7.43 (br s, 1H), 7.37-7.42 (m, 1H), 7.25 (dd, J = 9.0, 2.3 Hz,

1H), 7.18 (br d, J = 7.0 Hz, 1H), 7.03 (d, J = 9.0 Hz, 1H), 4.10 (br s, 2H), 3.28 (br s, 4H), 3.09 (br s, 4H) ppm.

^{13}C NMR (101 MHz, DMSO- d_6) δ = 159.0, 153.3, 139.1, 132.5, 131.1, 129.1, 128.9, 126.5, 125.8, 123.0, 122.3, 120.8, 118.1, 105.9, 60.0, 48.2, 41.4 ppm. Quaternary carbon peaks missing.

HRMS (ESI $^+$): m/z calcd. for $\text{C}_{21}\text{H}_{23}\text{ClN}_5\text{O}_2^+$ ($[M+H]^+$) 412.1535, measured 412.1529.

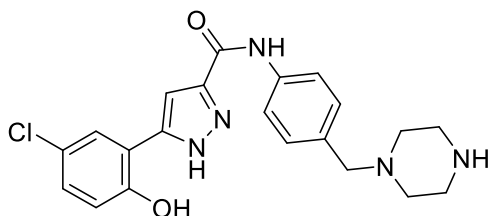
tert-Butyl 4-(3-(5-(5-chloro-2-hydroxyphenyl)-1H-pyrazole-3-carboxamido)benzyl)piperazine-1-carboxylate (**3B**):



Compound **3B** was prepared following GP-1, chromene amide **40** (114 mg, 0.23 mmol) was reacted with hydrazine hydrate (92 mg, 1.83 mmol). The reaction mixture stirred for 15 min at reflux. The solvent was removed under reduced pressure to obtain **3B** as off-white powder in quantitative yield (125 mg, 0.23 mmol).

^1H NMR (400 MHz, DMSO- d_6) δ = 10.10 (br s, 1H), 7.70-7.81 (m, 3H), 7.42 (s, 1H), 7.29 (t, J = 7.8 Hz, 1H), 7.21 (br d, J = 7.8 Hz, 1H), 6.96-7.06 (m, 2H), 3.47 (s, 2H), 3.31 (br s, 4H), 2.32 (br s, 4H), 1.38 (br s, 9H) ppm.
 ^{13}C NMR (101 MHz, DMSO- d_6) δ = 159.5, 154.0, 153.9, 143.9, 143.3, 138.7, 138.4, 128.6, 128.4, 126.3, 124.2, 122.5, 120.6, 119.0, 118.5, 118.2, 105.2, 78.8, 62.1, 52.4, 28.1 ppm.
 HRMS (ESI $^+$): m/z calcd. for $\text{C}_{26}\text{H}_{31}\text{ClN}_5\text{O}_4^+$ ($[\text{M}+\text{H}]^+$) 512.2059, measured 512.2050.

5-(5-Chloro-2-hydroxyphenyl)-*N*-(4-(piperazin-1-ylmethyl)phenyl)-1*H*-pyrazole-3-carboxamide (**4A**):



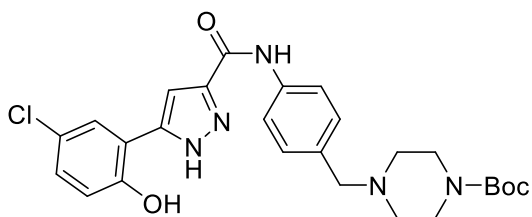
Compound **4A** was prepared following GP-2, *N*-Boc amine **4B** (153 mg, 0.30 mmol) was reacted with TFA (4.8 mmol) and the reaction mixture stirred for 1 h. Compound **4A** was obtained as beige powder in form of a TFA salt in quantitative yield (194 mg, 0.30 mmol).

^1H NMR (400 MHz, DMSO- d_6) δ = 10.72 (br s, 1H), 10.31 (br s, 1H), 9.19 (br s, 1H), 7.89 (d, J = 8.2 Hz, 2H), 7.81 (d, J = 2.4 Hz, 1H), 7.47 (br s, 1H), 7.44 (br d, J = 8.2 Hz, 2H), 7.24 (dd, J = 8.8, 2.4 Hz, 1H), 7.03 (d, J = 8.8 Hz, 1H), 4.12 (br s, 2H), 3.32 (br s, 4H), 3.13 (br s, 4H) ppm.

^{13}C NMR (101 MHz, DMSO- d_6) δ = 159.5, 153.8, 139.9, 131.6, 129.3, 126.9, 123.3, 123.3, 120.6, 118.5, 106.4, 59.7, 48.3, 41.5 ppm. Quaternary carbon peaks missing.

HRMS (ESI $^+$): m/z calcd. for $\text{C}_{21}\text{H}_{23}\text{ClN}_5\text{O}_2^+$ ($[\text{M}+\text{H}]^+$) 412.1535, measured 412.1509.

tert-Butyl 4-(4-(5-(5-chloro-2-hydroxyphenyl)-1*H*-pyrazole-3-carboxamido)benzyl)piperazine-1-carboxylate (**4B**):



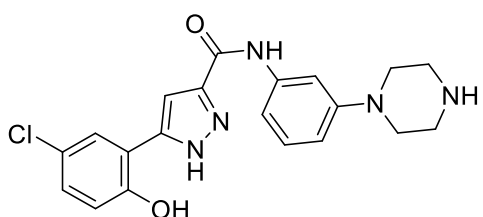
Compound **4B** was prepared following GP-1, chromene amide **41** (178 mg, 0.36 mmol) was reacted with hydrazine hydrate (143 mg, 2.86 mmol). The solvent was removed under reduced pressure to obtain **4B** as off-white powder in quantitative yield (183 mg, 0.36 mmol).

^1H NMR (400 MHz, DMSO- d_6) δ = 10.13 (br s, 1H), 7.80 (d, J = 2.0 Hz, 1H), 7.76 (d, J = 7.8 Hz, 2H), 7.34-7.59 (m, 1H), 7.26 (d, J = 7.8 Hz, 2H), 7.21-7.25 (m, 1H), 7.01 (br d, J = 8.6 Hz, 1H), 3.44 (br s, 2H), 3.31 (br s, 4H), 2.30 (br s, 4H), 1.38 (s, 9H) ppm.

^{13}C NMR (101 MHz, DMSO- d_6) δ = 154.3, 153.8, 138.0, 133.4, 129.6, 129.2, 126.9, 123.4, 120.5, 118.5, 106.1, 79.2, 62.0, 52.7, 28.5 ppm.

HRMS (ESI $^+$): m/z calcd. for $\text{C}_{26}\text{H}_{31}\text{ClN}_5\text{O}_4^+$ ($[\text{M}+\text{H}]^+$) 512.2059, measured 512.2051.

5-(5-Chloro-2-hydroxyphenyl)-*N*-(3-(piperazin-1-yl)phenyl)-1*H*-pyrazole-3-carboxamide (**5A**):



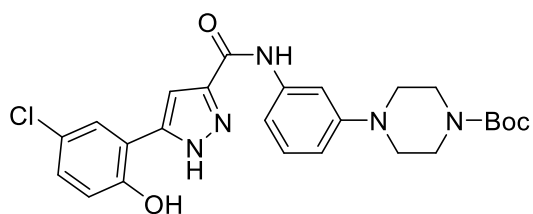
Compound **5A** was prepared following GP-2, *N*-Boc amine **5B** (254 mg, 0.51 mmol) was reacted with TFA (8.1 mmol) and the reaction mixture stirred for 24 h. Compound **5A** was obtained as white powder in form of a TFA salt in quantitative yield (258 mg, 0.51 mmol).

^1H NMR (400 MHz, DMSO- d_6) δ = 10.68 (br s, 1H), 10.03 (br s, 1H), 9.00 (br s, 2H), 7.81 (br s, 1H), 7.51 (br s, 1H), 7.39 (br d, J = 7.8 Hz, 1H), 7.44 (br s, 1H), 7.23 (br t, J = 8.6 Hz, 2H), 7.03 (br d, J = 8.6 Hz, 1H), 6.75 (br d, J = 7.8 Hz, 1H), 3.35 (br s, 4H), 3.27 (br s, 4H) ppm.

^{13}C NMR (101 MHz, DMSO- d_6) δ = 158.6, 153.4, 150.4, 139.6, 129.2, 128.8, 126.5, 122.9, 118.1, 112.1, 111.8, 108.0, 105.8, 45.7, 42.7 ppm. Quaternary carbon peaks missing.

HRMS (ESI $^+$): m/z calcd. for $\text{C}_{20}\text{H}_{21}\text{ClN}_5\text{O}_2^+$ ($[\text{M}+\text{H}]^+$) 398.1378, measured 398.1366.

tert-Butyl 4-(3-(5-(5-chloro-2-hydroxyphenyl)-1*H*-pyrazole-3-carboxamido)phenyl)piperazine-1-carboxylate (**5B**):



Compound **5B** was prepared following GP-1, chromene amide **42** (224 mg, 0.46 mmol) was reacted with hydrazine hydrate (185 mg, 3.71 mmol). The solvent was removed under reduced pressure to obtain **5B** as off-white powder (228 mg, 0.45 mmol, 99%).

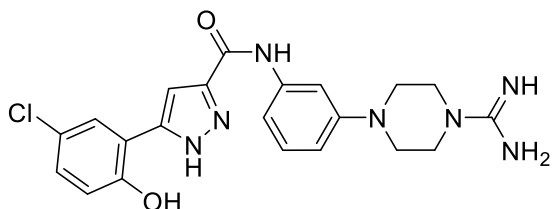
^1H NMR (400 MHz, DMSO- d_6) δ = 9.93 (br s, 1H), 7.80 (d, J = 2.0 Hz, 1H), 7.44 (br s, 1H), 7.34 (br d, J = 7.8 Hz, 1H),

7.24 (dd, J = 8.6, 2.0 Hz, 1H), 7.19 (br t, J = 7.8 Hz, 1H), 7.01 (d, J = 8.6 Hz, 1H), 6.71 (br d, J = 7.8 Hz, 1H), 3.47 (br s, 4H), 3.10 (br s, 4H), 1.42 (s, 9H) ppm. Pyrazole C–H is not a clear peak, likely very broad at 7.4 ppm due to annular tautomerism.

^{13}C NMR (101 MHz, DMSO- d_6) δ = 181.3, 153.9, 153.3, 151.2, 139.4, 129.1, 128.8, 126.5, 122.9, 122.1, 118.1, 111.6, 111.5, 107.9, 79.0, 48.4, 43.6, 28.1 ppm. Quaternary carbons missing.

HRMS (ESI $^-$): m/z calcd. for $\text{C}_{25}\text{H}_{27}\text{ClN}_5\text{O}_4^-$ ($[M-H]^-$) 496.1757, measured 496.1745.

N-(3-(4-Carbamimidoylpiperazin-1-yl)phenyl)-5-(5-chloro-2-hydroxyphenyl)-1*H*-pyrazole-3-carboxamide (**5G**):



Compound **5G** was prepared following GP-3, amine **5A** (97 mg, 0.19 mmol) was reacted with DIPEA (156 mg, 1.2 mmol) and guanidinylation agent **65** (45 mg, 0.31 mmol). The reaction mixture stirred for 24 h and **5G** was obtained as grey solid in form of a TFA salt in quantitative yield (106 mg, 0.19 mmol).

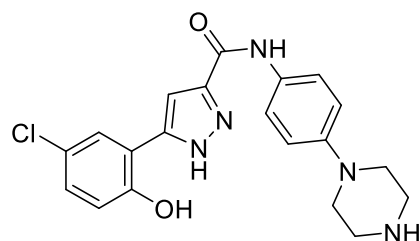
^1H NMR (400 MHz, DMSO- d_6 , 120 $^\circ\text{C}$): δ = 7.46 (br s,

1H), 7.43 (br s, 1H), 7.26 (br d, J = 7.6 Hz, 1H), 7.17 (br t, J = 7.6 Hz, 1H), 6.99 (br s, 1H), 6.89 (br s, 1H), 6.72 (br d, J = 8.2 Hz, 1H), 6.64 (br d, J = 7.4 Hz, 1H), 3.63 (br s, 4H), 3.31 (br s, 4H) ppm.

^{13}C NMR (101 MHz, DMSO- d_6 , 120 $^\circ\text{C}$): δ = 161.3, 157.1, 156.2, 150.1, 150.0, 145.5, 139.8, 128.4, 125.1, 123.5, 119.9, 119.4, 117.5, 110.3, 109.6, 106.3, 99.1, 46.9, 44.3 ppm.

HRMS (ESI $^+$): m/z calcd. for $\text{C}_{21}\text{H}_{23}\text{ClN}_7\text{O}_2^+$ ($[M+H]^+$) 440.1596, measured 440.1587.

5-(5-Chloro-2-hydroxyphenyl)-*N*-(4-(piperazin-1-yl)phenyl)-1*H*-pyrazole-3-carboxamide (**6A**):



Compound **6A** was prepared following GP-2, *N*-Boc amine **6B** (150 mg, 0.30 mmol) was reacted with TFA (9.6 mmol) and the reaction mixture stirred for 2.5 h. Compound **6A** was obtained as off-white solid in form of a TFA salt in quantitative yield (153 mg, 0.30 mmol).

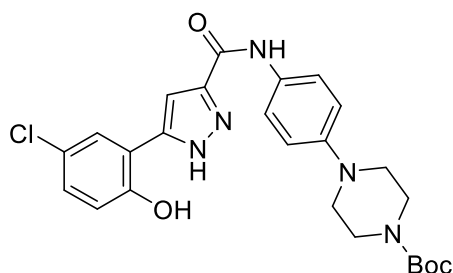
^1H NMR (400 MHz, DMSO- d_6 , 120 $^\circ\text{C}$): δ = 9.64 (br s, 1H), 7.73 (d, J = 2.2 Hz, 1H), 7.67 (d, J = 8.6 Hz, 2H), 7.37 (s, 1H), 7.21 (br dd, J = 8.8, 2.2 Hz, 1H), 7.02 (d, J = 8.8 Hz, 1H), 6.99 (d, J = 8.6 Hz, 2H), 3.38

(s, 4H), 3.27 (s, 4H) ppm.

^{13}C NMR (101 MHz, DMSO- d_6 , 120 $^\circ\text{C}$): δ = 158.1, 153.0, 145.9, 131.1, 128.1, 127.9, 126.1, 125.9, 122.7, 121.2, 121.0, 118.1, 117.8, 116.0, 115.9, 104.5, 104.3, 45.6, 42.4 ppm.

HRMS (ESI $^+$): m/z calcd. for $\text{C}_{20}\text{H}_{21}\text{ClN}_5\text{O}_2^+$ ($[M+H]^+$) 398.1378, measured 398.1366.

tert-Butyl 4-(4-(5-(5-chloro-2-hydroxyphenyl)-1*H*-pyrazole-3-carboxamido)phenyl)piperazine-1-carboxylate (**6B**):



Compound **6B** was prepared following GP-1, chromene amide **43** (212 mg, 0.44 mmol) was reacted with hydrazine hydrate (175 mg, 3.5 mmol). The mixture stirred for 2 h and the solvent was removed under reduced pressure to obtain **6B** as white solid in quantitative yield (220 mg, 0.44 mmol).

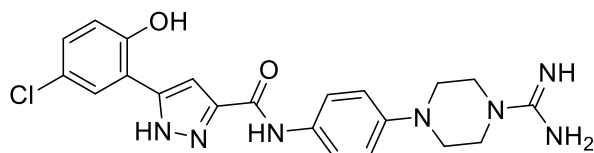
^1H NMR (400 MHz, DMSO- d_6) δ = 7.80 (d, J = 2.7 Hz, 1H), 7.66 (br d, J = 8.4 Hz, 2H), 7.24 (br dd, J = 8.6, 2.0 Hz, 1H), 7.00 (d, J = 8.6 Hz, 1H), 0.01 (d, J = 8.4 Hz, 2H), 3.46 (t, J = 4.5 Hz, 4H), 3.06 (br t,

$J = 4.5$ Hz, 4H), 1.42 (s, 9H) ppm. Pyrazole C–H is not a clear peak, likely very broad between peaks 7.66 and 7.24 ppm due to annular tautomerism.

^{13}C NMR (101 MHz, DMSO- d_6) $\delta = 153.9, 153.4, 147.4, 131.0, 128.8, 126.4, 122.9, 122.1, 121.4, 118.1, 116.3, 79.0, 48.9, 48.4, 28.1$ ppm. Quaternary carbon and pyrazole C–H peaks missing.

HRMS (ESI⁺): m/z calcd. for $\text{C}_{25}\text{H}_{29}\text{ClN}_5\text{O}_4^+$ ($[M+H]^+$) 498.1903, measured 498.1890.

N-(4-(4-Carbamimidoylpiperazin-1-yl)phenyl)-5-(5-chloro-2-hydroxyphenyl)-1*H*-pyrazole-3-carboxamide (**6G**):



Compound **6G** was prepared following GP-3 with adaptations. Amine **6A** (102 mg, 0.20 mmol) was reacted with DIPEA (216 mg, 1.7 mmol) and guanidinylation agent **65** (45 mg, 0.31 mmol). The reaction mixture stirred for 20 h and the crude (156 mg) was triturated with MeOH (2 mL).

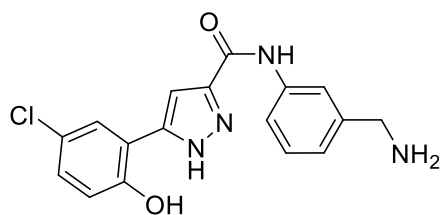
Compound **6G** was obtained as grey solid in form of a TFA salt (38 mg, 0.069 mmol, 34%).

^1H NMR (400 MHz, DMSO- d_6 , 120 °C): $\delta = 9.68$ (br s, 1H), 7.73 (br s, 1H), 7.66 (d, $J = 8.2$ Hz, 2H), 7.42 (br s, 2H), 7.38 (s, 1H), 7.21 (d, $J = 8.6$ Hz, 1H), 7.04 (d, $J = 8.6$ Hz, 1H), 6.97 (d, $J = 8.2$ Hz, 2H), 3.64 (br s, 4H), 3.26 (br s, 4H) ppm.

^{13}C NMR (101 MHz, DMSO- d_6 , 120 °C): $\delta = 161.5, 158.7, 156.3, 153.0, 146.2, 130.6, 128.0, 125.9, 122.6, 121.1, 117.7, 115.5, 108.9, 104.4, 47.4, 44.4$ ppm.

HRMS (ESI⁺): m/z calcd. for $\text{C}_{21}\text{H}_{23}\text{ClN}_7\text{O}_2^+$ ($[M+H]^+$) 440.1596, measured 440.1585.

N-(3-(Aminomethyl)phenyl)-5-(5-chloro-2-hydroxyphenyl)-1*H*-pyrazole-3-carboxamide (**7A**):



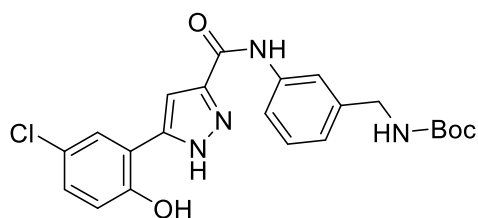
Compound **7A** was prepared following GP-2, *N*-Boc amine **7B** (161 mg, 0.36 mmol) was reacted with TFA (5.8 mmol) and the reaction mixture stirred for 1 h. Compound **7A** was obtained as off-white powder in form of a TFA salt in quantitative yield (165 mg, 0.36 mmol).

^1H NMR (400 MHz, DMSO- d_6) $\delta = 10.65$ (br s, 1H), 10.23 (br s, 1H), 8.24 (br s, 2H), 8.01 (br s, 1H), 7.81 (d, $J = 2.3$ Hz, 1H), 7.74 (br d, $J = 8.0$ Hz, 1H), 7.42 (br t, $J = 8.0$ Hz, 1H), 7.25 (dd, $J = 8.6, 2.3$ Hz, 1H), 7.21 (br d, $J = 8.0$ Hz, 1H), 7.03 (d, $J = 8.6$ Hz, 1H), 4.04 (br d, $J = 5.1$ Hz, 2H) ppm.

^{13}C NMR (101 MHz, DMSO- d_6) $\delta = 158.4, 158.1, 157.8, 153.5, 139.2, 134.6, 129.2, 129.0, 126.7, 124.1, 123.1, 120.9, 120.7, 118.3, 106.1, 42.7$ ppm. Quaternary carbon peaks missing.

HRMS (ESI⁻): m/z calcd. for $\text{C}_{17}\text{H}_{14}\text{ClN}_4\text{O}_2^-$ ($[M-H]^-$) 341.08108, measured 341.0798.

tert-Butyl (3-(5-(5-chloro-2-hydroxyphenyl)-1*H*-pyrazole-3-carboxamido)benzyl)carbamate (**7B**):



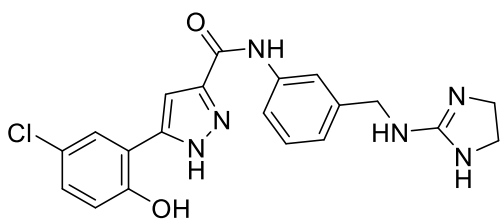
Compound **7B** was prepared following GP-1, chromene amide **44** (400 mg, 0.93 mmol) was reacted with hydrazine hydrate (374 mg, 7.46 mmol). The solvent was removed under reduced pressure to obtain compound **7B** as white solid in quantitative yield (440 mg, 0.93 mmol).

^1H NMR (400 MHz, DMSO- d_6) $\delta = 10.13$ (br s, 1H), 7.81 (br s, 1H), 7.64-7.75 (m, 2H), 7.48 (br s, 1H), 7.34-7.41 (m, 1H), 7.21-

7.32 (m, 2H), 6.89-7.09 (m, 2H), 4.13 (br s, 2H), 1.40 (br s, 9H) ppm.

^{13}C NMR (101 MHz, DMSO- d_6) $\delta = 155.6, 153.2, 140.6, 138.4, 128.6, 128.3, 126.3, 122.8, 122.1, 118.7, 118.6, 117.9, 105.6, 77.6, 43.3, 28.1$ ppm. Quaternary carbon peaks missing.

HRMS (ESI⁻): m/z calcd. for $\text{C}_{22}\text{H}_{22}\text{ClN}_4\text{O}_4^-$ ($[M-H]^-$) 441.1335, measured 441.1327.

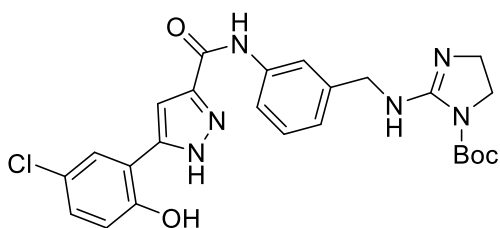
5-(5-Chloro-2-hydroxyphenyl)-*N*-(3-(((4,5-dihydro-1*H*-imidazol-2-yl)amino)methyl)phenyl)-1*H*-pyrazole-3-carboxamide (**7C**):

Compound **7C** was prepared following GP-2, *N*-Boc guanidine **7D** (163 mg, 0.32 mmol) was reacted with TFA (5.1 mmol) and the reaction mixture stirred overnight. Compound **7C** was obtained as off-white powder in form of a TFA salt in quantitative yield (169 mg, 0.32 mmol).

¹H NMR (400 MHz, DMSO-*d*₆) δ = 10.64 (br s, 1H), 10.10 (br s, 1H), 8.74 (br s, 1H), 7.89 (br s, 1H), 7.80 (s, 1H), 7.69 (d, *J* = 7.6 Hz, 1H), 7.35 (t, *J* = 7.6 Hz, 1H), 7.26 (d, *J* = 7.6 Hz, 2H), 7.03 (br s, 1H), 7.01 (s, 1H), 4.39 (br d, *J* = 5.5 Hz, 2H), 3.63 (s, 4H) ppm.

¹³C NMR (101 MHz, DMSO-*d*₆) δ = 160.5, 159.6, 158.5, 158.2, 153.3, 139.0, 137.6, 128.9, 126.5, 122.9, 122.3, 119.5, 118.9, 118.7, 118.1, 115.7, 105.9, 45.5, 42.6 ppm.

HRMS (ESI⁺): *m/z* calcd. for C₂₀H₂₀ClN₆O₂⁺ ([*M*+*H*]⁺) 411.1331, measured 411.1308.

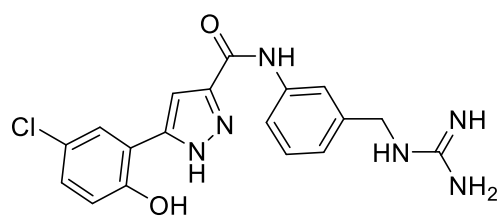
tert-Butyl 2-((3-(5-(5-chloro-2-hydroxyphenyl)-1*H*-pyrazole-3-carboxamido)benzyl)amino)-4,5-dihydro-1*H*-imidazole-1-carboxylate (**7D**):

Compound **7D** was prepared following GP-3, amine **3A** (200 mg, 0.44 mmol) was reacted with DIPEA (80 mg, 0.66 mmol) and guanidinylation agent **64** (284 mg, 1.31 mmol). The reaction mixture stirred for 24 h, and compound **7D** was obtained as off-white solid (182 mg, 0.36 mmol, 82%). Product contains 5% Boc-protected compound **7C**.

¹H NMR (400 MHz, DMSO-*d*₆) δ = 10.12 (br s, 1H), 7.79 (br d, *J* = 1.6 Hz, 1H), 7.69-7.76 (m, 2H), 7.43 (br s, 1H), 7.30 (br t, *J* = 7.8 Hz, 1H), 7.23 (br s, 1H), 7.05 (br d, *J* = 8.6 Hz, 1H), 6.99 (br d, *J* = 8.6 Hz, 1H), 4.36 (s, 2H), 3.69 (t, *J* = 8.0 Hz, 2H), 3.48 (t, *J* = 8.0 Hz, 2H), 1.46 (s, 9H) ppm.

¹³C NMR (101 MHz, DMSO-*d*₆) δ = 158.9, 153.1, 152.1, 151.5, 139.8, 138.3, 128.2, 128.1, 125.9, 122.3, 122.2, 118.7, 118.4, 118.0, 117.7, 105.1, 81.1, 47.7, 46.0, 45.3, 27.4 ppm.

HRMS (ESI⁺): *m/z* calcd. for C₂₅H₂₈ClN₆O₄⁺ ([*M*+*H*]⁺) 511.1855, measured 511.1838.

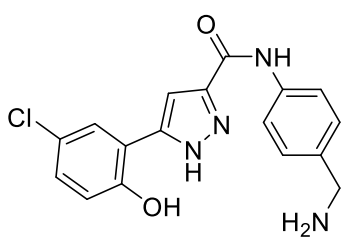
5-(5-Chloro-2-hydroxyphenyl)-*N*-(3-(guanidinomethyl)phenyl)-1*H*-pyrazole-3-carboxamide (**7G**):

Compound **7G** was prepared following GP-3, amine **7A** (108 mg, 0.24 mmol) was reacted with DIPEA (183 mg, 1.4 mmol) and guanidinylation agent **65** (52 mg, 0.36 mmol). The reaction mixture stirred for 5 h, and **7G** was obtained as white solid in form of a TFA salt (74 mg, 0.23 mmol, 63%).

¹H NMR (400 MHz, DMSO-*d*₆) δ = 9.92 (br s, 1H), 7.92 (br s, 1H), 7.70 (br d, *J* = 7.0 Hz, 1H), 7.49 (br s, 1H), 7.31 (t, *J* = 7.0 Hz, 1H), 7.15 (br s, 1H), 6.96 (br s, 2H), 6.71 (br d, *J* = 7.0 Hz, 1H), 4.37 (br s, 2H) ppm.

¹³C NMR (101 MHz, DMSO-*d*₆) δ = 162.1, 158.0, 156.9, 149.3, 146.0, 139.9, 137.5, 128.8, 125.9, 124.1, 121.2, 120.2, 119.5, 118.5, 118.4, 118.0, 100.0, 44.3 ppm.

HRMS (ESI⁺): *m/z* calcd. for C₁₈H₁₈ClN₆O₂⁺ ([*M*+*H*]⁺) 385.1174, measured 385.1166.

N-(4-(Aminomethyl)phenyl)-5-(5-chloro-2-hydroxyphenyl)-1*H*-pyrazole-3-carboxamide (**8A**):

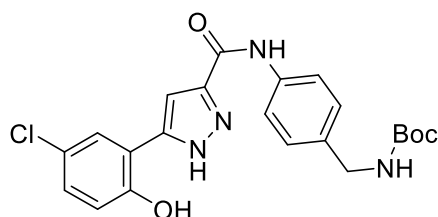
Compound **8A** was prepared following GP-2, *N*-Boc amine **8B** (289 mg, 0.65 mmol) was reacted with TFA (10.4 mmol) and the reaction mixture stirred overnight. Compound **8A** was obtained as off-white solid in form of a TFA salt in quantitative yield (299 mg, 0.65 mmol).

¹H NMR (400 MHz, DMSO-*d*₆) δ = 10.24 (br s, 1H), 7.85 (br d, *J* = 8.2 Hz, 2H), 7.81 (br d, *J* = 2.7 Hz, 1H), 7.42 (br d, *J* = 8.2 Hz, 2H), 7.34 (br s, 1H), 7.25 (br dd, *J* = 8.6, 2.7 Hz, 1H), 7.02 (d, *J* = 8.6 Hz, 1H), 4.00 (s, 2H) ppm.

¹³C NMR (101 MHz, DMSO-*d*₆, 120 °C): δ = 158.7, 153.0, 138.4, 138.3, 128.6, 128.4, 128.1, 126.1, 122.7, 119.9, 117.9, 117.8, 104.7, 41.8 ppm.

HRMS (ESI⁻): *m/z* calcd. for C₁₇H₁₄ClN₄O₂⁻ ([*M*-*H*]⁻) 341.0811, measured 341.0799.

tert-Butyl(4-(5-(5-chloro-2-hydroxyphenyl)-1*H*-pyrazole-3-carboxamido)benzyl)carbamate (**8B**):



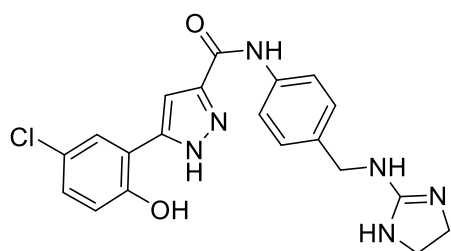
Compound **8B** was prepared following GP-1, chromene amide **45** (280 mg, 0.65 mmol) was reacted with hydrazine hydrate (261 mg, 5.2 mmol). The solvent was removed under reduced pressure obtaining **8B** as white solid in quantitative yield (290 mg, 0.65 mmol).

^1H NMR (400 MHz, $\text{DMSO-}d_6$) δ = 10.08 (br s, 1H), 7.80 (d, J = 2.7 Hz, 1H), 7.73 (br d, J = 8.2 Hz, 2H), 7.35 (br s, 1H), 7.24 (dd, J = 8.8, 2.7 Hz, 1H), 7.21 (d, J = 8.2 Hz, 2H), 7.01 (d, J = 8.8 Hz, 1H), 4.09 (d, J = 5.9 Hz, 2H), 1.40 (s, 9H) ppm.

^{13}C NMR (101 MHz, $\text{DMSO-}d_6$) δ = 155.8, 153.3, 137.2, 135.4, 128.7, 127.2, 126.4, 122.9, 120.2, 118.1, 105.7, 77.7, 43.0, 28.3 ppm. Quaternary carbon peaks missing.

HRMS (ESI⁻): m/z calcd. for $\text{C}_{22}\text{H}_{22}\text{ClN}_4\text{O}_4^-$ ($[M-H]^-$) 441.1335, measured 441.13266.

5-(5-Chloro-2-hydroxyphenyl)-*N*-(4-(((4,5-dihydro-1*H*-imidazol-2-yl)amino)methyl)phenyl)-1*H*-pyrazole-3-carboxamide(**8C**):



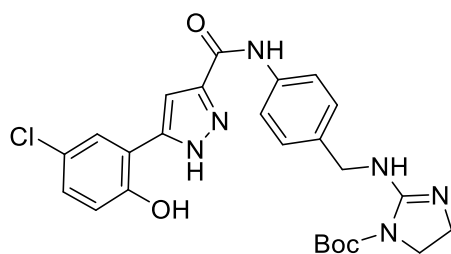
Compound **8C** was prepared following GP-2, *N*-Boc guanidine **8D** (21 mg, 0.042 mmol) was reacted with TFA (1.4 mmol) and the reaction mixture stirred for 24 h. Compound **8C** was obtained as light brown powder in form of a TFA salt (21 mg, 0.040 mmol, 96%).

^1H NMR (400 MHz, $\text{DMSO-}d_6$) δ = 13.50 (s, 2H), 10.64 (br s, 1H), 10.15 (br s, 1H), 8.80 (br s, 1H), 8.46 (br s, 1H), 8.45 (br s, 1H), 7.83 (br s, 2H), 7.18-7.38 (m, 3H), 7.03 (br s, 1H), 4.35 (s, 2H), 3.62 (s, 2H), 3.11 (br s, 2H) ppm.

^{13}C NMR (101 MHz, $\text{DMSO-}d_6$) δ = 159.9, 158.6, 158.3, 153.7, 138.6, 132.6, 129.2, 128.1, 126.9, 123.3, 120.8, 118.5, 106.3, 54.0, 46.1, 45.5, 43.0 ppm.

HRMS (ESI⁺): m/z calcd. for $\text{C}_{20}\text{H}_{20}\text{ClN}_6\text{O}_2^+$ ($[M+H]^+$) 411.1331, measured 411.1317.

tert-Butyl 2-(((4-(5-(5-chloro-2-hydroxyphenyl)-1*H*-pyrazole-3-carboxamido)benzyl)amino)-4,5-dihydro-1*H*-imidazole-1-carboxylate (**8D**):



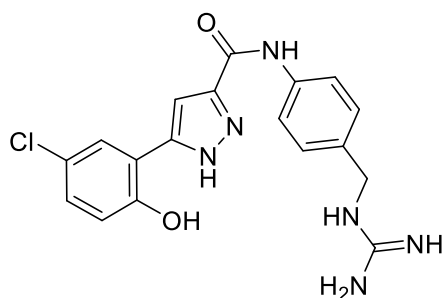
Compound **8D** was prepared following GP-4 with adaptations. Amine **8A** (74 mg, 0.17 mmol) was reacted with DIPEA (129 mg, 1.0 mmol) and guanidinylation agent **64** (107 mg, 0.49 mmol), the reaction mixture stirred for 150 h. It was quenched with water (10 mL) and extracted with EtOAc (3 x 10 mL). The combined organic layers were washed with brine, dried over anhydrous MgSO_4 , filtered, and concentrated *in vacuo*, obtaining of a viscous brown oil (129 mg). The crude was purified

by flash column chromatography using 10% MeOH in DCM as eluent to obtain **8D** as a white solid (41 mg, 0.080 mmol, 47%).

^1H NMR (400 MHz, $\text{DMSO-}d_6$) δ = 10.25 (br s, 1H), 10.20 (br s, 1H), 8.79 (br s, 1H), 7.95 (br s, 1H), 7.76-7.84 (m, 3H), 7.43 (br s, 1H), 7.28-7.35 (m, 2H), 7.24 (dd, J = 8.8, 2.3 Hz, 1H), 7.05 (dd, J = 8.8, 2.9 Hz, 1H), 3.80 (t, J = 8.4 Hz, 2H), 3.61 (s, 2H), 3.54 (t, J = 8.4 Hz, 2H), 1.48 (s, 9H) ppm.

^{13}C NMR (101 MHz, $\text{DMSO-}d_6$) δ = 162.3, 159.4, 153.4, 151.5, 138.2, 137.8, 133.3, 132.1, 128.7, 127.8, 127.7, 126.4, 122.8, 120.3, 120.3, 118.1, 105.8, 82.8, 45.4, 45.1, 42.5, 27.7 ppm.

HRMS (ESI⁺): m/z calcd. for $\text{C}_{25}\text{H}_{28}\text{ClN}_6\text{O}_4^+$ ($[M+H]^+$) 511.1855, measured 511.1829.

5-(5-Chloro-2-hydroxyphenyl)-*N*-(4-(guanidinomethyl)phenyl)-1*H*-pyrazole-3-carboxamide (**8G**):

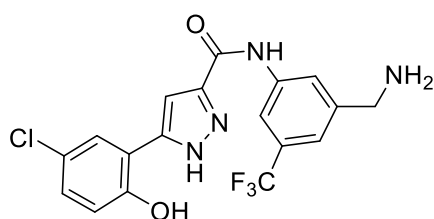
Compound **8G** was prepared following GP-3, amine **8A** (65 mg, 0.15 mmol) was reacted with DIPEA (124 mg, 0.96 mmol) and guanidinylation agent **65** (37 mg, 0.25 mmol). The reaction mixture stirred for 3.5 h and **8G** was obtained as off-white solid in form of a TFA salt (53 mg, 0.11 mmol, 74%).

^1H NMR (500 MHz, $\text{DMSO-}d_6$) δ = 10.21 (br s, 1H), 8.24 (br s, 1H), 7.78 (br d, J = 8.2 Hz, 2H), 7.75 (br s, 1H), 7.39 (br s, 1H), 7.26 (br d, J = 8.1 Hz, 2H), 7.18 (br d, J = 8.1 Hz, 1H), 7.00 (d, J = 8.1 Hz, 1H), 4.30 (br d, J = 4.7 Hz, 2H) ppm.

^{13}C NMR (101 MHz, $\text{DMSO-}d_6$) δ = 158.5, 156.9, 153.4, 138.1,

132.2, 128.8, 127.6, 126.4, 122.9, 120.4, 118.6, 118.1, 115.6, 112.7, 105.8, 43.7 ppm.

HRMS (ESI⁺): m/z calcd. for $\text{C}_{18}\text{H}_{18}\text{ClN}_6\text{O}_2^+$ ($[M+H]^+$) 385.1174, measured 385.1176.

N-(3-(Aminomethyl)-5-(trifluoromethyl)phenyl)-5-(5-chloro-2-hydroxyphenyl)-1*H*-pyrazole-3-carboxamide (**9A**):

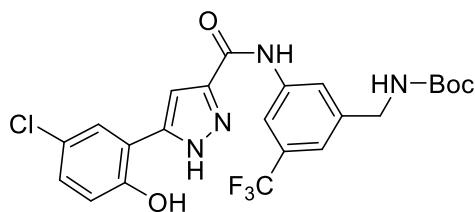
Compound **9A** was prepared following GP-2, *N*-Boc amine **9B** (138 mg, 0.27 mmol) was reacted with TFA (6.7 mmol) and the reaction mixture stirred for 24 h. Compound **9A** was obtained as off-white solid in form of a TFA salt in quantitative yield (141 mg, 0.27 mmol).

^1H NMR (400 MHz, $\text{DMSO-}d_6$) δ = 10.68 (br s, 1H), 10.53 (br s, 1H), 8.24-8.40 (m, 3H), 8.20 (br s, 1H), 7.81 (d, J = 2.3 Hz, 1H), 7.60 (s, 1H), 7.30 (br s, 1H), 7.26 (br dd, J = 7.4, 2.3 Hz, 2H), 7.04 (d, J = 7.4 Hz, 1H), 4.12 (br s, 2H) ppm.

^{13}C NMR (101 MHz, $\text{DMSO-}d_6$) δ = 158.2, 153.7, 140.3, 136.4, 130.2, 129.9, 129.5, 127.0, 125.7, 123.0, 120.6, 118.5, 117.0, 106.6, 42.5 ppm. Quaternary carbon peaks missing.

^{19}F NMR (376 MHz, $\text{DMSO-}d_6$) δ = -61.38, -73.61 ppm.

HRMS (ESI⁺): m/z calcd. for $\text{C}_{18}\text{H}_{15}\text{ClF}_3\text{N}_4\text{O}_2^+$ ($[M+H]^+$) 411.0830, measured 411.0811.

tert-Butyl (3-(5-(5-chloro-2-hydroxyphenyl)-1*H*-pyrazole-3-carboxamido)-5-(trifluoromethyl)benzyl)carbamate (**9B**):

Compound **9B** was prepared following GP-1, chromene amide **46** (137 mg, 0.28 mmol) was reacted with hydrazine hydrate (111 mg, 2.2 mmol). The mixture stirred for 2.5 h and the solvent was removed under reduced pressure to obtain **9B** as yellow solid in quantitative yield (143 mg, 0.28 mmol).

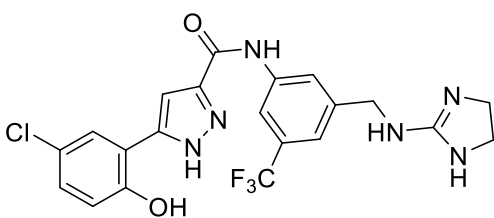
^1H NMR (500 MHz, $\text{DMSO-}d_6$) δ = 10.49 (br s, 1H), 8.15 (s, 1H), 8.02 (br s, 1H), 7.81 (d, J = 2.4 Hz, 1H), 7.51 (br t, J = 6.0 Hz, 1H),

7.30 (s, 1H), 7.25 (br dd, J = 8.7, 2.4 Hz, 1H), 7.01 (d, J = 8.7 Hz, 1H), 4.20 (d, J = 6.0 Hz, 2H), 1.41 (s, 9H) ppm.

^{13}C NMR (126 MHz, $\text{DMSO-}d_6$) δ = 156.3, 153.8, 142.9, 140.1, 129.9, 129.6, 129.3, 127.9, 127.0, 125.7, 123.6, 123.4, 122.6, 118.5, 115.3, 106.6, 78.5, 43.7, 28.7 ppm.

^{19}F NMR (470 MHz, $\text{DMSO-}d_6$) δ = -61.28 ppm.

HRMS (ESI⁻): m/z calcd. for $\text{C}_{23}\text{H}_{21}\text{ClF}_3\text{N}_4\text{O}_4^-$ ($[M-H]^-$) 509.1209, measured 509.1194.

5-(5-Chloro-2-hydroxyphenyl)-*N*-(3-(((4,5-dihydro-1*H*-imidazol-2-yl)amino)methyl)-5-(trifluoromethyl)phenyl)-1*H*-pyrazole-3-carboxamide (**9C**):

Compound **9C** was prepared following GP-2, *N*-Boc guanidine **9D** (50 mg, 0.086 mmol) was reacted with TFA (1.3 mmol) and the reaction mixture stirred overnight. Compound **9C** was obtained as light grey solid in form of a TFA salt in quantitative yield (51 mg, 0.086 mmol).

^1H NMR (400 MHz, $\text{acetone-}d_6$) δ = 10.40 (br s, 1H), 10.00 (br s, 1H), 8.39 (s, 1H), 8.15 (br s, 1H), 7.75 (s, 1H), 7.59 (br s, 1H), 7.45 (s, 1H), 7.21 (d, J = 8.0 Hz, 1H), 7.06 (br d, J = 8.0 Hz,

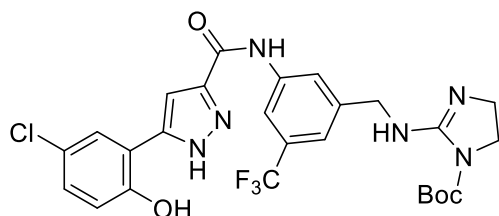
1H), 4.65 (br s, 2H), 4.04 (br s, 2H), 3.78 (br s, 4H) ppm.

^{13}C NMR (101 MHz, acetone- d_6) δ = 171.9, 160.9, 154.3, 140.3, 139.7, 131.3, 129.4, 126.8, 125.9, 124.3, 123.2, 122.3, 119.2, 118.6, 118.0, 115.9, 104.3, 45.9, 45.5, 43.1 ppm.

^{19}F NMR (376 MHz, acetone- d_6) δ = -63.12, -75.77 ppm.

HRMS (ESI⁺): m/z calcd. for $\text{C}_{21}\text{H}_{19}\text{ClF}_3\text{N}_6\text{O}_2^+$ ($[\text{M}+\text{H}]^+$) 479.1205, measured 479.1192.

tert-Butyl 2-((3-(5-(5-chloro-2-hydroxyphenyl)-1*H*-pyrazole-3-carboxamido)-5-(trifluoromethyl)benzyl)amino)-4,5-dihydro-1*H*-imidazole-1-carboxylate (**9D**):



Compound **9D** was prepared following GP-3, amine **9A** (200 mg, 0.44 mmol) was reacted with DIPEA (80 mg, 0.66 mmol) and guanidinylation agent **64** (26 mg, 0.20 mmol). The reaction mixture stirred for 48 h, and compound **9D** was obtained as off-white powder (54 mg, 0.93 mmol, 70%). Product contains 5% Boc-deprotected compound **9C**.

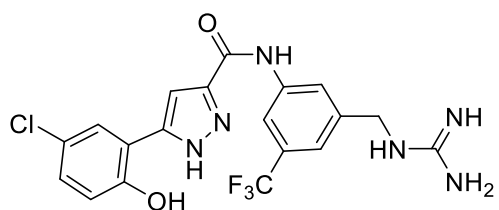
^1H NMR (500 MHz, DMSO- d_6) δ = 10.50 (br s, 1H), 8.19 (s, 1H), 8.04 (s, 1H), 7.81 (d, J = 2.3 Hz, 1H), 7.45 (br s, 1H), 7.40 (s, 1H), 7.25 (dd, J = 8.7, 2.3 Hz, 1H), 7.02 (d, J = 8.7 Hz, 1H), 4.45 (s, 2H), 3.73-3.78 (m, 2H), 3.69-3.73 (m, 2H), 1.48 (s, 9H) ppm.

^{13}C NMR (126 MHz, DMSO- d_6) δ = 158.2, 153.9, 153.1, 152.3, 142.7, 140.0, 129.8, 129.5, 129.3, 126.9, 125.8, 123.6, 123.0, 119.2, 118.6, 115.4, 106.4, 82.1, 47.8, 47.0, 45.7, 28.3 ppm.

^{19}F NMR (470 MHz, DMSO- d_6) δ = -61.14 ppm.

HRMS (ESI⁺): m/z calcd. for $\text{C}_{26}\text{H}_{27}\text{ClF}_3\text{N}_6\text{O}_4^+$ ($[\text{M}+\text{H}]^+$) 579.1729, measured 579.1713.

5-(5-Chloro-2-hydroxyphenyl)-*N*-(3-(guanidinomethyl)-5-(trifluoromethyl)phenyl)-1*H*-pyrazole-3-carboxamide (**9G**):



Compound **9G** was prepared following GP-3 with adaptations, amine **9A** (40 mg, 0.076 mmol) was reacted with DIPEA (59 mg, 0.46 mmol) and guanidinylation agent **65** (17 mg, 0.11 mmol). The reaction mixture stirred for 30 h obtaining an off-white solid (54 mg). Part of the crude (15 mg, 28%) was purified by preparative HPLC to afford **9G** as white powder (5 mg, 0.09 mmol, 43%).

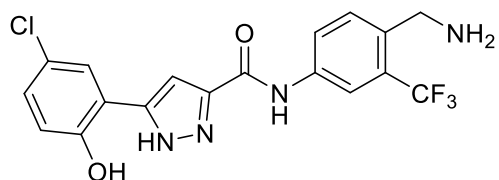
^1H NMR (500 MHz, DMSO- d_6) δ = 10.61 (s, 1H), 8.90 (br s, 1H), 8.41 (s, 1H), 8.21 (s, 1H), 8.14 (s, 1H), 7.85 (br s, 2H), 7.78 (d, J = 2.6 Hz, 1H), 7.39 (s, 1H), 7.36 (s, 1H), 7.21 (dd, J = 8.8, 2.6 Hz, 1H), 7.01 (d, J = 8.8 Hz, 1H), 4.46 (d, J = 4.1 Hz, 2H) ppm.

^{13}C NMR (126 MHz, DMSO- d_6) δ = 167.0, 160.8, 157.9, 154.5, 140.5, 140.4, 130.0, 129.8, 129.0, 126.7, 125.7, 122.9, 122.5, 118.8, 118.6, 115.8, 106.0, 43.9 ppm.

^{19}F NMR (470 MHz, DMSO- d_6) δ = -61.24 ppm.

HRMS (ESI⁺): m/z calcd. for $\text{C}_{19}\text{H}_{17}\text{ClF}_3\text{N}_6\text{O}_2^+$ ($[\text{M}+\text{H}]^+$) 453.1048, measured 453.1028.

N-(4-(Aminomethyl)-3-(trifluoromethyl)phenyl)-5-(5-chloro-2-hydroxyphenyl)-1*H*-pyrazole-3-carboxamide (**10A**):



Compound **10A** was prepared following GP-2, *N*-Boc amine **10B** (1910 mg, 3.74 mmol) was reacted with TFA (94.0 mmol) and the reaction mixture stirred for 3 h. Compound **10A** was obtained as light orange solid in form of a TFA salt in quantitative yield (1999 mg, 3.74 mmol).

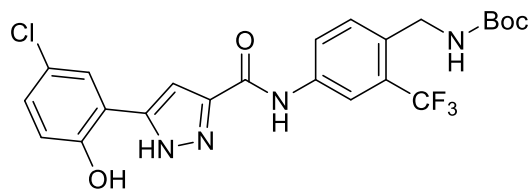
^1H NMR (400 MHz, DMSO- d_6) δ = 10.69 (br s, 1H), 10.63 (br s, 1H), 8.44 (br s, 2H), 8.38 (s, 1H), 8.21 (d, J = 8.2 Hz, 1H), 7.82 (br s, 1H), 7.69 (d, J = 8.2 Hz, 1H), 7.41 (br s, 1H), 7.25 (d, J = 8.6 Hz, 1H), 7.04 (d, J = 8.6 Hz, 1H), 4.16 (s, 2H) ppm.

^{13}C NMR (101 MHz, DMSO- d_6) δ = 160.2, 158.7, 153.4, 139.6, 131.5, 128.9, 127.7, 126.6, 126.2, 125.3, 123.6, 122.9, 122.6, 118.2, 117.4, 115.4, 106.3, 38.5 ppm

^{19}F NMR (376 MHz, DMSO- d_6) δ = -58.24, -73.93 ppm.

HRMS (ESI⁻): m/z calcd. for $\text{C}_{18}\text{H}_{13}\text{ClF}_3\text{N}_4\text{O}_2^-$ ($[\text{M}-\text{H}]^-$) 409.0685, measured 409.0674.

tert-Butyl (4-(5-(5-chloro-2-hydroxyphenyl)-1*H*-pyrazole-3-carboxamido)-2-(trifluoromethyl)benzyl)carbamate (**10B**):



Compound **10B** was prepared following GP-1, chromene amide **47** (2000 mg, 4.02 mmol) was reacted with hydrazine hydrate (1621 mg, 32.4 mmol). The mixture stirred for 3 h and the solvent was removed under reduced pressure obtaining **10B** as white solid (1972 mg, 3.86 mmol, 96%).

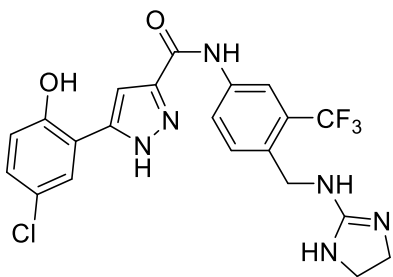
^1H NMR (400 MHz, $\text{DMSO-}d_6$) δ = 10.46 (s, 1H), 8.27 (s, 1H), 8.09 (d, J = 8.2 Hz, 1H), 7.81 (br d, J = 2.2 Hz, 1H), 7.48 (br s, 1H), 7.46 (br s, 1H), 7.43 (br s, 1H), 7.24 (dd, J = 8.6, 2.2 Hz, 1H), 7.02 (d, J = 8.6 Hz, 1H), 4.30 (d, J = 3.9 Hz, 2H), 1.41 (s, 9H) ppm.

^{13}C NMR (101 MHz, $\text{DMSO-}d_6$) δ = 160.3, 156.2, 153.8, 144.5, 142.7, 138.2, 133.2, 129.2, 126.9, 126.7, 126.4, 126.1, 124.1, 123.4, 123.3, 120.6, 118.5, 117.7, 106.4, 78.6, 28.6 ppm.

^{19}F NMR (376 MHz, $\text{DMSO-}d_6$) δ = -59.19 ppm.

HRMS (ESI⁻): m/z calcd. for $\text{C}_{23}\text{H}_{21}\text{ClF}_3\text{N}_4\text{O}_4^-$ ($[\text{M-H}]^-$) 509.1209, measured 509.1189.

5-(5-Chloro-2-hydroxyphenyl)-*N*-(4-(((4,5-dihydro-1*H*-imidazol-2-yl)amino)methyl)-3-(trifluoromethyl)phenyl)-1*H*-pyrazole-3-carboxamide (**10C**):



Compound **10C** was prepared following GP-2, *N*-Boc guanidine **10D** (122 mg, 0.21 mmol) was reacted with TFA (3.4 mmol) and the reaction mixture stirred for 48 h. Compound **10C** was obtained as brown solid in form of a TFA salt in quantitative yield (125 mg, 0.21 mmol).

^1H NMR (400 MHz, $\text{DMSO-}d_6$) δ = 10.59 (s, 1H), 8.78 (t, J = 5.8 Hz, 1H), 8.36 (d, J = 1.8 Hz, 1H), 8.17 (dd, J = 8.4, 1.8 Hz, 1H), 7.82 (d, J = 2.3 Hz, 1H), 7.53 (d, J = 8.4 Hz, 2H), 7.43 (br s, 1H), 7.26 (dd, J = 8.6, 2.3 Hz, 1H), 7.04 (d, J = 8.6 Hz, 1H), 4.53 (br d, J = 5.8 Hz, 2H), 3.66 (s, 4H)

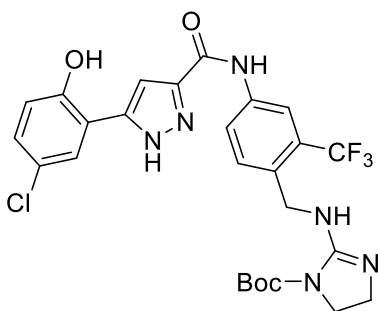
ppm.

^{13}C NMR (101 MHz, $\text{DMSO-}d_6$) δ = 159.6, 158.6, 158.3, 153.3, 138.9, 130.1, 129.0, 128.9, 127.0, 126.5, 125.5, 123.7, 122.9, 122.7, 118.1, 117.7, 106.2, 42.6, 42.5 ppm.

^{19}F NMR (376 MHz, $\text{DMSO-}d_6$) δ = -58.85, -74.55 ppm.

HRMS (ESI⁺): m/z calcd. for $\text{C}_{21}\text{H}_{19}\text{ClF}_3\text{N}_6\text{O}_2^+$ ($[\text{M+H}]^+$) 479.1205, measured 479.1186.

tert-Butyl 2-((4-(5-(5-chloro-2-hydroxyphenyl)-1*H*-pyrazole-3-carboxamido)-2-(trifluoromethyl)benzyl)amino)-4,5-dihydro-1*H*-imidazole-1-carboxylate (**10D**):



Compound **10D** was prepared following GP-3 with adaptations. Amine **10A** (314 mg, 0.62 mmol) was reacted with DIPEA (471 mg, 3.6 mmol) and guanidinylation agent **64** (392 mg, 1.81 mmol). The reaction mixture stirred for 6 days. The obtained precipitate was filtered and purified by column chromatography using 10% MeOH in DCM as eluent to obtain **10D** as a white powder (186 mg, 0.32 mmol, 52%).

^1H NMR (400 MHz, $\text{DMSO-}d_6$) δ = 10.50 (br s, 1H), 8.28 (br s, 1H), 8.07 (br d, J = 8.2 Hz, 1H), 7.81 (br d, J = 2.4 Hz, 1H), 7.55 (br d, J = 8.2 Hz, 1H), 7.42 (br s, 1H), 7.25 (br dd, J = 8.6, 2.3 Hz, 1H), 7.02 (br d, J = 8.6 Hz, 1H), 4.54 (br s, 1H), 3.72 (br t, J = 8.2 Hz, 2H), 3.47 (t, J = 8.2 Hz, 2H),

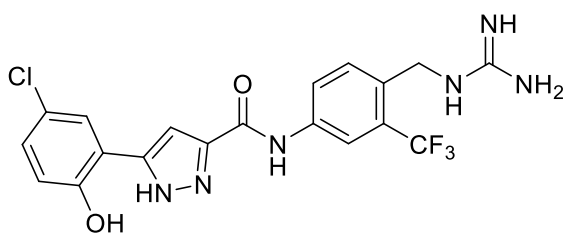
1.47 (s, 9H) ppm.

^{13}C NMR (101 MHz, $\text{DMSO-}d_6$) δ = 153.4, 152.6, 151.9, 141.7, 141.6, 138.0, 132.2, 129.7, 128.8, 126.5, 126.2, 125.7, 123.7, 123.0, 122.9, 118.1, 117.4, 106.1, 81.8, 47.7, 46.5, 42.2, 27.8 ppm.

^{19}F NMR (376 MHz, $\text{DMSO-}d_6$) δ = -59.05 ppm.

HRMS (ESI⁺): m/z calcd. for $\text{C}_{26}\text{H}_{27}\text{ClF}_3\text{N}_6\text{O}_4^+$ ($[\text{M+H}]^+$) 579.1729, measured 579.1710.

5-(5-Chloro-2-hydroxyphenyl)-*N*-(4-(guanidinomethyl)-3-(trifluoromethyl)phenyl)-1*H*-pyrazole-3-carboxamide (**10G**):



Compound **10G** was prepared following GP-3, amine **10A** (260 mg, 0.51 mmol) was reacted with DIPEA (402 mg, 3.1 mmol) and guanidinylation agent **65** (114 mg, 0.78 mmol). The reaction mixture stirred for 3.5 h and **10G** was obtained as light yellow solid in form of a TFA salt (190 mg, 0.37 mmol, 75%).

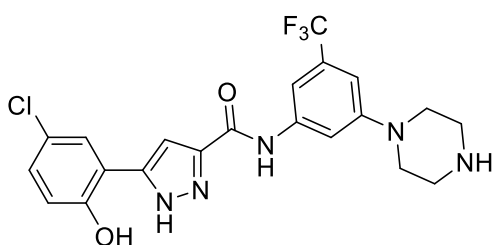
^1H NMR (400 MHz, DMSO- d_6) δ = 10.62 (br s, 1H), 8.37 (s, 1H), 8.17 (d, J = 8.2 Hz, 1H), 8.02 (br s, 1H), 7.82 (s, 1H), 7.53 (br d, J = 8.2 Hz, 1H), 7.44 (br s, 2H), 7.25 (br d, J = 8.2 Hz, 1H), 7.06 (br d, J = 8.2 Hz, 1H), 4.51 (br s, 2H) ppm.

^{13}C NMR (101 MHz, DMSO- d_6) δ = 158.6, 157.1, 153.4, 138.9, 130.2, 129.2, 128.9, 128.2, 127.1, 126.5, 125.5, 123.7, 122.9, 118.6, 118.1, 117.7, 115.6, 106.2, 41.3 ppm.

^{19}F NMR (376 MHz, DMSO- d_6) δ = -58.65, -73.55 ppm.

HRMS (ESI $^+$): m/z calcd. for $\text{C}_{19}\text{H}_{17}\text{ClF}_3\text{N}_6\text{O}_2^+$ ($[\text{M}+\text{H}]^+$) 453.1048, measured 453.1028.

5-(5-Chloro-2-hydroxyphenyl)-*N*-(3-(piperazin-1-yl)-5-(trifluoromethyl)phenyl)-1*H*-pyrazole-3-carboxamide (**11A**):



Compound **11A** was prepared following GP-2 with adaptations, *N*-Boc amine **11B** (500 mg, 0.88 mmol) was reacted with TFA (27 mmol) and the reaction mixture stirred overnight. A precipitate appeared which was filtered and washed with ice-cold EtOH (2 mL) to obtain **11A** as white powder in form of a TFA salt (393 mg, 0.70 mmol, 79%).

^1H NMR (400 MHz, DMSO- d_6 , 120 $^\circ\text{C}$): δ = 10.01 (br s, 1H), 7.73-7.77 (m, 2H), 7.72 (br s, 1H), 7.39 (s, 1H), 7.22 (br d, J =

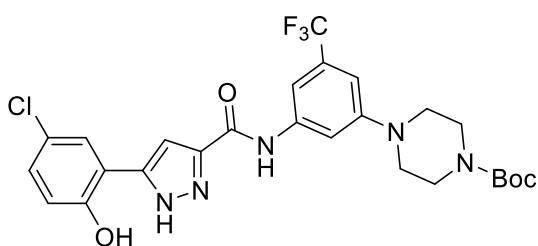
8.6 Hz, 1H), 7.04 (br d, J = 8.6 Hz, 1H), 6.99 (br s, 1H), 3.46-3.55 (m, 4H), 3.26-3.35 (m, 4H) ppm.

^{13}C NMR (101 MHz, DMSO- d_6 , 120 $^\circ\text{C}$): δ = 159.0, 152.9, 150.2, 142.9, 139.9, 130.2, 129.9, 128.1, 126.1, 125.0, 122.7, 117.8, 117.7, 110.1, 107.5, 106.8, 104.9, 44.8, 42.2 ppm.

^{19}F NMR (376 MHz, DMSO- d_6) δ = -61.27, -73.55 ppm.

HRMS (ESI $^+$): m/z calcd. for $\text{C}_{21}\text{H}_{20}\text{ClF}_3\text{N}_5\text{O}_2^+$ ($[\text{M}+\text{H}]^+$) 466.1252, measured 466.1229.

tert-Butyl 4-(3-(5-(5-chloro-2-hydroxyphenyl)-1*H*-pyrazole-3-carboxamido)-5-(trifluoromethyl)phenyl)piperazine-1-carboxylate (**11B**):



Compound **11B** was prepared following GP-1, chromene amide **48** (611 mg, 1.1 mmol) was reacted with hydrazine hydrate (438 mg, 8.7 mmol). The mixture stirred for 1 h and the solvent was removed under reduced pressure to obtain **11B** as white solid in quantitative yield (614 mg, 1.1 mmol).

^1H NMR (400 MHz, DMSO- d_6) δ = 10.27 (br s, 10H), 7.80 (d, J = 2.5 Hz, 1H), 7.77 (s, 1H), 7.68 (s, 1H), 7.39 (br s,

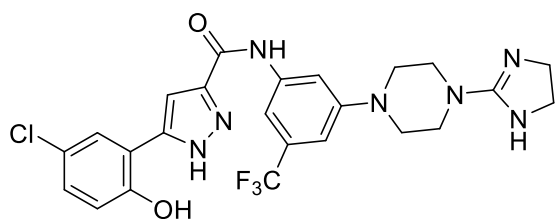
1H), 7.24 (dd, J = 8.8, 2.5 Hz, 1H), 7.01 (d, J = 8.8 Hz, 1H), 6.96 (s, 1H), 3.48 (t, J = 5.4 Hz, 4H), 3.20 (br t, J = 5.4 Hz, 4H), 1.42 (s, 9H) ppm.

^{13}C NMR (101 MHz, DMSO- d_6) δ = 154.6, 153.9, 152.0, 140.8, 131.4, 131.1, 130.8, 129.2, 127.1, 126.2, 123.8, 123.4, 118.9, 118.8, 110.8, 107.7, 107.4, 105.9, 79.6, 48.3, 43.6, 28.6 ppm.

^{19}F NMR (376 MHz, DMSO- d_6) δ = -61.29 ppm.

HRMS (ESI $^-$): m/z calcd. for $^-$ ($[\text{M}-\text{H}]^-$) 564.1631, measured 564.1617.

5-(5-Chloro-2-hydroxyphenyl)-*N*-(3-(4-(4,5-dihydro-1*H*-imidazol-2-yl)piperazin-1-yl)-5-(trifluoromethyl)phenyl)-1*H*-pyrazole-3-carboxamide (**11C**):



Compound **11C** was prepared following GP-3 with adaptations. Amine **11A** (91 mg, 0.16 mmol) was reacted with DIPEA (152 mg, 1.2 mmol) and guanidinylation agent **63** (122 mg, 0.50 mmol), the reaction mixture stirred for 20 h. After water (20 mL) addition, the obtained precipitate was filtered off and purified by flash column chromatography using

NH₄OH:MeOH:DCM (1:4:15) as eluent system to obtain **11C** as white solid (20 mg, 0.037, 23%).

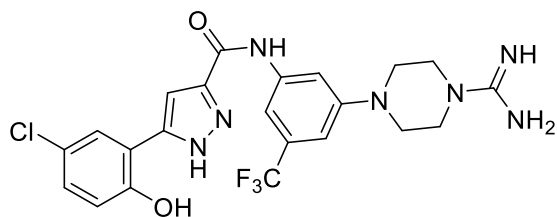
¹H NMR (600 MHz, DMSO-*d*₆, 50 °C): δ = 10.07 (br s, 1H), 7.85 (s, 1H), 7.69 (s, 1H), 7.56 (d, *J* = 2.5 Hz, 1H), 7.07 (s, 1H), 7.01 (dd, *J* = 8.6, 2.5 Hz, 1H), 6.93 (s, 1H), 6.81 (d, *J* = 8.6 Hz, 1H), 3.63 (s, 4H), 3.57 (t, *J* = 5.0 Hz, 4H), 3.36 (t, *J* = 5.0 Hz, 4H) ppm.

¹³C NMR (151 MHz, DMSO-*d*₆, 50 °C): δ = 161.6, 159.6, 156.4, 150.8, 147.5, 145.2, 140.9, 130.1, 126.4, 125.2, 124.5, 120.5, 119.6, 118.0, 109.3, 106.4, 106.1, 101.4, 46.7, 45.3, 43.5 ppm

¹⁹F NMR (376 MHz, DMSO-*d*₆) δ = -61.2 (s, 1F) ppm.

HRMS (ESI⁺): *m/z* calcd. for C₂₄H₂₄ClF₃N₇O₂⁺ ([*M*+*H*]⁺) 534.1627, measured 534.1601

N-(3-(4-Carbamimidoylpiperazin-1-yl)-5-(trifluoromethyl)phenyl)-5-(5-chloro-2-hydroxyphenyl)-1*H*-pyrazole-3-carboxamide (**11G**):



Compound **11G** was prepared following GP-3, amine **11A** (94 mg, 0.17 mmol) was reacted with DIPEA (152 mg, 1.17 mmol) and guanidinylation agent **65** (36 mg, 0.25 mmol). The reaction mixture stirred for 48 h to obtain **11G** as light grey solid (38 mg, 0.08 mmol, 46%).

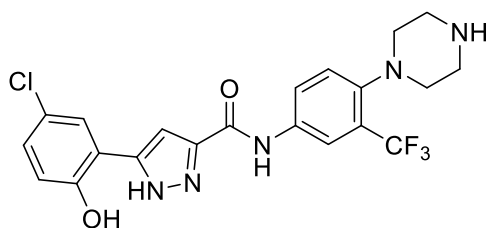
¹H NMR (400 MHz, DMSO-*d*₆) δ = 10.64 (br s, 1H), 7.82 (br s, 2H), 7.74 (br s, 1H), 7.65 (br s, 3H), 7.44 (br s, 1H), 7.24 (br d, *J* = 6.6 Hz, 2H), 7.08 (br d, *J* = 6.6 Hz, 1H), 7.01 (br s, 1H), 3.62 (s, 4H), 3.35 (s, 4H) ppm.

¹³C NMR (151 MHz, DMSO-*d*₆) δ = 160.8, 156.3, 153.4, 150.8, 146.7, 140.5, 139.7, 130.1, 128.9, 126.5, 125.2, 122.8, 118.1, 117.2, 109.7, 106.9, 106.9, 106.2, 46.8, 44.5 ppm.

¹⁹F NMR (376 MHz, DMSO-*d*₆) δ = -61.23 ppm.

HRMS (ESI⁺): *m/z* calcd. for C₂₂H₂₂ClF₃N₇O₂⁺ ([*M*+*H*]⁺) 508.1470, measured 508.1443.

5-(5-Chloro-2-hydroxyphenyl)-*N*-(4-(piperazin-1-yl)-3-(trifluoromethyl)phenyl)-1*H*-pyrazole-3-carboxamide (**12A**):



Compound **12A** was prepared following GP-2 with adaptations, *N*-Boc amine **12B** (140 mg, 0.25 mmol) was reacted with TFA (6.2 mmol) and the reaction mixture stirred for 20 h. A precipitate appeared which was filtered and washed with DCM (1 mL) to obtain **12A** as light grey solid in form of a TFA salt (113 mg, 0.20 mmol, 81%).

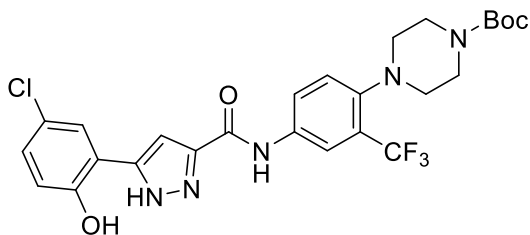
¹H NMR (400 MHz, DMSO-*d*₆) δ = 10.60 (br s, 1H), 10.49 (s, 1H), 8.83 (br s, 2H), 8.25 (s, 1H), 8.15 (dd, *J* = 8.6, 2.3 Hz, 1H), 7.81 (d, *J* = 2.3 Hz, 1H), 7.56 (d, *J* = 8.6 Hz, 1H), 7.37 (br s, 1H), 7.25 (dd, *J* = 8.6, 2.3 Hz, 1H), 7.02 (d, *J* = 8.6 Hz, 1H), 3.21 (br s, 4H), 3.04 (br s, 4H) ppm.

¹³C NMR (101 MHz, DMSO-*d*₆) δ = 158.8, 158.4, 153.4, 145.8, 136.7, 128.9, 127.9, 126.5, 126.1, 125.9, 125.1, 124.9, 122.9, 122.4, 118.5, 118.1, 106.1, 50.0, 43.6 ppm.

¹⁹F NMR (376 MHz, DMSO-*d*₆) δ = -59.31, -73.81 ppm.

HRMS (ESI⁺): *m/z* calcd. for C₂₁H₂₀ClF₃N₅O₂⁺ ([*M*+*H*]⁺) 466.1252, measured 466.1227.

tert-Butyl 4-(4-(5-(5-chloro-2-hydroxyphenyl)-1*H*-pyrazole-3-carboxamido)-2-(trifluoromethyl)phenyl)piperazine-1-carboxylate (**12B**):



Compound **12B** was prepared following GP-1 with adaptations, chromene amide **49** (401 mg, 0.83 mmol) was reacted with hydrazine hydrate (338 mg, 6.8 mmol) and the mixture stirred for 30 min. A precipitate appeared, which was filtered and washed with ice-cold EtOH (1 mL) to obtain **13B** as beige solid (405 mg, 0.81 mmol, 98%).

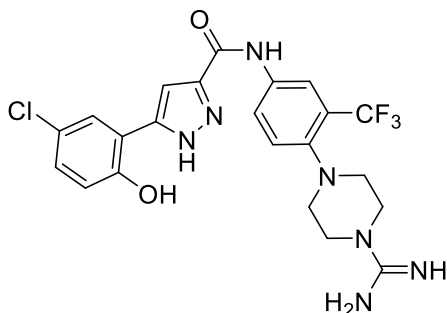
^1H NMR (400 MHz, DMSO- d_6) δ = 10.40 (br s, 1H), 8.24 (d, J = 2.3 Hz, 1H), 8.08 (dd, J = 8.6, 2.3 Hz, 1H), 7.76 (d, J = 2.3 Hz, 1H), 7.57 (d, J = 8.6 Hz, 1H), 7.34 (s, 1H), 7.20 (dd, J = 8.6, 2.3 Hz, 1H), 6.97 (d, J = 8.6 Hz, 1H), 3.43 (br s, 4H), 2.79 (br t, J = 4.7 Hz, 4H), 1.43 (s, 9H) ppm.

^{13}C NMR (101 MHz, DMSO- d_6) δ = 159.6, 153.9, 153.3, 147.1, 136.2, 128.8, 126.5, 126.1, 125.8, 125.5, 125.3, 124.8, 122.9, 122.5, 118.3, 118.1, 106.0, 79.0, 53.0, 44.2, 28.1 ppm.

^{19}F NMR (376 MHz, DMSO- d_6) δ = -59.08 ppm.

HRMS (ESI $^+$): m/z calcd. for $\text{C}_{26}\text{H}_{28}\text{ClF}_3\text{N}_5\text{O}_4^+$ ($[\text{M}+\text{H}]^+$) 566.1776, measured 566.1755.

N-(4-(4-Carbamimidoylpiperazin-1-yl)-3-(trifluoromethyl)phenyl)-5-(5-chloro-2-hydroxyphenyl)-1*H*-pyrazole-3-carboxamide (**12G**):



Compound **12G** was prepared following GP-3, amine **12A** (260 mg, 0.51 mmol) was reacted with DIPEA (403 mg, 3.12 mmol) and guanidinylation agent **65** (114 mg, 0.78 mmol). The reaction mixture stirred for 20 h and **4G** was obtained as off-white solid in form of a TFA salt (190 mg, 0.37 mmol, 75%).

^1H NMR (400 MHz, DMSO- d_6): δ = 10.51 (br s, 1H), 8.26 (br s, 1H), 8.12 (br s, 1H), 7.81 (br s, 1H), 7.61 (br s, 4H), 7.44 (br s, 1H), 7.25 (br s, 1H), 7.05 (br s, 1H), 3.54 (br s, 4H), 2.91 (br s, 4H) ppm.

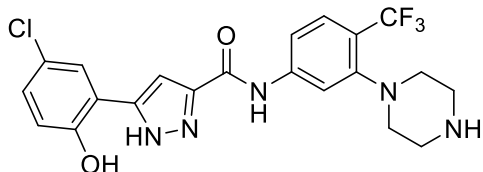
^{13}C NMR (151 MHz, DMSO- d_6) δ = 158.4, 158.2, 156.4, 153.3, 146.2, 136.5, 128.8, 126.5, 126.0, 125.5, 124.8, 124.7, 122.9,

122.9, 121.1, 118.3, 118.1, 106.1, 52.3, 45.7 ppm.

^{19}F NMR (376 MHz, DMSO- d_6) δ = -59.13, -73.65 ppm.

HRMS (ESI $^+$): m/z calcd. for $\text{C}_{22}\text{H}_{22}\text{ClF}_3\text{N}_7\text{O}_2^+$ ($[\text{M}+\text{H}]^+$) 508.1470, measured 508.1441.

5-(5-Chloro-2-hydroxyphenyl)-*N*-(3-(piperazin-1-yl)-4-(trifluoromethyl)phenyl)-1*H*-pyrazole-3-carboxamide (**13A**):



Compound **13A** was prepared following GP-2, *N*-Boc amine **13B** (150 mg, 0.27 mmol) was reacted with TFA (8.0 mmol) and the reaction mixture stirred for 3 h. Compound **13A** was obtained as white solid in form of a TFA salt in quantitative yield (150 mg, 0.27 mmol).

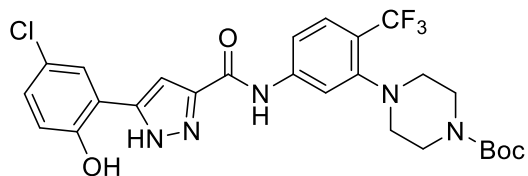
^1H NMR (400 MHz, DMSO- d_6) δ = 10.69 (br s, 1H), 10.55 (s, 1H), 8.97 (s, 1H), 8.08 (br s, 1H), 7.90 (d, J = 8.8 Hz, 1H), 7.82 (d, J = 2.4 Hz, 1H), 7.67 (d, J = 8.8 Hz, 1H), 7.41 (br s, 1H), 7.26 (dd, J = 8.8, 2.4 Hz, 1H), 7.04 (d, J = 8.8 Hz, 1H), 3.23 (br s, 4H), 3.07 (br s, 4H) ppm.

^{13}C NMR (101 MHz, DMSO- d_6) δ = 158.2, 153.3, 151.3, 143.6, 128.9, 128.1, 127.8, 126.5, 125.4, 122.9, 122.7, 120.1, 119.8, 118.1, 116.6, 115.2, 106.2, 50.0, 43.6 ppm.

^{19}F NMR (376 MHz, DMSO- d_6) δ = -58.28, -74.01 ppm.

HRMS (ESI $^+$): m/z calcd. for $\text{C}_{21}\text{H}_{20}\text{ClF}_3\text{N}_5\text{O}_2^+$ ($[\text{M}+\text{H}]^+$) 466.1252, measured 466.1227.

tert-Butyl 4-(5-(5-(5-chloro-2-hydroxyphenyl)-1*H*-pyrazole-3-carboxamido)-2-(trifluoromethyl)phenyl)piperazine-1-carboxylate (**13B**):



Compound **13B** was prepared following GP-1, chromene amide **50** (170 mg, 0.31 mmol) was reacted with hydrazine hydrate (141 mg, 2.8 mmol). The mixture stirred for 2 h and the solvent was removed under reduced pressure to obtain **13B** as white solid (169 mg, 0.30 mmol, 96%).

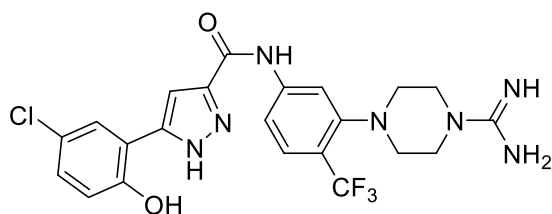
¹H NMR (400 MHz, DMSO-*d*₆) δ = 10.42 (br s, 1H), 7.99 (s, 1H), 7.90 (br d, *J* = 8.6 Hz, 1H), 7.81 (d, *J* = 2.5 Hz, 1H), 7.65 (d, *J* = 8.6 Hz, 1H), 7.41 (br s, 1H), 7.25 (dd, *J* = 8.8, 2.5 Hz, 1H), 7.02 (d, *J* = 8.8 Hz, 1H), 3.46 (br s, 4H), 2.81 (t, *J* = 4.5 Hz, 4H), 1.43 (s, 9H) ppm.

¹³C NMR (101 MHz, DMSO-*d*₆) δ = 153.9, 153.3, 152.4, 143.4, 128.9, 127.6, 126.5, 125.5, 122.9, 122.8, 120.1, 119.8, 118.1, 116.1, 115.4, 106.1, 79.0, 53.1, 28.1 ppm. Quaternary carbon peaks missing.

¹⁹F NMR (376 MHz, DMSO-*d*₆) δ = -58.03 ppm.

HRMS (ESI⁺): *m/z* calcd. for C₂₆H₂₈ClF₃N₅O₄⁺ ([*M*+*H*]⁺) 566.1776, measured 566.1751.

N-(3-(4-Carbamimidoylpiperazin-1-yl)-4-(trifluoromethyl)phenyl)-5-(5-chloro-2-hydroxyphenyl)-1*H*-pyrazole-3-carboxamide (**13G**):



Compound **13G** was prepared following GP-3, amine **13A** (129 mg, 0.23 mmol) was reacted with DIPEA (190 mg, 1.47 mmol) and guanidinylation agent **65** (52 mg, 0.36 mmol). The reaction mixture stirred for 6 h and **13G** was obtained as white solid in form of a TFA salt (103 mg, 0.20 mmol, 88%).

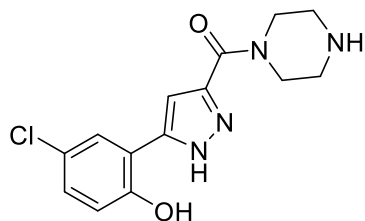
¹H NMR (400 MHz, DMSO-*d*₆) δ = 8.11 (s, 1H), 7.89 (d, *J* = 9.0 Hz, 1H), 7.61 (d, *J* = 9.0 Hz, 1H), 7.53 (br d, *J* = 2.3 Hz, 1H), 7.02 (s, 1H), 6.98 (dd, *J* = 8.6, 2.3 Hz, 1H), 6.76 (d, *J* = 8.6 Hz, 1H), 3.56 (br s, 4H), 2.93 (br s, 4H) ppm.

¹³C NMR (101 MHz, DMSO-*d*₆): δ = 162.8, 157.2, 156.7, 152.1, 149.6, 146.0, 144.7, 128.0, 126.5, 124.7, 123.4, 121.0, 120.6, 119.3, 118.5, 116.0, 115.1, 101.3, 52.8, 46.2 ppm.

¹⁹F NMR (376 MHz, DMSO-*d*₆): δ = -57.82 ppm.

HRMS (ESI⁺): *m/z* calcd. for C₂₂H₂₂ClF₃N₇O₂⁺ ([*M*+*H*]⁺) 508.1470, measured 508.1451.

(5-(5-Chloro-2-hydroxyphenyl)-1*H*-pyrazol-3-yl)(piperazin-1-yl)methanone (**14A**):



Compound **14A** was prepared following GP-2. *N*-Boc amine **14B** (280 mg, 0.69 mmol) was reacted with TFA (15 mmol) and the reaction mixture stirred overnight. Compound **4A** was obtained as grey powder in form of a TFA salt (270 mg, 0.67 mol, 98%).

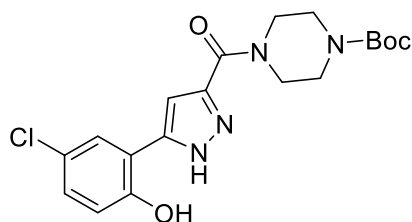
¹H NMR (400 MHz, DMSO-*d*₆) δ = 13.41 (br s, 1H), 10.71 (br s, 1H), 9.04 (br s, 2H), 7.75 (br s, 1H), 7.24 (d, *J* = 7.4 Hz, 1H), 7.14 (s, 1H), 7.00 (d, *J* = 7.4 Hz, 1H), 4.27 (br s, 2H), 3.84 (br s, 2H), 3.25-3.73 (m, 4H) ppm.

¹³C NMR (101 MHz, DMSO-*d*₆) δ = 161.9, 153.3, 146.3, 139.0, 128.9, 126.6, 122.9, 118.6, 118.1, 107.9, 43.4, 42.8 ppm.

¹⁹F NMR (376 MHz, DMSO-*d*₆) δ = -73.70 ppm.

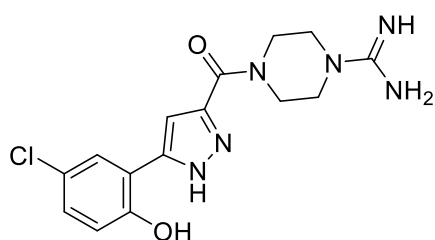
HRMS (ESI⁺): *m/z* calcd. for C₁₄H₁₆ClN₄O₂⁺ ([*M*+*H*]⁺) 307.0956, measured 307.0938.

tert-Butyl 4-(5-(5-chloro-2-hydroxyphenyl)-1*H*-pyrazole-3-carbonyl)piperazine-1-carboxylate (**14B**):



Compound **14B** was prepared following GP-1 with adaptations, chromene amide **51** (405 mg, 1.03 mmol) was reacted with hydrazine hydrate (422 mg, 8.4 mmol) and the mixture stirred for 2 h. A precipitate appeared, which was filtered and washed with ice-cold water (2 mL) to obtain **14B** as white solid (350 mg, 0.86 mmol, 83%). The product was used without further purification.

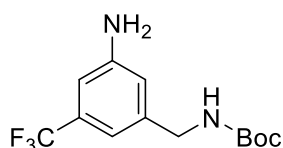
¹H NMR (400 MHz, DMSO-*d*₆) δ = 7.79 (s, 1H), 7.22 (d, *J* = 7.6 Hz, 1H), 7.15 (s, 1H), 6.98 (d, *J* = 7.6 Hz, 1H), 3.90 (br s, 1H), 3.62 (br s, 4H), 3.33 (br s, 4H), 1.42 (br s, 9H) ppm.

4-(5-(5-Chloro-2-hydroxyphenyl)-1*H*-pyrazole-3-carbonyl)piperazine-1-carboximidamide (**14G**):

Compound **14G** was prepared following GP-3 with adaptations, amine **14A** (89 mg, 0.22 mmol) was reacted with DIPEA (175 mg, 1.35 mmol) and guanidinylation agent **65** (48 mg, 0.33 mmol). The reaction mixture stirred for 2 h obtaining an off-white solid (35 mg). Part of the crude (15 mg, 43%) was purified by preparative HPLC to afford **14G** as white powder (7 mg, 0.02 mmol, 18%).

$^1\text{H NMR}$ (500 MHz, $\text{DMSO-}d_6$) δ = 8.43 (s, 1H), 7.95 (br s, 3H), 7.76 (br s, 1H), 7.21 (br d, J = 7.8 Hz, 1H), 7.15 (s, 1H), 6.99 (br d, J = 7.8 Hz, 1H), 4.11 (br s, 2H), 3.73 (br s, 2H), 3.53 (br s, 4H) ppm.

$^{13}\text{C NMR}$ (126 MHz, $\text{DMSO-}d_6$) δ = 167.2, 162.2, 157.1, 154.3, 141.8, 129.1, 126.8, 123.0, 118.6, 118.2, 107.3, 45.8, 45.6, 44.9, 41.6 ppm.

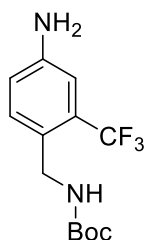
Intermediates 16–62*tert*-Butyl (3-amino-5-(trifluoromethyl)benzyl)carbamate (**16**):

To a solution of compound **54** (137 mg, 0.74 mmol, 1 eq.) in DCM (2 mL), NEt_3 (149 mg, 1.48 mmol, 2 eq.) was added and, at 0 °C Boc_2O (171 mg, 0.78 mmol, 1.06 eq.) in DCM (2 mL) was added dropwise. The mixture was allowed to slowly warm to r.t. and stirred overnight. Excess DCM was removed *in vacuo* and the crude was purified by column chromatography using 30% EtOAc in PE to obtain compound **16** (59 mg, 0.20 mmol, 28%) as a orange solid.

$^1\text{H NMR}$ (400 MHz, CDCl_3) δ = 6.89 (s, 1H), 6.79 (br s, 1H), 6.75 (br s, 1H), 4.27 (J = 4.7 Hz, 2H), 3.87 (s, 2H), 1.47 (s, 9H) ppm.

$^{13}\text{C NMR}$ (101 MHz, CDCl_3) δ = 155.9, 147.1, 141.2, 131.8, 124.0, 116.7, 113.7, 110.3, 79.7, 44.2, 28.3 ppm.

$^{19}\text{F NMR}$ (376 MHz, CDCl_3) δ = -62.96 ppm.

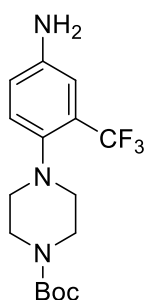
tert-Butyl (4-amino-2-(trifluoromethyl)benzyl)carbamate (**17**):

4-(aminomethyl)-3-(trifluoromethyl)aniline **55** (4126 mg, 21.7 mmol, 1 eq.) was dissolved in DCM (10 mL) and NEt_3 (4444 mg, 43.9 mmol, 2 eq.) was added. The reaction mixture was cooled to 0 °C and a cold solution of Boc_2O (4765 mg, 21.8 mmol, 1 eq) in DCM (10 mL) was added dropwise. After 6 h, the mixture was quenched with saturated bicarbonate aq. (50 mL) and extracted with DCM (3 x 50 mL). The combined organic layers were washed with brine, dried over anhydrous MgSO_4 , filtered, and concentrated *in vacuo*, obtaining an orange oil. The crude was purified by column chromatography using a gradient of 2–10% EtOAc in DCM as eluent to obtain compound **17** as orange solid (3543 mg, 12.2 mmol, 56%).

$^1\text{H NMR}$ (400 MHz, CDCl_3) δ = 7.33 (br d, J = 8.2 Hz, 1H), 6.91 (d, J = 2.0 Hz, 1H), 6.78 (dd, J = 2.0, 8.2 Hz, 1H), 4.83 (br s, 1H), 4.35 (d, J = 5.9 Hz, 2H), 3.84 (s, 2H), 1.45 (s, 9H) ppm.

$^{13}\text{C NMR}$ (101 MHz, CDCl_3) δ = 155.7, 145.7, 132.0, 128.4, 126.4, 124.3, 117.9, 112.1, 79.4, 40.8, 28.4 ppm.

$^{19}\text{F NMR}$ (376 MHz, CDCl_3) δ = -59.76 ppm.

tert-Butyl 4-(4-amino-2-(trifluoromethyl)phenyl)piperazine-1-carboxylate (**18**):

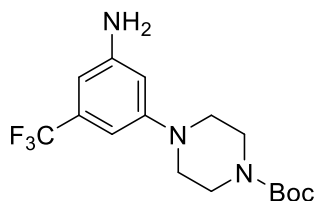
Compound **58** (136.4 mg, 0.36 mmol, 1 eq) was dissolved in EtOH (10 mL) and sodium dithionite (261.5 mg, 1.5 mmol, 4.1 eq) was added. The reaction mixture was heated to 90 °C. After 6 h the mixture was quenched with water (15 mL) and extracted with EtOAc (3 x 30 mL). The combined organic layers were washed with brine, dried over anhydrous MgSO_4 , filtered, and concentrated to dryness *in vacuo*. The resulting crude was purified by column chromatography using 30% EtOAc in PE to obtain compound **18** as a light brown powder (75.3 mg, 0.22 mmol, 60%).

$^1\text{H NMR}$ (400 MHz, CDCl_3) δ = 7.14 (d, J = 8.6 Hz, 1H), 6.91 (d, J = 2.5 Hz, 1H), 6.79 (dd, J = 2.5, 8.6 Hz, 1H), 3.76 (s, 2H), 3.52 (br s, 4H), 2.77 (br t, J = 4.5 Hz, 4H), 1.49 (s, 9H) ppm.

$^{13}\text{C NMR}$ (101 MHz, CDCl_3) δ = 154.7, 143.6, 142.7, 128.4, 125.1, 123.6, 118.3, 112.7, 79.4, 53.3, 44.4, 28.2 ppm.

^{19}F NMR (376 MHz, CDCl_3) $\delta = -60.88$ ppm.

tert-Butyl 4-(3-amino-5-(trifluoromethyl)phenyl)piperazine-1-carboxylate (**19**):



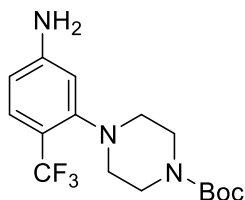
Compound **59** (2000 mg, 5.33 mmol, 1 eq.) was suspended in EtOH (20 mL) and heated to 80 °C. The solution was allowed to cool for 5 min and sodium dithionite (3794 mg, 21.8 mmol, 4.1 eq) was added under vigorous stirring. The reaction mixture was heated to 90 °C, the yellow suspension changed into a white colour and after 6 h the reaction was complete. The reaction mixture was filtered over celite while warm and water was added (50 mL). The mixture was extracted with EtOAc (3 x 50 mL) and the combined organic layers were washed with brine, dried over anhydrous MgSO_4 , filtered, and concentrated to dryness *in vacuo*. The resulting crude was purified by column chromatography using 2.5% MeOH in DCM to obtain compound **19** as a pale yellow powder (1181 mg, 3.42 mmol, 64%).

^1H NMR (400 MHz, CDCl_3) $\delta = 6.55$ (s, 1H), 6.44 (s, 1H), 6.34 (s, 1H), 3.79 (s, 2H), 3.60 (s, 4H), 3.11 (s, 4H), 1.49 (s, 9H) ppm.

^{13}C NMR (101 MHz, CDCl_3) $\delta = 154.6, 152.5, 147.7, 132.3, 125.0, 105.1, 103.4, 80.0, 48.9, 41.9, 28.4$ ppm.

^{19}F NMR (376 MHz, CDCl_3) $\delta = -63.15$ ppm.

tert-Butyl 4-(5-amino-2-(trifluoromethyl)phenyl)piperazine-1-carboxylate (**20**):



Compound **62** (3332 mg, 8.9 mmol, 1 eq.) was dissolved in EtOH (30 mL) and heated to 50 °C. Sodium dithionite (6284 mg, 36.1 mmol, 4.1 eq.) was added to the stirring solution. The reaction mixture stirred at reflux for 6 h and was filtered over celite while warm and water was added (50 mL). The mixture was extracted with EtOAc (3 x 50 mL) and the combined organic layers were washed with brine, dried over anhydrous MgSO_4 , filtered, and concentrated to dryness *in vacuo*. The resulting crude was purified by column chromatography using 15% EtOAc in DCM

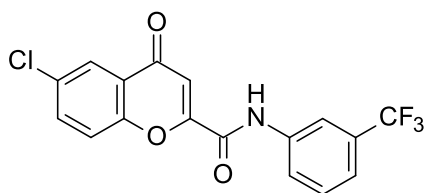
to obtain compound **20** as a pale yellow powder (506 mg, 1.46 mmol, 17%).

^1H NMR (400 MHz, CDCl_3) $\delta = 7.37$ (d, $J = 8.2$ Hz, 1H), 6.51 (s, 1H), 6.45 (d, $J = 8.6$ Hz, 1H), 3.99 (s, 2H), 3.57 (br t, $J = 4.5$ Hz, 4H), 2.82 (br t, $J = 4.5$ Hz, 4H), 1.48 (s, 9H) ppm.

^{13}C NMR (101 MHz, CDCl_3) $\delta = 154.9, 153.6, 150.4, 128.6, 124.5, 116.5, 110.5, 109.3, 79.6, 53.2, 44.6, 28.4$ ppm.

^{19}F NMR (376 MHz, CDCl_3) $\delta = -58.78$ ppm.

6-Chloro-4-oxo-*N*-[3-(trifluoromethyl)phenyl]chromene-2-carboxamide (**34**):



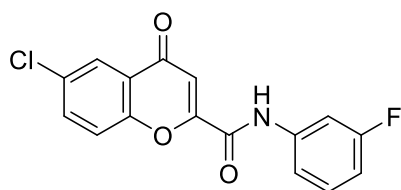
Compound **34** was prepared following GP-4, carboxylic acid **15** (537 mg, 2.33 mmol) was reacted with DIPEA (353 mg, 2.66 mmol), HATU (1037 mg, 2.66 mmol) and 3-(trifluoromethyl)aniline **21** (362 mg, 2.22 mmol). The reaction mixture stirred for 22 h and the resulting crude was washed with EtOH (2 mL), filtered, and evaporated to dryness to obtain compound **34** as white powder (419 mg, 1.14 mmol, 51%).

^1H NMR (400 MHz, $\text{DMSO}-d_6$): $\delta = 11.00$ (s, 1H), 8.19 (s, 1H), 8.06 (d, $J = 8.6$ Hz, 1H), 7.94 (d, $J = 8.6$ Hz, 1H), 7.85 (d, $J = 8.6$ Hz, 1H), 7.64 (t, $J = 8.0$ Hz, 1H), 7.53 (d, $J = 8.0$ Hz, 1H), 7.00 (s, 1H) ppm.

^{13}C NMR (101 MHz, $\text{DMSO}-d_6$): $\delta = 176.6, 158.3, 155.8, 154.1, 138.8, 135.5, 131.1, 130.6, 130.1, 129.8, 125.2, 125.0, 124.4, 121.9, 121.7, 117.6, 111.7$ ppm.

^{19}F NMR (470 MHz, $\text{DMSO}-d_6$) $\delta = -61.31$ ppm.

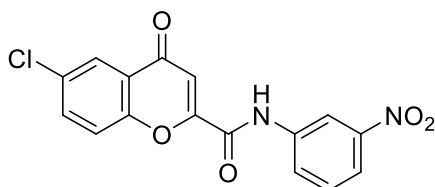
6-Chloro-*N*-(3-fluorophenyl)-4-oxo-4*H*-chromene-2-carboxamide (**35**):



Compound **35** was prepared following GP-4, carboxylic acid **15** (263 mg, 1.17 mmol) was reacted with DIPEA (182 mg, 1.41 mmol), HATU (534 mg, 1.41 mmol) and 3-fluoroaniline **22** (124 mg, 1.11 mmol). The reaction mixture stirred for 4 h at rt, obtaining compound **35** as yellow powder (335 mg, 1.05 mmol, 95%). The product was used without further purification.

^1H NMR (400 MHz, DMSO- d_6) δ = 10.85 (br s, 1H), 7.98 (d, J = 2.2 Hz, 1H), 7.96 (dd, J = 8.8, 2.2 Hz, 1H), 7.86 (br d, J = 8.8 Hz, 1H), 7.71 (br d, J = 11.7 Hz, 1H), 7.59 (br d, J = 8.2 Hz, 1H), 7.45 (dd, J = 8.2, 6.6 Hz, 1H), 7.03 (br t, J = 8.2 Hz, 1H), 6.99 (s, 1H) ppm.

6-Chloro-*N*-(3-nitrophenyl)-4-oxo-4*H*-chromene-2-carboxamide (**36**):

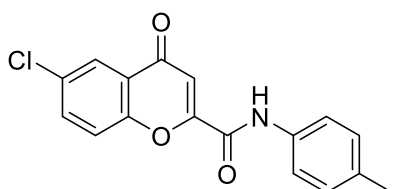


Compound **36** was prepared following GP-4 with adaptations, carboxylic acid **15** (263 mg, 1.17 mmol) was reacted with DIPEA (182 mg, 1.41 mmol), HATU (534 mg, 1.41 mmol) and 3-nitroaniline **23** (154 mg, 1.11 mmol) overnight at r.t. and at 80 °C for 20 h. The crude mixture was purified by flash column chromatography using 20% EtOAc in PE as eluent to obtain compound **36** as yellow powder (160 mg, 0.46 mmol, 34%).

^1H NMR (400 MHz, DMSO- d_6) δ = 11.07 (br s, 1H), 8.71 (s, 1H), 8.20 (d, J = 7.4 Hz, 1H), 8.02 (d, J = 7.8 Hz, 1H), 7.97 - 7.89 (m, 2H), 7.87 - 7.77 (m, 1H), 7.68 (t, J = 8.2 Hz, 1H), 6.99 (s, 1H) ppm.

^{13}C NMR (101 MHz, DMSO- d_6) δ = 176.6, 158.4, 155.6, 154.1, 148.3, 139.1, 135.5, 131.1, 130.8, 127.2, 125.2, 124.4, 121.8, 119.8, 115.6, 111.8 ppm.

6-Chloro-4-oxo-*N*-(*p*-tolyl)-4*H*-chromene-2-carboxamide (**37**):

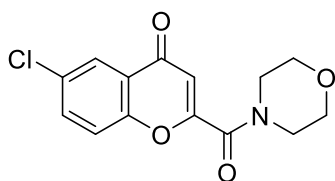


Compound **37** was prepared following GP-4, carboxylic acid **15** (200 mg, 0.89 mmol) was reacted with DIPEA (132 mg, 1.02 mmol), HATU (387 mg, 1.02 mmol) and *p*-toluidine **24** (91 mg, 0.85 mmol). The reaction mixture stirred for 2 h, obtaining compound **37** as off-white solid (122 mg, 0.39 mmol, 46%).

^1H NMR (400 MHz, DMSO- d_6) δ = 10.68 (br s, 1H), 8.01 (d, J = 2.3 Hz, 1H), 7.98 (br dd, J = 2.3, 9.0 Hz, 1H), 7.89 (br d, J = 9.3 Hz, 1H), 7.67 (br d, J = 8.2 Hz, 2H), 7.22 (br d, J = 8.2 Hz, 2H), 6.99 (s, 1H), 2.30 (s, 3H) ppm.

^{13}C NMR (101 MHz, DMSO- d_6) δ = 176.8, 157.7, 156.4, 154.2, 135.4, 135.4, 134.7, 131.0, 129.7, 125.3, 124.4, 122.0, 121.5, 111.4, 21.0 ppm.

6-Chloro-2-(morpholine-4-carbonyl)-4*H*-chromen-4-one (**38**):

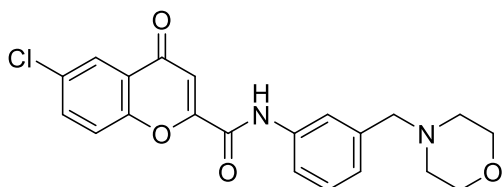


Compound **38** was prepared following GP-4, carboxylic acid **15** (308 mg, 0.89 mmol) was reacted with DIPEA (212 mg, 1.6 mmol), HATU (610 mg, 1.6 mmol) and morpholine **25** (109 mg, 1.25 mmol). The reaction mixture stirred for 24 h and was quenched with water (20 mL) and extracted with EtOAc (3 x 20 mL). The combined organic layers were washed with brine, dried over anhydrous MgSO_4 , filtered, and concentrated *in vacuo*, obtaining a yellow oil. The crude was purified by column chromatography using 10% MeOH in DCM to obtain compound **38** as yellow powder (110 mg, 0.37 mmol, 28%).

^1H NMR (400 MHz, DMSO- d_6) δ = 7.98 (d, J = 2.5 Hz, 1H), 7.90 (dd, J = 2.5, 9.0 Hz, 1H), 7.77 (d, J = 9.0 Hz, 1H), 6.63 (s, 1H), 3.54-3.71 (m, 8H) ppm.

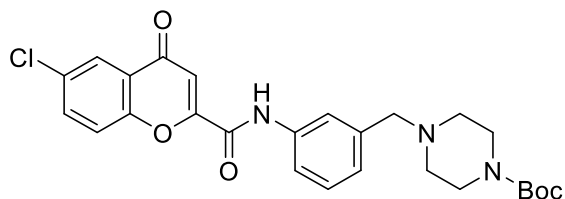
^{13}C NMR (101 MHz, DMSO- d_6) δ = 176.03, 160.40, 158.23, 154.51, 134.98, 130.84, 125.29, 124.29, 121.60, 111.19, 66.59, 66.12, 47.33, 42.54 ppm.

6-Chloro-*N*-(3-(morpholinomethyl)phenyl)-4-oxo-4*H*-chromene-2-carboxamide (**39**):



Compound **39** was prepared following GP-4, carboxylic acid **15** (200 mg, 0.89 mmol) was reacted with 3-(morpholinomethyl)aniline **26** (163 mg, 0.85 mmol) and the reaction mixture stirred for 4 h. White precipitate was filtered, obtaining compound **39** (277 mg, 0.69 mmol, 76%). The product was used without further purification.

^1H NMR (400 MHz, DMSO- d_6) δ = 11.13 (br s, 1H), 8.02 (br s, 1H), 8.03 - 7.92 (m, 2H), 7.85 (br d, J = 7.4 Hz, 1H), 7.56 (br s), 7.43 (br t, J = 7.4 Hz, 1H), 7.00 (s, 1H), 4.30 (br s, 2H), 3.84 (br s, 4H), 3.07 (br s, 4H) ppm.

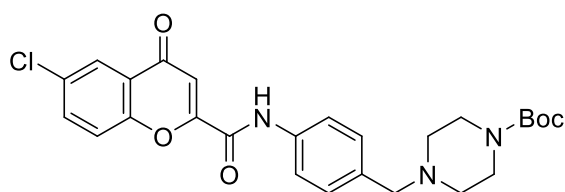
tert-Butyl 4-(3-(6-chloro-4-oxo-4H-chromene-2-carboxamido)benzyl)piperazine-1-carboxylate (40):

Compound **40** was prepared following GP-4, carboxylic acid **15** (250 mg, 1.11 mmol) was reacted with DIPEA (164 mg, 1.27 mmol), HATU (484 mg, 1.27 mmol) and *tert*-butyl 4-(3-aminobenzyl)piperazine-1-carboxylate **27** (309 mg, 1.06 mmol). The reaction mixture stirred for 2 h and the resulting crude was washed with DCM (2 mL), filtered,

and evaporated to dryness to obtain compound **40** as off-white powder (277 mg, 0.56 mmol, 50%).

^1H NMR (400 MHz, DMSO- d_6) δ = 10.90 (br s, 1H), 8.05 (br s, 1H), 8.03 - 7.94 (m, 2H), 7.87 (br d, J = 8.6 Hz, 1H), 7.78 (br d, J = 7.8 Hz, 1H), 7.54 (br t, J = 7.2 Hz, 1H), 7.34 (br d, J = 6.6 Hz, 1H), 7.01 (br s, 1H), 4.37 (br s, 2H), 3.06 (br s, 4H), 2.49 (br s, 4H), 1.41 (s, 9H) ppm.

^{13}C NMR (101 MHz, DMSO- d_6) δ = 176.7, 158.1, 156.1, 154.2, 153.7, 138.3, 135.5, 131.1, 130.0, 128.3, 125.3, 124.4, 124.1, 124.1, 122.8, 121.9, 111.6, 80.4, 59.5, 51.0, 40.6, 28.4 ppm.

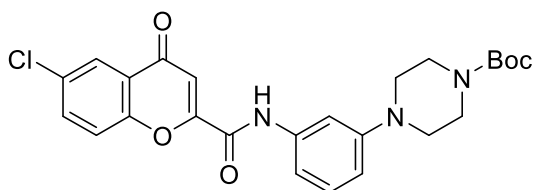
tert-Butyl 4-(4-(6-chloro-4-oxo-4H-chromene-2-carboxamido)benzyl)piperazine-1-carboxylate (41):

Compound **41** was prepared following GP-4, carboxylic acid **15** (250 mg, 1.11 mmol) was reacted with DIPEA (164 mg, 1.27 mmol), HATU (484 mg, 1.27 mmol) and *tert*-butyl 4-(4-aminobenzyl)piperazine-1-carboxylate **28** (309 mg, 1.06 mmol). The reaction mixture stirred for 2 h and the crude was purified by flash column

chromatography using 5% MeOH in DCM as eluent to obtain compound **41** as off-white powder (172 mg, 0.35 mmol, 31%).

^1H NMR (400 MHz, DMSO- d_6) δ = 10.72 (br s, 1H), 8.00 (br d, J = 2.3 Hz, 1H), 7.97 (br dd, J = 2.3, 8.6 Hz, 1H), 7.88 (br d, J = 7.0 Hz, 1H), 7.73 (br d, J = 8.6 Hz, 2H), 7.33 (br d, J = 8.2 Hz, 2H), 6.99 (br s, 1H), 3.46 (br s, 2H), 3.30 - 3.24 (m, 4H), 2.30 (br t, J = 5.4 Hz, 4H), 1.37 (s, 9H) ppm.

^{13}C NMR (101 MHz, DMSO- d_6) δ = 176.7, 157.8, 156.4, 154.3, 154.2, 136.8, 135.4, 135.0, 131.0, 129.8, 125.3, 124.4, 122.0, 121.3, 111.4, 79.2, 61.9, 52.8, 43.4, 28.5 ppm.

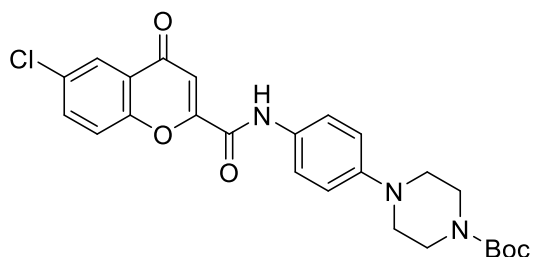
tert-Butyl 4-(3-(6-chloro-4-oxo-4H-chromene-2-carboxamido)phenyl)piperazine-1-carboxylate (42):

Compound **42** was prepared following GP-4, carboxylic acid **15** (310 mg, 1.38 mmol) was reacted with DIPEA (204 mg, 1.58 mmol), HATU (600 mg, 1.58 mmol) and *tert*-butyl 4-(3-aminophenyl)piperazine-1-carboxylate **29** (365 mg, 1.32 mmol). The reaction mixture stirred for 1 h and the resulting crude was impregnated on silica and purified by flash column chromatography using 5%

MeOH in DCM as eluent to obtain compound **42** as off-white powder (230 mg, 0.48 mmol, 34%).

^1H NMR (400 MHz, DMSO- d_6) δ = 10.59 (br s, 1H), 8.03 - 7.95 (m, 2H), 7.89 (br d, J = 9.2 Hz, 1H), 7.40 (br s, 1H), 7.31 - 7.22 (m, 2H), 6.98 (br s, 1H), 6.80 (br d, J = 6.2 Hz, 1H), 3.48 (br s, 4H), 3.12 (br s, 4H), 1.42 (s, 9H) ppm.

^{13}C NMR (101 MHz, DMSO- d_6): δ = 176.7, 157.7, 156.4, 154.4, 154.2, 151.7, 138.7, 135.4, 131.0, 129.7, 125.3, 124.4, 122.0, 113.3, 112.6, 111.4, 109.0, 79.5, 48.7, 28.5 ppm.

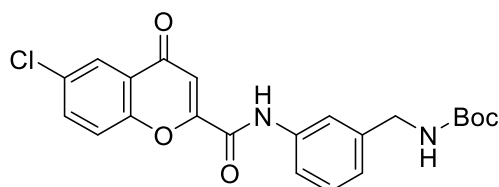
tert-Butyl 4-(4-(6-chloro-4-oxo-4H-chromene-2-carboxamido)phenyl)piperazine-1-carboxylate (43):

Compound **43** was prepared following GP-4, carboxylic acid **15** (250 mg, 1.11 mmol) was reacted with DIPEA (164 mg, 1.27 mmol), HATU (484 mg, 1.27 mmol) and *tert*-butyl 4-(4-aminophenyl)piperazine-1-carboxylate **30** (294 mg, 1.06 mmol). The reaction mixture stirred for 1 h the resulting crude was washed with EtOAc (2 mL) to obtain compound **43** as yellow powder (220mg, 0.45 mmol, 41%).

^1H NMR (400 MHz, $\text{DMSO-}d_6$) δ = 10.59 (br s, 1H), 8.00 (br d, J = 2.5 Hz, 1H), 7.96 (dd, J = 2.5, 9.0 Hz, 1H), 7.87 (d, J = 9.0 Hz, 1H), 7.65 (d, J = 9.0 Hz, 2H), 6.99 (d, J = 9.0 Hz, 2H), 6.96 (s, 1H), 3.46 (br t, J = 5.3 Hz, 4H), 3.10 (br t, J = 5.1 Hz, 4H), 1.42 (s, 9H) ppm.

^{13}C NMR (101 MHz, $\text{DMSO-}d_6$) δ = 176.7, 157.2, 156.6, 154.3, 148.6, 135.4, 131.0, 129.9, 125.3, 124.4, 123.4, 122.5, 121.8, 116.7, 111.2, 79.4, 49.3, 48.8, 28.5 ppm.

tert-Butyl (3-(6-chloro-4-oxo-4*H*-chromene-2-carboxamido)benzyl)carbamate (**44**):

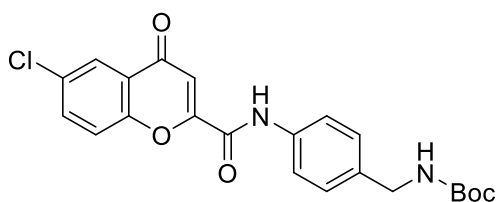


Compound **44** was prepared following GP-4, carboxylic acid **15** (250 mg, 1.11 mmol) was reacted with DIPEA (164 mg, 1.27 mmol), HATU (484 mg, 1.27 mmol) and *tert*-butyl (3-aminobenzyl)carbamate **27** (236 mg, 1.06 mmol). The reaction mixture stirred for 2 h, obtaining compound **44** as off-white powder (232 mg, 0.54 mmol, 49%).

^1H NMR (400 MHz, $\text{DMSO-}d_6$) δ = 10.76 (br s, 1H), 8.03 - 7.95 (m, 2H), 7.89 (br d, J = 9.4 Hz, 1H), 7.73 - 7.63 (m, 2H), 7.44 (br s, 1H), 7.36 (t, J = 7.8 Hz, 1H), 7.08 (br d, J = 7.4 Hz, 1H), 6.99 (br s, 1H), 4.15 (br d, J = 5.5 Hz, 2H), 1.40 (s, 9H) ppm.

^{13}C NMR (101 MHz, $\text{DMSO-}d_6$) δ = 176.8, 157.9, 156.4, 156.3, 154.2, 141.5, 137.9, 135.4, 131.0, 129.2, 125.3, 124.4, 124.1, 122.0, 120.1, 119.9, 111.4, 78.3, 43.8, 28.7 ppm.

tert-Butyl (4-(6-chloro-4-oxo-4*H*-chromene-2-carboxamido)benzyl)carbamate (**45**):

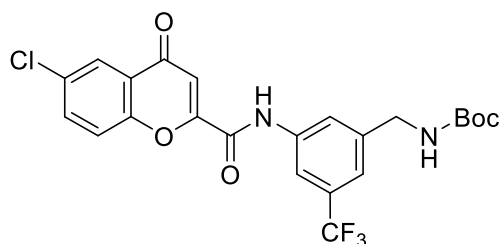


Compound **45** was prepared following GP-4, carboxylic acid **15** (250 mg, 1.11 mmol) was reacted with DIPEA (164 mg, 1.27 mmol), HATU (484 mg, 1.27 mmol) and *tert*-butyl (4-aminobenzyl)carbamate **28** (236 mg, 1.06 mmol). The reaction mixture stirred for 1 h, the crude was washed with acetone (2 mL) to obtain compound **45** as off-white powder (188 mg, 0.44 mmol, 39%).

^1H NMR (400 MHz, $\text{DMSO-}d_6$) δ = 10.73 (br s, 1H), 8.03 - 7.94 (m, 2H), 7.88 (br d, J = 8.9 Hz, 1H), 7.72 (br d, J = 7.0 Hz, 2H), 7.39 (br s, 1H), 7.28 (br d, J = 8.5 Hz, 2H), 6.99 (br s, 1H), 4.12 (br d, J = 3.6 Hz, 2H), 1.40 (s, 9H) ppm.

^{13}C NMR (101 MHz, $\text{DMSO-}d_6$) δ = 176.7, 157.8, 156.3, 156.2, 154.2, 137.4, 136.4, 135.4, 131.0, 127.8, 125.3, 124.4, 122.0, 121.5, 111.4, 78.3, 43.5, 28.7 ppm.

tert-Butyl (3-(6-chloro-4-oxo-4*H*-chromene-2-carboxamido)-5-(trifluoromethyl)benzyl)carbamate (**46**):

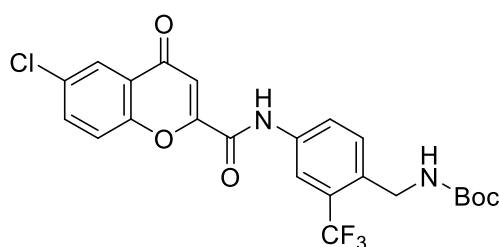


Compound **46** was prepared following GP-4, carboxylic acid **15** (105 mg, 0.47 mmol) was reacted with DIPEA (74 mg, 0.57 mmol), HATU (216 mg, 0.57 mmol) and aniline **16** (138 mg, 0.48 mmol). The reaction mixture stirred for 48 h, obtaining compound **46** as yellow powder (220 mg, 0.44 mmol, 95%).

^1H NMR (400 MHz, $\text{DMSO-}d_6$) δ = 11.01 (br s, 1H), 8.11 (s, 1H), 8.00 (s, 1H), 7.97 (s, 1H), 7.87 (d, J = 8.6 Hz, 1H), 7.55 (br s, 1H), 7.41 (s, 1H), 7.02 (s, 1H), 4.24 (d, J = 5.1 Hz, 2H), 1.41 (s, 9H) ppm.

^{19}F NMR (376 MHz, $\text{DMSO-}d_6$) δ = -61.41 ppm.

tert-Butyl *N*-[[4-[(6-chloro-4-oxo-chromene-2-carbonyl)amino]-2-(trifluoromethyl)phenyl]methyl]carbamate (**47**):



Compound **47** was prepared following GP-4 with adaptations, carboxylic acid **15** (2559 mg, 11.4 mmol) was reacted with DIPEA (1693 mg, 13.1 mmol), HATU (4968 mg, 13.1 mmol) and aniline **17** (3171 mg, 10.9 mmol). The reaction mixture stirred for 4 h, quenched with water (100 mL) and extracted with EtOAc (3 x 100 mL). The combined organic layers were washed with brine, dried over anhydrous MgSO_4 , filtered, and concentrated under

2. Chapter

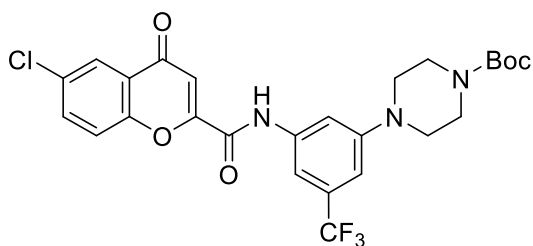
reduced pressure. The crude was triturated with MeOH (10 mL) to obtain compound **47** as yellow powder (2050 mg, 4.1 mmol, 38%).

^1H NMR (400 MHz, DMSO- d_6) δ = 10.98 (s, 1H), 8.18 (s, 1H), 8.09 (d, J = 8.2 Hz, 1H), 8.00 (s, 1H), 7.87 (d, J = 9.0 Hz, 1H), 7.54 (d, J = 8.6 Hz, 1H), 7.51 (s, 1H), 7.02 (s, 1H), 4.31 (d, J = 5.1 Hz, 2H), 1.42 (s, 9H) ppm.

^{13}C NMR (101 MHz, DMSO- d_6) δ = 176.2, 157.7, 155.8, 155.4, 153.6, 136.5, 135.0, 134.4, 130.6, 128.9, 126.4, 124.8, 124.4, 123.9, 122.8, 121.4, 118.0, 111.2, 78.2, 40.1, 28.2 ppm.

^{19}F NMR (376 MHz, DMSO- d_6) δ = -59.32 ppm.

tert-Butyl 4-[3-[(6-chloro-4-oxo-chromene-2-carbonyl)amino]-5-(trifluoromethyl)phenyl]piperazine-1-carboxylate (**48**):



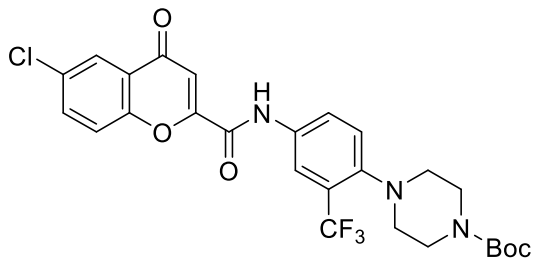
Compound **48** was prepared following GP-4, carboxylic acid **15** (530 mg, 2.36 mmol) was reacted with DIPEA (363 mg, 2.8 mmol), HATU (1074 mg, 2.8 mmol) and aniline **19** (138 mg, 0.48 mmol). The reaction mixture stirred for 24 h, and the crude was washed with ice-cold EtOH (5 mL) to obtain compound **48** as pale yellow powder (646.6 mg, 1.17 mmol, 52%).

^1H NMR (400 MHz, DMSO- d_6) δ = 8.01 (s, 1H), 7.98 (d, J = 2.7 Hz, 1H), 7.88 (d, J = 9.0 Hz, 1H), 7.65 (s, 1H), 7.64 (s, 1H), 7.06 (s, 1H), 7.01 (s, 1H), 3.49 (br s, 4H), 3.23 (br s, 4H), 1.43 (s, 9H) ppm.

^{13}C NMR (101 MHz, DMSO- d_6) δ = 176.2, 157.7, 155.49, 153.9, 153.6, 151.5, 139.1, 135.0, 130.6, 130.4, 130.1, 129.8, 130.1, 128.2, 125.5, 124.0, 121.4, 121.5, 111.1, 110.6, 108.1, 107.4, 79.1, 47.6, 39.9, 28.1 ppm.

^{19}F NMR (376 MHz, DMSO- d_6) δ = -61.38 ppm.

tert-Butyl 4-[4-[(6-chloro-4-oxo-chromene-2-carbonyl)amino]-2-(trifluoromethyl)phenyl]piperazine-1-carboxylate (**49**):



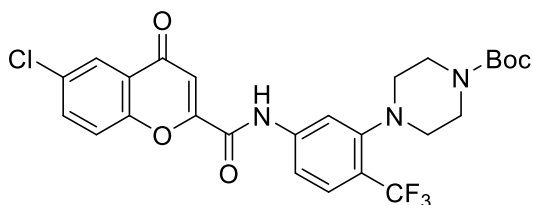
Compound **49** was prepared following GP-4, carboxylic acid **15** (248 mg, 1.1 mmol) was reacted with DIPEA (176 mg, 1.34 mmol), HATU (509 mg, 1.34 mmol) and aniline **18** (138 mg, 0.48 mmol). The reaction mixture stirred for 24 h, and the crude was washed with diethyl ether (3 mL) to obtain compound **49** as white powder (311 mg, 0.56 mmol, 51%).

^1H NMR (400 MHz, DMSO- d_6) δ = 10.93 (s, 1H), 8.15 (s, 1H), 8.08 (d, J = 9.0 Hz, 1H), 8.00 (s, 1H), 7.97 (br s, 1H), 7.87 (d, J = 8.6 Hz, 1H), 7.63 (d, J = 8.2 Hz, 1H), 7.01 (s, 1H), 3.43 (br s, 4H), 2.81 (br s, 4H), 1.43 (s, 9H) ppm.

^{13}C NMR (101 MHz, DMSO- d_6) δ = 153.9, 153.3, 147.1, 136.2, 128.8, 126.5, 126.1, 125.8, 125.5, 125.3, 124.8, 122.9, 123.9, 118.3, 118.1, 106.0, 79.0, 53.0, 44.1, 28.1 ppm.

^{19}F NMR (376 MHz, DMSO- d_6) δ = -58.99 ppm.

tert-Butyl 4-[5-[(6-chloro-4-oxo-chromene-2-carbonyl)amino]-2-(trifluoromethyl)phenyl]piperazine-1-carboxylate (**50**):



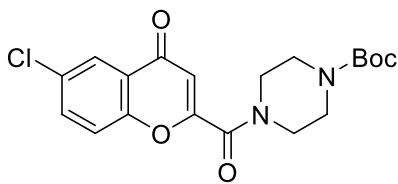
Compound **50** was prepared following GP-4, carboxylic acid **15** (295 mg, 1.3 mmol) was reacted with DIPEA (210 mg, 1.6 mmol), HATU (592 mg, 1.6 mmol) and aniline **20** (421 mg, 1.22 mmol). The reaction mixture stirred for 24 h, and the crude was purified by column chromatography using 5% MeOH in DCM to obtain compound **50** as pale yellow powder (204 mg,

0.37 mmol, 28%).

^1H NMR (400 MHz, DMSO- d_6) δ = 10.89 (s, 1H), 7.97 (s, 1H), 7.95 (d, J = 1.0 Hz, 1H), 7.91 (s, 1H), 7.85 (d, J = 9.8 Hz, 1H), 7.81 (br d, J = 8.6 Hz, 1H), 7.69 (d, J = 8.6 Hz, 1H), 7.00 (s, 1H), 3.46 (br s, 4H), 2.82 (br t, J = 3.9 Hz, 4H), 1.43 (s, 9H) ppm.

^{13}C NMR (101 MHz, DMSO- d_6) δ = 176.1, 157.8, 155.2, 153.8, 153.6, 152.4, 142.0, 135.0, 130.6, 127.9, 124.8, 123.9, 123.9, 121.4, 121.2, 116.9, 116.0, 111.3, 79.0, 53.1, 43.5, 28.0 ppm.

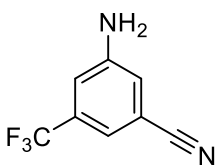
^{19}F NMR (376 MHz, DMSO- d_6) δ = 58.35 ppm.

tert-Butyl 4-(6-chloro-4-oxo-chromene-2-carbonyl)piperazine-1-carboxylate (51):

Compound **51** was prepared following GP-4 with adaptations, carboxylic acid **15** (996.0 mg, 4.43 mmol) was reacted with DIPEA (700 mg, 5.4 mmol), HATU (2037 mg, 5.4 mmol) and *tert*-butyl piperazine-1-carboxylate **33** (797 mg, 4.3 mmol). The reaction mixture stirred for 72 h, quenched with water (25 mL) and extracted with EtOAc (3 x 25 mL). The combined organic layers were washed with brine, dried over anhydrous MgSO₄, filtered, and the solvent was removed under reduced pressure. The resulting crude was triturated with ice-cold MeOH (5 mL) to obtain compound **51** as light grey powder (463 mg, 1.18 mmol, 27%).

¹H NMR (400 MHz, DMSO-*d*₆) δ = 7.96 (br s, 1H), 7.88 (br s, 1H), 7.76 (br d, *J* = 2.3 Hz, 1H), 6.61 (br s, 1H), 3.53 (s, 4H), 3.29 (br s, 4H), 1.39 (br s, 9H) ppm.

¹³C NMR (101 MHz, DMSO-*d*₆) δ = 175.6, 160.1, 157.9, 154.1, 153.7, 134.6, 130.4, 124.8, 123.8, 121.2, 110.7, 79.3, 46.2, 41.6, 28.0 ppm.

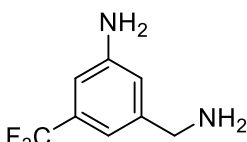
3-Amino-5-(trifluoromethyl)benzonitrile (53):

3-Nitro-5-(trifluoromethyl)benzonitrile **52** (2471 mg, 11.4 mmol, 1 eq.) and ammonium chloride (2446.0 mg, 46.4 mmol, 4 eq.) were dissolved and stirred in EtOH (25 mL) and water (12.5 mL). After heating to 90 °C for 30 minutes, 70 mesh >99% iron powder (2593.2 mg, 46.4 mmol, 4.1 eq) was added. TLC (20% EtOAc/PE) overnight showed full conversion of the starting material. The mixture was quenched with saturated bicarbonate solution (30 mL) and extracted with EtOAc (30 mL). The combined organic layers were washed with brine, dried over anhydrous MgSO₄, filtered, and concentrated *in vacuo*. The crude was purified by column chromatography 25% EtOAc in petroleum ether (PE) to obtain compound **53** as a yellow oil (1362 mg, 7.3 mmol, 64%).

¹H NMR (400 MHz, CDCl₃) δ = 7.24 (s, 1H), 7.08 (s, 1H), 7.05 (s, 1H), 4.15 (s, 2H) ppm.

¹³C NMR (101 MHz, CDCl₃) δ = 147.5, 133.1, 122.9, 120.1, 117.9, 115.1, 113.9 ppm.

¹⁹F NMR (376 MHz, CDCl₃) δ = -63.52 ppm.

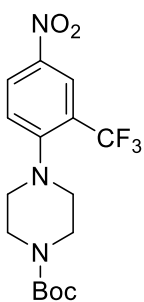
3-(Aminomethyl)-5-(trifluoromethyl)aniline (54):

A solution of nitrile **53** (1340 mg, 7.20 mmol, 1 eq.) in THF (5 mL) was added dropwise to a solution of LiAlH₄ (15 mL, 36 mmol, 2.4 M) in THF (20 mL). After the addition was completed, the reaction mixture was heated to reflux and after 4 h quenched with slow addition of NaOH aq. (50 mL, 1M). A solution of Rochelle salt (500 mg) in water (10 mL) was added, and the mixture extracted with EtOAc (3 x 30 mL). The combined organic layers were washed with brine, dried over anhydrous MgSO₄, and filtered. The solvent was removed under reduced pressure to obtain compound **54** in quantitative yield (1577 mg, 8.29 mmol). The product was used without further purification.

¹H NMR (400 MHz, CDCl₃) δ = 6.94 (s, 1H), 6.84 (br s, 2H), 6.77 (s, 1H), 4.38 (s, 2H), 3.83 (s, 2H) ppm.

¹³C NMR (101 MHz, CDCl₃) δ = 147.0, 145.1, 131.7, 124.1, 116.5, 113.6, 109.9, 46.0 ppm.

¹⁹F NMR (376 MHz, CDCl₃) δ = -62.83 ppm.

tert-Butyl 4-(4-nitro-2-(trifluoromethyl)phenyl)piperazine-1-carboxylate (58):

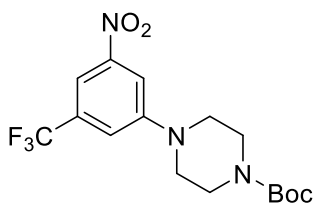
To a solution of 1-fluoro-4-nitro-2-(trifluoromethyl)benzene **56** (500 mg, 2.39 mmol, 1 eq.) in DMSO (5 mL), *tert*-butyl piperazine-1-carboxylate **33** (668 mg, 3.59 mmol, 1.5 eq.) and potassium carbonate (690 mg, 5.0 mmol, 2.1 eq) were added and the reaction mixture stirred for 18 h at 100 °C. Once completed, the reaction was quenched with water (10 mL) and extracted with EtOAc (3 x 30 mL). The combined organic layers were washed with brine, dried over anhydrous MgSO₄, filtered, and concentrated to dryness *in vacuo* to obtain a sticky solid (883 mg). Part of the crude (364 mg, 41%) was purified by column chromatography (25% EtOAc in PE) to obtain compound **10** as a yellow solid (187 mg, 0.50 mmol, 50%).

¹H NMR (400 MHz, CDCl₃) δ = 8.52 (d, *J* = 2.7 Hz, 1H), 8.35 (dd, *J* = 2.7, 9.0 Hz, 1H), 7.30 (d, *J* = 9.0 Hz, 1H), 3.60 (t, *J* = 5.1 Hz, 4H), 3.06 (t, *J* = 4.7 Hz, 4H), 1.49 (s, 9H) ppm.

¹³C NMR (101 MHz, CDCl₃) δ = 157.0, 154.6, 142.7, 127.9, 125.2, 124.4, 122.8, 123.0, 80.1, 52.7, 44.1, 28.4 ppm.

^{19}F NMR (376 MHz, CDCl_3) δ = -60.23 ppm.

tert-Butyl 4-[3-nitro-5-(trifluoromethyl)phenyl]piperazine-1-carboxylate (**59**):



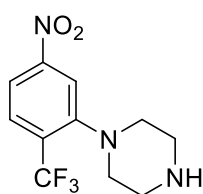
To a solution of 1-fluoro-3-nitro-5-(trifluoromethyl)benzene **57** (1506 mg, 7.2 mmol, 1 eq.) in DMSO (10 mL), *tert*-butyl piperazine-1-carboxylate **33** (1473 mg, 7.91 mmol, 1.1 eq.) and potassium carbonate (1995 mg, 14.4 mmol, 2 eq.) were added and the mixture was heated to 100 °C. After 20 h the reaction was complete and was quenched with water (50 mL). The mixture was extracted with EtOAc (3 x 50 mL) and the combined organic layers were washed with brine, dried over anhydrous MgSO_4 , filtered, and concentrated to dryness *in vacuo*. The resulting crude was purified by column chromatography (10% EtOAc in PE) to obtain compound **59** (2001 mg, 5.33 mmol, 74%) as an orange powder.

^1H NMR (400 MHz, CDCl_3) δ = 7.90 (s, 1H), 7.86 (t, J = 2.1 Hz, 1H), 7.36 (s, 1H), 3.64 (br t, J = 3.1 Hz, 4H), 3.34 (br t, J = 5.5 Hz, 4H), 1.50 (s, 9H) ppm.

^{13}C NMR (101 MHz, CDCl_3) δ = 154.5, 151.9, 149.4, 143.2, 132.8, 123.0, 116.9, 112.3, 110.3, 80.4, 47.9, 41.9, 28.4 ppm.

^{19}F NMR (376 MHz, CDCl_3) δ = -63.11 ppm.

1-(5-Nitro-2-(trifluoromethyl)phenyl)piperazine (**61**):



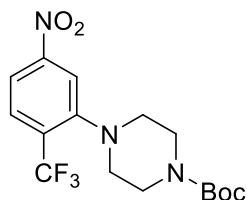
Piperazine (6211 mg, 72 mmol, 6 eq.) and K_2CO_3 (3340 mg, 24 mmol, 2 eq.) were suspended in DMSO (20 mL). To the stirring solution was added 2-fluoro-4-nitro-1-(trifluoromethyl)benzene **60** (2516.3 mg, 12 mmol, 1 eq.) and it was heated to 100 °C. After 24 h the reaction was complete, quenched with water (50 mL) and extracted with EtOAc (3 x 50 mL). The combined organic layers were washed with brine and saturated NH_4Cl , dried over anhydrous MgSO_4 , filtered, and concentrated *in vacuo* to obtain compound **61** as an orange oil (3088 mg, 11.2 mmol, 93%).

^1H NMR (400 MHz, CDCl_3) δ = 8.14 (s, 1H), 8.02 (d, J = 8.6 Hz, 1H), 7.81 (d, J = 8.2 Hz, 1H), 3.03 (br s, 4H), 2.97 (br s, 4H) ppm.

^{13}C NMR (101 MHz, CDCl_3) δ = 154.1, 150.7, 132.1, 128.8, 123.0, 118.8, 118.6, 54.5, 46.0 ppm.

^{19}F NMR (376 MHz, CDCl_3) δ = -61.14 ppm.

tert-Butyl 4-[5-nitro-2-(trifluoromethyl)phenyl]piperazine-1-carboxylate (**62**):



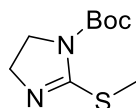
To a solution of di-*tert*-butyl dicarbonate (5409 mg, 24.8 mmol, 2.2 eq) in DCM (5 mL), compound **61** (3000 mg, 10.9 mmol, 1 eq.) as solution in DCM (10 mL) and DMAP (141 mg, 1.15 mmol, 0.1 eq.) were added and the mixture was stirred for 72 h. The resulting crude was purified by column chromatography (15% EtOAc in PE) to obtain compound **62** as a yellow oil (3462 mg, 9.22 mmol, 85%).

^1H NMR (400 MHz, CDCl_3) δ = 8.12 (br s, 1H), 8.06 (br d, J = 8.6 Hz, 1H), 7.83 (dd, J = 3.1, 8.6 Hz, 1H), 3.59 (br d, J = 3.9 Hz, 4H), 2.94 (br d, J = 3.5 Hz, 4H), 1.48 (s, J = 3.5 Hz, 9H) ppm.

^{13}C NMR (101 MHz, CDCl_3) δ = 154.6, 153.6, 150.7, 132.5, 128.8, 122.9, 119.5, 118.8, 80.0, 53.3, 43.9, 28.4 ppm.

^{19}F NMR (376 MHz, CDCl_3) δ = -60.84 ppm.

tert-Butyl 2-(methylthio)-4,5-dihydro-1*H*-imidazole-1-carboxylate (**64**):



To a solution of 2-(methylthio)-4,5-dihydro-1*H*-imidazole **63** (2256 mg, 9.24 mmol, 1 eq.) in DCM (10 mL) and triethylamine (2.6 mL, 18.5 mmol, 2 eq.), was added a solution of di-*tert*-butyl di-carbonate (2078 mg, 9.52 mmol, 1 eq.) in DCM (10 mL). After 24 h the solvent was removed under reduced pressure, and the resulting crude was purified by flash column chromatography using 50% EtOAc in PE as eluent to obtain compound **63** as colourless crystals (1747 mg, 8.07 mmol, 87 %).

^1H NMR (400 MHz, CDCl_3) δ = 3.80-3.88 (m, 4H), 2.39 (s, 3H), 1.51 (s, 9H) ppm.

^{13}C NMR (101 MHz, CDCl_3) δ = 159.6, 150.8, 82.5, 53.4, 47.6, 28.2, 15.0 ppm.

***P. falciparum* culturing and *in vitro* drug sensitivity assay on asexual blood stage parasites**

The *Plasmodium falciparum* NF54 wild-type parasites were cultured in RPMI 1640 medium that was supplemented with 25 mM HEPES, 0.36 mM hypoxanthine, 24 mM NaHCO₃ (pH = 7.3), 0.5% Albumax II and 100 µg/mL neomycin. The parasites were maintained at 37 °C with the mixed gas containing 3% O₂, 4% CO₂, and 93% N₂ and kept in an incubator under atmospheric pressure. The compounds were tested for *in vitro* drug sensitivity using the [³H]-hypoxanthine incorporation assay as described.⁷ Briefly, compounds were dissolved in DMSO at 10 mM and was diluted in hypoxanthine-free culture medium. The compounds were then titrated in duplicates over a 64-fold range in a 6-step twofold dilution in a 96-well plate. The parasites were then added (100µL) to each well and mixed with the compound to obtain a final parasitemia of 0.3% and haematocrit of 1.25%. The plates were then incubated for 48 h and 0.25 µCi of [³H]-hypoxanthine was added per well and was incubated for an addition 24 h. The parasites were then harvested on a glass-fiber filter using a Microbeta FilterMate cell harvester (Perkin Elmer, Waltham, US) and radioactivity was counted using a MicroBeta2 liquid scintillation counter (Perkin Elmer, Waltham, US). The results were recorded and expressed as percentage of untreated controls. The fifty percent inhibitory concentration (IC₅₀) was estimated by linear interpolation as described.⁸

Determination of *in vitro* antibacterial activity

Minimal inhibitory concentration (MIC) values were determined in 96-well plates (Sarstedt, Nümbrecht, Germany) against, *Escherichia coli* ΔtolC, *E. coli* K12, *Acinetobacter baumannii*, *Pseudomonas aeruginosa* PA14, *Staphylococcus aureus* ssp. *Aureus*, and *Streptococcus pneumoniae* (DSM20566). As bacteria start OD₆₀₀ 0.03 was used in a total volume of 200 µL in lysogeny broth (LB) medium containing the compounds dissolved in DMSO (DMSO concentration in the experiment: 1%). Final compound concentrations (in duplicates) were prepared by serial dilution ranging from 0.02–100 µg/mL depending on their antibacterial activity and solubility in growth medium. The ODs were measured using a CLARIOstar platereader (BMG labtech, Ortenberg, Germany) after inoculation and after incubation for 18 h at 37 °C with 50 rpm (200 rpm for *P. aeruginosa* PA14). Given MIC values are means of at least two independent determinations and defined as the lowest concentration of compound that reduced the OD₆₀₀ by ≥ 95%.

Determination of *in vitro* anti-tubercular activity and solubility in 7H9 medium

Anti-tubercular tests were performed as previously described.⁹ In brief, 7H9 complete medium (BD Difco; Becton Dickinson, Maryland, USA) supplemented with 10% OADC (BD), 0.2% glycerol, and 0.05% Tween80 as previously described,¹⁰ was used to culture *Mycobacterium tuberculosis* (*Mtb*) strain H37Rv (ATCC 25618) carrying a mCherry-expressing plasmid (pCherry10).¹¹ Cultures were harvested at mid-log phase and frozen in aliquots at –80 °C. Prior to testing aliquots were thawed followed by centrifugation and the pellet was resuspended in 7H9 medium with 10% OADC (without glycerol and Tween80). This was further thoroughly resuspended by passing it through a syringe with a 26-gauge needle to avoid clumping of the bacteria. 2×10⁵ CFU (colony forming units) were then cultured in a total volume of 100 µL culture medium (triplicates) to test the non-precipitating compounds for the anti-tubercular activity at the concentrations indicated. For these assays, 96-well flat clear bottom black polystyrene microplates (Corning® CellBIND®, Merck, New York, USA) were used. Each plate had Rifampicin (at 1 µg/ml and 0.1 µg/ml) (National Reference Center, Borstel) as a reference compound. Plates were sealed with an air-permeable membrane (Porvair Sciences, Wrexham, UK) in a 37 °C incubator with mild agitation (TiMix5, Edmund Bühler, Germany). The activity of compounds was determined after 7 days by measuring the bacterial growth as relative light units (RLU) from the fluorescence intensity obtained at an excitation wavelength of 575 nm and an emission wavelength of 635 nm in a microplate reader (Synergy 2, BioTek Instruments, Vermont, USA). Two independent experiments (each in triplicates) were performed, and all values were normalized to untreated control sample (100%) in each experiment.

Cytotoxicity assay

To obtain information regarding the toxicity of our compounds, their impact on the viability of human cells was investigated. HepG2 cells (2×10⁴ cells per well) were seeded in 96-well, flat-bottomed culture plates in 100 µL culture medium (DMEM containing 10% fetal calve serum, 1% penicillin-streptomycin). Twenty-four hours after seeding the cells, medium was removed and replaced by medium containing test compounds in a final DMSO concentration of 1%. Compounds were tested in duplicates at a single concentration or, for CC₅₀ determination, at 8 concentrations that were prepared via 2-fold serial dilutions in 1% DMSO/medium. Epirubicin and doxorubicin were used as positive controls in serial dilutions starting

from 10 μM , and rifampicin was used as a negative control (at 100 μM). The living cell mass was determined 48 h after treatment with compounds by adding 0.1 volumes of 3-(4,5-dimethylthiazol-2-yl)-2,5-diphenyltetrazolium bromide (MTT) solution (5 mg/mL sterile PBS) (Sigma, St. Louis, MO) to the wells. After incubating the cells for 30 min at 37 $^{\circ}\text{C}$ (atmosphere containing 5% CO_2), medium was removed and MTT crystals were dissolved in 75 μL of a solution containing 10% SDS and 0.5% acetic acid in DMSO. The optical density (OD) of the samples was determined photometrically at 570 nm in a PHERAstar Omega plate reader (BMG labtech, Ortenberg, Germany). To obtain percent viability for each sample, their ODs were related to those of DMSO controls. At least two independent measurements were performed for each compound. The calculation of CC_{50} was performed using the nonlinear regression function of GraphPad Prism 10 (GraphPad Software, San Diego, CA, USA).

Measurement of *in vitro* cytotoxicity by XTT assay

An 2,3-bis-(2-methoxy-4-nitro-5-sulphophenyl)-2H-tetrazolium-5-carboxanilide (XTT) assay was used to determine the cytotoxicity of the selected compounds (Table S2). Human Monocyte-derived Macrophages (hMdm) were differentiated from peripheral blood mononuclear cells (PBMC) of healthy volunteers and cultured as previously described.¹² 5×10^4 cells/well in RPMI medium containing 10% (v/v) heat-inactivated Fetal Bovine Serum and 2 mmol/L L-glutamine (Biochrom, Berlin, Germany) were seeded in presence of 2-fold dilution concentrations (64 μM to 1 μM) of the compound for 24 h with a final volume of 200 μL /well. For this assay, 96-well clear flat bottom plates (Nunclon™ Delta Surface, ThermoScientific, Denmark) were used. Triton™-X 100 (Sigma-Aldrich, Missouri, USA; 1% in RPMI medium) was used as a positive control. Cells were incubated with 200 μL of Triton-X 100 and incubated for 10 min at 37 $^{\circ}\text{C}$. XTT dye from the kit (SERVA Electrophoresis GmbH; 50 μL) was added to each well and resuspended thoroughly and further incubated for 3–4 hours at 37 $^{\circ}\text{C}$. Subsequently, absorbance values were measured at 490 nm on a multi-well plate reader (Synergy 2, BioTek Instruments, Vermont, USA). Untreated cells were used as negative control. The Cytotoxic Concentration 50 (CC_{50}) was determined by plotting a curve using GraphPad Prism version 9.4.1.

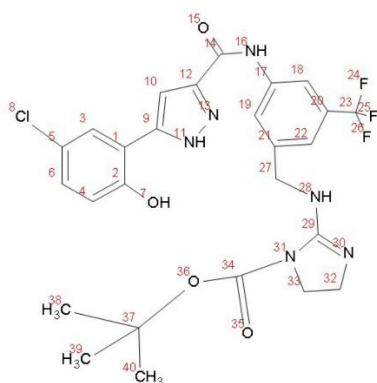
Supplementary Tables and Figures

Computational evaluation of pKa

Software name and version: ACD/Percepta 14.50.0 (Build 3200)

Compound name:

Structure:



1.7 \pm 0.9 (Atom number: 13), 100% MS1
 5.1 \pm 0.5 (Atom number: 30), 100% MS2
 9.2 \pm 0.8 (Atom number: 7), 100% MS3
 15.0 \pm 0.4 (Atom number: 16), 100% MS4

Strongest pKa(Acid): 9.2 \pm 0.8
 Strongest pKa(Base): 5.1 \pm 0.5

Molecular Weight: 578.97
 No. of Hydrogen Bond Donors: 4
 No. of Hydrogen Bond Acceptors: 10
 TPSA: 131.94
 No. of Rotatable Bonds: 9
 LogP: 4.09
 C Ratio: 0.65
 N Ratio: 0.15
 NO Ratio: 0.25
 Hetero Ratio: 0.25
 Halogen Ratio: 0.10
 Number of Rings: 4
 Number of Aromatic Rings: 3
 Number of Rings (size 3): 0
 Number of Rings (size 4): 0
 Number of Rings (size 5): 2
 Number of Rings (size 6): 2
 Log(BCF): 2.53
 Log(Koc): 3.35
 Dielectric Constant: not calculated
 Parachor, cm^3 : 1044.74
 Index of Refraction: 1.63
 Surface Tension, dyne/cm : 48.87
 Density, g/cm^3 : 1.47
 Polarizability, $10 \times 10^{-24} \text{ cm}^3$: 55.53
 Molar Volume, cm^3 : 395.13
 Molar Refractivity, cm^3 : 140.07

Figure S1. Computational evaluation of pKa of 9D.

Biological evaluation of compounds

Table S1. Biological activity of pyrazole-amide class in *Escherichia coli* (*EcΔtolC* and *EcK12*), *Acinetobacter baumannii* (*Ab*), *Pseudomonas aeruginosa* (PA14) including standard deviation.

Cmp	<i>EcΔtolC</i> MIC ₉₅ (μM)	<i>EcΔtolC</i> inh. at 50 μM (%)	<i>EcK12</i> inh. at 50 μM (%)	<i>Ab</i> inh. at 50 μM (%)	PA14 inh. at 50 μM (%)
1a	-	<10	<10	<10	<10
1b	-	sol. issues	n.d.	n.d.	n.d.
1c	-	sol. issues	n.d.	n.d.	n.d.
1d	-	<10	n.d.	n.d.	n.d.
1e	-	23 ± 3	n.d.	n.d.	n.d.
2	-	24 ± 12	n.d.	n.d.	n.d.
3A	45 ± 1	-	28 ± 12	21 ± 2	50 ± 4
3B	-	sol. issues	<10	n.d.	n.d.
4A	40 ± 8	-	34 ± 5	24.2 ± 7.7	62 ± 3
4B	-	sol. issues	17 ± 13	n.d.	n.d.
5A	21 ± 2	-	83 ± 8	34.3 ± 0.4	60 ± 3
5B	-	19 ± 14	<10	n.d.	n.d.
5G	11 ± 2	-	32 ± 9	<10	31 ± 14
6A	22.5 ± 0.0	-	49 ± 6	37 ± 2	63 ± 9
6B	-	<10	n.d.	n.d.	n.d.
6G	9 ± 3	-	45 ± 5	32 ± 6	55 ± 16
7A	47 ± 1	-	27 ± 10	15 ± 3	44 ± 6
7B	-	<10	<10	n.d.	n.d.
7C	13 ± 3	-	29.4 ± 0.6	33 ± 6	41 ± 19
7D	14 ± 4	-	56 ± 2	77 ± 4	54.8 ± 0.8
7G	13 ± 3	-	61 ± 6	24 ± 5	56.0 ± 0.0
8A	-	44 ± 16	n.d.	n.d.	n.d.
8B	-	<10	n.d.	n.d.	n.d.
8C	21.5 ± 0.0	-	<10	12 ± 9	10 ± 3
8D	-	18.5 ± 0.8	n.d.	n.d.	n.d.
8G	47.5 ± 0.0	-	29 ± 11	19.9 ± 0.6	41 ± 6
9A	8 ± 3	-	<10	MIC ₉₅ = 48.9 ± 0.5	<10
9B	-	48 ± 8	n.d.	n.d.	n.d.
9C	7 ± 1	-	84 ± 2	47 ± 4	18 ± 21
9D	24.0 ± 0.0	-	<10	81.6 ± 0.6	21 ± 18
9G	5 ± 2	-	MIC ₉₅ = 46 ± 2	59 ± 8	50 ± 4
10A	22.9 ± 0.1	-	61 ± 17	86 ± 7	<10
10B	-	<10	<10	<10	n.d.
10C	5.5 ± 0.8	-	77 ± 10	49.6 ± 0.9	29 ± 12
10D	18 ± 6	-	17 ± 6	<10	<10
10G	3.5 ± 0.8	-	86 ± 2	49 ± 24	55 ± 2
11A	7 ± 2	-	72 ± 5	MIC ₉₅ = 22 ± 3	<10
11B	-	18 ± 4	n.d.	<10	n.d.
11C	7 ± 2	-	63 ± 3	53 ± 12	<10
11G	4 ± 1	-	MIC ₉₅ = 48 ± 5	MIC ₉₅ = 17 ± 5	25 ± 10
12A	18.9 ± 0.5	-	12 ± 2	29 ± 1	<10
12B	-	<10	n.d.	<10	n.d.
12G	2.8 ± 0.3	-	51 ± 6	33 ± 5	<10
13A	-	46 ± 5	n.d.	<10	<10
13B	-	<10	n.d.	n.d.	n.d.
13G	5 ± 2	-	59 ± 8	46 ± 26	17 ± 10
14A	-	18 ± 4	n.d.	n.d.	n.d.
14G	-	18 ± 9	n.d.	n.d.	n.d.

n.d. = not determined

Table S2. Biological activity of pyrazole-amide class in *Plasmodium falciparum* (PfNF54), *Streptococcus pneumoniae* (Sp), *Staphylococcus aureus* (Sa), human liver cells (HepG2) including standard deviation. In addition, for selected compounds; human Monocyte-derived Macrophages (hMdm) toxicity, and solubility in 7h9 media.

Cmp	PfNF54 IC ₅₀	Sp MIC ₉₅ (μM)	Sa MIC ₉₅ (μM)	HepG2 CC ₅₀ (μM)	hMdm CC ₉₀ (μM)	7h9 media Sol. (μM)
1a	0.21 ± 0.02	>50	>50	>50	-	<8
1b	0.7 ± 0.2	>50	>50	n.d.	-	<8
1c	0.51 ± 0.05	>50	>50	n.d.	-	32
1d	2.40 ± 0.03	>50	>50	>50	-	-
1e	>5	>50	>50	>50	-	-
2	1.1 ± 0.2	>50	>50	49 ± 7%	-	16
3A	0.62 ± 0.03	40 ± 7	>50	12 ± 2	-	64
3B	1.0 ± 0.3	>50	>50	25 ± 4	-	-
4A	0.27 ± 0.03	40 ± 7	>50	13 ± 3	-	64
4B	0.2 ± 0.1	>50	>50	7.4 ± 0.7	-	-
5A	0.13 ± 0.03	26 ± 1	37 ± 10	9 ± 2	-	64
5B	0.9 ± 0.3	>50	>50	>50	-	-
5G	0.93 ± 0.02	48 ± 1	23.1 ± 0.5	>50	-	-
6A	0.14 ± 0.02	45 ± 0	>50	11.8 ± 0.9	-	16
6B	1.61 ± 0.01	>50	>50	>50	-	-
6G	0.44 ± 0.06	25 ± 2	26 ± 2	>50	-	-
7A	0.30 ± 0.08	43 ± 11	>50	28.4 ± 0.2	-	64
7B	1.1 ± 0.3	>50	>50	>50	-	-
7C	0.39 ± 0.01	48.2 ± 0.8	22.3 ± 0.6	>50	-	-
7D	0.36 ± 0.07	31 ± 11	24.0 ± 0.0	19 ± 4	-	-
7G	0.21 ± 0.02	49.0 ± 0.0	22 ± 2	>50	-	-
8A	1.8 ± 0.5	>50	>50	30 ± 3	-	16
8B	1.7 ± 0.3	>50	>50	>50	-	<8
8C	0.67 ± 0.02	>50	49 ± 1	>50	-	-
8D	>5	>50	>50	>50	-	-
8G	0.42 ± 0.02	>50	22 ± 1	>50	-	-
9A	0.082 ± 0.001	10.8 ± 2.5	12.1 ± 0.6	7 ± 2	-	-
9B	0.2033 ± 0.0003	30 ± 5	>50	5.0 ± 0.8	-	-
9C	0.517 ± 0.004	15 ± 4	9 ± 2	>50	-	-
9D	0.15 ± 0.02	21 ± 9	12 ± 3	14 ± 2	-	-
9G	0.078 ± 0.003	>50	8 ± 3	>50	-	-
10A	0.15 ± 0.02	23 ± 3	29 ± 3	13 ± 4	-	-
10B	0.19 ± 0.01	>50	>50	>50	-	-
10C	0.404 ± 0.002	14 ± 2	8 ± 2	>50	-	-
10D	0.14 ± 0.04	>50	11.6 ± 0.2	11 ± 3	-	-
10G	0.25 ± 0.09	16 ± 5	5 ± 1	>50	>32	-
11A	0.05 ± 0.01	5 ± 1	6 ± 2	9 ± 3	-	-
11B	0.13 ± 0.06	>50	>50	4.0 ± 0.4	-	<8
11C	0.59 ± 0.08	7 ± 2	8 ± 2	>50	-	-
11G	0.5 ± 0.2	28 ± 15	3.2 ± 0.1	>25	>32	-
12A	0.06 ± 0.01	8 ± 2	14 ± 2	6 ± 1	-	-
12B	0.56 ± 0.06	>50	>50	>50	-	<8
12G	0.2 ± 0.1	31 ± 6	2.4 ± 0.3	30 ± 1	32	-
13A	0.160 ± 0.008	29 ± 2	>50	8 ± 3	-	-
13B	0.3418 ± 0.0006	n.d.	n.d.	2.8 ± 0.7	-	-
13G	0.5 ± 0.2	16 ± 6	2.5 ± 0.3	>25	>32	-
14A	3.3 ± 0.6	>50	>50	>50	-	-
14G	>5	>50	>50	>50	-	-

Supplementary References

- (1) Santos, C. M. M.; Silva, V. L. M.; Silva, A. M. S. Synthesis of Chromone-Related Pyrazole Compounds. *Molecules* **2017**, *22* (10). <https://doi.org/10.3390/molecules22101665>.
- (2) Svenningsen, S. W.; Frederiksen, R. F.; Counil, C.; Ficker, M.; Leisner, J. J.; Christensen, J. B. Synthesis and Antimicrobial Properties of a Ciprofloxacin and PAMAM-Dendrimer Conjugate. *Molecules* **2020**, *25* (6). <https://doi.org/10.3390/molecules25061389>.
- (3) Dardonville, C.; Caine, B. A.; Navarro De La Fuente, M.; Martín Herranz, G.; Corrales Mariblanca, B.; Popelier, P. L. A. Substituent Effects on the Basicity (pK_a) of Aryl Guanidines and 2-(Arylimino)imidazolidines: Correlations of PH-Metric and UV-Metric Values with Predictions from Gas-Phase Ab Initio Bond Lengths. *New J Chem* **2017**, *41* (19), 11016–11028. <https://doi.org/10.1039/c7nj02497e>.
- (4) Ueno, H.; Yokota, K.; Hoshi, J. I.; Yasue, K.; Hayashi, M.; Hase, Y.; Uchida, I.; Aisaka, K.; Katoh, S.; Cho, H. Synthesis and Structure-Activity Relationships of Novel Selective Factor Xa Inhibitors with a Tetrahydroisoquinoline Ring. *J Med Chem* **2005**, *48* (10), 3586–3604. <https://doi.org/10.1021/jm058160e>.
- (5) Aoyagi, N.; Endo, T. Synthesis of Five- and Six-Membered Cyclic Guanidines by Guanylation with Isothiouonium Iodides and Amines under Mild Conditions. *Synth Commun* **2017**, *47* (5), 442–448. <https://doi.org/10.1080/00397911.2016.1269927>.
- (6) Gaspar, A.; Reis, J.; Matos, M. J.; Uriarte, E.; Borges, F. In Search for New Chemical Entities as Adenosine Receptor Ligands: Development of Agents Based on Benzo- γ -Pyrone Skeleton. *Eur J Med Chem* **2012**, *54*, 914–918. <https://doi.org/10.1016/j.ejmech.2012.05.033>.
- (7) Snyder, C.; Chollet, J.; Santo-Tomas, J.; Scheurer, C.; Wittlin, S. In Vitro and in Vivo Interaction of Synthetic Peroxide RBx11160 (OZ277) with Piperaquine in Plasmodium Models. *Exp Parasitol* **2007**, *115* (3), 296–300. <https://doi.org/10.1016/j.exppara.2006.09.016>.
- (8) Huber, W.; Koella, J. C. A Comparison of Three Methods of Estimating EC₅₀ in Studies of Drug Resistance of Malaria Parasites. *Acta Trop* **1993**, *55* (4), 257–261. [https://doi.org/10.1016/0001-706X\(93\)90083-N](https://doi.org/10.1016/0001-706X(93)90083-N).
- (9) Jumde, R. P.; Guardigni, M.; Gierse, R. M.; Alhayek, A.; Zhu, D.; Hamid, Z.; Johannsen, S.; Elgaher, W. A. M.; Neusens, P. J.; Nehls, C.; Haupenthal, J.; Reiling, N.; Hirsch, A. K. H. Hit-Optimization Using Target-Directed Dynamic Combinatorial Chemistry: Development of Inhibitors of the Anti-Infective Target 1-Deoxy-D-Xylulose-5-Phosphate Synthase. *Chem Sci* **2021**, *12* (22), 7775–7785. <https://doi.org/10.1039/D1SC00330E>.
- (10) Kolbe, K.; Möckl, L.; Sohst, V.; Brandenburg, J.; Engel, R.; Malm, S.; Bräuchle, C.; Holst, O.; Lindhorst, T. K.; Reiling, N. Azido Pentoses: A New Tool To Efficiently Label *Mycobacterium Tuberculosis* Clinical Isolates. *ChemBioChem* **2017**, *18* (13), 1172–1176. <https://doi.org/10.1002/cbic.201600706>.
- (11) Zelmer, A.; Carroll, P.; Andreu, N.; Hagens, K.; Mahlo, J.; Redinger, N.; Robertson, B. D.; Wiles, S.; Ward, T. H.; Parish, T.; Ripoll, J.; Bancroft, G. J.; Schaible, U. E. A New in Vivo Model to Test Anti-Tuberculosis Drugs Using Fluorescence Imaging. *J. Antimicrob. Chemother.* **2012**, *67* (8), 1948–1960. <https://doi.org/10.1093/jac/dks161>.
- (12) Reiling, N.; Homolka, S.; Walter, K.; Brandenburg, J.; Niwinski, L.; Ernst, M.; Herzmann, C.; Lange, C.; Diel, R.; Ehlers, S.; Niemann, S. Clade-Specific Virulence Patterns of *Mycobacterium Tuberculosis* Complex Strains in Human Primary Macrophages and Aerogenically Infected Mice. *mBio* **2013**, *4* (4). <https://doi.org/10.1128/mBio.00250-13>.

3. Chapter:

Guanylated α / γ -Substituted Aza-Fosmidomycin Derivatives

Fosmidomycin is a natural product with antimalarial potency, its structure consists of a phosphonic acid linked to a hydroxamic acid through a propyl spacer (Figure 1).¹ This highly polar structure inhibits the metalloenzyme deoxy-D-xylulose-5-phosphate reductoisomerase (DXR). Co-crystal structures confirm the binding mode to the active site; the hydroxamate chelates Mg^{2+} or Mn^{2+} , and the phosphonate forms hydrogen bonds with three amino acid residues. DXR is the second enzyme of the 2-C-methyl-D-erythritol 4-phosphate (MEP) pathway, which is a promising anti-infective target present in *Plasmodium falciparum* and many pathogenic bacteria.² Fosmidomycin is the only MEP-pathway inhibitor that has been studied in clinical trials but it suffers from poor oral bioavailability and a short plasma half-life.³ In the past four decades, extensive research efforts aimed at improving the drug-like properties of fosmidomycin led to a good understanding of the structure–activity relationship (SAR).¹ The two acid moieties are essential for activity and cannot be replaced with other acids. In the case of the phosphonic acid, the only replacements that did not lead to loss of inhibition of DXR were phosphates.⁴ Similarly, the hydroxamic acid can be *N*-acetylated, and reversed by linking the carbonyl to the propyl chain instead of the nitrogen atom.⁵ Other metal binding groups and isosteres led to a loss in activity.⁶ Modifications on the chain, proved to be the best tolerated, likely given that it is the only part not involved in binding DXR. Substitutions on the α -position led to a boost in activity especially with halogens directly bound to the propyl or through a phenyl ring.^{7,8} β - and γ -substituted analogues are scarcer and seem to be detrimental to activity.^{9,10} Exchanging the β -carbon of the chain with heteroatoms is possible, especially in the case of sulfur excellent activities have been reported.^{11,12}

Recent unpublished work in the group of Van Calenbergh involved the synthesis of reverse fosmidomycin derivatives with a nitrogen atom in the β -position (class-1 & -2, Figure 2). The design of these aza-derivatives was inspired by the eNTRY rules, which aim at improving accumulation in Gram-negative bacteria (GNB). These guidelines suggest that molecules with flat and rigid structures containing ionisable nitrogens have an enhanced compound accumulation in *Escherichia coli*. In the case of class-1,

and -2, the aza-moiety is an ionisable secondary amine and the α -aryl makes the compound flatter and more drug-like compared to fosmidomycin. Additionally, in class-2, the cyclisation from the γ -position to the nitrogen of the hydroxamate adds rigidity, while simultaneously positioning the hydroxamic acid into its active metal binding *E*-conformation. Both classes, cyclised and not, have excellent DXR inhibitory profiles, with the best examples achieving unprecedented subnanomolar affinities. Despite this excellent target-engagement, and more importantly the more eNTRY-compliant structural properties, the vast majority are inactive against *E. coli*. Only three examples show a moderate effect (> 50% at 100 μ M) on the *acrB* efflux pump deficient *E. coli* strain. Nevertheless, promising antimalarial activities, in the submicromolar range were obtained. These values are comparable, and in some cases exceed the potency of fosmidomycin.

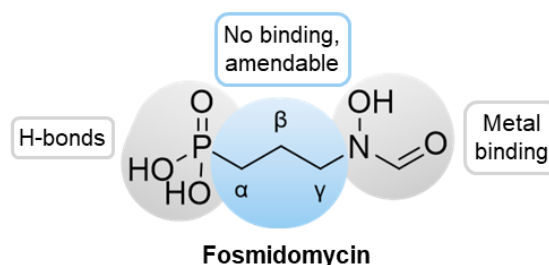


Figure 1. Chemical structure of fosmidomycin. Phosphonic, -and hydroxamic acid are involved in binding unlike the propyl linker.

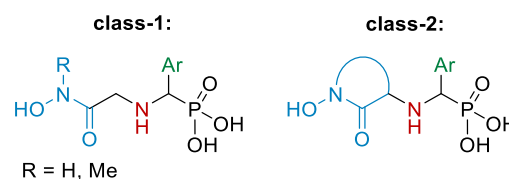


Figure 2. Chemical scaffold of α -substituted β -aza reverse fosmidomycin derivatives (class 1 & 2); hydroxamic acid in blue, β -nitrogen in red, α -aryl in green.

Herein, we expand the library of α -substituted β -aza reverse fosmidomycin derivatives (class-1 & -2) with the aim of obtaining antibacterial activity. Studies on the eNTRY rules indicate that primary amines and *N*-alkyl guanidines are more beneficial for *E. coli* accumulation than secondary or tertiary amines. We recently unlocked promising broad-spectrum anti-infective activity in an antimalarial chemical class by addition of (cyclised) *N*-alkyl guanidines (Chapter A).¹³ Therefore, we decided to apply a similar strategy to the reverse aza-fosmidomycin class by introducing (cyclised) *N*-alkyl guanidiniums as well as primary amines. We designed distinct synthetic strategies to introduce these ionisable moieties at α -, β -, and γ -positions (Figure 3). The α -derivatives contain the positive groups attached to the aromatic ring via an ether linkage. According to co-crystal structures of class-1, the aromatic ring points towards a solvent-exposed area, which could be beneficial for the attached positively charged groups. In contrast, the aza moiety only has a small space available for substitutions, therefore we opted for directly aza-guanylated β -derivatives. In the case of the γ -position, class-2 shows that cyclisation to the hydroxamate is beneficial for activity. However, no other substitutions were studied in this context, which led us to explore γ -alkyl substitutions and potentially add ionisable nitrogen functionalities. With this multifaceted approach, we aimed to cover a broad structure–activity, and structure–uptake relationship to subsequently design more focused target molecules.

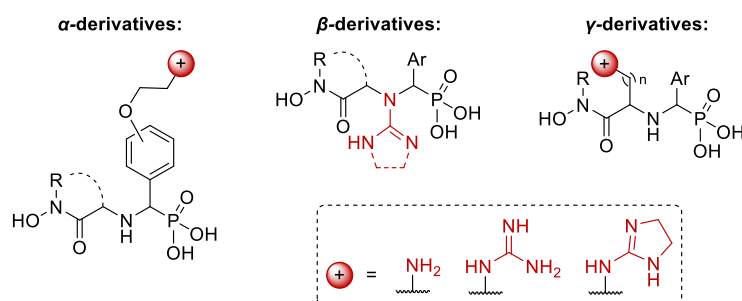
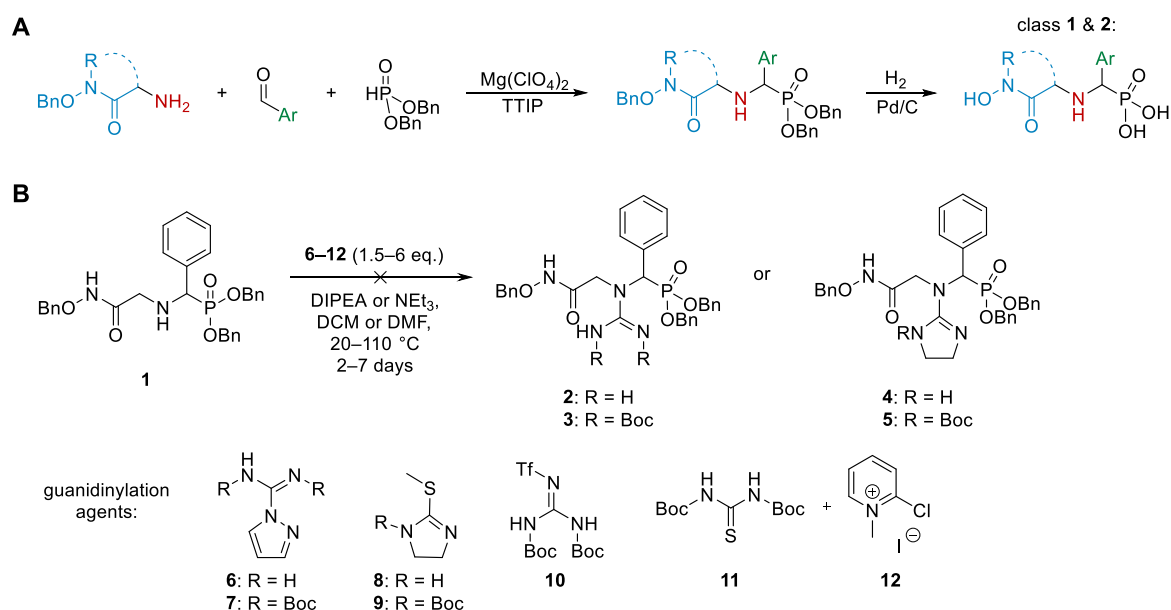


Figure 3. Chemical scaffolds of class-1 & -2, including ionisable nitrogen groups at α -, β -, and γ -positions.

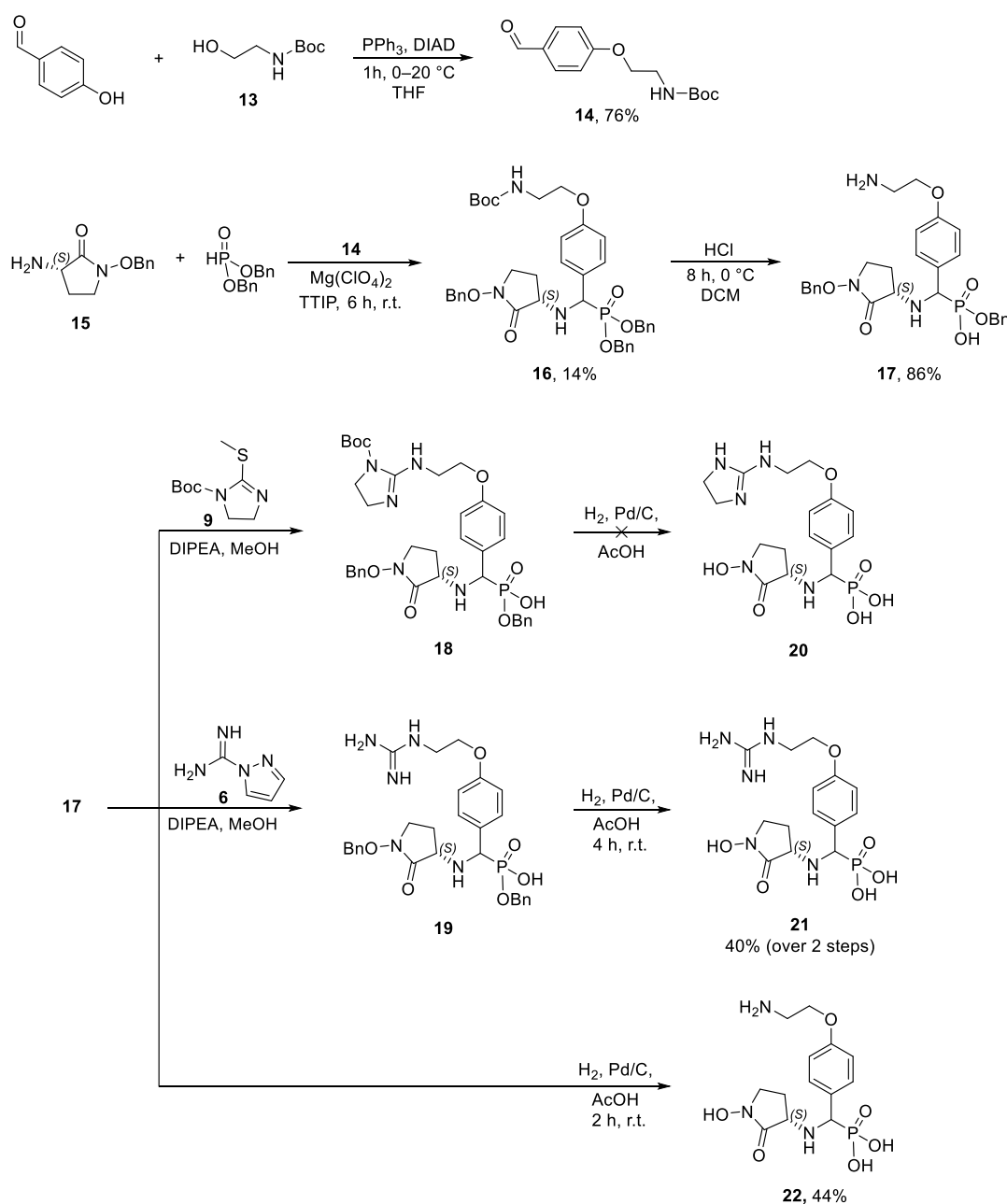
Given that the synthesis of class-1, and -2 had been thoroughly optimised, our aim was to maintain the key three-component reaction step in the synthesis of our new target molecules. This Kabachnik–Fields reaction affords the structural scaffold of the two classes, which subsequently undergo hydrogenation to afford the target molecules of class-1, and -2 (Scheme 1A). The simplest option of introducing our ionisable groups while keeping modifications of the synthetic route to the minimum, seemed to be the β -derivatives.



Scheme 1. A) General synthesis scheme of the last two steps that afford compounds of class 1 and 2. B) Proposed synthesis to afford β -derivatives.

We proposed to add a guanidinylation step before the hydrogenation. For this purpose, we screened different reaction conditions using test compound **1** and various guanidinylation agents (Scheme 1B). The reaction did not proceed in any of our attempts, involving long reaction times of up to seven days, different bases, solvents, and increased temperatures. Elevating the temperature to 110 °C led to slow degradation of **1**. This led us to conclude that the secondary amine is a very weak nucleophile and performed a final attempt with thiourea **11** and Mukaiyama's reagent **12**. This combination of reagents has been used to guanidylate weakly nucleophilic secondary amines likely through the formation of a highly electrophilic carbodiimide intermediate.¹⁴ In our case no guanylated product was detected, concluding that steric hinderance may be an additional factor explaining why the reaction did not proceed.

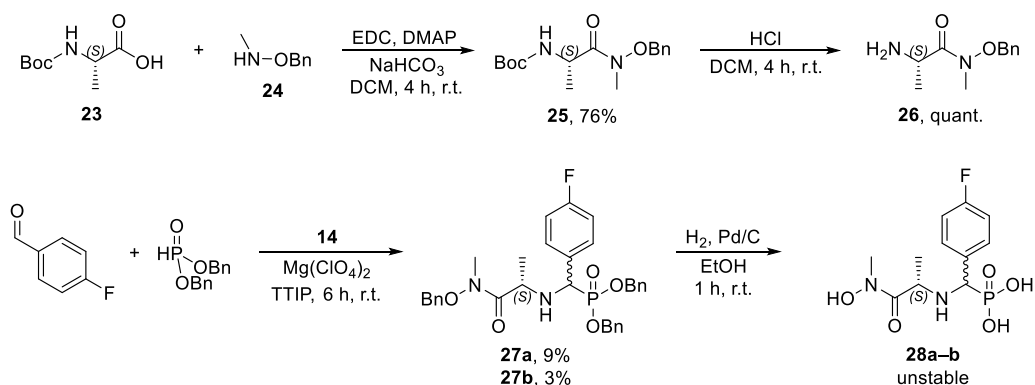
Given that **1** was unreactive under our tested guanidinylation conditions, we decided to use it to our advantage and perform a late-stage guanidinylation to obtain the α -class. We strategically designed benzaldehyde **14** to contain an *N*-Boc protected primary amine, which could later serve as a handle for



Scheme 2. Synthesis of α -aryl aza-fosmidomycin compounds with a positively charged group.

guanidinylation (Scheme 2). We synthesised intermediate **14** in one step from 4-hydroxybenzaldehyde and aminoethanol **13** via a Mitsunobu reaction. To build our aza-scaffold **16** via a Kabachnik–Fields reaction, we used **14** in combination with enantiomerically pure aminopyrrolidin-2-one **15**, chosen based on favourable results obtained with the (*S*)-isomers of five-membered cyclic hydroxamates of class-2. At this stage, we deprotected the primary amine, maintaining a low temperature and sequentially adding hydrochloric acid to control the reaction. Despite this careful Boc-deprotection, the phosphonate was partially debenzylated affording key intermediate **17**. We decided to move forward with the guanidinylation regardless, affording guanidines **18** and **19** using reagents **6** and **9**, respectively (Scheme 2). The reactions proceeded nicely, although the debenzylated phosphonate led to an increased hydrophilicity making the isolation and purification of products challenging. The added lipophilicity of the Boc-protected cycle in guanidine **18** did not appear to make a big difference. Lastly, compounds **17–19** were hydrogenated to obtain the final deprotected products containing ionisable nitrogen groups; amine **21** and *N*-alkyl guanidine **22**. To our disappointment the reaction did not succeed for cyclic guanidine **18**. We hypothesise that the palladium catalyst was poisoned with by-products from the previous reaction, given that we did not purify compound **18** due to its high polarity. In the case of amine **17** and guanidine **19** the hydrogenation proceeded only with addition of acetic acid, and was significantly slower with the guanidine than the amine. These findings suggest that the positively charged groups slow down the rate of debenzylation. Nevertheless, this synthetic approach was largely successful and synthetic efforts towards obtaining respective analogues of class-1 are ongoing.

Similarly, to the α -derivatives, the synthesis of the γ -substituted compounds was based on a convergent strategy, designing key starting materials for the Kabachnik–Fields reaction. In this case, the amine had to be adapted to include the desired γ -substituent. We first decided to investigate this position with a methyl substitution to assess the feasibility; partially from a synthetic perspective and mainly to assess the activity, given that γ -substitutions were detrimental to activity in fosmidomycin derivatives.¹⁰ For this purpose, we synthesised amine **26** in two steps, starting from *N*-Boc protected *L*-alanine (Scheme 4). First, we introduced the protected hydroxamate moiety and subsequently we removed the Boc group. The Kabachnik–Fields reaction using **26** and 4-fluorobenzaldehyde went smoothly, although purification by column chromatography only partially removed by-products. We purified a small fraction *via* prep-HPLC and were able to separate diastereomers in a 3 : 1 (**27a** : **27b**) ratio. The hydrogenation of the major product yielded **28a** as a fine white powder. Unfortunately, this was not the case for the other isomer (**27b**), the debenzylated product **28b** degraded during lyophilisation. To our disappointment, product **28a** transformed into an oil after 2 days and LCMS analysis revealed compound degradation. We monitored the degradation progress, however, after the second month, an equilibrium had been reached. The ratio of degraded and intact product stayed at 3 : 2 and we were unable to identify the structure of the by-product.



Scheme 3. Synthesis of α -aryl aza-fosmidomycin with γ -methyl substituent **28** via Kabachnik-Fields reaction and hydrogenation.

In conclusion, we developed a promising synthetic strategy to obtain α -substituted β -aza reverse fosmidomycin derivatives containing positively charged functionalities. We successfully obtained two derivatives containing a guanidine (**21**) and amine (**22**) moiety linked to the α -aromatic substituent. The synthesis of amine **22** did not encounter any obstacles. However, a milder Boc-deprotection step could improve the synthesis of the guanidine derivatives, especially in the case of cyclic guanidines, given that purification by prep-HPLC of partially debenzylated **18** is necessary before making another hydrogenation attempt to obtain **20** as a third final product. The biological evaluation of **21** and **22** is currently ongoing and results will be used to improve the design of new eNTRY-compliant analogues. The synthesis of γ -substituted derivatives went smoothly and shows that the use of amino acids can be an effective way to access underexplored γ -fosmidomycin analogues. However, our alanine derived product was unstable and the mechanism of its degradation needs to be investigated further.

Experimental Section

General. All reactions using oxygen- and/or moisture-sensitive materials were carried out in dry solvents (*vide infra*) under a nitrogen atmosphere using oven-dried glassware. The reaction progress was monitored on thin layer chromatography (TLC) on Machery Nagel ALUGRAM Xtra SIL G UV254 sheets or by liquid chromatography-mass spectrometry (LC-MS). LC-MS analysis for reaction monitoring and purity analyses were carried out on a Waters Autopurification system equipped with a Waters CORTECS column (4.6x100 mm, C18, 2.7 μ m) and using a water/acetonitrile/formic acid linear gradient. Peak detection was achieved using mass spectrometry (ESI-MD) and a photo-diode-array detector (PDA). Purification by column chromatography was performed on a Reveleris X2 automated flash chromatography system (Grace/Büchi) using disposable silica gel cartridges (Agela). Nuclear magnetic resonance analyses including ^1H - and ^{13}C -spectra were carried out on a Bruker Avance Neo 400MHz spectrometer equipped with an autosampler and using TOPSPIN/ICON-NMR. Chemical shifts are given in ppm (δ) relative to the solvent peak. NMR solvents included CDCl_3 (7.26 ppm in ^1H NMR, 77.16 ppm in ^{13}C NMR) or $\text{DMSO}-d_6$ (2.50 ppm in ^1H NMR and 39.52 ppm in ^{13}C NMR) and were all purchased from Euriso-Top (Saint Aubin, France). Systematic nomenclature was used to name the synthesized compounds. High-resolution mass spectrometry was performed on a Waters Premier XE HRMS system that is calibrated using a solution of Le-enkephalin. Infusion of the analyte into the HRMS system was done as a solution (0.5 ng/mL) in UPLC grade water and acetonitrile. All solvents utilized (HPLC grade or equivalent or superior purity) were purchased from ChemLab (Zedelgem, Belgium) and used as received. All building blocks and reagents were purchased from common chemical suppliers including but not limited to: Fluorochem (Glossop, Derbyshire UK), Apollo Scientific (Bredbury/Stockport Cheshire UK), Sigma-Aldrich (Diegem, Belgium), and Fisher Scientific (Merelbeke, Belgium). All obtained final compounds had purity > 95%, as assayed by analytical HPLC (UV) using a linear gradient Water/ MeCN 0 -> 98 % + 0.1 % formic acid in 10 min on a Waters CORTECS column (4.6x100 mm, C18, 2.7 μ m).

General procedure for Kabachnik–Fields reaction (GP-1).

The synthesis of the β -aza fosmidomycin backbone was prepared following a similar procedure reported in the literature.¹⁵ To the respective amine (1 eq.) and magnesium perchlorate (0.05 eq.), the respective aldehyde (1.05 eq.) and subsequently dibenzyl phosphite (2 eq.) was added slowly. The mixture stirred gently until a homogeneous viscous oil was formed (0.5–1h). Every 15 min, titanium(IV) isopropoxide (TTIP, 0.1 eq.) was added dropwise. After the reaction was complete, the mixture was added to Na_2CO_3 sat. (100 mL) and EtOAc (50 mL), and filtered over celite. The mixture was extracted with EtOAc (3 x 50 mL). The combined organic layers were washed with brine, dried over anhydrous Na_2SO_4 , filtered, and concentrated to dryness *in vacuo*. The resulting crude was purified by column chromatography using EtOAc/PE, concentrated to dryness *in vacuo*, followed by repurification using MeOH/DCM to obtain the pure product.

Dibenzyl (((2-((benzyloxy)amino)-2-oxoethyl)amino)(phenyl)methyl)phosphonate (**1**).

Prepared by T. Quennesson according to GP-1.

^1H NMR (400 MHz, CDCl_3) δ = 9.29 (s, 1H), 7.26-7.39 (m, 18H), 7.08-7.14 (m, 2H), 4.73-4.99 (m, 6H), 4.59 (t, J = 9.8 Hz, 1H), 3.80 (d, J = 21.3 Hz, 1H), 3.30 (d, J = 16.8 Hz, 1H), 3.10 (d, J = 16.8 Hz, 1H). ^{31}P NMR (162 MHz, CDCl_3) δ = 23.55 ppm.

1,3-Di-Boc-2-(trifluoromethylsulfonyl)guanidine (**10**).

Prepared according to the literature procedure.¹⁶ ^1H NMR (400 MHz, CDCl_3) δ = 9.98 (br s, 2H), 1.54 (s, 18H) ppm. ^{19}F NMR (377 MHz, CDCl_3) δ = -78.74 ppm.

tert-Butyl (2-(4-formylphenoxy)ethyl)carbamate (**14**).

Prepared according to the literature procedure.¹⁷ ¹H NMR (400 MHz, CDCl₃) δ = 9.84 (s, 1H), 7.75-7.83 (m, 2H), 6.92-7.00 (m, 2H), 5.13 (br s, 1H), 4.08 (t, *J* = 5.2 Hz, 2H), 3.53 (q, *J* = 5.2 Hz, 2H), 1.42 (s, 9H) ppm.

(S)-3-amino-1-(benzyloxy)pyrrolidin-2-one (**15**).

Prepared by T. Quennesson according to the literature procedure.¹⁸

¹H NMR (400 MHz, DMSO-*d*₆) δ = 9.67 (s, 3H), 7.45-7.49 (m, 2H), 7.36-7.42 (m, 3H), 4.96 (s, 2H), 3.97 (t, *J* = 9.8 Hz, 1H), 3.44-3.50 (m, 2H), 2.32-2.41 (m, 1H), 1.90-1.99 (m, 1H).

tert-Butyl (2-(4-(((*S*)-1-(benzyloxy)-2-oxopyrrolidin-3-yl)amino)(bis(benzyloxy)phosphoryl)methyl)phenoxy)ethyl)carbamate (**16**).

Prepared from compounds **14** (532 mg, 2 mmol) and **15** (515 mg, 1.9 mmol) according to GP-1 to obtain a white powder (192 mg, 0.27 mmol, 14%). ¹H NMR (400 MHz, CDCl₃) δ = 7.36-7.42 (m, 3H), 7.26-7.36 (m, 12H), 7.13-7.19 (m, 2H), 6.81-6.86 (m, 2H), 5.30 (s, 1H), 4.85-5.13 (m, 6H), 4.72-4.82 (m, 1H), 4.02 (d, *J* = 11.9 Hz, 1H), 3.99 (br d, *J* = 5.4 Hz, 2H), 3.53 (br d, *J* = 5.4 Hz, 2H), 3.48 (s, 1H), 3.02-3.23 (m, 3H), 1.90-2.02 (m, 1H), 1.51-1.58 (m, 1H), 1.45 (s, 9H) ppm. ¹³C NMR (101 MHz, CDCl₃) δ = 169.6, 158.6, 136.3, 135.2, 130.4, 129.8, 129.7, 129.4, 128.9, 128.6, 128.5, 128.4, 128.2, 128.0, 127.8, 127.0, 114.7, 76.9, 68.6, 68.2, 67.2, 58.5, 57.0, 52.9, 44.7, 40.1, 28.4, 24.5 ppm. ³¹P NMR (162 MHz, CDCl₃) δ = 23.57 ppm.

Benzyl hydrogen ((4-(2-aminoethoxy)phenyl)(((*S*)-1-(benzyloxy)-2-oxopyrrolidin-3-yl)amino)methyl)phosphonate (**17**).

To a solution of compound **16** (280 mg, 0.39 mmol) in DCM (5 mL) at 0 °C, HCl (100 μL, 4M, 1 eq.) in dioxane was added portion wise (every 2 h, 3x). After 8 h, the reaction mixture was dried *in vacuo* affording compound **17** as HCl salt (190 mg, 0.34 mmol, 86%) and was used without further purification. ¹H NMR (400 MHz, CD₃OD): δ = 7.60 (br d, *J* = 8.5 Hz, 2H), 7.28-7.49 (m, 10H), 7.14 (br d, *J* = 8.5 Hz, 2H), 5.00-5.17 (m, 2H), 4.28 (t, *J* = 6.0 Hz, 2H), 3.47 (t, *J* = 6.0 Hz, 2H), 3.39 (br s, 3H), 3.33-3.36 (m, 1H), 2.37-2.50 (m, 1H), 1.97-2.17 (m, 1H) ppm. ¹³C NMR (101 MHz, CD₃OD): δ = 165.7, 160.6, 138.2, 136.1, 133.1, 132.5, 130.7, 130.2, 129.7, 129.7, 129.4, 129.0, 124.5, 116.6, 78.1, 65.6, 54.5, 45.0, 40.4, 22.3 ppm. ³¹P NMR (162 MHz, CD₃OD): δ = 11.79 ppm.

tert-Butyl 2-((2-(4-(((benzyloxy)(hydroxy)phosphoryl)(((*S*)-1-(benzyloxy)-2-oxopyrrolidin-3-yl)amino)methyl)phenoxy)ethyl)amino)-4,5-dihydro-1H-imidazole-1-carboxylate (**18**).

Compound **17** (105 mg, 0.19 mmol, 1 eq.) was suspended in MeOH (3 mL), *tert*-butyl 2-(methylthio)-4,5-dihydro-1H-imidazole-1-carboxylate **9** (121 mg, 0.56 mmol, 3 eq.) and DIPEA (82 mg, 0.56 mmol, 3 eq.) was added. The reaction mixture was heated to 40 °C for 2 days and dried *in vacuo*. The resulting residue was washed with diethyl ether affording compound **18** as grey solid (96 mg, 0.14 mmol, 74%) and was used without further purification.

Benzyl hydrogen (((*S*)-1-(benzyloxy)-2-oxopyrrolidin-3-yl)amino)(4-(2-guanidinoethoxy)phenyl)methyl)phosphonate (**19**).

Compound **17** (130 mg, 0.23 mmol, 1 eq.) was suspended in MeOH (4 mL), 1H-pyrazole-1-carboximidamide hydrochloride (51 mg, 0.35 mmol, 1.5 eq.) and DIPEA (180 mg, 1.4 mmol, 6 eq.) was added. The reaction mixture was heated to 40 °C for 2 days and dried *in vacuo*. The resulting residue was washed with diethyl ether affording compound **19** as off white solid (110 mg, 0.18 mmol, 84%) and was used without further purification.

((4-(2-Guanidinoethoxy)phenyl)(((S)-1-hydroxy-2-oxopyrrolidin-3-yl)amino)methyl)phosphonic acid (**21**).

To a solution of compound **19** (110 mg, 0.18 mmol, 1 eq.) in MeOH/H₂O/AcOH (2:2:1, 5 mL), a catalytic amount of Pd/C (10%) was added. The reaction mixture was then stirred under a hydrogen atmosphere for 4 h. The mixture was filtered and dried *in vacuo*, redissolved in H₂O, frozen, and lyophilised. The resulting solid was purified by preparative HPLC to obtain compound **21** as off-white solid (34 mg, 48 %). ¹H NMR (400 MHz, D₂O) δ = 8.38 (s, 2H), 7.40 (dd, *J* = 8.6, 1.5 Hz, 2H), 7.00 (d, *J* = 8.6 Hz, 2H), 4.18 (t, *J* = 4.9 Hz, 2H), 3.56 (br t, *J* = 4.9 Hz, 2H), 3.41-3.49 (m, 1H), 3.12-3.18 (m 3H), 2.25-2.37 (m, 1H), 1.92-2.05 (m, 1H) ppm. ¹³C NMR (101 MHz, D₂O) δ = 170.6, 167.2, 157.9, 130.3, 126.5, 115.1, 66.5, 58.9, 57.6, 42.5, 40.8, 21.4 ppm. ³¹P NMR (162 MHz, D₂O) δ = 12.98 ppm. HRMS (ESI⁺): *m/z* calcd. for C₁₄H₂₃N₅O₆P⁺ ([M+H]⁺) 388.1380, measured 388.1383.

((4-(2-Aminoethoxy)phenyl)(((S)-1-hydroxy-2-oxopyrrolidin-3-yl)amino)methyl)phosphonic acid (**22**).

To a solution of compound **17** (155 mg, 0.28 mmol, 1 eq.) in MeOH/H₂O/AcOH (2:2:1, 5 mL), a catalytic amount of Pd/C (10%) was added. The reaction mixture was then stirred under a hydrogen atmosphere for 2 h. The mixture was filtered and dried *in vacuo*, redissolved in H₂O, frozen, and lyophilised to obtain an orange powder (70 mg). Part of the crude (35 mg, 50%) was purified by preparative HPLC to obtain

compound **21** as pale yellow solid (21 mg, 0.12 mmol, 44%). ¹H NMR (400 MHz, D₂O) δ = 7.47 (d, *J* = 8.8 Hz, 2H), 7.06 (d, *J* = 8.8 Hz, 2H), 4.21-4.39 (m, 3H), 3.82 (t, *J* = 8.8 Hz, 1H), 3.61 (t, *J* = 8.8 Hz, 1H), 3.51 (q, *J* = 8.4 Hz, 1H), 3.42 (br t, *J* = 4.8 Hz, 1H), 2.31-2.46 (m, 1H), 1.99-2.16 (m, 1H) ppm. ¹³C NMR (101 MHz, D₂O) δ = 167.3, 157.6, 130.3, 114.9, 64.0, 59.0, 53.4, 46.4, 38.9, 23.7, 23.5, 21.5, 16.3 ppm. ³¹P NMR (162 MHz, D₂O) δ = 11.71 ppm. HRMS (ESI⁻): *m/z* calcd. for C₁₃H₁₉N₃O₆P⁻ ([M-H]⁻) 344.1017, measured 344.1010.

tert-Butyl (*S*)-1-((benzyloxy)(methyl)amino)-1-oxopropan-2-yl)carbamate (**25**).

NaHCO₃ (2.44 g, 29.1 mmol, 1.1 eq.) was suspended in a solution of *O*-benzyl-*N*-methylhydroxylamine hydrochloride **24** (5.05 mg, 29.0 mmol, 1.1 eq.) and DMAP (3.87 g, 31.7 mmol, 1.2 eq.) in DCM (150 mL) and stirred for 15 min. The mixture was added slowly to a solution of (*tert*-butoxycarbonyl)-*L*-alanine **23** (5.00 g, 26.4 mmol, 1 eq.) and EDC (6.08 g, 31.7 mmol, 1.2 eq.) in DCM (250 mL). The reaction mixture stirred for 4 h and excess solvent was removed under reduced pressure to obtain a concentrated mixture (80 mL) that was quenched with citric acid aq. (0.5 M). The mixture was extracted with DCM (3 x 50 mL) and the combined organic layers were washed with NaOH aq. (50 mL, 1M), brine, dried over anhydrous Na₂SO₄, filtered, and concentrated to dryness *in vacuo*. The resulting crude was purified by column chromatography using a gradient of 10–40% EtOAc in PE to obtain compound **25** as off-white solid (6.22 g, 20.2 mmol, 76%). ¹H NMR (400 MHz, CDCl₃) δ = 7.35-7.44 (m, 5H), 5.27 (d, *J* = 7.0 Hz, 1H), 4.86-5.05 (m, 2H), 3.23 (s, 3H), 1.76 (br s, 1H), 1.46 (s, 9H), 1.30 ppm (d, *J* = 7.0 Hz, 3H). ¹³C NMR (101 MHz, CDCl₃) δ = 167.7, 155.2, 134.1, 129.3, 129.0, 128.8, 79.5, 76.8, 46.8, 28.4, 18.6 ppm.

(*S*)-2-Amino-*N*-(benzyloxy)-*N*-methylpropanamide (**26**).

To a solution of compound **25** (5.8 g, 18.8 mmol, 1 eq.) in DCM (20 mL), HCl (19 mL, 4M, 4 eq.) in dioxane was added slowly. The reaction mixture stirred for 4 h and the excess solvent was evaporated *in vacuo* to obtain compound **26** as pure HCl salt in form of a white powder in quantitative yield (4.8 g, 19 mmol). ¹H NMR (400 MHz, CDCl₃) δ = 8.57 (br s, 2H), 7.39-7.46 (m, 2H), 7.31-7.38 (m, 3H), 5.09 (d, *J* = 10.3 Hz, 1H), 4.98 (d, *J* = 10.3 Hz, 1H), 4.67 (br s, 1H), 3.16 (s, 3H), 1.64 (d, *J* = 7.0 Hz, 3H) ppm. ¹³C NMR (101 MHz, CDCl₃) δ = 170.4, 134.1, 129.4, 129.0, 128.8, 76.4, 48.3, 34.1, 16.2 ppm.

Dibenzyl (((*S*)-1-((benzyloxy)(methyl)amino)-1-oxopropan-2-yl)amino)(4-fluorophenyl)methylphosphonate (**27a–b**).

Prepared from compound **26** (760 mg, 3.1 mmol, 1 eq.) and 4-fluorobenzaldehyde (370 μL, 3.3 mmol, 1.05 eq.) according to GP-1. The diastereoisomers were separated by preparative HPLC to obtain **27a** as white powder (155 mg, 0.27 mmol, 9%) and **27b** as off-white powder (55 mg, 0.10, 3%). **27a**: ¹H NMR (400 MHz, CDCl₃) δ = 7.27-7.37 (m, 11H), 7.17-7.25 (m, 6H), 6.95 (t, *J* = 8.6 Hz, 2H), 4.84-5.05 (m, 4H), 4.70 (d, *J* = 10.2 Hz, 1H), 4.64 (d, *J* = 10.2 Hz, 1H), 4.03 (d, *J* = 15.8 Hz, 1H), 3.96 (br d, *J* = 6.7 Hz, 1H), 3.04 (s, 3H), 2.44 (br s, 1H), 1.11 (d, *J* = 6.7 Hz, 3H) ppm. ¹³C NMR (101 MHz, CDCl₃) δ = 176.1, 162.5, 136.4, 136.3, 134.2, 131.8, 131.8, 130.6, 130.5, 129.2, 129.0, 128.7, 128.6, 128.5, 128.3, 127.9, 127.8, 115.2, 77.2, 76.5, 68.4, 68.2, 59.5, 52.2, 18.5 ppm. ¹⁹F NMR (377 MHz, CDCl₃) δ = -114.14 ppm. ³¹P NMR (162 MHz, CDCl₃) δ = 23.51 ppm. **27b**: ¹H NMR (400 MHz, CDCl₃) δ = 7.38-7.51 (m, 2H), 7.27-7.36 (m, 10H), 7.22-7.26 (m, 2H), 7.00 (t, *J* = 8.6 Hz, 2H), 6.85-6.94 (m, 2H), 4.97 (d, *J* = 8.2 Hz, 2H), 4.93 (d, *J* = 8.2 Hz, 2H), 4.51 (br d, *J* = 9.6 Hz, 1H), 4.24 (d, *J* = 17.0 Hz, 1H), 3.95 (br d, *J* = 9.6 Hz, 1H), 3.63 (br d, *J* = 5.5 Hz, 1H), 3.18 (br s, 3H), 1.17 (d, *J* = 6.6 Hz, 3H) ppm. ¹³C NMR (101 MHz, CDCl₃) δ = 176.0, 163.9, 136.2, 133.7, 130.9, 130.5, 129.0, 128.8, 128.6, 128.5, 128.3, 128.0, 127.9, 115.5, 77.2, 76.6, 68.2, 58.5, 50.7, 33.6, 18.9 ppm. ¹⁹F NMR (377 MHz, CDCl₃) δ = -113.96 ppm. ³¹P NMR (162 MHz, CDCl₃) δ = 23.38 ppm.

Notes

This project was carried out under supervision of Thibaut Quennesson and Serge Van Calenbergh at the Laboratory for Medicinal Chemistry, Ghent University, Ottergemsesteenweg 460, B-9000, Ghent, Belgium.

Funding

This project has received funding from the European Union's Horizon 2020 research and innovation programme under the Marie Skłodowska-Curie grant agreement No. 860816 (Serge Van Calenbergh).

References

- (1) Knak, T.; Abdullaziz, M. A.; Höfmann, S.; Alves Avelar, L. A.; Klein, S.; Martin, M.; Fischer, M.; Tanaka, N.; Kurz, T. Over 40 Years of Fosmidomycin Drug Research: A Comprehensive Review and Future Opportunities. *Pharmaceuticals* **2022**, *15* (12). <https://doi.org/10.3390/ph15121553>.
- (2) Jomaa, H.; Wiesner, J.; Sanderbrand, S.; Altincicek, B.; Weidemeyer, C.; Hintz, M.; Türbachova, I.; Eberl, M.; Zeidler, J.; Lichtenthaler, H. K.; Soldati, D.; Beck, E. Inhibitors of the Nonmevalonate Pathway of Isoprenoid

3. Chapter

- Biosynthesis as Antimalarial Drugs. *Science* **1999**, 285 (5433), 1573–1576. <https://doi.org/10.1126/science.285.5433.1573>.
- (3) Ashley, E. A.; Phyto, A. P. Drugs in Development for Malaria. *Drugs* **2018**, 78 (9), 861–879. <https://doi.org/10.1007/s40265-018-0911-9>.
- (4) Munier, M.; Tritsch, D.; Krebs, F.; Esque, J.; Hemmerlin, A.; Rohmer, M.; Stote, R. H.; Grosdemange-Billiard, C. Synthesis and Biological Evaluation of Phosphate Isosters of Fosmidomycin and Analogs as Inhibitors of Escherichia Coli and Mycobacterium Smegmatis 1-Deoxyxylulose 5-Phosphate Reductoisomerases. *Bioorg Med Chem* **2017**, 25 (2), 684–689. <https://doi.org/10.1016/j.bmc.2016.11.040>.
- (5) Kuntz, L.; Tritsch, D.; Grosdemange-Billiard, C.; Hemmerlin, A.; Willem, A.; Bach, T. J.; Rohmer, M. Isoprenoid Biosynthesis as a Target for Antibacterial and Antiparasitic Drugs: Phosphonohydroxamic Acids as Inhibitors of Deoxyxylulose Phosphate Reducto-Isomerase. *Biochemical Journal* **2005**, 386 (1), 127–135. <https://doi.org/10.1042/BJ20041378>.
- (6) Chofor, R.; Risseeuw, M. D. P.; Pouyez, J.; Johnny, C.; Wouters, J.; Dowd, C. S.; Couch, R. D.; Van Calenbergh, S. Synthetic Fosmidomycin Analogues with Altered Chelating Moieties Do Not Inhibit 1-Deoxy-d-Xylulose 5-Phosphate Reductoisomerase or Plasmodium Falciparum Growth in Vitro. *Molecules* **2014**, 19 (2), 2571–2587. <https://doi.org/10.3390/molecules19022571>.
- (7) Devreux, V.; Wiesner, J.; Jomaa, H.; Rozenski, J.; Van der Eycken, J.; Van Calenbergh, S. Divergent Strategy for the Synthesis of α -Aryl-Substituted Fosmidomycin Analogues. *J Org Chem* **2007**, 72 (10), 3783–3789. <https://doi.org/10.1021/jo0700981>.
- (8) Verbrugghen, T.; Cos, P.; Maes, L.; Van Calenbergh, S. Synthesis and Evaluation of α -Halogenated Analogues of 3-(Acetylhydroxyamino)Propylphosphonic Acid (FR900098) as Antimalarials. *J Med Chem* **2010**, 53 (14), 5342–5346. <https://doi.org/10.1021/jm100211e>.
- (9) Chofor, R.; Sooriyaarachchi, S.; Risseeuw, M. D. P.; Bergfors, T.; Pouyez, J.; Johnny, C.; Haymond, A.; Everaert, A.; Dowd, C. S.; Maes, L.; Coenye, T.; Alex, A.; Couch, R. D.; Jones, T. A.; Wouters, J.; Mowbray, S. L.; Van Calenbergh, S. Synthesis and Bioactivity of β -Substituted Fosmidomycin Analogues Targeting 1-Deoxy-D-Xylulose-5-Phosphate Reductoisomerase. *J Med Chem* **2015**, 58 (7), 2988–3001. <https://doi.org/10.1021/jm5014264>.
- (10) Kurz, T.; Schlüter, K.; Kaula, U.; Bergmann, B.; Walter, R. D.; Geffken, D. Synthesis and Antimalarial Activity of Chain Substituted Pivaloyloxymethyl Ester Analogues of Fosmidomycin and FR900098. *Bioorg Med Chem* **2006**, 14 (15), 5121–5135. <https://doi.org/10.1016/j.bmc.2006.04.018>.
- (11) Brücher, K.; Illarionov, B.; Held, J.; Tschan, S.; Kunfermann, A.; Pein, M. K.; Bacher, A.; Gräwert, T.; Maes, L.; Mordmüller, B.; Fischer, M.; Kurz, T. α -Substituted β -Oxa Isosteres of Fosmidomycin: Synthesis and Biological Evaluation. *J Med Chem* **2012**, 55 (14), 6566–6575. <https://doi.org/10.1021/jm300652f>.
- (12) Lienau, C.; Gräwert, T.; Alves Avelar, L. A.; Illarionov, B.; Held, J.; Knaab, T. C.; Lungerich, B.; van Geelen, L.; Meier, D.; Geissler, S.; Cynis, H.; Riederer, U.; Buchholz, M.; Kalscheuer, R.; Bacher, A.; Mordmüller, B.; Fischer, M.; Kurz, T. Novel Reverse Thia-Analogs of Fosmidomycin: Synthesis and Antiplasmodial Activity. *Eur J Med Chem* **2019**, 181, 111555. <https://doi.org/10.1016/j.ejmech.2019.07.058>.
- (13) Braun-Cornejo, M.; Platteschorre, M.; de Vries, V.; Bravo, P.; Sonawane, V.; Hamed, M. M.; Hauptenthal, J.; Reiling, N.; Rottmann, M.; Piet, D.; Maas, P.; Diamanti, E.; Hirsch, A. K. H. A Positive Charge in an Antimalarial Compound Unlocks Broad-Spectrum Antibacterial Activity. *ChemRxiv* **2024**, 1–14. <https://doi.org/10.26434/chemrxiv-2024-rs2v8>. This content is a preprint and has not been peer-reviewed.
- (14) Yong, Y. F.; Kowalski, J. A.; Lipton, M. A. Facile and Efficient Guanylation of Amines Using Thioureas and Mukaiyama's Reagent. *J Org Chem* **1997**, 62 (5), 1540–1542. <https://doi.org/10.1021/jo962196k>.
- (15) Bhagat, S.; Chakraborti, A. K. An Extremely Efficient Three-Component Reaction of Aldehydes/Ketones, Amines, and Phosphites (Kabachnik–Fields Reaction) for the Synthesis of α -Aminophosphonates Catalyzed by Magnesium Perchlorate. *J Org Chem* **2007**, 72 (4), 1263–1270. <https://doi.org/10.1021/jo062140i>.
- (16) Perlmutter, S. J.; Geddes, E. J.; Drown, B. S.; Motika, S. E.; Lee, M. R.; Hergenrother, P. J. Compound Uptake into E. Coli Can Be Facilitated by N-Alkyl Guanidiniums and Pyridiniums. *ACS Infect Dis* **2021**, 7 (1), 162–173. <https://doi.org/10.1021/acsinfecdis.0c00715>.
- (17) Ward, R. A.; Brassington, C.; Breeze, A. L.; Caputo, A.; Critchlow, S.; Davies, G.; Goodwin, L.; Hassall, G.; Greenwood, R.; Holdgate, G. A.; Mrosek, M.; Norman, R. A.; Pearson, S.; Tart, J.; Tucker, J. A.; Vogtherr, M.; Whittaker, D.; Wingfield, J.; Winter, J.; Hudson, K. Design and Synthesis of Novel Lactate Dehydrogenase A Inhibitors by Fragment-Based Lead Generation. *J Med Chem* **2012**, 55 (7), 3285–3306. <https://doi.org/10.1021/jm201734r>.
- (18) Leeson, P. D.; Williams, B. J. [3R]-3-Amino-1-Hydroxy Pyrrolidin-2-One and Its Use as a Neuroprotective Agent, 1989. US 4863953 A.

4. Chapter:

Target-Directed Dynamic Combinatorial Chemistry Affords Binders of *Mycobacterium tuberculosis* IspE

Maria Braun-Cornejo, Camilla Ornago, Vidhisha Sonawane, Jörg Haupenthal, Andreas M. Kany, Eleonora Diamanti, Gwenaëlle Jézéquel, Norbert Reiling, Wulf Blankenfeldt, Peter Maas, and Anna K. H. Hirsch.

Manuscript submitted on May 28th 2024 to ACS Medicinal Chemistry Letters and is available on the preprint server ChemRxiv ([10.26434/chemrxiv-2024-dh07n](https://doi.org/10.26434/chemrxiv-2024-dh07n)).

Author Contributions

M. Braun-Cornejo was involved in designing the project, performing and evaluating the tdDCC experiments, synthesising compounds, designing and analysing the docking experiment, and writing the manuscript. C. Ornago purified *Mtb*IspE, performed and evaluated the binding and docking studies. V. Sonawane performed and evaluated the 7H9 solubility and *Mtb*H37Rv activity tests. J. Haupenthal coordinated and evaluated the *E. coli* tests. A. M. Kany coordinated and evaluated the PBS solubility tests. G. Jézéquel was involved in designing and supervising the project, and analysing the docking results. E. Diamanti, N. Reiling, and W. Blankenfeld were involved in supervising the project. P. Maas was involved in evaluating the tdDCC equilibrium, designing and supervising the project. A. K. H. Hirsch was involved in designing and supervising the project. All authors edited or approved the submitted manuscript.

Note: Please refer to ChemRxiv for full Supporting Information including NMR, HRSM, and LCMS spectra not included in this thesis.

Target-Directed Dynamic Combinatorial Chemistry Affords Binders of *Mycobacterium Tuberculosis* IspE

Maria Braun-Cornejo,^{1,2,3} Camilla Ornago,⁴ Vidhisha Sonawane,⁵ Jörg Haupenthal,³ Andreas M. Kany,³ Eleonora Diamanti,³ Gwenaëlle Jézéquel,³ Norbert Reiling,^{5,6} Wulf Blankenfeldt,⁴ Peter Maas,¹ and Anna K. H. Hirsch^{2,3*}

¹ Specs Research Laboratory, Specs Compound Handling, B.V., Bleiswijkseweg 55, 2712 PB, Zoetermeer, The Netherlands.

² Saarland University, Department of Pharmacy, Campus Building E8.1, 66123 Saarbrücken, Germany.

³ Helmholtz Institute for Pharmaceutical Research Saarland (HIPS) – Helmholtz Centre for Infection Research (HZI), Campus Building E8.1, 66123 Saarbrücken, Germany.

⁴ Department Structure and Function of Proteins Helmholtz Centre for Infection Research Inhoffenstrasse 7, 38124 Braunschweig, Germany.

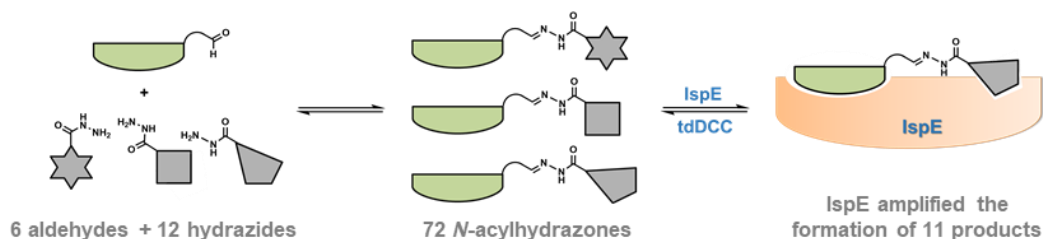
⁵ RG Microbial Interface Biology, Research Center Borstel Leibniz Lung Center, Parkallee 1-40, 23845 Borstel, Germany.

⁶ German Center for Infection Research (DZIF), Partner Site Hamburg-Lübeck-Borstel-Riems, 23845 Borstel, Germany.

*Corresponding author: Anna.Hirsch@helmholtz-hips.de

Abstract

In the search for new antitubercular compounds, we leveraged target-directed dynamic combinatorial chemistry (tdDCC) as an efficient hit-identification method. In tdDCC, the target selects its own binders from a dynamic library generated *in situ*, reducing the number of compounds that require synthesis and evaluation. We combined a total of twelve hydrazides and six aldehydes to generate 72 structurally diverse *N*-acylhydrazones. To amplify the best binders, we employed anti-infective target 4-diphosphocytidyl-2C-methyl-D-erythritol kinase (IspE) from *Mycobacterium tuberculosis* (*Mtb*). We successfully validated the use of tdDCC as hit-identification method for IspE and optimised the analysis of tdDCC hit determination. From the 72 possible *N*-acylhydrazones, we synthesised twelve of them revealing several new starting points for the development of IspE inhibitors as antibacterial agents.



Keywords: Target-directed dynamic combinatorial chemistry, *N*-acylhydrazones, antitubercular, antibacterial, *Mycobacterium tuberculosis*.

Introduction

Target-directed dynamic combinatorial chemistry (tdDCC) has evolved into an effective hit-identification method for medicinal chemistry. A set of “building blocks” with complementary reactivities engage in a reversible bond-forming reaction, resulting in a dynamic combinatorial library (DCL) that comprises all possible building block combinations.¹ A target protein can influence this equilibrium by stabilising binders, resulting in their amplification. This selective amplification circumvents the need to synthesise the entire library, making tdDCC particularly efficient in the time- and cost-sensitive early stages of drug

discovery.²⁻⁴ Recent literature highlights the application of new targets, analytical methods, and reaction types for tdDCC, resulting in robust protocols and an increasing number of success stories.⁵⁻⁸ One of the frequently used reactions in tdDCC is the formation of acylhydrazones from aldehydes and hydrazides. In 2021, we applied this reaction to DXPS, the first enzyme of the 2C-methyl-D-erythritol 4-phosphate (MEP) pathway obtaining promising new anti-infective compounds.⁶

While all enzymes of the MEP-pathway are considered potential antibiotic drug targets, few inhibitors have been reported since its discovery in the 1990s.⁹⁻¹¹ This pathway is vital for critical pathogens, such as *Mycobacterium tuberculosis* (*Mtb*), and Gram-negative bacteria to afford the essential isoprenoid precursors isopentenyl diphosphate (IDP) and dimethylallyl diphosphate (DMADP).¹² Moreover, it is absent in mammals, where the mevalonate pathway yields the same building blocks, making target-related toxicity less of a concern.^{9,13} The identification of new inhibitors against the fourth enzyme of the pathway, 4-diphosphocytidyl-2C-methyl-D-erythritol kinase (IspE), is challenging. Most available crystal structures of IspE homologues are co-crystals with the natural substrates. So far, only one IspE structure in complex with an inhibitor has been published, likely due to its structural similarity to the natural IspE substrate and to its high potency.¹⁴ With single-digit micromolar activity, this compound is the most potent known IspE inhibitor, but it lacks whole-cell activity. A few more IspE inhibitors have been discovered, however, activities are moderate and no significant improvements in whole-cell activity have been achieved.¹⁵ Recent efforts to discover IspE hits have included structure-based virtual screening, however, only a very limited number of hits could be identified. In particular, we focused on filtering the screening library for compounds with properties that aid accumulation in *Escherichia coli* (*Ec*). The applied filter seemed successful, but optimisation of the affinity for *Ec*IspE proved to be difficult.¹⁶ Most IspE studies, use protein homologues from model organisms like *E. coli* and *Aquifex aeolicus*. Very recently, Choi *et al.* took a step towards the identification of antitubercular IspE inhibitors by screening 15 million compounds *in silico* against *Mtb*IspE (PDB: 3PYG). On this basis, one hit was confirmed, but could not be optimised thus far.¹⁷ To the author's knowledge, no other inhibitors targeting *Mtb*IspE have been reported. Therefore, we highlight the need for additional efforts towards investigating IspE from critical pathogen homologues like *M. tuberculosis*.

We explored a new avenue in IspE hit-discovery by assessing the compatibility of *Mtb*IspE with tdDCC. This targeted approach allows to explore novel scaffolds without relying on knowledge of protein structure or pre-existing inhibitors. One of the limitations of tdDCC is the need of a substantial amount of protein, which has to be stable under the reaction conditions. Therefore, more robust proteins originating from model organism are often used in place of pathogenic proteins. Recently, we optimised the production of *Mtb*IspE (Supporting Information - SI) and could verify its stability under the conditions necessary to build an acylhydrazone DCL (Figure S1).⁶ Therefore, we are confident that tdDCC can be a valuable method to obtain new specific starting points for MEP-pathway inhibitors using the pathogen homolog *Mtb*IspE.

Results and Discussion

Design of dynamic combinatorial libraries

In this study, we used *Mtb*IspE as target protein and the reversible reaction of hydrazides and aldehydes to form dynamic combinatorial libraries (DCLs) of acylhydrazones. To accelerate the reaction at neutral pH, aniline was used as catalyst.^{2,4,18} We analysed the protein's effect on the DCLs by comparing HPLC-MS/MS data of blank vs protein-templated (PT) experiments. The experiments spanned three days, with periodic sampling (every 2 hours, followed by two samples per day after 8 hours), addition of NaOH prior to analysis ensured the sample composition was preserved.¹⁸ Templated experiments were conducted in duplicate, and the protein was denatured and removed prior to HPLC-MS/MS analysis.

Employing a randomised tdDCC hit-identification approach, we covered a wide chemical space, not relying on any structural information of the protein or its ligands. We selected diverse commercially available aldehyde and hydrazide building blocks with various geometries, sizes, and functional groups, including (hetero)aromatic rings (six- and five-membered, electron-rich/-poor), aliphatic moieties (morpholine,

piperazine, adamantane), and various types of spacers. To ensure the HPLC-MS/MS analysis would be feasible, not too cluttered, nor contain isobaric products, we designed four distinct DCLs, each comprising 18 acylhydrazones. The building blocks were organised into two clusters of hydrazides (**A–M**) with six building blocks each and two clusters of aldehydes (**1–6**) with three building blocks each. To cover all possible combinations, we reacted aldehydes from cluster 1 with hydrazides from cluster 1 in DCL-1, aldehydes from cluster 2 with hydrazides from cluster 2 in DCL-2, aldehydes from cluster 1 with hydrazides from cluster 2 in DCL-3, and aldehydes from cluster 2 with hydrazides from cluster 1 in DCL-4, theoretically leading to 72 products (Figure 1).

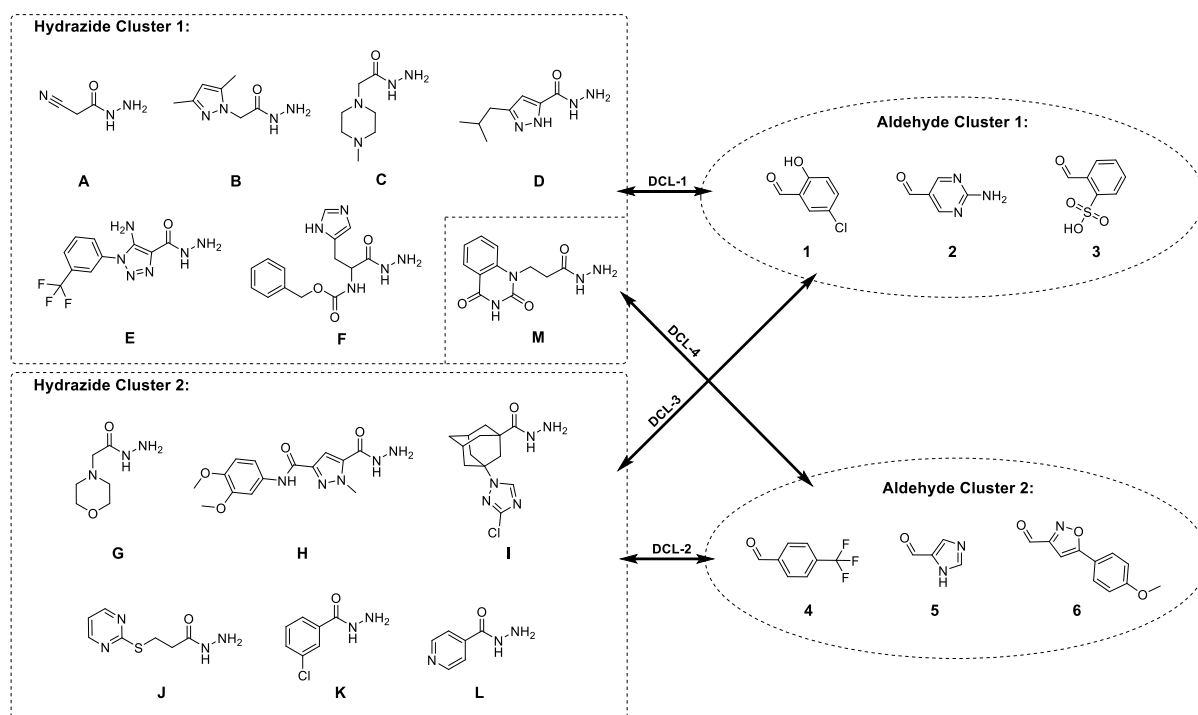


Figure 1. Clusters of hydrazides (**A–M**) and aldehydes (**1–6**) building blocks used in four dynamic combinatorial libraries (DCLs).

Determination of tdDCC IspE hits

The tdDCC hits and thus potential *Mtb*IspE binders are amplified in the PT experiment compared to the blank experiment. The first step in the analysis of DCLs is the determination of the equilibrium since the amplification factors need to be calculated when the concentration of products is stable. To determine the evolution of the possible products, it is important to measure the characteristic UV absorbance of the acylhydrazones linker (310 nm) during the HPLC-MS/MS run. The resulting UV peaks are assigned to each product using the MS data (Figure S2–S5). The sum of all peak areas is normalised to 100% in order to obtain the respective relative peak area (RPA) for each product. The RPA values represent relative concentrations, determined at each time point of the blank experiment until the values stabilise. Plotting the RPAs over time shows the evolution of the products: in DCL-1 the four most abundant compounds are visibly flattening from eight hours (h) onwards (Figure 2A). However, the rest of the compounds are out of range, making a visual inspection difficult. Given that we do not want to neglect the importance of low-abundant compounds on the equilibrium, we normalised the RPA values using decimal scaling, confirming that the library starts stabilising from 8 h onwards (Figure 2B). To determine the slope reaches zero, we calculated the change in RPA for each time interval and represented it in a stacked bar chart (Figure 2C), showing that the compounds' concentration was most stable in the time interval 8–24 h and remained largely stable thereafter. The other three libraries behaved the same way, reaching equilibrium within 24 h and also

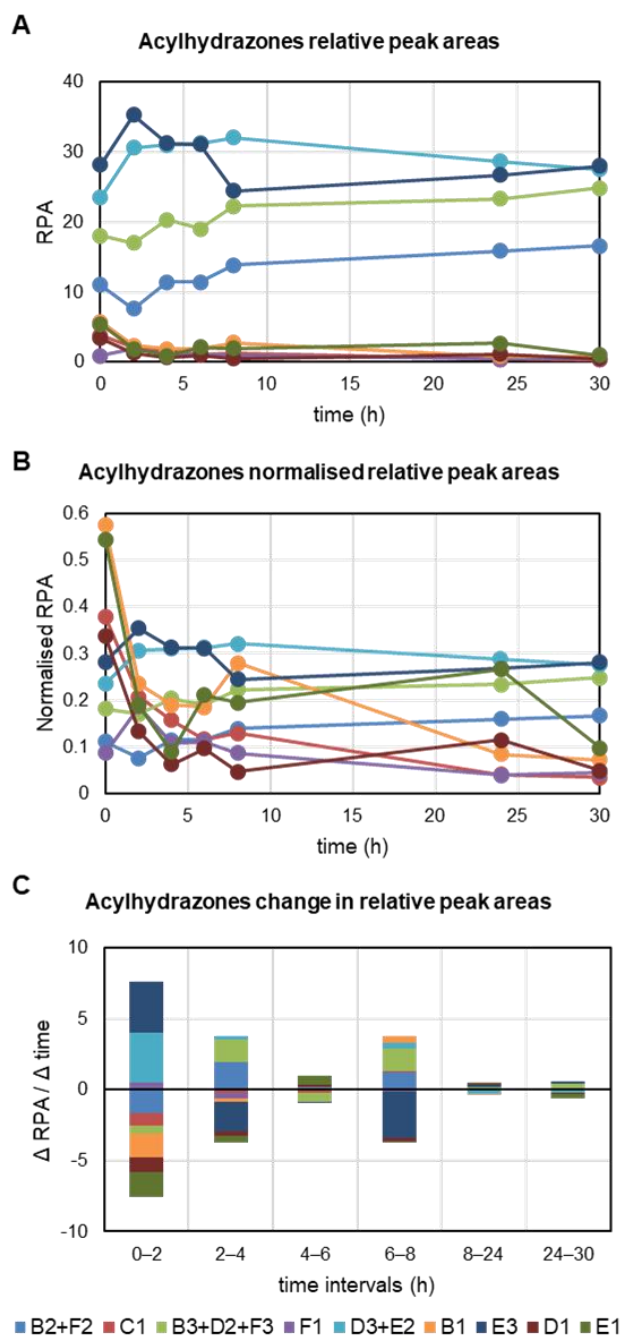


Figure 2. Graphical determination of equilibrium in blank DCL-1. A) Evolution of relative peak areas (RPA) of formed acylhydrazones over time. B) Normalised RPAs over time. C) Change of RPA in each time interval.

the strongly electron-withdrawing nitrile and carbonyl groups. When adding NaOH for sample preparation, compounds containing **A** were likely deprotonated, followed by degradation or formation of undesired byproducts.

In the case of DCL-2, despite employing a higher protein concentration compared to DCL-1, there was no significant amplification of any product at 24 h or the subsequent time point, 35 h. The product amplifications remained largely unchanged in both time points, indicating that the PT experiments also had reached equilibrium. We selected compound **K4** as a control since our protein seemingly did not have any influence on its formation (Figure S9).

maintained stable concentrations beyond (Figure S6–S8). To determine the tdDCC hits, we compared the RPAs of the PT experiments to the blanks at 24 h and set a threshold of at least 50% increase in compound formation. In total, eleven acylhydrazones passed our criteria, with amplification factors ranging from 0.5 to 15.5, qualifying them for resynthesis and further evaluation (Figure 3). During the analysis of chromatograms, challenges arose concerning product identification. Some compound peaks were not neatly separated, forcing us to consider them in clusters, others presented two peaks, likely due to isomers, and were considered separately in our evaluation. Lastly, some compounds were detected by MS, but their respective UV signal interfered with the injection peak or was too low for integration (<1%), both in the blank and PT experiments. Consequently, we excluded these compounds from the analysis (Figure S2–S5).

In DCL-1 at 24 h, one potential hit, **E1**, reported a small amplification factor of 0.5 (Figure 3A). The protein concentration used for the PT experiments was rather low with 25 mol% *MtblspE*, a higher concentration should intensify amplification factors, therefore we decided to use 40 mol% from DCL-2 onwards.⁶ Nevertheless, we decided to also determine the product amplifications at 30 h for DCL-1 since the equilibrium remained stable (Figure 2). Interestingly, at 30 h, the amplification of **E1** amplification grows extremely, and two more products, **C1** and **D1**, pass our amplification threshold, indicating that the PT experiment's equilibrium is not in line with the blank experiment (Figure 3A). It is noteworthy that no product containing hydrazide **A** could be identified in the chromatograms of DCL-1. We believe that **A**'s methylene is rather acidic due to

DCL-3 yielded four potential hits at 24 h, **L1**, **H1**, **I1** and **K1**, however, the latter two products were clustered together due to their significant peak overlap (Figure S4). Regarding **H1**, a complication arose as it appeared as a single peak in one PT duplicate, while in the other PT sample and the blank, it appeared as two overlapping peaks (Figure S4). This discrepancy may be due to **H1** existing as different isomers. However, the lone peak was insufficient to compensate for the missing area of the two peaks in the duplicate, resulting in a significant error in **H1**'s RPA. Despite the differences in RPA, both PT duplicates showcased substantial amplification compared to the blank, with amplification factors of 11.4 and 4.2, firmly establishing **H1** as a tdDCC hit (Figure 3B and Figure S4).

Given the reactivity issue for hydrazide **A** in DCL-1, we opted for its substitution in cluster 1 with a structurally very different hydrazide, **M** (Figure 1). One product, **M5**, could not be detected despite these modifications. Nevertheless, we identified four potential hits, namely, **B6**, **D6**, **E4** and **E6**, each exhibiting relatively modest amplification factors ranging from 0.7 to 2.3 at 24 h (Figure 3C).

To validate these eleven preliminary hits and assess their biological relevance, we synthesised them in a one-step reaction. The corresponding hydrazides and aldehydes were refluxed in methanol overnight, affording the acylhydrazones in moderate to excellent yields (SI).

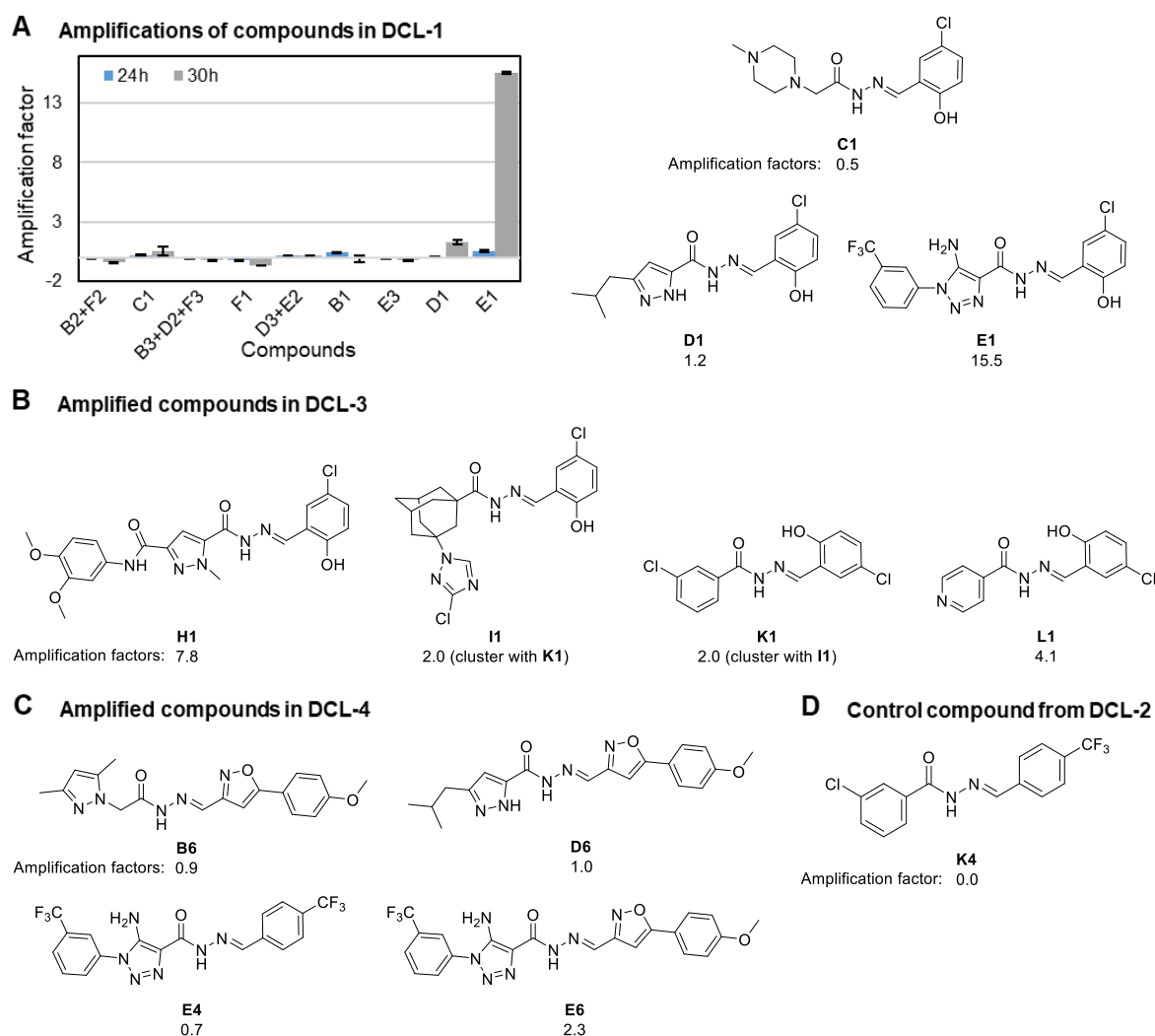


Figure 3. Structures of selected compounds for biological evaluation. A) Amplification of acylhydrazones in the protein-templated experiment of dynamic combinatorial library-1 (DCL-1) at 24 and 30 h, and the structures of selected preliminary hits. B) Amplified compounds in DCL-3. C) Amplified compounds in DCL-4. D) Selected control compound from DCL-2.

Structure–amplification relationship of tdDCC hits

Regarding the composition of the tdDCC hits (Figure 3), there is one building block that clearly stood out, aldehyde **1**. It is found in seven of the eleven potential hits, notably, the most amplified compounds (**E1**, **H1**, **L1**) all incorporate aldehyde **1**. This observation suggests that the arrangement of the aromatic scaffold with a *para*-substituted OH and Cl fit and interacted well in an IspE pocket. In addition, the structure of aldehyde **6** may also be interesting, since it is present in three potential hits **B6**, **D6** and **E6**. Aldehydes **2**, **3** and **5** are not included in any tdDCC hit. The most amplified aldehydes **1** and **6** both contain an electron-rich phenyl ring due to electron-donating substituents hydroxy and methoxy, which both can also be hydrogen-bond acceptors. In contrast, the aldehydes that were not amplified do all contain comparatively electron-deficient aromatic rings. The most prevalent hydrazide component found in the hits is **E**, which appears in **E1**, **E4**, and **E6**. Hydrazide **E** contains an electron-deficient phenyl ring that is linked to an electron-rich heterocycle. Hydrazides **F**, **G**, **J**, and **M** are not included in any tdDCC hit, possibly **F** and **M** are too bulky, and **J** is too electron-deficient. The lack of amplified compounds containing **C**, **G** and **I** indicates that aliphatic groups are not well-tolerated by IspE. Interestingly, the by far most amplified hit, **E1**, contains the two most prevalent building blocks of their kind, suggesting that their structural and electronic features align with complementary sites of the enzyme. These motifs along with their hydrogen-bond donor/acceptor geometry could be promising starting points for the development of new *Mtb*IspE inhibitors. It cannot be ruled out that the acylhydrazone linker may also contribute to favourable interactions, especially hydrogen bonds, and should be kept in mind.

In silico elucidation of tdDCC hits' binding mode

Docking simulations provided valuable insights that further rationalise the structure–amplification relationship within the active site of *Mtb*IspE. We generated ten binding poses for each compound across the four DCLs to analyse trends in the binding modes of the compounds. The defined binding site for the docking encompassed both natural substrates' binding pockets as defined in the published crystal structures of *Mtb*IspE (3PYE for CDP-ME and 3PYG for ADP).¹⁹ Importantly, we did not set any binding restraint to minimise bias, and we removed poses that were unrealistic due to bad torsion, or inter- and intramolecular clashes. The analysis of these compound poses revealed preferred binding tendencies for two of the three most common motifs in the tdDCC hits; fragment **1** and **E**, whereas fragment **6** did not show a particular binding tendency. Aldehyde **1** is by far the most frequently appearing fragment in the hits' structures and the docking results showed two pockets where the characteristic phenol moiety in **1** primarily bound. One pocket was the substrate binding site of CDP-ME, where the phenol bound slightly deeper within the pocket compared to the substrate's cytidine moiety (Figure S10). The other pocket was an unoccupied area adjacent to the ADP binding site. The poses in the CDP-ME binding pocket showed a clear orientation directing the hydroxy substituent towards amino acid Ser182 with distances of 2.6–3 Å suggesting the possibility of an H-bond. Interestingly, these poses belonged to hit compounds, whereas the poses adjacent to the ADP binding site belonged to both protein-amplified and not amplified compounds, and did not present such a clear orientation. Similarly, the hits containing hydrazide **E**, had the trifluoromethyl-substituted phenyl positioned deep inside the CDP-ME binding site (Figure S11). In the case of **E1**, containing both of the fragments with the same binding tendency, motif **1** bound to a third unoccupied and very narrow pocket. This unique binding mode was the same for all poses of **E1** (Figure S12) and gives a possible explanation for its exceptionally high amplification compared to the rest of the hits. Lastly, these findings suggest a link between the CDP-ME binding site and enhanced amplification.

Acylhydrazones' low solubility hinders biological evaluation

Prior to biological evaluation of the tdDCC hits, we tested their solubility in a standard buffer as well as in *M. tuberculosis* 7H9 growth medium. Our results revealed a major issue, most compounds' solubility lies between 20 and 30 μM in PBS with 5% DMSO, representing a challenge for our established hit-verification methods. Merely product **C1** reaches a good solubility close to 1 mM, **L1** and **B6** show moderate

solubilities. Regrettably, with 3.3 μM the least soluble compound is **E1**, making our most amplified, and promising compound unsuitable for biological evaluation. We assessed the solubility in *Mtb* growth medium given that it is a complex, nutrient-rich environment with a distinct solubility profile. However, the trend continued, only seven hits are soluble at 8 μM or above, the remaining five compounds, including **E1**, were not eligible for antitubercular activity testing (Table 1).

Evaluation of tdDCC hits *Mtb*lspE binding

The compounds' low solubility prevents the determination of binding affinities (K_D). Nevertheless, qualitative binding assessments were conducted for all compounds, except **E1** and **I1**, using MicroScale Thermophoresis at 20 μM in triplicate. **C1**, **K1**, and **E4** consistently demonstrated binding across all measurements. Compound **B6** exhibited inconsistent binding, as it bound in two out of three measurements, while our negative control, **K4**, showed binding in only one measurement. These two compounds' irreproducible binding may be due to non-specific interactions. As an orthogonal method to determine qualitative binding of the hits, we performed thermal shift assays. The protein needs to reach a certain level of saturation in order to exhibit a change in melting temperature (ΔT_m), therefore compounds with a lower solubility than 20 μM (**E4**, **E1**, **I1**) could not be tested. Minimal ΔT_m values were obtained and have to be interpreted carefully, since they are close to the inherent error of the method. **K1**, **K4** and **E6** showed $\Delta T_m = +0.7^\circ\text{C}$, providing some assurance in the binding of **K1**, which shows a consistent response in both methods.

Table 1. Solubility determination and biological evaluation of tdDCC hits on *Mycobacterium tuberculosis*, HepG2, *Escherichia coli* and IspE.

DCL	Cmp	Solubility 5% DMSO in PBS (μM)	Solubility in 7H9 (μM)	<i>Mtb</i> lspE binding at 20 μM	<i>Mtb</i> lspE ΔT_m at 20 μM ($^\circ\text{C}$)	<i>Mtb</i> H37Rv MIC ₉₀ (μM)	<i>Ec</i> TolC %inh. at 50 μM	<i>Ec</i> K12 %inh. at 50 μM	HepG2 CC ₅₀ (μM)
1	C1	>800	16	Yes	<0.3	no inh. at max. sol.	17.1 \pm 0.1	<10	>50
	D1	22 \pm 9	insoluble	No	<0.3	n.d.	28 \pm 11	11 \pm 4	7.9 \pm 0.8
	E1	3.3 \pm 1	insoluble	n.d.	n.d.	n.d.	< 10	n.d.	>50
2	K4	21 \pm 6	8	1/3	+0.7	no inh. at max. sol.	38 \pm 4	12 \pm 4	>50
3	H1	28 \pm 6	32	No	<0.3	no inh. at max. sol.	< 10	n.d.	32 \pm 5
	I1	8.0 \pm 4	64	n.d.	n.d.	no inh. at max. sol.	33 \pm 3	<10	n.d.
	K1	25 \pm 4	insoluble	Yes	+0.7	n.d.	39 \pm 8	<10	7 \pm 3
	L1	108 \pm 3	16	No	<0.3	no inh. at max. sol.	52 \pm 3	18 \pm 6	~50
4	B6	65 \pm 35	16	2/3	<0.3	no inh. at max. sol.	< 10	n.d.	>50
	D6	20 \pm 10	16	No	<0.3	no inh. at max. sol.	39 \pm 6	<10	>50
	E4	12 \pm 6	insoluble	Yes	n.d.	n.d.	< 10	n.d.	>50
	E6	29 \pm 10	insoluble	No	+0.7	n.d.	< 10	n.d.	>50

n.d.: not determined

Antibacterial activity against *M. tuberculosis* and *E. coli*

M. tuberculosis is known to be notoriously hard to target,²⁰ and once again our compounds' poor solubility posed a significant obstacle to their antibacterial evaluation. Nevertheless, our final goal is to obtain antitubercular compounds. Therefore, we assessed the antitubercular activity of our hits at the

concentration of their maximum solubility in 7H9 growth medium (Table 1). Regrettably, no compound presented inhibitory activity against *MtbH37Rv* (Table 1). This lack of inhibitory effects may be attributed to permeability and efflux issues inherent to the pathogen. It is noteworthy that assay conditions were constrained, only one compound could be tested at high concentrations (64 μM) and almost half of our compounds could not be tested at all (Table 1).

The identity of *MtbIspE* and its *E. coli* ortholog are high,¹⁹ therefore we decided to test the TolC efflux pump deficient *E. coli* strain to obtain further insights into our compounds' antibacterial profile. To assess possible efflux issues of our compounds, we tested the *EcTolC* active compounds against the *E. coli* wild-type strain K12. All compounds, regardless of their solubilities, were tested at 50 μM against the *E. coli* strains. Seven of our hits displayed moderate inhibition of *EcTolC*, with more than 10% inhibition, including **K1** that was shown to bind to *IspE*. Notably, compound **L1** demonstrated the most promising result with 52% inhibition, which may be due to its higher solubility compared to most other active compounds. **L1** is also the only compound showing an appreciable effect on the growth of *E. coli* K12 wild type, indicating that the structures are prone to efflux. Additionally, a toxicity assessment conducted on HepG2 cells revealed that the majority of the compounds are non-toxic. Nevertheless, compounds **D1** and **K1** exhibited notable cytotoxicity, with IC_{50} values below 10 μM . These findings provide valuable insights into the inhibitory potential and safety profile of the compounds tested, emphasising the need for further exploration of these antibacterial starting points.

Conclusions

We have successfully demonstrated the compatibility of *MtbIspE* with acylhydrazone-based tdDCC conditions, providing a solid foundation for further exploration in drug-discovery efforts using pathogenic targets for hit-identification. In addition, we optimised the analysis of the tdDCC equilibrium for the determination of hit compounds. We identified the majority of the 72 possible *N*-acylhydrazones using HPLC-MS/MS and *in silico* evaluation of these components gave insights into the possible binding modes of our privileged scaffolds **1** and **E**. The most challenging aspect in our work was the hit validation due to the poor solubility of our eleven tdDCC hits. Despite this challenge, our study successfully verified one compound, **K1**, as targeting *IspE* and it also showed moderate activity on *EcTolC*. Compound **L1** turned out to be the most potent inhibitor of *E. coli* growth. These positive outcomes position **K1** and **L1** as starting points for further optimisation. Since the acylhydrazone moiety is likely to be the major contributor to poor solubility and thus is a critical point of improvement, we propose its replacement with bioisosteres such as oxazoles or amides. For future endeavours, however, we suggest a more careful building-block selection, including considerations such as logS values. Furthermore, contemplating alternative reactions to create dynamic combinatorial libraries with a more soluble linker should be considered as well. We urge for continuous refinement and exploration in our goal to develop anti-infective agents.

Author Contributions

M. Braun-Cornejo was involved in designing the project, performing and evaluating the tdDCC experiments, synthesising compounds, designing and analysing the docking experiment, and writing the manuscript. C. Ornago purified *MtbIspE*, performed and evaluated the binding and docking studies. V. Sonawane performed and evaluated the 7H9 solubility and *MtbH37Rv* activity tests. J. Hauptenthal coordinated and evaluated the *E. coli* tests. A. M. Kany coordinated and evaluated the PBS solubility tests. G. Jézéquel was involved in designing and supervising the project, and analysing the docking results. E. Diamanti, N. Reiling, and W. Blankenfeld were involved in supervising the project. P. Maas was involved in evaluating the tdDCC equilibrium, designing and supervising the project. A. K. H. Hirsch was involved in designing and supervising the project. All authors edited or approved the submitted manuscript.

Acknowledgements

This project has received funding from the European Union's Horizon 2020 research and innovation programme under the Marie Skłodowska-Curie grant agreement No. 860816 (A. K. H. Hirsch & P. Maas). The

authors thank Dr. Marcus Gastreich and the BioSolveIT team for expert technical support and for providing the pre-release version 13.1 of SeeSAR.

Notes

The authors declare no competing financial interest.

References

- (1) Lehn, J. M. Perspectives in Chemistry - Aspects of Adaptive Chemistry and Materials. *Angew Chem Int Ed* **2015**, *54* (11), 3276–3289. <https://doi.org/10.1002/anie.201409399>.
- (2) Frei, P.; Hevey, R.; Ernst, B. Dynamic Combinatorial Chemistry: A New Methodology Comes of Age. *Chem. Eur. J.* **2019**, *25*, 60–73. <https://doi.org/10.1002/chem.201803365>.
- (3) Mondal, M.; Hirsch, A. K. H. Dynamic Combinatorial Chemistry: A Tool to Facilitate the Identification of Inhibitors for Protein Targets. *Chem Soc Rev* **2015**, *44* (8), 2455–2488. <https://doi.org/10.1039/c4cs00493k>.
- (4) Hartman, A. M.; Gierse, R. M.; Hirsch, A. K. H. Protein-Templated Dynamic Combinatorial Chemistry: Brief Overview and Experimental Protocol. *European J Org Chem* **2019**, *22*, 3581–3590. <https://doi.org/10.1002/ejoc.201900327>.
- (5) Frei, P.; Pang, L.; Silbermann, M.; Eriş, D.; Mühlethaler, T.; Schwardt, O.; Ernst, B. Target-Directed Dynamic Combinatorial Chemistry: A Study on Potentials and Pitfalls as Exemplified on a Bacterial Target. *Chem. Eur. J.* **2017**, *23* (48), 11570–11577. <https://doi.org/10.1002/chem.201701601>.
- (6) Jumde, R. P.; Guardigni, M.; Gierse, R. M.; Alhayek, A.; Zhu, D.; Hamid, Z.; Johannsen, S.; Elgaher, W. A. M.; Neusens, P. J.; Nehls, C.; Haupenthal, J.; Reiling, N.; Hirsch, A. K. H. Hit-Optimization Using Target-Directed Dynamic Combinatorial Chemistry: Development of Inhibitors of the Anti-Infective Target 1-Deoxy-D-Xylulose-5-Phosphate Synthase. *Chem Sci* **2021**, *12* (22), 7775–7785. <https://doi.org/10.1039/D1SC00330E>.
- (7) Ekström, A. G.; Wang, J. T.; Bella, J.; Campopiano, D. J. Non-Invasive ¹⁹F NMR Analysis of a Protein-Templated N-Acylhydrazone Dynamic Combinatorial Library. *Org Biomol Chem* **2018**, *16* (43), 8144–8149. <https://doi.org/10.1039/c8ob01918e>.
- (8) Exapicheidou, I. A.; Shams, A.; Ibrahim, H.; Tsarenko, A.; Backenköhler, M.; Hamed, M. M.; Diamanti, E.; Volkamer, A.; Slotboom, D. J.; Hirsch, A. K. H. Hit Optimization by Dynamic Combinatorial Chemistry on Streptococcus Pneumoniae Energy-Coupling Factor Transporter ECF-PanT. *Chem. Commun.* **2024**, *60* (870). <https://doi.org/10.1039/d3cc04738e>.
- (9) Hunter, W. N. The Non-Mevalonate Pathway of Isoprenoid Precursor Biosynthesis. *J. Biol. Chem.* **2007**, *282* (30), 21573–21577. <https://doi.org/10.1074/jbc.R700005200>.
- (10) Allamand, A.; Piechowiak, T.; Lièvreumont, D.; Rohmer, M.; Grosdemange-Billiard, C. The Multifaceted MEP Pathway: Towards New Therapeutic Perspectives. *Molecules* **2023**, *28* (1403). <https://doi.org/10.3390/molecules28031403>.
- (11) Masini, T.; Hirsch, A. K. H. Development of Inhibitors of the 2C-Methyl-D-Erythritol 4-Phosphate (MEP) Pathway Enzymes as Potential Anti-Infective Agents. *J Med Chem* **2014**, *57* (23), 9740–9763. <https://doi.org/10.1021/jm5010978>.
- (12) Hale, I.; O'Neill, P. M.; Berry, N. G.; Odom, A.; Sharma, R. The MEP Pathway and the Development of Inhibitors as Potential Anti-Infective Agents. *MedChemComm* **2012**, *3* (4), 418. <https://doi.org/10.1039/c2md00298a>.
- (13) Coppens, I. Targeting Lipid Biosynthesis and Salvage in Apicomplexan Parasites for Improved Chemotherapies. *Nat Rev Microbiol.* December 2013, pp 823–835. <https://doi.org/10.1038/nrmicro3139>.
- (14) Hirsch, A. K. H.; Lauw, S.; Gersbach, P.; Schweizer, W. B.; Rohdich, F.; Eisenreich, W.; Bacher, A.; Diederich, F. Nonphosphate Inhibitors of IspE Protein, a Kinase in the Non-Mevalonate Pathway for Isoprenoid Biosynthesis and a Potential Target for Antimalarial Therapy. *ChemMedChem* **2007**, *2* (6), 806–810. <https://doi.org/10.1002/cmdc.200700014>.
- (15) Ropponen, H. K.; Diamanti, E.; Siemens, A.; Illarionov, B.; Haupenthal, J.; Fischer, M.; Rottmann, M.; Witschel, M.; Hirsch, A. K. H. Assessment of the Rules Related to Gaining Activity against Gram-Negative Bacteria. *RSC Med Chem* **2021**, *12* (4), 593–601. <https://doi.org/10.1039/d0md00409j>.
- (16) Ropponen, H.; Diamanti, E.; Johannsen, S.; Illarionov, B.; Hamid, R.; Jaki, M.; Sass, P.; Fischer, M. Exploring the Translational Gap of a Novel Class of Escherichia Coli IspE Inhibitors. *ChemMedChem* **2023**, *e202300346* (18). <https://doi.org/10.1002/cmdc.202300346>.
- (17) Choi, S.; Narayanasamy, P. Investigating Novel IspE Inhibitors of the MEP Pathway in Mycobacterium. *Microorganism* **2024**, *12* (18). <https://doi.org/https://doi.org/10.3390/microorganisms12010018>.
- (18) Bhat, V. T.; Caniard, A. M.; Luksch, T.; Brenk, R.; Campopiano, D. J.; Greaney, M. F. Nucleophilic Catalysis of Acylhydrazone Equilibration for Protein-Directed Dynamic Covalent Chemistry. *Nat Chem* **2010**, *2* (6), 490–497. <https://doi.org/10.1038/nchem.658>.

4. Chapter

- (19) Shan, S.; Chen, X.; Liu, T.; Zhao, H.; Rao, Z.; Lou, Z. Crystal Structure of 4-diphosphocytidyl-2-C-methyl-D-erythritol Kinase (IspE) from *Mycobacterium Tuberculosis*. *FASEB J.* **2011**, *25* (5), 1577–1584. <https://doi.org/10.1096/fj.10-175786>.
- (20) Dalberto, P. F.; de Souza, E. V.; Abbadi, B. L.; Neves, C. E.; Rambo, R. S.; Ramos, A. S.; Macchi, F. S.; Machado, P.; Bizarro, C. V.; Basso, L. A. Handling the Hurdles on the Way to Anti-Tuberculosis Drug Development. *Front. Chem.* **2020**, *8* (586294). <https://doi.org/10.3389/fchem.2020.586294>.

4.1 Supporting Information

Target-Directed Dynamic Combinatorial Chemistry Affords Binders of *Mycobacterium Tuberculosis* IspE

Maria Braun-Cornejo,^{1,2,3} Camilla Ornago,⁴ Vidhisha Sonawane,⁵ Jörg Hauptenthal,³ Andreas M. Kany,³ Eleonora Diamanti,³ Gwenaëlle Jézéquel,³ Norbert Reiling,⁵ Wulf Blankenfeldt,⁴ Peter Maas,¹ and Anna K. H. Hirsch^{2,3*}

¹ Specs Research Laboratory, Specs Compound Handling, B.V., Bleiswijkseweg 55, 2712 PB, Zoetermeer, The Netherlands.

² Saarland University, Department of Pharmacy, Campus Building E8.1, 66123 Saarbrücken, Germany.

³ Helmholtz Institute for Pharmaceutical Research Saarland (HIPS) – Helmholtz Centre for Infection Research (HZI), Campus Building E8.1, 66123 Saarbrücken, Germany.

⁴ Department Structure and Function of Proteins Helmholtz Centre for Infection Research Inhoffenstrasse 7, 38124 Braunschweig, Germany.

⁵ RG Microbial Interface Biology, Research Center Borstel Leibniz Lung Center, Parkallee 1-40, 23845 Borstel, Germany.

⁶ German Center for Infection Research (DZIF), Partner Site Hamburg-Lübeck-Borstel-Riems, 23845 Borstel, Germany.

*Corresponding author: Anna.Hirsch@helmholtz-hips.de

Table of Contents

Supplementary Methods.....	83
General information.....	83
Chemicals.....	83
General procedure for tdDCC experiments	83
Experimental conditions of tdDCC.....	84
Assessment of amplification factors	84
General procedure for acylhydrazones synthesis.....	85
Characterization of acylhydrazone products	85
<i>Mtb</i> IspE expression and purification	88
<i>Mtb</i> IspE stability study <i>via</i> thermal shift assay	88
<i>In silico</i> elucidation of tdDCC hits' binding mode.....	89
Kinetic turbidimetric solubility	89
<i>Mtb</i> IspE binding study <i>via</i> MicroScale Thermophoresis	89
<i>Mtb</i> IspE binding study <i>via</i> thermal shift assay.....	89
Determination of <i>E. coli</i> activity.....	89
Determination of <i>in vitro</i> anti-tubercular activity and solubility in 7H9 medium.....	89
Cytotoxicity assay.....	90
Supplementary Figures	90
<i>Mtb</i> IspE stability study <i>via</i> thermal shift assay	90
HPLC-MS/MS peak assignments and determination of equilibrium.....	91

4. Chapter

Amplification of <i>N</i> -acylhydrazones in the PT experiments	96
<i>In silico</i> elucidation of tdDCC hits' binding mode.....	97
Supplementary references.....	98

Supplementary Methods

General information

High-resolution mass (HRMS) of final products was determined by HPLC-MS/MS using a Thermo Scientific Q Exactive Focus Orbitrap LC-MS/MS system. All compounds were analysed for purity by LCMS on Acquity UPLC-SQD system from Waters with a gradient elution of Water (Formic acid 0.1%)/Acetonitrile on an HSS-T3 column (2.1 x 50 mm, Waters), 1.8 μm , at 30°C, PDA detection between 240-320 nm, and MS detection by simultaneous ES+/ES- ionization in a mass range of 150-800. The flow is set to 0.9 ml/min, and the gradient time is 1.5 min. NMR spectra were recorded on an Agilent 400 MHz or a Bruker Avance Neo 500 MHz. Chemical shifts (δ) are reported in ppm relative to residual solvent signals. The following abbreviations are used to describe peak patterns when appropriate: s (singlet), d (doublet), t (triplet), q (quartet), quint (quintet), sex (sextet), sept (septuplet), m (multiplet), br (broad). Coupling constants (J) are reported in Hertz (Hz). Reactions were monitored with thin layer chromatography (TLC) on silica gel-coated aluminum (silica gel F254, SiliCycle).

The periodic progress and analysis of tdDCC were monitored by HPLC-MS/MS (ThermoScientific Dionex Ultimate 3000 UHPLC System coupled to a ThermoScientific Q Exactive Focus with an electrospray ion source) using an Acquity Waters Column (BEH, C8 1.7 μm , 2.1 x 150 mm, Waters, Germany) at a flow rate of 0.250 mL/min with detection set at 210, 254, 290, and 310 nm, and the mass spectrum recorded in a positive mode in the range of 100–700 m/z. The solvent system was 0.1% formic acid in H₂O (Solvent-A) and 0.1% formic acid in MeCN (Solvent-B). The gradient program began with 5% of Solvent-B for 1 min and was then increased to 95% of Solvent-B over 17 min and held for 2 min, followed by a decrease of Solvent-B to 5% over 0.1 min, where it was held for 2 min.

Chemicals

All reagents and solvents were purchased from Sigma-Aldrich, Specs, Fluorochem, or Acros Organics, were reagent grade, and used without purification unless indicated otherwise. All reactions were conducted under nitrogen atmosphere using oven-dried glassware. Purifications by flash chromatography were done using silica gel (Screening Devices 60-200 μm). All new compounds were fully characterised by ¹H and ¹³C NMR and HRMS techniques. The purity of the final products was determined by HPLC-MS and found to be >95%.

General procedure for tdDCC experiments

Blank DCL preparation (GP-1): DCL without protein is prepared following a similar published procedure.¹ To a well of a 24-well plate, containing Tris-HCl buffer (pH 7.0) were added hydrazides (300 μM each, in DMSO), aldehydes (100 μM each, in DMSO), aniline (20 mM, in DMSO), and an additional amount of DMSO to reach a final concentration of 5% in the DCL with 0.5 mL of end-volume. The DCL was allowed to mix on a plate shaker at room temperature (r.t.) and was frequently monitored via LCMS-MS. For analysis, 30 μL of the corresponding library was mixed with 42 μL acetonitrile and 3 μL of NaOH (1 M), the mixture was centrifuged, and filtered before analysis.

Protein-templated (PT) DCL preparation (GP-2): DCL with protein is prepared following a similar published procedure.¹

To a well of a 24-well plate, containing Tris-HCl buffer (pH 7.0) were added hydrazides (300 μM each, in DMSO), aldehydes (100 μM each, in DMSO), aniline (20 mM, in DMSO), the protein *MtblSpE* (25 or 40 μM in Tris-HCl buffer at pH 7.0), and an additional amount of DMSO to reach a final concentration of 5% in the DCL with 0.5 mL of end-volume. The DCL with the protein was allowed to gently mix on a plate shaker (50 rpm) at r.t. and was frequently monitored via LCMS-MS and the traces were compared with the blank composition. For analysis, 20 μL of the corresponding library was mixed with 80 μL acetonitrile and 4 μL of NaOH (1 M), the mixture was centrifuged, and the supernatant was used for the analysis.

Note: The protein-templated DCLs were run as duplicates.

Experimental conditions of tdDCC

DCL-1:

This experiment library consists of three aldehydes (**1–3**) and six hydrazides (**A–F**). The tdDCC experiment was carried out according to the GP-1 (blank) and GP-2 (PT) in Tris-HCl buffer at pH 7.0 and 5% DMSO. The composition of DCL-1 is as below:

Entry	Blank		PT-I		PT-II	
	amount	final conc. in DCL	amount	final conc. in DCL	amount	final conc. in DCL
Tris-HCl buffer	475 μ L	-	436.3 μ L	-	436.3 μ L	-
Hydrazide (100 mM)	6 \times 1.5 μ L (9 μ L)	(6 \times 300 μ M)	6 \times 1.5 μ L (9 μ L)	(6 \times 300 μ M)	6 \times 1.5 μ L (9 μ L)	(6 \times 300 μ M)
Aldehyde (100 mM)	3 \times 0.5 μ L (1.5 μ L)	(3 \times 100 μ M)	3 \times 0.5 μ L (1.5 μ L)	(3 \times 100 μ M)	3 \times 0.5 μ L (1.5 μ L)	(3 \times 100 μ M)
Aniline (1 M)	10 μ L	20 mM	10 μ L	20 mM	10 μ L	20 mM
DMSO	4.5 μ L	5%	4.5 μ L	5%	4.5 μ L	5%
MtblspE (324 μ M)	0	-	38.7 μ L	25 μ M	38.7 μ L	25 μ M

DCL-2:

This experiment library consists of three aldehydes (**4–6**) and six hydrazides (**G–L**). The tdDCC experiment was carried out according to the GP-1 (blank) and GP-2 (PT) in Tris-HCl buffer at pH 7.0 and 5% DMSO.

DCL-3:

This experiment library consists of three aldehydes (**4–6**) and six hydrazides (**A–F**). The tdDCC experiment was carried out according to the GP-1 (blank) and GP-2 (PT) in Tris-HCl buffer at pH 7.0 and 5% DMSO.

DCL-4:

This experiment library consists of three aldehydes (**1–3**) and six hydrazides (**B–F**, and **M**). The tdDCC experiment was carried out according to the GP-1 (blank) and GP-2 (PT) in Tris-HCl buffer at pH 7.0 and 5% DMSO.

The composition of DCL-2, -3, and -4 is as below:

Entry	Blank		PT-I		PT-II	
	amount	final conc. in DCL	amount	final conc. in DCL	amount	final conc. in DCL
Tris-HCl buffer	475 μ L	-	413.2 μ L	-	413.2 μ L	-
Hydrazide (100 mM)	6 \times 1.5 μ L (9 μ L)	(6 \times 300 μ M)	6 \times 1.5 μ L (9 μ L)	(6 \times 300 μ M)	6 \times 1.5 μ L (9 μ L)	(6 \times 300 μ M)
Aldehyde (100 mM)	3 \times 0.5 μ L (1.5 μ L)	(3 \times 100 μ M)	3 \times 0.5 μ L (1.5 μ L)	(3 \times 100 μ M)	3 \times 0.5 μ L (1.5 μ L)	(3 \times 100 μ M)
Aniline (1 M)	10 μ L	20 mM	10 μ L	20 mM	10 μ L	20 mM
DMSO	4.5 μ L	5%	4.5 μ L	5%	4.5 μ L	5%
MtblspE (324 μ M)	0	-	61.8 μ L	40 μ M	61.8 μ L	40 μ M

Assessment of amplification factors

The amplification factor for each product of the DCL was assessed at the time of equilibrium of the blank experiment. The relative peak area (RPA) was determined for each experiment; blank and protein-templated (PT) duplicates, using ACD/Labs (Figure S2–S5, p. 12). All products of the DCL were integrated and their sum set to 100% in order to obtain the respective RPA for each product. The amplification factor was calculated for each PT duplicate individually as $\left(\frac{RPA_{PT} - RPA_{blank}}{RPA_{blank}}\right)^2$. The mean of the amplification factors and its standard deviation were reported for each product in form of bar charts with error bars, for DCL-1 in the main text (Figure 3A) and for DCL-2, -3, and -4 in Figure S9 (p. 17).

General procedure for acylhydrazones synthesis

General procedure for acylhydrazone formation (GP-3):

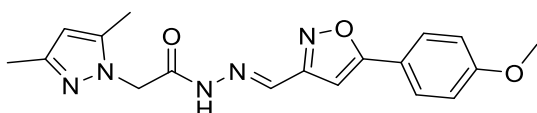
To an oven-dried round-bottom flask, under nitrogen atmosphere, the corresponding hydrazide (1.0 eq) and aldehyde (1.0–1.8 eq) were suspended in MeOH (0.02–0.2 M) and refluxed for 1–5 h; its progress was followed on TLC. After the reaction was completed, the solvent was removed under reduced pressure to afford the corresponding acylhydrazone product in 85 – 99% isolated yields.

General procedure for small scale acylhydrazone formation (GP-4):

To an oven-dried test tube with a magnetic stirrer, under nitrogen atmosphere the corresponding hydrazide (1.0 eq) and aldehyde (1.0–1.1 eq) were suspended in MeOH (0.02–0.12 M). The reaction mixture was refluxed for 2–5 h, using Radleys Parallel Synthesiser™. The reaction progress was followed by TLC. Once the reaction was completed, the mixture was cooled to 0 °C and the precipitate filtered over a 20 µm filter and washed with cold MeOH. The residual solvent was removed under reduced pressure to afford the corresponding acylhydrazone product in 28 – 99% isolated yields.

Characterization of acylhydrazone products

(*E*)-2-(3,5-diMethyl-1*H*-pyrazol-1-yl)-*N'*-((5-(4-methoxyphenyl)isoxazol-3-yl)methylene)acetohydrazide (**B6**):



Compound **B6** was synthesised according to GP-4, hydrazide **B** (12.8 mg, 0.076 mmol) and aldehyde **6** (15.7 mg, 0.077 mmol) stirred in MeOH (1.5 mL) for 5 h to afford compound **B6** as white airy powder (18.9 mg,

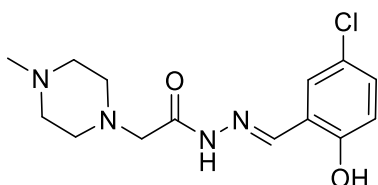
0.054 mmol, 70%). ¹H NMR indicates the presence of two isomers, possibly *trans* and *cis* conformers of the amide. We did not assign the peaks to a specific conformer and will refer to them as *A* and *B* (*A*:*B* = 2:1).

¹H NMR (400 MHz, DMSO-*d*₆) δ = 11.99 (br s, 1H, *A*&*B*), 8.33 (s, 1H, *B*), 8.09 (s, 1H, *A*), 7.91 (br d, *J* = 8.6 Hz, 2H, *B*), 7.87 (br d, *J* = 8.2 Hz, 2H, *A*), 7.34 (s, 1H, *A*), 7.21 (s, 1H, *B*), 7.11 (br d, *J* = 8.2 Hz, 2H, *A*), 7.07 (br s, 2H, *B*), 5.84 (s, 1H, *A*&*B*), 5.26 (s, 1H, *A*), 4.80 (s, 1H, *B*), 3.83 (s, 3H, *A*&*B*), 2.20 (s, 1H, *B*), 2.16 (s, 3H, *A*), 2.08 (s, 3H, *A*&*B*) ppm.

¹³C NMR (101 MHz, DMSO-*d*₆) δ = 169.5, 169.0, 161.1, 160.7, 146.0, 140.1, 133.6, 127.4, 119.1, 114.7, 104.8, 95.9, 55.4, 49.3, 13.3, 10.6 ppm.

HRMS (ESI⁺): *m/z* calcd. for C₁₈H₂₀N₅O₃⁺ (*[M+H]*⁺) 354.1561, measured 354.1543.

(*E*)-*N'*-(5-Chloro-2-hydroxybenzylidene)-2-(4-methylpiperazin-1-yl)acetohydrazide (**C1**):



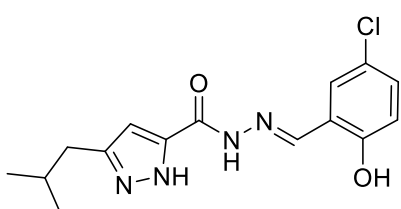
Compound **C1** was synthesised according to GP-4, with adaptations. Hydrazide **C** (21.0 mg, 0.122 mmol) and aldehyde **1** (19.1 mg, 0.122 mmol) stirred in MeOH (1 mL) for 2 h. The solvent was removed under reduced pressure to afford compound **C1** as yellow oil (37.9 mg, 0.122 mmol, >99%).

¹H NMR (400 MHz, CDCl₃) δ = 10.11 (br s, 1H), 8.41 (s, 1H), 7.21-7.25 (m, 1H), 7.18 (d, *J* = 2.3 Hz, 1H), 6.93 (d, *J* = 8.6 Hz, 1H), 3.46-3.49 (m, 1H), 3.20 (s, 2H), 2.60-2.68 (m, 4H), 2.51 (br s, 4H), 2.32 (s, 3H) ppm.

¹³C NMR (101 MHz, CDCl₃) δ = 166.0, 157.0, 149.7, 131.6, 129.9, 123.9, 118.7, 118.4, 60.9, 55.0, 53.6, 45.9 ppm.

HRMS (ESI⁺): *m/z* calcd. for C₁₄H₂₀ClN₄O₂⁺ (*[M+H]*⁺) 311.1269, measured 311.1254.

(*E*)-*N'*-(5-Chloro-2-hydroxybenzylidene)-3-isobutyl-1*H*-pyrazole-5-carbohydrazide (**D1**):



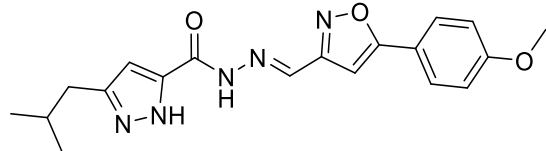
Compound **D1** was synthesised according to GP-3, hydrazide **D** (51.7 mg, 0.284 mmol) and aldehyde **1** (46.5 mg, 0.297 mmol) stirred in MeOH (5 mL) for 2.5 h to afford compound **D1** as pale yellow solid (88.8 mg, 0.277 mmol, 98%).

¹H NMR (400 MHz, DMSO-*d*₆) δ = 13.14 (br s, 1H), 12.05 (s, 1H), 11.39 (s, 1H), 8.64 (s, 1H), 7.56 (br s, 1H), 7.30 (dd, *J* = 8.6, 2.5 Hz, 1H), 6.94 (d, *J* = 8.6 Hz, 1H), 6.54 (s, 1H), 2.53 (br d, *J* = 7.0 Hz, 2H), 1.91 (spt, *J* = 6.6 Hz, 1H), 0.89 (d, *J* = 6.6 Hz, 6H) ppm.

^{13}C NMR (101 MHz, DMSO- d_6) δ = 158.4, 156.0, 145.8, 145.2, 143.8, 130.5, 127.9, 122.8, 120.7, 118.2, 104.7, 33.8, 28.2, 22.0 ppm.

HRMS (ESI $^+$): m/z calcd. for $\text{C}_{15}\text{H}_{18}\text{ClN}_4\text{O}_2^+$ ($[M+H]^+$) 321.1113, measured 321.1105.

(*E*)-3-Isobutyl-*N'*-((5-(4-methoxyphenyl)isoxazol-3-yl)methylene)-1*H*-pyrazole-5-carbohydrazide (**D6**):



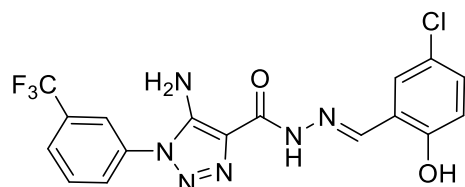
Compound **D6** was synthesised according to GP-3, hydrazide **D** (47.0 mg, 0.258 mmol) and aldehyde **6** (53.1 mg, 0.261 mmol) stirred in MeOH (5 mL) for 2.5 h to afford compound **D6** as white powder (92.0 mg, 0.250mmol, 97%).

^1H NMR (400 MHz, DMSO- d_6) δ = 13.17 (s, 1H), 12.08 (s, 1H), 8.62 (s, 1H), 7.92 (d, J = 8.7 Hz, 2H), 7.24 (s, 1H), 7.09 (d, J = 8.7 Hz, 2H), 6.56 (s, 1H), 3.84 (s, 3H), 2.54 (br d, J = 7.0 Hz, 2H), 1.92 (spt, J = 6.6 Hz, 1H), 0.90 (d, J = 6.6 Hz, 6H) ppm.

^{13}C NMR (101 MHz, DMSO- d_6) δ = 169.6, 161.2, 161.0, 158.6, 145.3, 144.0, 137.0, 127.5, 119.2, 114.7, 104.9, 95.8, 55.4, 33.8, 28.2, 22.0 ppm.

HRMS (ESI $^+$): m/z calcd. for $\text{C}_{19}\text{H}_{22}\text{N}_5\text{O}_3^+$ ($[M+H]^+$) 368.1717, measured 368.1701.

(*E*)-5-Amino-*N'*-(5-chloro-2-hydroxybenzylidene)-1-(3-(trifluoromethyl)phenyl)-1*H*-1,2,3-triazole-4-carbohydrazide (**E1**):



Compound **E1** was synthesised according to GP-4, hydrazide **E** (10.0 mg, 0.035 mmol) and aldehyde **1** (6.1 mg, 0.039 mmol) stirred at reflux in MeOH (1.5 mL) for 5 h and at r.t. overnight to afford compound **E1** as off-white solid (11.4 mg, 0.027mmol, 77%).

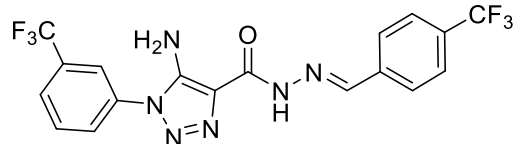
^1H NMR (500 MHz, DMSO- d_6) δ = 12.43 (br s, 1H), 11.48 (br s, 1H), 8.66 (s, 1H), 8.00 (s, 1H), 7.92-7.97 (m, 2H), 7.87 (t, J = 7.8 Hz, 1H), 7.57 (br s, 1H), 7.31 (dd, J = 8.1, 2.3 Hz, 1H), 6.95 (d, J = 8.1 Hz, 1H), 6.83 (br s, 2H) ppm.

^{13}C NMR (126 MHz, DMSO- d_6) δ = 158.3, 156.0, 146.0, 145.7, 135.2, 131.1, 130.4, 128.7, 128.1, 126.0, 124.7, 122.8, 121.5, 120.6, 120.1, 118.2 ppm.

^{19}F NMR (470 MHz, DMSO- d_6) δ = -61.13 ppm.

HRMS (ESI $^+$): m/z calcd. for $\text{C}_{17}\text{H}_{13}\text{ClF}_3\text{N}_6\text{O}_2^+$ ($[M+H]^+$) 425.0735, measured 425.0726.

(*E*)-5-Amino-*N'*-(4-(trifluoromethyl)benzylidene)-1-(3-(trifluoromethyl)phenyl)-1*H*-1,2,3-triazole-4-carbohydrazide (**E4**):



Compound **E4** was synthesised according to GP-4, hydrazide **E** (10.0 mg, 0.035 mmol) and aldehyde **4** (6.3 mg, 0.036 mmol) stirred at reflux in MeOH (1.5 mL) for 5h and at r.t. overnight to afford compound **E4** as off-white solid (4.3 mg, 0.010 mmol, 28%). ^1H NMR, ^{19}F NMR, and HPLC-

MS indicate the presence of two isomers, possibly *trans* and *cis* conformers of the amide. We did not assign the peaks to a specific conformer and will refer to them as *A* and *B* (*A*:*B* = 1:1).

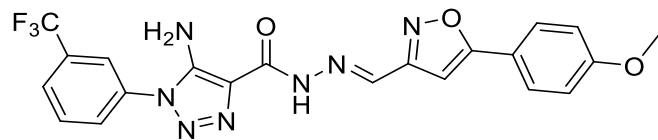
^1H NMR (500 MHz, DMSO- d_6) δ = 12.30 (br s, 1H, *A*), 12.17 (s, 1H, *B*), 8.88 (s, 1H, *A*), 8.59 (br s, 2H, *A*), 8.13 (br s, 1H, *A*), 8.00 (s, 1H, *B*), 7.87-7.98 (m, 7H, *A* & *B*), 7.77-7.86 (m, 6H, *A* & *B*), 7.52 (br t, J = 7.6 Hz, 1H, *B*), 7.23 (br d, J = 7.6 Hz, 1H, *B*), 6.78 ppm (s, 2H, *A*).

^{13}C NMR (126 MHz, DMSO- d_6) δ = 158.6, 146.2, 146.0, 141.9, 138.6, 135.2, 131.2, 130.0, 129.6, 128.7, 127.6, 127.5, 125.8, 123.1, 121.5, 120.4, 120.2, 112.1 ppm.

^{19}F NMR (470 MHz, DMSO- d_6) δ = -61.11 (*A*), -61.13 (*B*), -61.17 (*A*), -61.24 (*B*) ppm.

HRMS (ESI $^+$): m/z calcd. for $\text{C}_{18}\text{H}_{13}\text{F}_6\text{N}_6\text{O}^+$ ($[M+H]^+$) 443.1050, measured 443.1022.

(*E*)-5-Amino-*N'*-((5-(4-methoxyphenyl)isoxazol-3-yl)methylene)-1-(3-(trifluoromethyl)phenyl)-1*H*-1,2,3-triazole-4-carbohydrazide (**E6**):



Compound **E6** was synthesised according to GP-4, hydrazide **E** (10.0 mg, 0.035 mmol) and aldehyde **6** (7.1 mg, 0.035 mmol) stirred at reflux in MeOH (1.5 mL) for 5 h and at r.t.

overnight to afford compound **E6** as off-white solid (6.9 mg, 0.015 mmol, 42%).

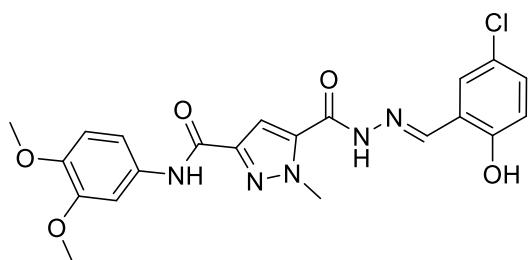
^1H NMR (500 MHz, DMSO- d_6): δ = 12.41 (s, 1H), 8.63 (s, 1H), 8.01 (s, 1H), 7.94-7.98 (m, 2H), 7.93 (d, J = 8.5 Hz, 2H), 7.88 (t, J = 8.1 Hz, 1H), 7.22 (s, 1H), 7.10 (d, J = 8.5 Hz, 2H), 6.81 (s, 2H), 3.84 (s, 3H) ppm.

^{13}C NMR (126 MHz, DMSO- d_6): δ = 169.6, 161.2, 161.0, 158.6, 146.2, 136.6, 135.2, 131.2, 130.3, 128.8, 127.6, 126.1, 121.59, 121.57, 120.2, 119.2, 114.7, 95.7, 55.4 ppm.

^{19}F NMR (470 MHz, DMSO- d_6): δ = -61.12 ppm.

HRMS (ESI $^+$): m/z calcd. for $\text{C}_{21}\text{H}_{17}\text{F}_3\text{N}_7\text{O}_3^+$ [$M+\text{H}$] $^+$ 472.1339, measured 472.1325.

(*E*)-5-(2-(5-Chloro-2-hydroxybenzylidene)hydrazine-1-carbonyl)-*N*-(3,4-dimethoxyphenyl)-1-methyl-1*H*-pyrazole-3-carboxamide (**H1**):



Compound **H1** was synthesised according to GP-3, hydrazide **H** (27.8 mg, 0.087 mmol) and aldehyde **1** (24.0 mg, 0.153 mmol) stirred in MeOH (4 mL) for 3 h to afford compound **H1** as pale yellow solid (37.3 mg, 0.086 mmol, 94%).

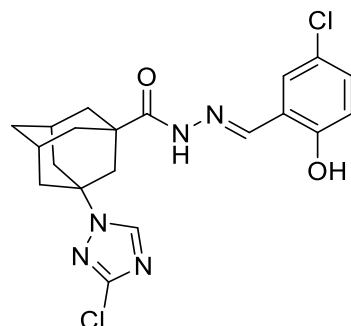
^1H NMR (500 MHz, DMSO- d_6) δ = 12.28 (br s, 1H), 11.07 (br s, 1H), 10.06 (s, 1H), 8.62 (s, 1H), 7.69 (d, J = 2.4 Hz, 1H), 7.52 (s, 1H), 7.51 (d, J = 2.1 Hz, 1H), 7.43 (dd, J = 8.7, 2.1 Hz, 1H), 7.33 (dd, J = 8.7, 2.4 Hz, 1H), 6.96 (d, J =

8.7 Hz, 1H), 6.91 (d, J = 8.7 Hz, 1H), 4.23 (s, 3H), 3.75 (s, 3H), 3.73 (s, 3H) ppm.

^{13}C NMR (126 MHz, DMSO- d_6) δ = 158.9, 156.0, 155.2, 148.5, 146.1, 145.2, 145.0, 135.4, 132.2, 131.1, 127.2, 123.1, 120.8, 118.3, 112.2, 111.9, 108.8, 105.6, 55.7, 55.4, 39.8 ppm.

HRMS (ESI $^+$): m/z calcd. for $\text{C}_{21}\text{H}_{21}\text{ClN}_5\text{O}_5^+$ [$M+\text{H}$] $^+$ 458.1226, measured 458.1198.

(1*r*,3*s*,5*R*,7*S*)-3-(3-Chloro-1*H*-1,2,4-triazol-1-yl)-*N'*-((*Z*)-5-chloro-2-hydroxybenzylidene)adamantane-1-carbohydrazide (**I1**):



Compound **I1** was synthesised according to GP-4, hydrazide **I** (14.5 mg, 0.049 mmol) and aldehyde **1** (7.9 mg, 0.050 mmol) stirred in MeOH (1 mL) for 2 h to afford compound **I1** as off-white solid (6.5 mg, 0.015 mmol, 31%).

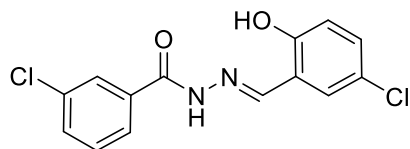
^1H NMR (500 MHz, DMSO- d_6): δ = 11.35 (s, 1H), 11.28 (s, 1H), 8.70 (s, 1H), 8.52 (s, 1H), 7.59 (d, J = 2.6 Hz, 2H), 7.29 (dd, J = 8.8, 2.6 Hz, 2H), 6.92 (d, J = 8.8 Hz, 1H), 2.32 (br s, 1H), 2.25 (s, 1H), 2.13 (d, J = 12.0 Hz, 2H), 2.07 (d, J = 12.0 Hz, 2H), 1.93 (d, J = 11.6 Hz, 2H), 1.87 (d, J = 11.6 Hz, 2H), 1.70 (br s, 2H) ppm.

^{13}C NMR (126 MHz, DMSO- d_6): δ = 171.6, 156.0, 150.2, 145.2, 142.9, 130.6, 127.6, 122.9, 120.6, 118.2, 59.6, 42.4, 41.8, 40.4, 36.8, 34.2, 28.6

ppm.

HRMS (ESI $^+$): m/z calcd. for $\text{C}_{20}\text{H}_{22}\text{Cl}_2\text{N}_5\text{O}_2^+$ [$M+\text{H}$] $^+$ 434.1145, measured 434.1135.

(*E*)-3-Chloro-*N'*-(5-chloro-2-hydroxybenzylidene)benzohydrazide (**K1**):



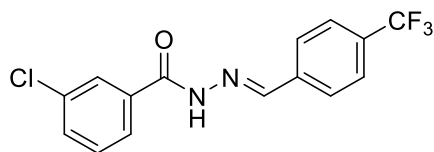
Compound **K1** was synthesised according to GP-3, hydrazide **K** (85.0 mg, 0.498 mmol) and aldehyde **1** (80.0 mg, 0.511 mmol) stirred in MeOH (5 mL) for 2h to afford compound **K1** as off-white solid (154.0 mg, 0.498 mmol, >99%). HPLC-MS indicates the presence of two isomers, possibly *trans* and *cis* conformers of the amide. We

did not assign the peaks to a specific conformer and will refer to them as A and B (A:B = 93:7).

^1H NMR (400 MHz, DMSO- d_6) δ = 12.24 (s, 1H), 11.19 (br s, 1H), 8.63 (s, 1H), 7.98 (t, J = 1.6 Hz, 1H), 7.90 (dt, J = 7.8, 1.6 Hz, 1H), 7.66-7.70 (m, 2H), 7.58 (t, J = 7.8 Hz, 1H), 7.32 (dd, J = 8.9, 2.7 Hz, 1H), 6.96 (d, J = 8.9 Hz, 1H) ppm.

^{13}C NMR (101 MHz, DMSO- d_6) δ = 161.6, 156.1, 146.1, 134.8, 133.4, 131.9, 131.0, 130.6, 127.4, 126.6, 123.1, 120.7, 118.3, 109.6 ppm.

HRMS (ESI $^+$): m/z calcd. for $\text{C}_{14}\text{H}_{11}\text{Cl}_2\text{N}_2\text{O}_2^+$ [$M+\text{H}$] $^+$ 309.0192, measured 309.0186.

(E)-3-Chloro-N'-(4-(trifluoromethyl)benzylidene)benzohydrazide (K4):

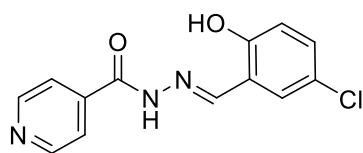
Compound **K4** was synthesised according to GP-3, with some adaptations. Hydrazide **K** (100.0 mg, 0.586 mmol) and aldehyde **4** (103.0 mg, 0.592 mmol, 1 mL MeOH) stirred in MeOH (3 mL) for 1 h. The crude was purified by flash column chromatography (EtOAc:PE, product at 1:1) to afford **K4** as a white powder (162.0 mg, 0.496 mmol, 85%).

$^1\text{H NMR}$ (400 MHz, $\text{DMSO-}d_6$) δ = 12.12 (br s, 1H), 8.52 (s, 1H), 7.93-7.99 (m, 3H), 7.89 (br d, J = 7.8 Hz, 1H), 7.81 (br d, J = 8.2 Hz, 2H), 7.68 (d, J = 7.8 Hz, 1H), 7.58 (t, J = 7.8 Hz, 1H) ppm.

$^{13}\text{C NMR}$ (126 MHz, $\text{DMSO-}d_6$) δ = 161.9, 146.6, 138.2, 135.2, 133.3, 131.8, 130.6, 129.8, 127.8, 127.4, 126.6, 125.8, 124.1 ppm.

$^{19}\text{F NMR}$ (470 MHz, $\text{DMSO-}d_6$) δ = -61.20 ppm.

HRMS (ESI⁺): m/z calcd. for $\text{C}_{15}\text{H}_{11}\text{ClF}_3\text{N}_2\text{O}^+$ $[M+H]^+$ 327.0507, measured 327.0493.

(E)-N'-(5-Chloro-2-hydroxybenzylidene)isonicotinohydrazide (L1):

Compound **L1** was synthesised according to GP-3, with some adaptations. Hydrazide **L** (53.2 mg, 0.388 mmol) and aldehyde **1** (61.3 mg, 0.392 mmol) were stirred at reflux in MeOH (2 mL) for 5 h and at r.t. overnight. Compound **L1** was afforded as pale yellow solid (105.2 mg, 0.382 mmol, 98%).

$^1\text{H NMR}$ (400 MHz, $\text{DMSO-}d_6$) δ = 12.35 (s, 1H), 11.11 (s, 1H), 8.80 (d, J = 6.2 Hz, 2H), 8.66 (s, 1H), 7.84 (d, J = 6.2 Hz, 2H), 7.70 (d, J = 2.5 Hz, 1H), 7.33 (dd, J = 8.6, 2.5 Hz, 1H), 6.96 (d, J = 8.6 Hz, 1H) ppm.

$^{13}\text{C NMR}$ (101 MHz, $\text{DMSO-}d_6$) δ = 161.5, 156.1, 150.4, 146.5, 139.9, 131.1, 127.2, 123.1, 121.5, 120.7, 118.3 ppm.

HRMS (ESI⁺): m/z calcd. for $\text{C}_{13}\text{H}_{11}\text{ClN}_3\text{O}_2^+$ $[M+H]^+$ 276.0534, measured 276.0526.

MtblSpE expression and purification

The synthetic gene encoding for *MtblSpE* was purchased from GenScript, GmbH cloned inside the plasmid pvp008, downstream a *N*-terminal StrepII tag followed by a TEV site. The plasmid was transformed into RB-competent *E. coli* Arctic express (DE3). Transformed *E. coli* cells were grown in LB medium at 37 °C until OD_{600} reached 0.6; after that, protein expression was induced adding 0.5 mM IPTG and the protein was expressed at 16°C for 48 hours. Cells were harvested by centrifugation at 5000 rpm for 20 minutes. The pellet was resuspended in wash buffer (50 mM HEPES pH 7, 100 mM NaCl, 5 mM MgCl_2 , 5 mM DTT) and sonicated for cell disruption. The lysate was cleared by centrifugation for 45 minutes at 16000 rpm at 4 °C. The supernatant was syringe-filtered and loaded onto a self-packed StreptActin-HC column equilibrated in was buffer. *MtblSpE* was eluted with a single step 40 mL gradient at 100% elution buffer (50 mM HEPES pH 7, 100 mM NaCl, 5 mM MgCl_2 , 5 mM DTT, 5 mM desthiobiotin). Protein purity was verified via SDS-PAGE. The purification yield was 2 mg/L.

MtblSpE stability study via thermal shift assay

The stability of *MtblSpE* in the DCL buffer conditions was studied for 10 days by measuring its melting temperature (T_m) using thermal shift assay (TSA). *MtblSpE* incubated at a final concentration of 0.2 mg/mL in Tris-HCl buffer at pH 7.0 with 5%, -and 10% DMSO at r.t. and samples were measured in duplicate at t = 0, 1, 2, 6, 8 & 10 days (10% DMSO sampling stopped after day 6). The experiments were performed in a 96-well PCR plate (Thermoscientific). The final volume per well was 20 μL , consisting of 18 μL of *MtblSpE* sample (as mentioned above), and 2 μL of GloMelt dye (diluted 20x with H_2O). The plate was centrifuged for 1 min at r.t. at 1200 rpm. The T_m of the protein was measured using a Real-time PCR machine (Step one plus, Applied Biosystem). The conditions of the experiment were adjusted using Step One 2.3 software. The starting temperature, the ending temperature and the heating rate were set as 21 °C, 95 °C and 0.5 °C / min, respectively. The melting curves were analyzed using Protein Thermal Shift 1.3 software. T_m of *MtblSpE* under these conditions was found to range from 50.4 °C to 51.3 °C, with one duplicate of day 6 (5% DMSO sample) discarded due to anomalies in the measurement. As expected *MtblSpE* is more stable and has higher T_m at 5% DMSO than 10% DMSO. The T_m of *MtblSpE* with 5% DMSO steadily declines from day 6 (Figure S1).

***In silico* elucidation of tdDCC hits' binding mode**

Docking studies were performed using a pre-release of SeeSAR 13.1 (BioSolveIT, GmbH, Sankt Augustin, Germany), provided for beta-test by the company. Two published *MtblspE* crystal structures in complex with ADP and CDP-ME (PDB accession code: 3PYF and 3PYE respectively) were superimposed and the 47 amino-acid in the binding region of both ADP and CDP-ME were used to define active site on 3PYF structure. All 72 possible product combinations (DCL-1, -2, -3, and -4) were docked on the active site defined as described above generating a maximum of 10 poses per molecule using standard docking parameters of SeeSAR software. The 720 poses generated were clustered by fragment and filtered basing on calculated torsion quality and molecular clashes. The binding pose of each fragment in the different molecules was visually analysed to determine whether a tendency in predicted binding pose of such fragments was found (Figure S10–S12, p. 11).

Kinetic turbidimetric solubility

The desired compounds were sequentially diluted in DMSO in a 96-well plate. 7.5 μ L of each well were transferred into another 96-well plate and mixed with 142.5 μ L of PBS. Plates were shaken for 5 min at 600 rpm at r.t., and the absorbance at 620 nm was measured. Absorbance values were normalized by blank subtraction and plotted using GraphPad Prism 8.4.2 (GraphPad Software, San Diego, CA, USA). Solubility (S) was determined based on the First X value of AUC function using a threshold of 0.005.

***MtblspE* binding study via MicroScale Thermophoresis**

MtblspE buffer was exchanged to 50 mM HEPES pH 7, 100mM NaCl, 5 mM MgCl₂, 5 mM TCEP before protein labelling. The enzyme was labelled with Cy5 following the protocol indicated by NanoTemper. Labelled *MtblspE* was diluted to 400 nM and used mixed 1:1 with 40 μ M of each ligand. MicroScale Thermophoresis experiment was performed with a Monolith N.115 (Nanotemper Technologies, GmbH, Munich, Germany) using Standard Capillaries (Nanotemper Technologies, GmbH, Munich, Germany). Each binding event was evaluated at a final concentration of 200 nM *MtblspE* and 20 μ M of each ligand. All the measurements were performed in triplicates. Data analysis was automatically performed by Mololith NT.115 Control and Analysis software (Nanotemper Technologies, GmbH, Munich, Germany).

***MtblspE* binding study via thermal shift assay**

The shifts in T_m of *MtblspE* induced by the compounds were determined *via* TSA. *MtblspE* (15 μ M) was incubated with 20 μ M of each compound for 30 min in 50 mM HEPES (pH 7.0, 100 mM NaCl, 5 mM MgCl₂, 5 mM DTT). After that, SYPRO ORANGE fluorescent dye (Thermo Fisher) was added at a final concentration of 5X. Melting curves of each sample was measured increasing the temperature from 10 °C to 95 °C with an increase of 1 °C/30 sec and recording fluorescence of SYPRO ORANGE after every temperature increase using CFX96 real-time system-C1000 Thermal Cycler (Bio-Rad). Melting temperature (T_m) of each sample were calculated using CFX manager 2.0 software (Bio-Rad). Data analysis and visualization was performed using Excel and GraphPad 9.8.

Determination of *E. coli* activity

Growth inhibition values were determined in 96-well plates (Sarstedt, Nümbrecht, Germany) against *Escherichia coli* K12 and *E. coli* Δ tolC. As bacteria start OD₆₀₀ 0.03 was used in a total volume of 200 μ L in lysogeny broth (LB) medium containing the compounds dissolved in DMSO (DMSO concentration in the experiment: 1%) at a concentration of 50 μ M. The OD values were measured using a CLARIOstar platereader (BMG labtech, Ortenberg, Germany) after inoculation and after incubation for 18 h at 37 °C with 50 rpm. Based on these values, percent inhibition values were calculated in relation to the DMSO control.

Determination of *in vitro* anti-tubercular activity and solubility in 7H9 medium

Anti-tubercular tests were performed as previously described.¹ In brief, 7H9 complete medium (BD Difco; Becton Dickinson, Maryland, USA) supplemented with 10% OADC (BD), 0.2% glycerol, and 0.05% Tween80 as previously described,³ was used to culture *Mycobacterium tuberculosis* (*Mtb*) strain H37Rv (ATCC 25618) carrying a mCherry-expressing plasmid (pCherry10).⁴ Cultures were harvested at mid-log phase and frozen in aliquots at – 80 °C. Prior to testing aliquots were thawed followed by centrifugation and the pellet was resuspended in 7H9 medium with 10% OADC (without glycerol and Tween80). This was further thoroughly resuspended by passing it through a syringe with a 26-gauge needle to avoid clumping of the

bacteria. 2×10^5 CFU (colony forming units) were then cultured in a total volume of 100 μ l culture medium (triplicates) to test the non-precipitating compounds for the anti-tubercular activity at the concentrations indicated. For these assays, 96-well flat clear bottom black polystyrene microplates (Corning® CellBIND®, Merck, New York, USA) were used. Each plate had Rifampicin (at 1 μ g/ml and 0.1 μ g/ml) (National Reference Center, Borstel) as a reference compound. Plates were sealed with an air-permeable membrane (Porvair Sciences, Wrexham, UK) in a 37 °C incubator with mild agitation (TiMix5, Edmund Bühler, Germany). The activity of compounds was determined after 7 days by measuring the bacterial growth as relative light units (RLU) from the fluorescence intensity obtained at an excitation wavelength of 575 nm and an emission wavelength of 635 nm in a microplate reader (Synergy 2, BioTek Instruments, Vermont, USA). Two independent experiments (each in triplicates) were performed, and all values were normalized to untreated control sample (100%) in each experiment.

Cytotoxicity assay

To obtain information regarding the toxicity of our compounds, their impact on the viability of human cells was investigated. HepG2 cells (2×10^4 cells per well) were seeded in 96-well, flat-bottomed culture plates in 100 μ L culture medium (DMEM containing 10% fetal calve serum, 1% penicillin-streptomycin). Twenty-four hours after seeding the cells, medium was removed and replaced by medium containing test compounds in a final DMSO concentration of 1%. Compounds were tested in duplicates at a single concentration or, for CC50 determination, at 8 concentrations that were prepared via 2-fold serial dilutions in 1% DMSO/medium. Epirubicin and doxorubicin were used as positive controls in serial dilutions starting from 10 μ M, and rifampicin was used as a negative control (at 100 μ M). The living cell mass was determined 48 h after treatment with compounds by adding 0.1 volumes of 3-(4,5-dimethylthiazol-2-yl)-2,5-diphenyltetrazolium bromide (MTT) solution (5 mg/mL sterile PBS) (Sigma, St. Louis, MO) to the wells. After incubating the cells for 30 min at 37 °C (atmosphere containing 5% CO₂), medium was removed and MTT crystals were dissolved in 75 μ L of a solution containing 10% SDS and 0.5% acetic acid in DMSO. The optical density (OD) of the samples was determined photometrically at 570 nm in a PHERAstar Omega plate reader (BMG labtech, Ortenberg, Germany). To obtain percent viability for each sample, their ODs were related to those of DMSO controls. At least two independent measurements were performed for each compound. The calculation of CC50 was performed using the nonlinear regression function of GraphPad Prism 10 (GraphPad Software, San Diego, CA, USA).

Supplementary Figures

*Mtb*lspE stability study *via* thermal shift assay

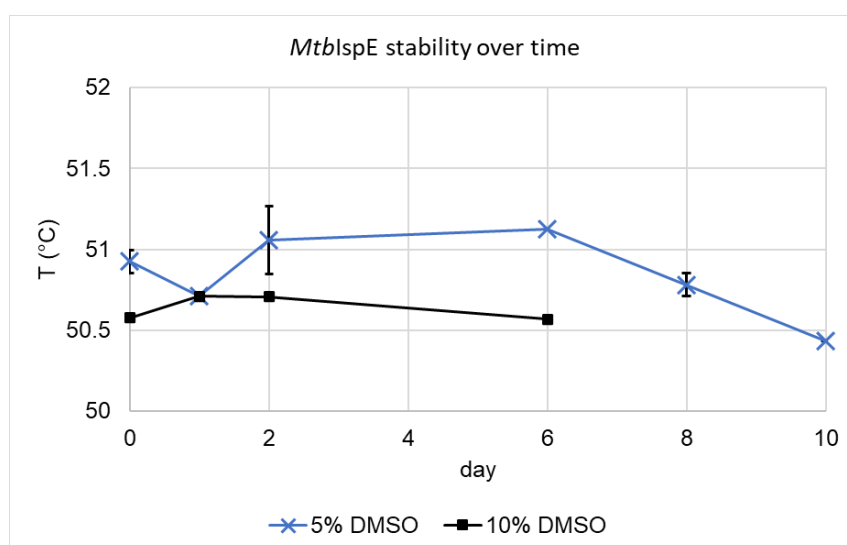
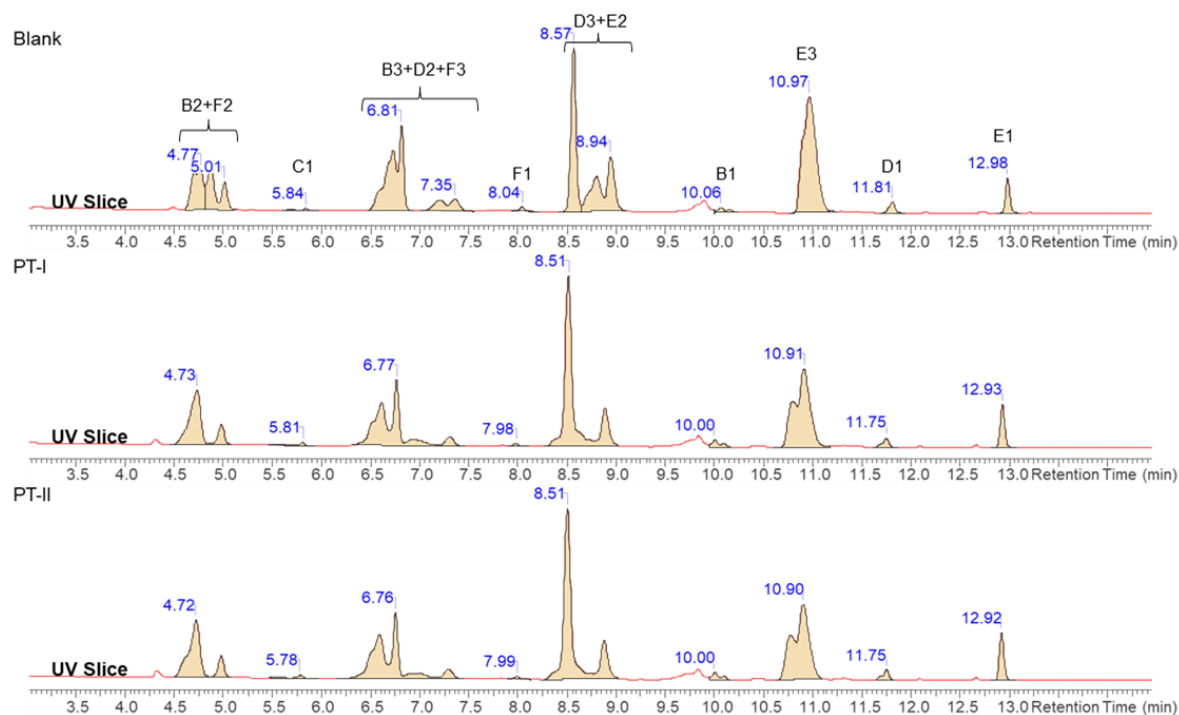


Figure S1. *Mtb*lspE melting temperature evolution over a period of 10 days at pH = 7.0 in Tris-HCl buffer with 5%, and 10% DMSO.

HPLC-MS/MS peak assignments and determination of equilibrium

A. DCL-1, 24h



B. DCL-1, 30h

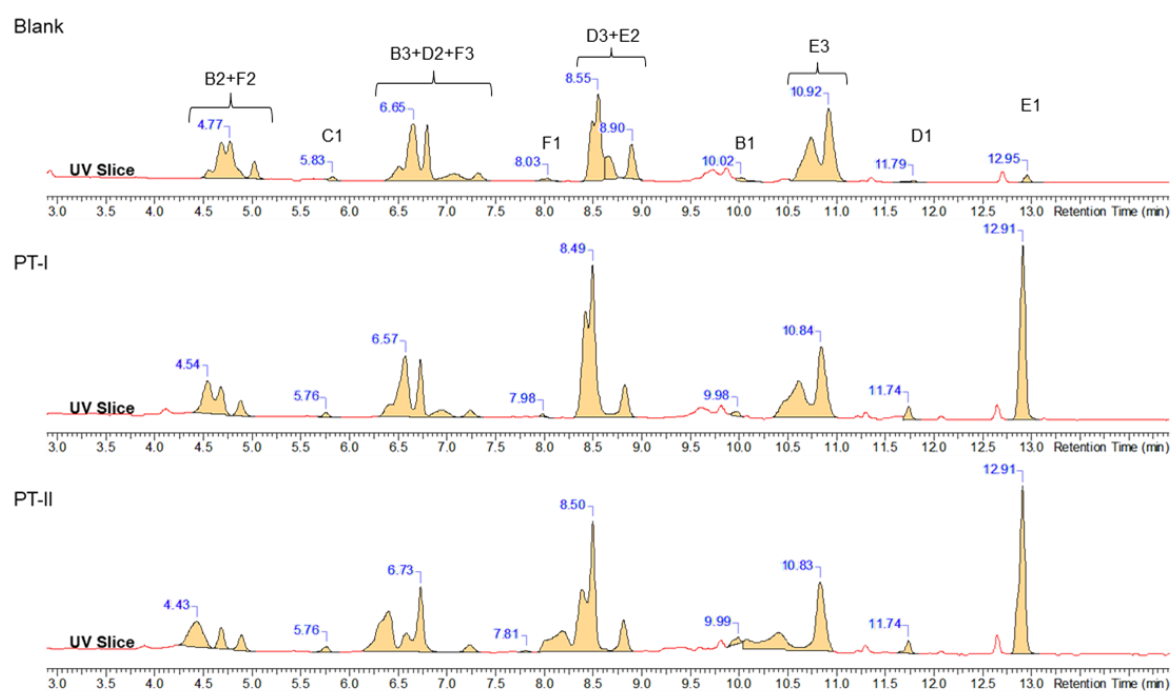


Figure S2. Product peak assignment for tdCC analysis. HPLC UV absorbance at 310nm of DCL-1 at A) 24 h and B) 30 h of blank and protein-templated duplicates. The following products were not considered: **A1–A3** (not found), **C2** (interference with injection peak), **C3** (RPA <1%).

4. Chapter

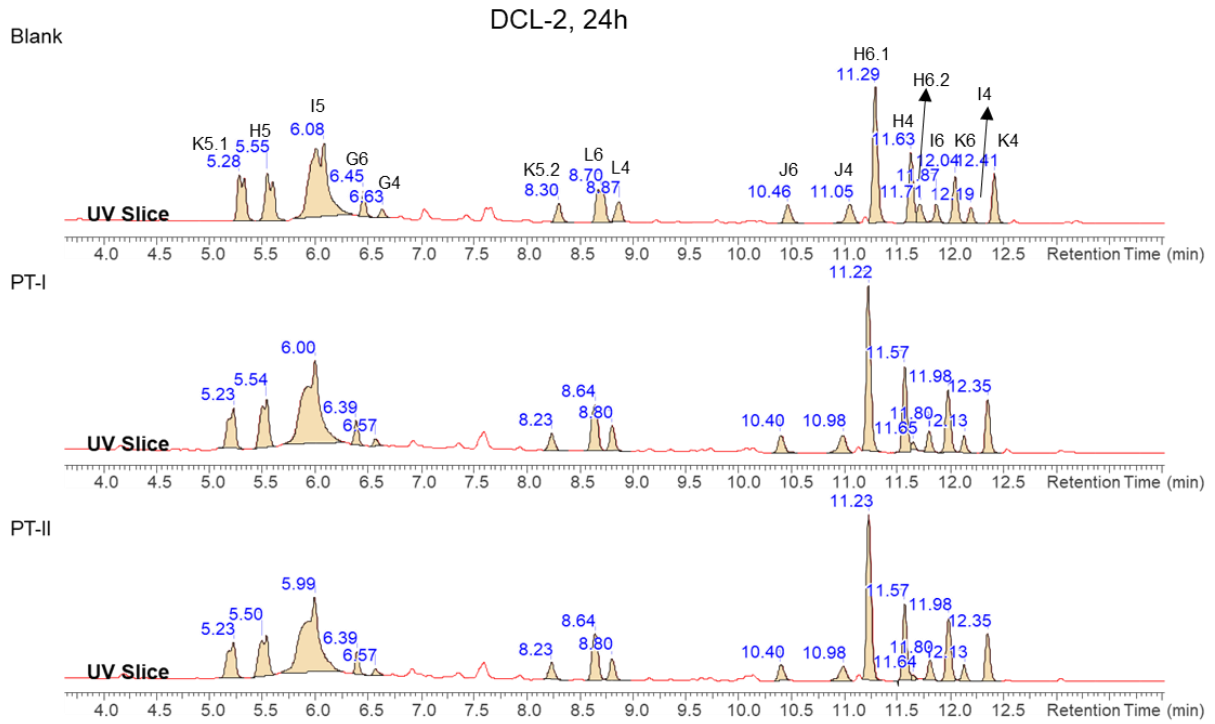


Figure S3. Product peak assignment for tdDCC analysis. HPLC UV absorbance at 310nm of DCL-2 at 24 h of blank and protein-templated duplicates. The following products were not considered: **G5** (interference with injection peak), **L5** and **J5** (RPA <1%).

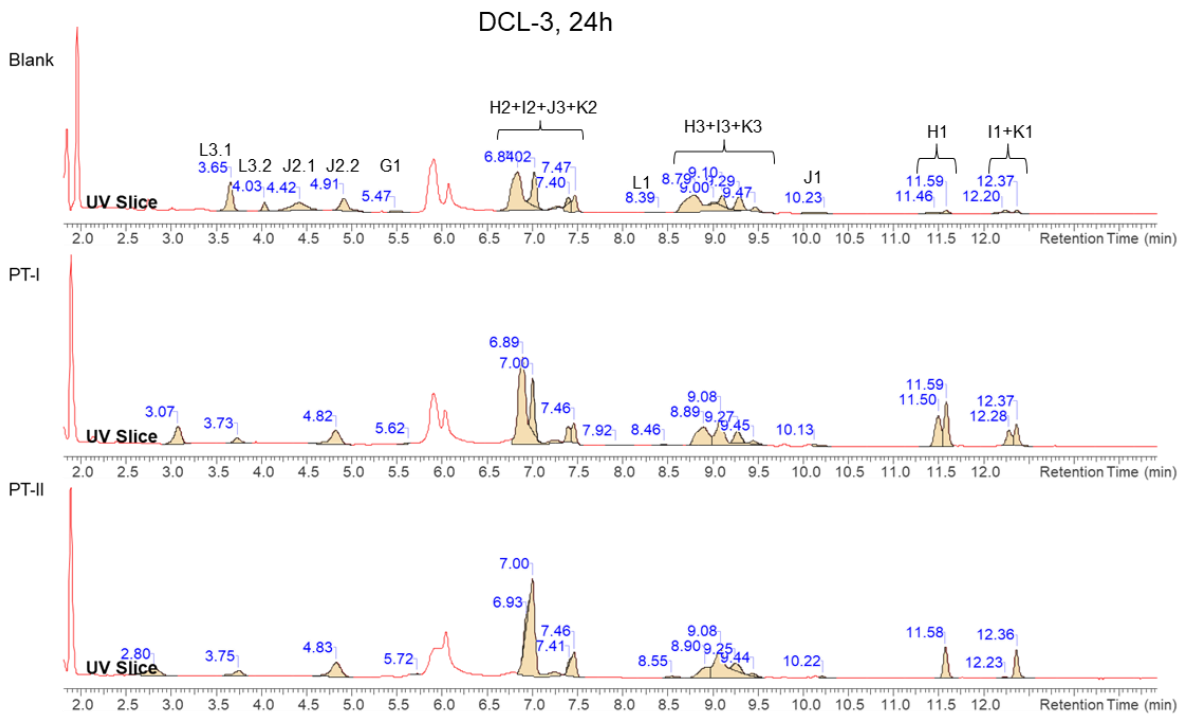


Figure S4. Product peak assignment for tdDCC analysis. HPLC UV absorbance at 310nm of DCL-3 at 24 h of blank and protein-templated duplicates. The following products were not considered: **G2**, **G3** and **L2** (interference with injection peak).

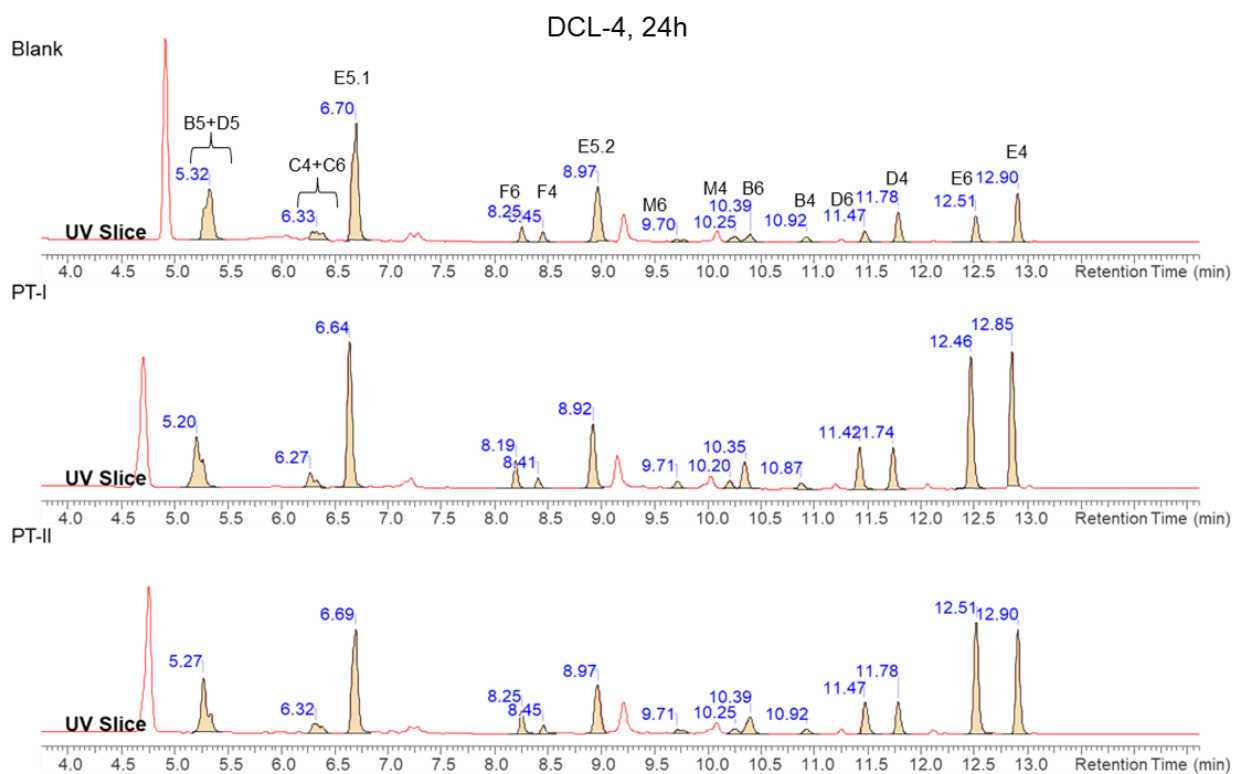


Figure S5. Product peak assignment for tdDCC analysis. HPLC UV absorbance at 310nm of DCL-4 at 24 h of blank and protein-templated duplicates. The following products were not considered: **C5** (interference with injection peak), **F5** (RPA <1%), and **M5** (not found).

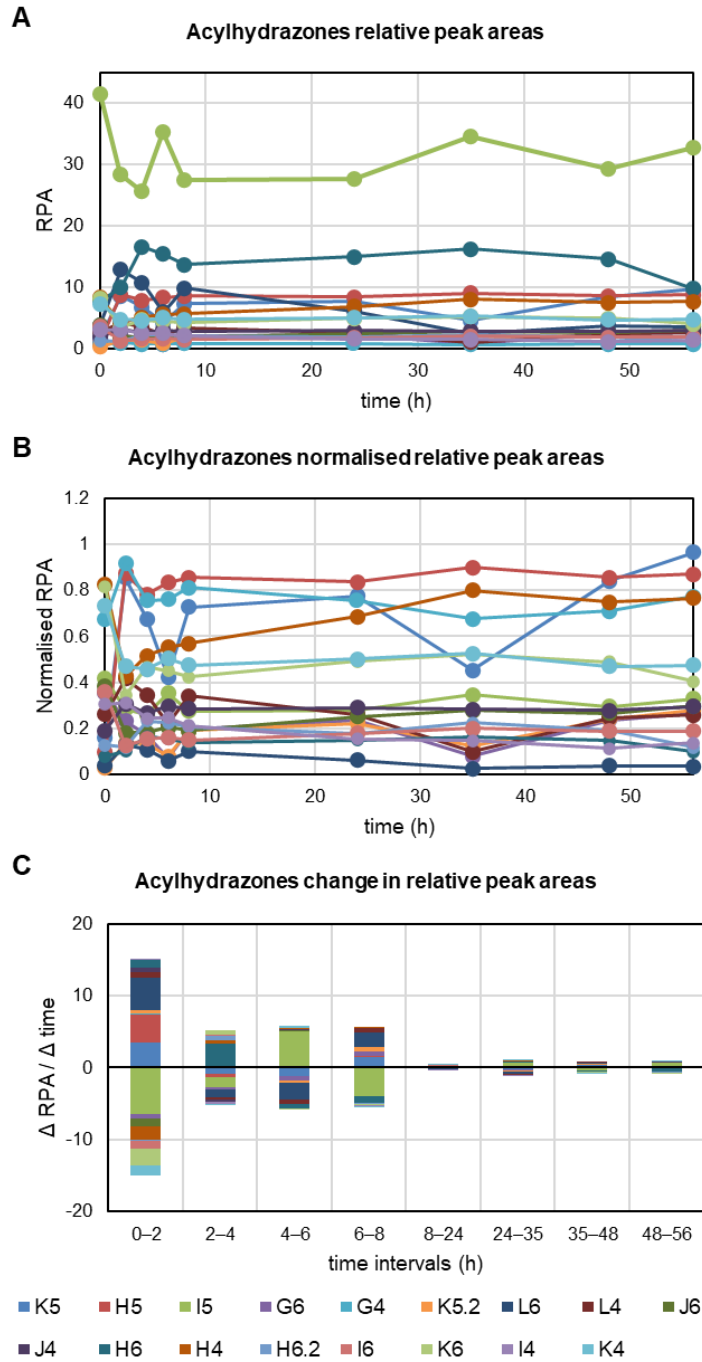


Figure S6. Graphical determination of equilibrium in blank DCL-2. A) Evolution of relative peak areas (RPA) of formed acylhydrazones over time. B) Normalised RPAs over time. C) Change of RPA in each time interval.

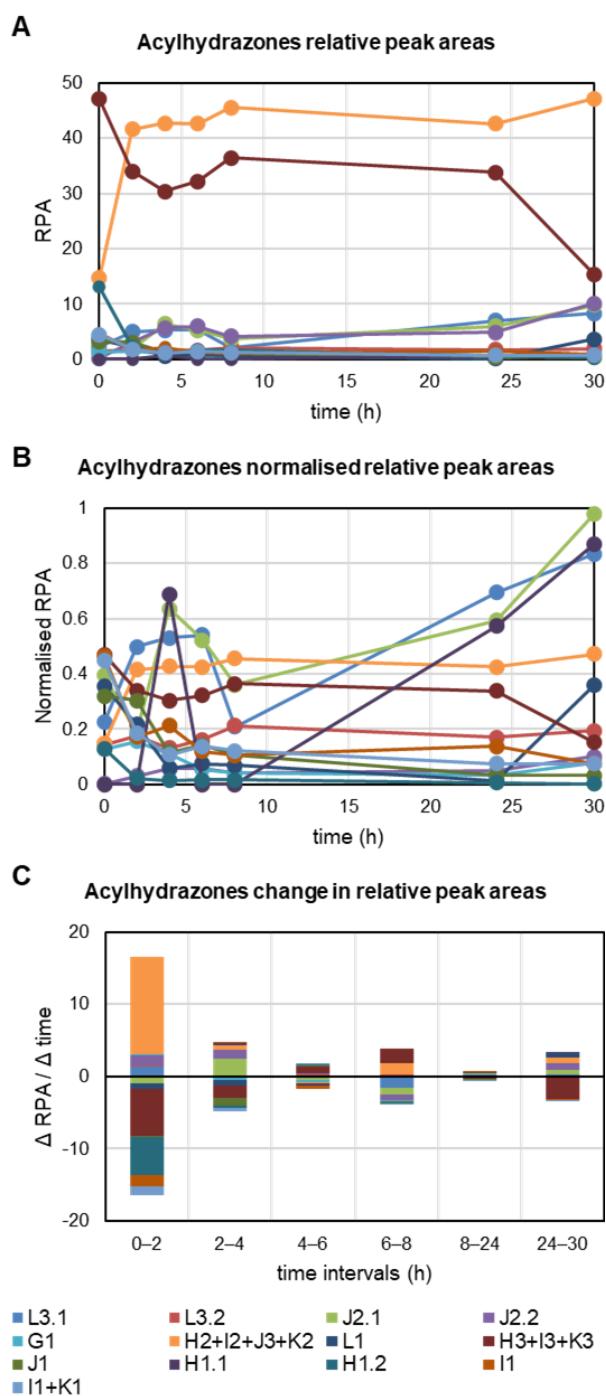


Figure S7. Graphical determination of equilibrium in blank DCL-3. A) Evolution of relative peak areas (RPA) of formed acylhydrazones over time. B) Normalised RPAs over time. C) Change of RPA in each time interval.

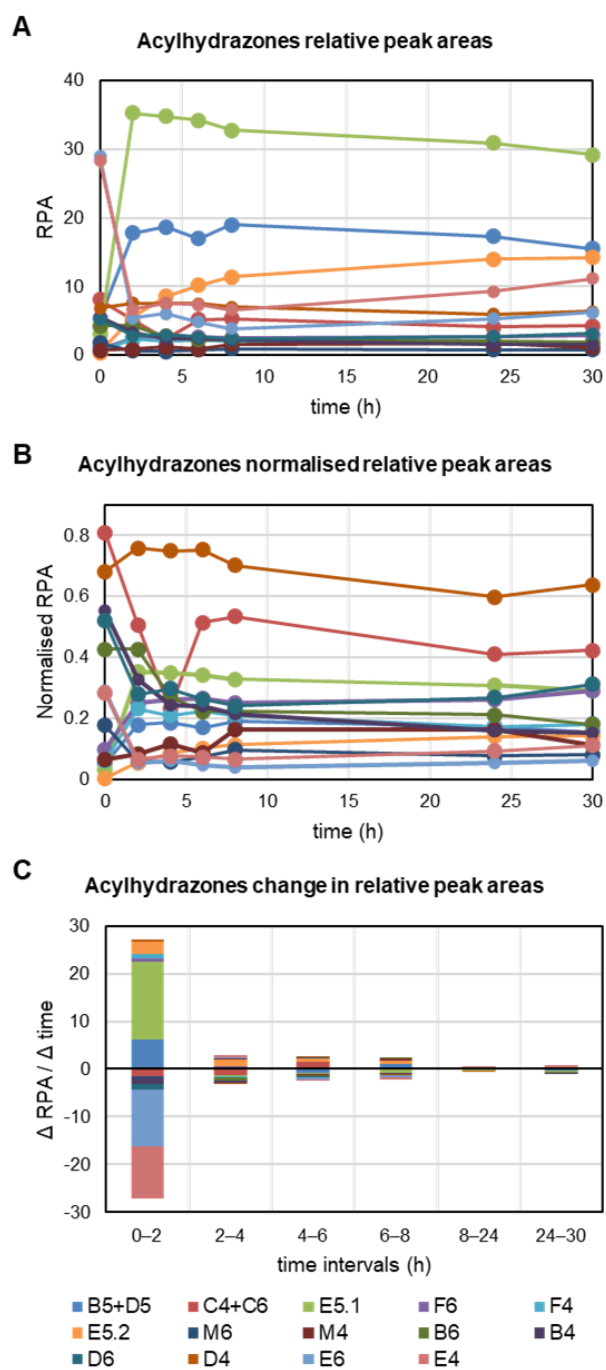


Figure S8. Graphical determination of equilibrium in blank DCL-4. A) Evolution of relative peak areas (RPA) of formed acylhydrazones over time. B) Normalised RPAs over time. C) Change of RPA in each time interval.

Amplification of *N*-acylhydrazones in the PT experiments

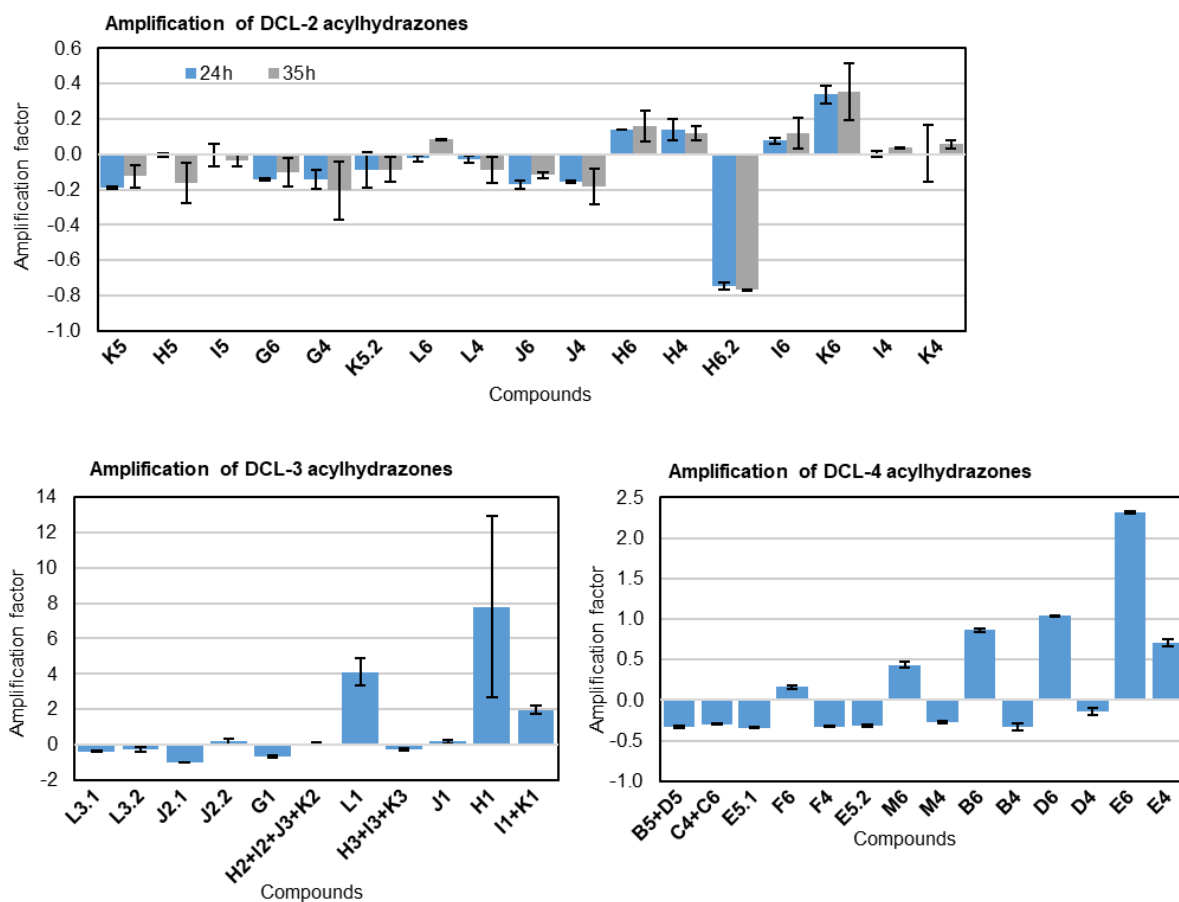


Figure S9. Amplifications of *N*-acylhydrazone products in protein-templated experiments DCL-2,-3, and-4 at 24 h. In the case of DCL-2, also at 35 h.

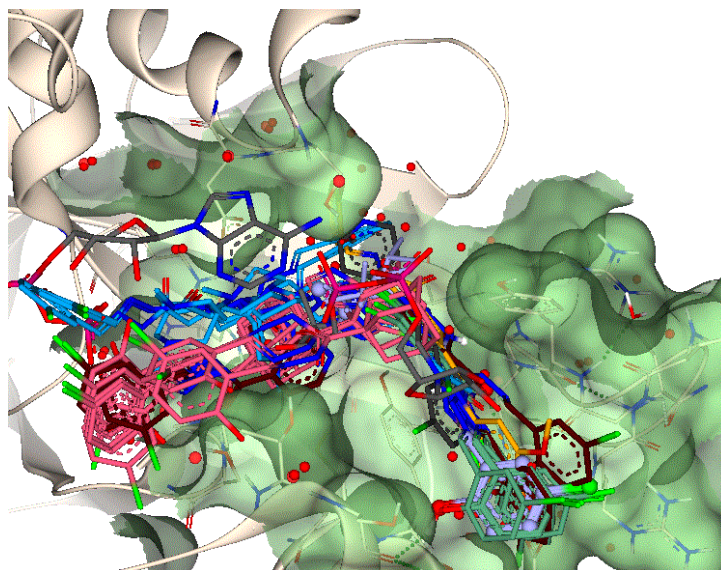
***In silico* elucidation of tdDCC hits' binding mode**

Figure S10. Binding poses of hit-structures containing fragment **1** and natural substrates. Molecules are represented with the following colours: **C1** in blue; **D1** in violet, **H1** in yellow, **I1** in pink, **K1** in green, **L1** in brown, CDP-ME and ADP in grey.

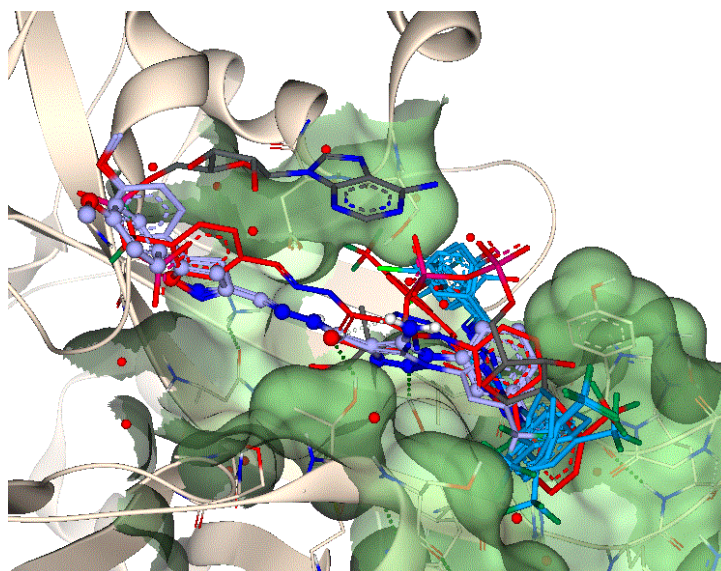


Figure S11. Binding poses of hit-structures containing fragment **E** and natural substrates. Molecules are represented with the following colours: **E1** in blue, **E4** in red, **E6** in violet, CDP-ME and ADP in grey.

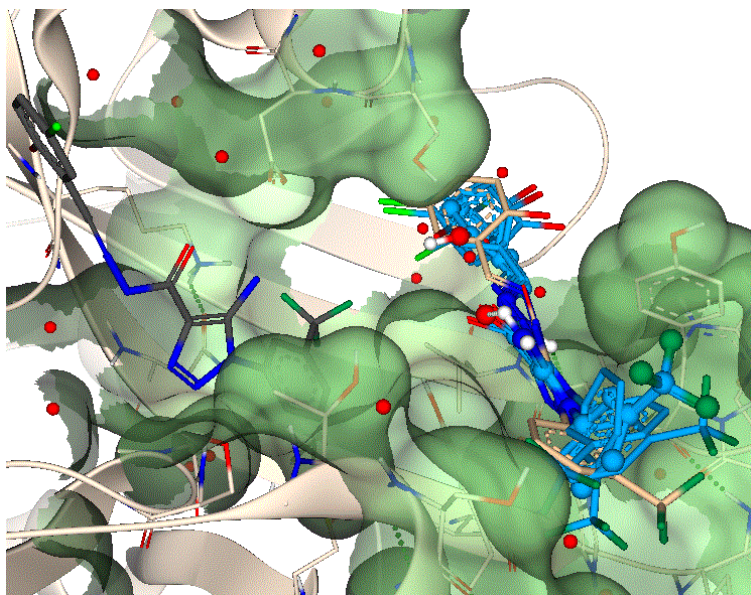


Figure S12. Binding poses of hit-structure **E1** and natural substrates. Molecules are represented with the following colours: **E1** in blue, CDP-ME and ADP in grey.

Supplementary references

- (1) Jumde, R. P.; Guardigni, M.; Gierse, R. M.; Alhayek, A.; Zhu, D.; Hamid, Z.; Johannsen, S.; Elgaher, W. A. M.; Neusens, P. J.; Nehls, C.; Hauptenthal, J.; Reiling, N.; Hirsch, A. K. H. Hit-Optimization Using Target-Directed Dynamic Combinatorial Chemistry: Development of Inhibitors of the Anti-Infective Target 1-Deoxy-D-Xylulose-5-Phosphate Synthase. *Chem Sci* **2021**, *12* (22), 7775–7785. <https://doi.org/10.1039/D1SC00330E>.
- (2) Hartman, A. M.; Gierse, R. M.; Hirsch, A. K. H. Protein-Templated Dynamic Combinatorial Chemistry: Brief Overview and Experimental Protocol. *European J Org Chem* **2019**, *22*, 3581–3590. <https://doi.org/10.1002/ejoc.201900327>.
- (3) Kolbe, K.; Möckl, L.; Sohst, V.; Brandenburg, J.; Engel, R.; Malm, S.; Bräuchle, C.; Holst, O.; Lindhorst, T. K.; Reiling, N. Azido Pentoses: A New Tool To Efficiently Label *Mycobacterium Tuberculosis* Clinical Isolates. *ChemBioChem* **2017**, *18* (13), 1172–1176. <https://doi.org/10.1002/cbic.201600706>.
- (4) Zelmer, A.; Carroll, P.; Andreu, N.; Hagens, K.; Mahlo, J.; Redinger, N.; Robertson, B. D.; Wiles, S.; Ward, T. H.; Parish, T.; Ripoll, J.; Bancroft, G. J.; Schaible, U. E. A New in Vivo Model to Test Anti-Tuberculosis Drugs Using Fluorescence Imaging. *J. Antimicrob. Chemother.* **2012**, *67* (8), 1948–1960. <https://doi.org/10.1093/jac/dks161>.

5. Chapter:

Exploring Protein-Templated and Biophysical Approaches for Fragment Discovery using IspE from Gram-Negative Bacteria

Maria Braun-Cornejo, Camilla Ornago, Rawia Hamid, Virgyl Camberlein, Boris Illarionov, Eleonora Diamanti, Wulf Blankenfeldt, Peter Maas, and Anna K. H. Hirsch

Manuscript In Preparation.

Author Contributions

M. Braun-Cornejo was involved in designing the project, performing the KTGS experiments, synthesising compounds, selecting compounds for screening, and writing of the manuscript. C. Ornago was involved in designing the project, purifying *PaIspE* and *AaIspE*, performing and evaluating TSA, MST, and *PaIspE* activity test. R. Hamid purified *EclspE*. V. Camberlein was involved in synthesising compounds and supervising the project. B. Illarionov coordinated and evaluated the *EclspE* activity tests. E. Diamanti was involved in supervising the. W. Blankenfeldt was involved in supervising the project. P. Maas was involved in selecting compounds for screening, designing, and supervising the project. A. K. H. Hirsch was involved in designing, and supervising the project. All authors edited or approved the submitted manuscript.

Exploring Protein-Templated and Biophysical Approaches for Fragment Discovery using IspE from Gram-Negative Bacteria

Maria Braun-Cornejo,^{1,2,3} Camilla Ornago,⁴ Rawia Hamid,^{2,3} Virgyl Camberlein,^{2,3} Boris Illarionov,⁵ Eleonora Diamanti,³ Wulf Blankenfeldt,⁴ Peter Maas,¹ and Anna K. Hirsch^{2,3*}

¹ Specs Research Laboratory, Specs Compound Handling, B.V., Bleiswijkseweg 55, 2712 PB, Zoetermeer, The Netherlands.

² Saarland University, Department of Pharmacy, Campus Building E8.1, 66123 Saarbrücken, Germany.

³ Helmholtz Institute for Pharmaceutical Research Saarland (HIPS) – Helmholtz Centre for Infection Research (HZI), Campus Building E8.1, 66123 Saarbrücken, Germany.

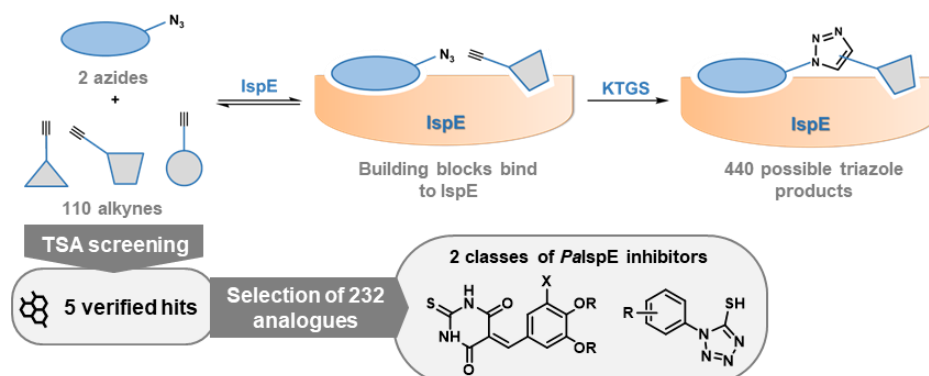
⁴ Department Structure and Function of Proteins, HZI, Inhoffenstrasse 7, 38124 Braunschweig, Germany.

⁵ Hamburg School of Food Science, Institute of Food Chemistry, Grindelallee 117, 20146 Hamburg, Germany

* Corresponding author: Anna.Hirsch@helmholtz-hips.de

Abstract

In this study, we built a diverse fragment library comprising 110 alkynes to perform kinetic target-guided synthesis (KTGS) based on the azide-alkyne cycloaddition. This technique exploits the catalytic potential of biological targets, to accelerate the cyclisation between azides and alkynes, effectively forming their own selective triazole ligands. KTGS is an ideal hit-optimisation and -expansion strategy, yet, our tailored azide did not perform as hoped and no triazole products were formed by our target: 4-diphosphocytidyl-2C-methyl-D-erythritol kinase (IspE). We successfully changed direction towards fragment-based hit-identification, screening the alkyne library via thermal shift assay obtaining several hits. Five diverse hit structures were verified and used to select over 200 additional compounds leading to the identification of five compounds that inhibit IspE from *Pseudomonas aeruginosa* (*Pa*). Notably, these structures are the first reported inhibitors of *Pa*IspE, and pave the way to targeting IspE in this critical Gram-negative bacterial pathogen.



Keywords: kinetic-target guided synthesis, click chemistry, fragment-based screening, IspE, *Pseudomonas aeruginosa*.

Introduction

With antimicrobial resistance posing a significant global health threat,^{1,2} the application of novel and effective medicinal-chemistry approaches is key to accelerate the discovery of anti-infectives with unprecedented modes of action.^{3,4} In the search for promising drug targets, the 2-C-methyl-D-erythritol 4-phosphate (MEP) pathway has emerged as a compelling candidate as it is essential for numerous

pathogens, including the causative agents of malaria, tuberculosis, and all Gram-negative bacteria.^{5,6} These critical pathogens rely solely on the MEP pathway as a source of the vital isoprenoid precursors isopentenyl diphosphate (IDP) and dimethylallyl diphosphate (DMADP). Given that in humans IDP and DMADP are formed through the mevalonate pathway, this metabolic divergence minimises selectivity concerns. Despite research efforts spanning decades and all seven enzymes of the MEP-pathway being considered druggable, the discovery of potent inhibitors has proven challenging, presumably owing to the highly hydrophilic active sites.⁷ In our study, we focus on the fourth enzyme of the pathway: 4-diphosphocytidyl-2-C-methyl-D-erythritol kinase (IspE). While several inhibitor classes targeting IspE have been reported, the most potent example exhibits low single-digit micromolar activity with no whole-cell activity.⁸ It is also the only inhibitor class co-crystallised with IspE. Recently, we employed virtual screening to identify novel IspE inhibitors within a focused library designed for improved accumulation within *Escherichia coli* (*Ec*).⁹ Subsequent optimisation efforts regarding the inhibition of IspE, however, have encountered significant hurdles. Therefore, we sought to explore alternative strategies prioritising target specificity.

Kinetic target-guided synthesis (KTGS) is a powerful tool in early-stage drug discovery, facilitating hit-optimisation and the structural expansion of initial hits through protein-templated (PT) synthesis. In KTGS, the biological target itself assembles ligands from pre-defined building blocks. Suitable fragments bind to the target's dynamic surface and undergo accelerated covalent bond formation, leading directly to the creation of selective binders.¹⁰ Therefore, this method is best suited when initial hits with affinity for the target are available and less for hit-identification efforts. In addition, the reaction chosen for KTGS needs to be compatible with the biological target. The most widely used reaction in KTGS is the click chemistry of azides and alkynes to form triazoles. Click chemistry, recently recognised by the Nobel Prize, refers to simple, atom-economic reactions, comprising some possible bioorthogonal reactions like the forementioned cycloaddition.¹¹ A typical approach consists in using a small number of azides tailored to the target in combination with a larger number of alkynes (random or pre-filtered).¹⁰ Notably, only the compounds formed by the target require biological evaluation and thus synthesis, making KTGS a cost- and time-effective method. Following this approach, many successful studies have been reported, establishing KTGS as a robust drug discovery method for hit-optimisation, and expansion.¹²⁻¹⁶

Recognising the need for enhanced-affinity hits for IspE, this study explores KTGS for the identification of selective IspE inhibitors. We designed azides based on an *Ec*IspE hit **1** (Figure 2A) that originates from a recent study,¹⁷ and combined them with a diverse alkyne library. Unfortunately, no triazole hits could be identified, potentially due to a lack of target affinity of the designed azide fragments. Consequently, we switched strategies to pursue fragment-based hit-identification using the alkyne fragment library. This approach led to the identification of five alkyne fragment hits that were used to pursue hit-optimisation studies leading to the discovery of two new IspE inhibitor classes.

Results and Discussion

Selection, design and synthesis of building blocks for KTGS

We chose the well-established Huisgen 1,3-dipolar cycloaddition with azides and alkynes as a reaction for the KTGS experiments, following the typical approach using an excess of alkynes compared to azides.¹³ Therefore, we built an alkyne library of 110 diverse fragments containing one terminal alkyne (Supplementary Information (SI), Table S2). We filtered around 600 alkyne-containing compounds using favourable values of chemical descriptors (MW < 350, clogS > -7 etc.), and excluded any fragments containing reactive or otherwise problematic functional groups. We generated a chemical space map of these remaining candidates to ensure a diverse selection spanning a wide chemical space, thereby enhancing the library's potential for favourable interactions with the protein. From the 110 selected alkynes, 39 fragments originated from our in-house reagents, eight had been synthesised for previous studies in our group,¹⁸⁻²⁰ and 63 fragments belong to the Specs library (Figure 1). We grouped the fragments

into 16 clusters, containing six or seven alkynes each to combine with azide fragments in the KTGS experiment. For ease in the LCMS/MS analysis, all alkynes within a cluster had distinct molecular weights.

We designed the complementary azide fragments for the KTGS experiment based on *EclspE* inhibitor **1** (Figure 2A), recently identified in our group through a phenotypic screening against *Plasmodium falciparum* (*Pf*). Using the coupled *IspE* pyruvate kinase/lactate dehydrogenase (PK/LDH) assay, we determined a moderate inhibition of *IspE* by hit **1**. Unfortunately, as inhibition of PK/LDH was found, we discontinued our *IspE* structure–activity relationship (SAR) study of this class. Nevertheless, we opted to pursue hit **1** further using KTGS to improve its selectivity. Therefore, we designed azides **2–4** (Figure 2B), which maintain the left-hand side of **1** (highlighted in blue, Figure 2A) while removing the undesirable aromatic nitro scaffold. In the design of the building blocks, the azide functionality replaces the amide linker of **1**, either being directly bound to the pyrazole (azide **3**) or through a methylene for variable linker length (azide **2**). The methylene linker of azide **2** provides greater flexibility compared to azide **3**, enhancing its potential to align with bound alkynes and facilitate the formation of triazoles.²¹ In addition, we isolated acyl azide **4**, which was an intermediate in the synthesis of azide **3** (Scheme 1), with the aim to potentially investigate the development of a novel KTGS reaction. Electron-poor azides do not undergo click chemistry via copper(I)-catalysis to form triazoles,²² however, in the case of carbonyl azides, specific copper(I)-complexes can catalyse the formation of 2,5-substituted oxazoles through loss of nitrogen.²³ Therefore it is worth contemplating that enzymes or other biological targets could catalyse this oxazole formation as well (Figure 2B). The choice of maintaining the left-hand side of hit **1** in the azide building blocks aligns with our recent target-directed dynamic combinatorial (tdDCC) study using *IspE* from *Mycobacterium tuberculosis* (4. Chapter).²⁴ In this protein-templated experiment, the most frequently appearing building block in the hits contained the same phenyl with *para*-substituted OH and Cl functionalities as **1** (Figure 2C). Additionally, our phenotypic study revealed that the class of hit **1** retains its anti-infective activity regardless of the type of substituent on the right-hand aromatic ring (electron-withdrawing, electron-donating, small, and large). We wanted to further explore the malleability of this side (highlighted in grey Figure 2A). Thus, we maintained the phenol and the pyrazole scaffolds in the design of the azides for the KTGS experiment.

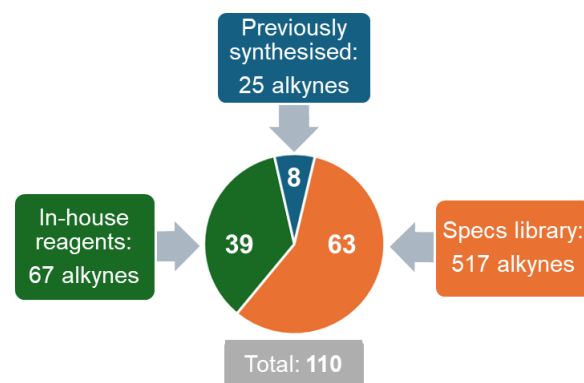


Figure 1. Origin of 110 selected alkyne building blocks.

Figure 2A shows the structure of compound **1** and its bioactivity. Figure 2B shows the designed azides for hit expansion based on **1**, and their potential KTGS products. Figure 2C shows the most common building block in a target-directed dynamic combinatorial (tdDCC) study using *IspE*.

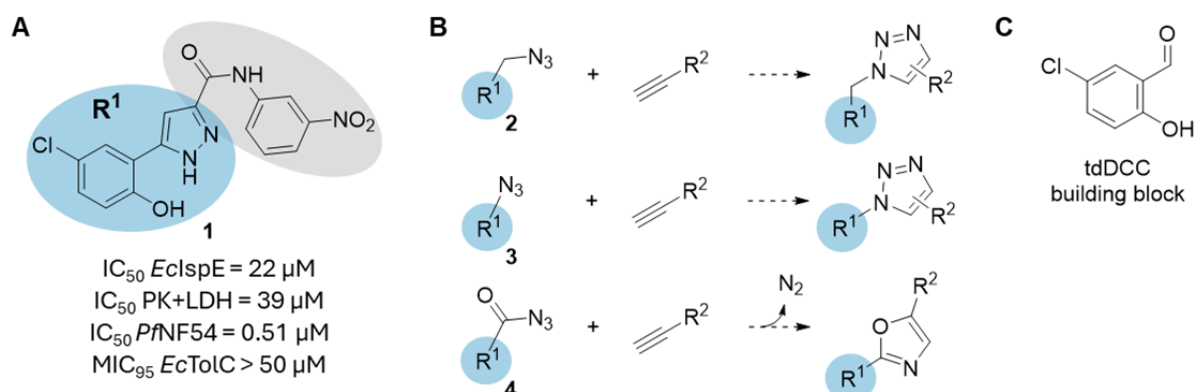
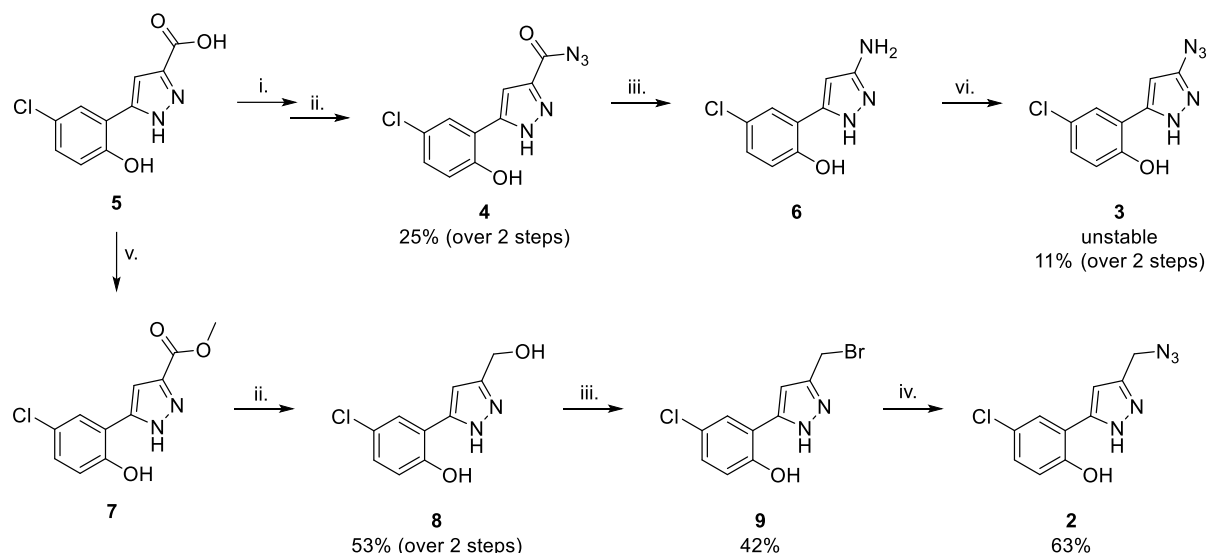


Figure 2. A) Structure of compound **1** and its bioactivity. B) Designed azides for hit expansion based on **1**, and their potential KTGS products. C) Most common building block in a target-directed dynamic combinatorial (tdDCC) study using *IspE*.

The synthesis of azides **2–4** started from the common building block **5**, which stems from our recent study on the class of hit **1** (Chapter A).¹⁷ The divergent manipulation of the carboxylic acid of derivative **5**, affords

the corresponding azides with **(2)** and without **(3)** the methylene linker. Acid chloride formation *in situ* and subsequent addition of sodium azide formed acyl azide **4**. Under aqueous acidic conditions, **4** underwent a Curtius rearrangement resulting in amine **6**, which gave azide **3** using the azide transfer reagent 1*H*-imidazole-1-sulfonyl azide. Azide **3** started to degrade at room temperature (r.t.) overnight, which precluded further investigations of the compound. To obtain azide **2**, a methyl esterification of **5**, followed by reduction using lithium aluminium hydride afforded primary alcohol **8**. A subsequent Appel reaction afforded alkyl bromide **9**, which finally resulted in our desired azide **2** through a substitution reaction with sodium azide, with acceptable yield (Scheme 1).



Scheme 1. Synthesis of azides **2–4**, reagents and conditions: i. SO_2Cl_2 , PhCH_3 , 110°C , 16 h; ii. NaN_3 , DMF, 0°C , 30 min; iii. $\text{AcOH}:\text{H}_2\text{O}$ (1:1), reflux, 1 h; iv. ZnCl_2 , K_2CO_3 , DIPEA, 1*H*-imidazole-1-sulfonyl azide hydrochloride, CH_3OH , 0°C –r.t., 3 h; v. H_2SO_4 , CH_3OH , reflux, 2.5 h; vi. LiAlH_4 , THF, 0°C , 2 h; vii. PPh_3 , CBr_4 , CH_2Cl_2 , 0°C –r.t., 2.5 h; viii. NaN_3 , KI, DMF, r.t., 1 h.

Experimental setup and analysis of KTGS

To our disappointment, the synthesised azides **2** and **4**, did not inhibit *EclspE*, therefore, we adapted our initial KTGS strategy. Aiming to increase the likelihood of hit identification, we broadened the structural diversity by including commercially available azide **10** (Figure 3). As mentioned above, acyl azide **4**, could be useful in the development of a new KTGS reaction forming oxazoles, however, due to its inactivity a proof-of-concept KTGS is highly unlikely to succeed. Therefore, we used azides **2** and **10** in combination with the alkyne library for our KTGS experiment. We investigated and optimised the experimental conditions, starting with the stability of the protein. We monitored the stability of *EclspE* over fourteen days at r.t. in HEPES and Tris buffer at pH = 7.0 and 8.0 with up to 10% DMSO by measuring its melting temperature (T_m) periodically (Table S1 and Figure S1). The protein was largely stable under the tested conditions, based on these results we chose to perform the KTGS experiment in HEPES buffer at pH = 7.0 with 5% DMSO. We determined the highest usable concentration of all the KTGS components under the chosen conditions resulting in 25 μM for *EclspE*, 250 μM for the azide building blocks, and 100 μM for the alkyne building blocks. We used these concentrations for the setup of the KTGS, incubating each azide individually with each of the 16 alkyne clusters in presence of *EclspE*, creating a total of 32 alkyne-azide mixtures. Considering a total of 110 alkynes and the possible formation of both 1,4- and 1,5-substituted triazoles, this provides 440 potential products.¹³ In addition to this protein-templated (PT) experiment, we included positive and negative controls to ensure the validation of potential KTGS hits. The negative control being identical to the PT experiment but excluding *EclspE*. For the positive control we increased the concentration of the azide building blocks and used CuSO_4 and ascorbic acid as catalysts generating 1,4-substituted triazoles

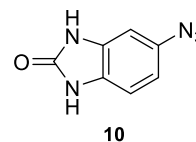


Figure 3. Chemical structure of azide **10**.

(copper(I)-catalysed azide-alkyne cycloaddition (CuAAC) conditions). The KTGS experiment spanned fourteen days, with periodic sampling (on day 4, 7, and 14). We prepared all samples in the same way; addition of ACN followed by centrifugation and collection of the supernatant for LCMS/MS analysis. The LCMS/MS data of the PT experiments were compared to the data of both control experiments to identify potential triazole hits. Regrettably, we were unable to identify any triazole product in the UV spectra of the LCMS/MS of the PT samples. To rule out that slow product formation led to insufficient UV absorption, we extracted the target ion data for all samples and analysed them in detail. We first compared the retention times (t_R) of the products from the positive control with the respective t_R in PT samples and found a few matches. Closer inspection, however, revealed them as noise or they were also found in the negative controls with similar intensity. We further broadened our search by excluding the t_R parameter, aiming to capture potential 1,5-triazoles with significant differences in t_R compared to the 1,4-regioisomer. Unfortunately, this approach also yielded no hits, concluding that our KTGS experiment was unsuccessful. The challenges we faced emphasise the importance of utilising verified binders as one of the two building blocks, not only for the design of the building blocks, but also to verify their affinity for the target once synthesised. Given that azide **2** did not show affinity for our target the KTGS experiment shifted from hit-expansion to hit-finding, two approaches with different building-block requirements. In the case of hit-finding the covered chemical space needs to be wide for both kinds of building blocks. We only employed two azides in our KTGS, heavily constraining the possibility of obtaining hits. In addition, hit-identification can be particularly difficult for certain protein targets with challenging binding pockets such as IspE's rather hydrophilic pocket.

Biophysical screening of the alkyne fragment library

Following the unsuccessful KTGS attempt applied to *EclspE*, we wanted to make use of our structurally diverse alkyne library, and pursued an alternative biophysical fragment-based hit-discovery approach. For the initial screening, we chose the thermal shift assay (TSA), which aims at identifying compounds binding to the protein of interest by observing the difference in thermal stability between the target alone and the target incubated with each potential ligand.²⁵ Based on this, we decided to exclude the alkyne fragments smaller than 150 Da, whose influence on the thermal stability of IspE was assumed to be too small to be detected via TSA. In addition, we decided to change the protein homologue, moving from *EclspE* the most studied homologue, to IspE from *Pseudomonas aeruginosa* (*Pa*), a highly critical Gram-negative bacterium not investigated in the context of IspE thus far.

For the TSA, we incubated the 79 fragments individually with the target protein and evaluated their impact on the melting temperature of IspE. Four alkyne fragments induced a significant change in T_m of *PaIspE* of at least 2 °C (Figure 4A), in all cases the induced shift was negative, indicating a decrease in the thermal stability of the protein. To further investigate the negative thermal shift, we decided to test the alkyne library also on *Aquifex aeolicus* (*Aa*) IspE. This model organism is a hyperthermophile, therefore its proteins usually display much higher thermal stability than the mesophiles' orthologues. We were interested in seeing if the thermal shifts would be amplified in a thermostable IspE. Indeed, this approach identified many fragments that induced a $\Delta T_m \geq 2$ °C. Consequently, we decided to set a higher ΔT_m threshold for *AaIspE* of $\Delta T_m > 8$ °C, also obtaining four preliminary hits (Figure 4B). However, only fragment **11** with the biggest ΔT_m in *PaIspE* of -8 °C, also showed a significant change in T_m for *AaIspE* of -6 °C. We decided to use an alternative biophysical method, microscale thermophoresis (MST), to verify the binding of *PaIspE* hits **11–14**. Once again, exclusively fragment **11** gave a positive response showing reproducible binding. Compounds **12–13** belong to the same class of compounds and could not be evaluated because they were aggregating. Compound **14** is a very small fragment and did not bind in the MST experiment. In the case of *AaIspE*, to verify the only hit stabilising the protein with a positive shift in T_m , we performed a dose-dependent TSA experiment evaluating the dissociation constant (K_D) using FoldAffinity, resulting in the verification of hit **18** with a good binding affinity for its small size ($K_D = 26$ μ M). We decided to evaluate the ΔT_m of the remaining *AaIspE* hits using Tycho TSA. This technique has an alternative read-out, detecting the

intrinsic fluorescence of the amino-acids tryptophan and tyrosine and has a much faster temperature gradient compared to the classical TSA, which follows protein unfolding using a fluorescent dye. We obtained significant T_m shifts using Tycho TSA, verifying that the compounds were binding to IspE. In conclusion, our alkyne fragment screening resulted in five hits (**11**, **15–18**), compound **11** stands out by binding both tested homologues of IspE, and fragment **18** is also very promising with a moderate affinity in the micromolar range.

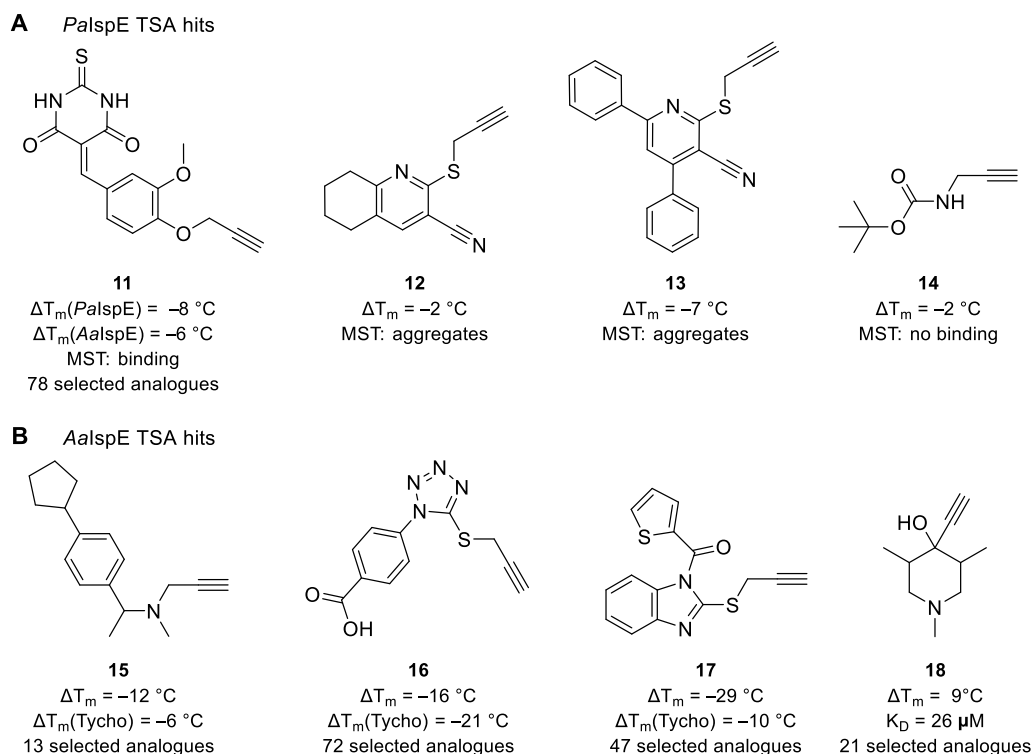
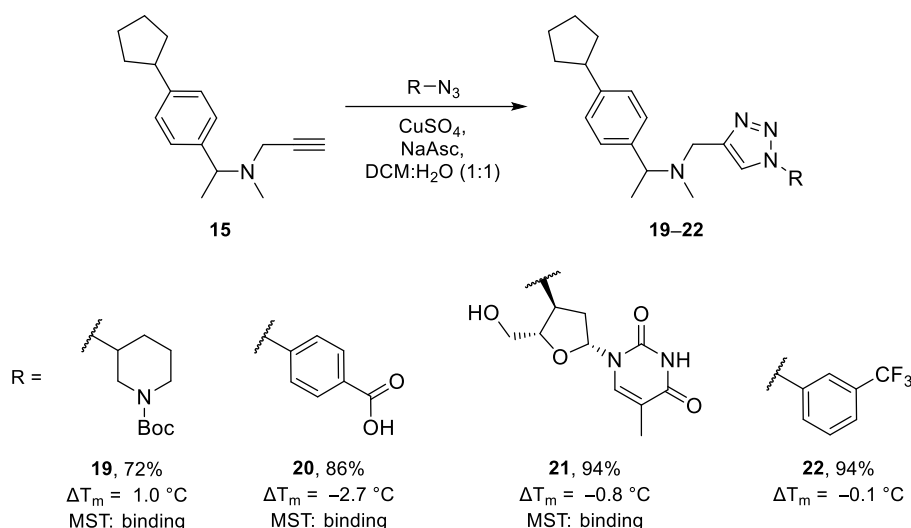


Figure 4. Structures of initial hits from the thermal shift assay (TSA). A) *Pseudomonas aeruginosa* (*Pa*) IspE hits. B) *Aquifex aeolicus* (*Aa*) IspE hits.

Hit expansion based on alkyne fragment hit structures

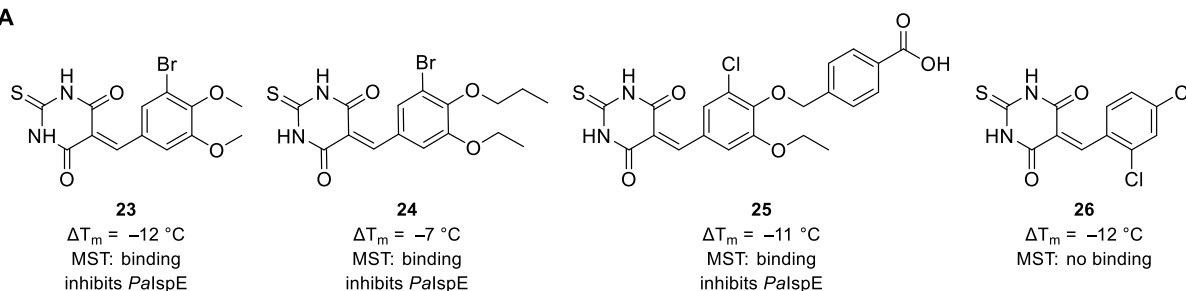
We selected over 200 compounds (Table S3) from the Specs library to follow up the verified hits **11**, and **15–18**. Given the small size of the structures, our goal was to primarily grow the compounds to increase the affinity and obtain more drug-like hits. Additionally, we also selected analogues similar in size to the alkyne hits with minor structural variations to get insights into the SAR. To achieve this, we first performed a substructure search of the hits, removing their alkyne handle. In addition, to increase the structural diversity, we performed similarity searches to allow variable linker-, ring-sizes, and heteroatoms. We filtered the lists obtained for favourable properties (MW < 500, clogP < 5, number of H-bonds etc.) before selecting compounds for biophysical screening. This final selection was mostly hand-picked to include the widest variety of drug-like compounds for each verified hit, selecting between 47 and 78 analogues for hits **11**, **16**, and **17** (Figure 4, Table S3). Given that the Specs library did not contain as many closely-related structures of hit **15** and **18**, we could only include thirteen and 22 analogues, respectively. Taking advantage of the fragments' alkyne handle, we attempted to establish a mid-throughput CuAAC workflow using a 24-tube parallel synthesiser, to grow the hits into triazole products using commercially available azides. For this purpose we chose non-miscible solvents, facilitating the isolation of products using phase-separation filters for a rapid work-up at small scales (< 100 μmol). Challenges arose as the stirring in the narrow parallel synthesiser tubes proved insufficient for thorough mixing of both phases, while ensuring complete solubilisation of all reagents. Consequently, we decided to only synthesise a few triazoles (**19–22**) in the standard fashion (Scheme 2).



Scheme 2. Copper(I)-catalysed alkyne-azide cycloaddition synthesis of triazoles **19–22** from alkyne hit **15** and their protein binding evaluation results.

The triazoles synthesised and the selection of analogues from the alkyne hits were tested in a similar workflow as the original alkyne library. For the synthesised products **19–22**, the changes in T_m of *Pal*spE were rather small, however, **19** and **21** showed positive shifts, indicating stabilisation of the protein (Scheme 2). Compound **22** showed no significant T_m shift and was not evaluated in MST binding experiments, the remaining triazole products bound to *Pal*spE, however, did not inhibit the protein. The 231 analogues from the Specs library yielded nine preliminary *Pal*spE hits originating from the alkyne hits **11** and **16**. The ΔT_m of these hits are in the same range as their parent fragments, between $-7\text{ }^\circ\text{C}$ and $-16\text{ }^\circ\text{C}$. The majority of the new hits could be verified with the MST binding assay (**23–25** and **27–29**, Figure 5).

A



B

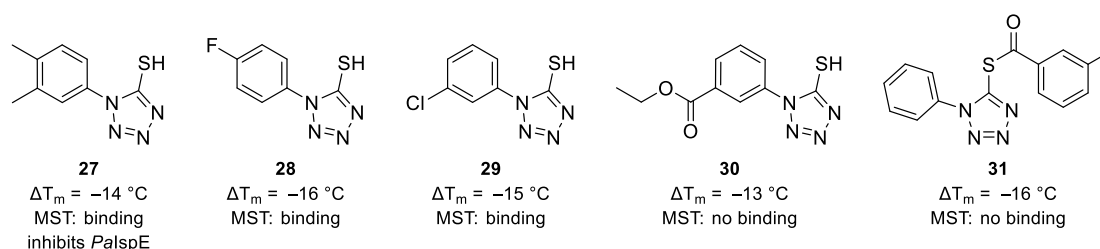


Figure 5. Hit compounds originating from screening 231 Specs compounds. A) structures based on fragment hit **11**. B) structures based on fragment **16**.

Furthermore, four of the six verified hits (**23–25**, and **27**), as well as alkyne fragment **11** showed inhibition ($\geq 50\%$) of *Pal*spE at $500\text{ }\mu\text{M}$ compound concentration. Inhibitors **23–25** belong to an interesting class of compounds as their structure contains a pyrimidine-like heterocycle with two carbonyls and a thiol substituent, linked to a phenyl with halogens and alkoxy substituents (Figure 5A). Notably, analogue **26**, which does not inhibit the enzyme, does not contain the alkoxy substituents but two chlorines. Inhibitor **25**, contains a benzoic acid linked *via* the alkoxy substituent serving as ester linkage, showing that we were able to grow the initial fragment hit **11** into a full-size drug-like compound. Unfortunately, this was not the case for the compounds **27–31**, originating from fragment hit **16** containing a benzoic acid linked to a

thiotetrazole. Despite screening over sixty diverse compounds that were bigger than alkyne **16**, we only obtained small-sized binders in the follow-up screening. The binders maintain the thiotetrazole motif from **16**, but have alternative substituents on the phenyl ring (**27–29**, Figure 5B). Inhibitor **27** has two methyl substituents on the phenyl and is the only compound of its class with inhibitory potency of *Pal*SpE, the halogenated analogues **28–29** did not inhibit the enzyme. These findings on the two newly discovered *Isp*E inhibitor classes give interesting structural insights into targeting *Pal*SpE, but more examples are needed to establish a more thorough SAR analysis. Nevertheless, these inhibitors, as well as alkyne fragment **18** are valuable starting points for further fragment growing, hit-optimisation, and -expansion efforts on *Isp*E.

Conclusions

Our study demonstrates compatibility of *Isp*E with KTGS, however, our hit-expansion strategy encountered setbacks given that the tailored azides did not exhibit the desired affinity for our target. Successful reports often originate from a verified binder and Peruzzotti *et al.* emphasised that *in silico* input or high-throughput fragment screening is essential in KTGS building block design.²⁶ The difficulty of true random hit-finding through KTGS is evident, as matching building blocks must bind simultaneously and align in the correct orientation within the protein pocket. Therefore, the fragment libraries used for hit-discovery must cover a wide structural diversity for both types of building blocks, as shown by the first successful report of this kind from last year. Kassu *et al.* obtained 12 bioactive hits by combining 38 sulfonyl azides with 45 thio acids giving 1710 potential *N*-acylsulfonamide combinations.²⁷ Ultimately, our approach was constrained by the limited chemical space explored, utilising only two azides. Another hit-discovery attempt would require expanding the azide library to cover a wider structural diversity. Given the proven potential of targeting *Isp*E with the alkyne library we built, KTGS holds potential in the context of hit-optimisation and -expansion once validated azide fragments are obtained for *Isp*E. Nevertheless, our shift in the strategy to target *Isp*E using the alkyne library yielded five hits in a fragment-based hit-identification workflow. These structurally diverse hits were followed up by screening hundreds of analogues, ultimately leading to five *Pal*SpE inhibitors from two distinct chemical classes. To the authors knowledge these are the first reported inhibitors of *Isp*E from *P. aeruginosa*, showcasing an important step towards targeting *Isp*E from critical pathogens. The pyrimidinedione inhibitor class is particularly promising as four analogues (**11**, **23–25**) showed inhibition of *Pal*SpE, indicating that the initial hit could be grown into a drug-like compound. We believe that hit-optimisation efforts can be promising for our identified starting points. In particular, the focus at this stage lies in obtaining structural information of the ligands' binding site in *Isp*E to pursue rational drug design strategies.

Author Contributions

M. Braun-Cornejo was involved in designing the project, performing the KTGS experiments, synthesising compounds, selecting compounds for screening, and writing of the manuscript. C. Ornago was involved in designing the project, purifying *Pal*SpE and *Aal*SpE, performing and evaluating TSA, MST, and *Pal*SpE activity test. R. Hamid purified *Ecl*SpE. V. Camberlein was involved in synthesising compounds and supervising the project. B. Illarionov coordinated and evaluated the *Ecl*SpE activity tests. E. Diamanti was involved in supervising the. W. Blankenfeld was involved in supervising the project. P. Maas was involved in selecting compounds for screening, designing, and supervising the project. A. K. H. Hirsch was involved in designing, and supervising the project. All authors edited or approved the submitted manuscript.

Acknowledgments

This project has received funding from the European Union's Horizon 2020 research and innovation programme under the Marie Skłodowska-Curie grant agreement No. 860816 (A. K. H. Hirsch, P. Maas & W. Blankenfeldt). The authors want to thank Antoine Lacour for support with StarDrop. R. Hamid thanks the Helmholtz Association's Initiative and Networking Fund, and the Schlumberger Foundation faculty for the future (FFTF) fellowships.

Notes

The authors declare no competing financial interest.

References

- (1) World Health Organization. *Global Priority List of Antibiotic-Resistant Bacteria to Guide Research, Discovery, and Development of New Antibiotics - 2017*; Geneva, 2017.
- (2) Murray, C. J.; Ikuta, K. S.; Sharara, F.; Swetschinski, L.; Robles Aguilar, G.; Gray, A.; Han, C.; Bisignano, C.; Rao, P.; Wool, E.; Johnson, S. C.; Browne, A. J.; Chipeta, M. G.; Fell, F.; Hackett, S.; Haines-Woodhouse, G.; Kashef Hamadani, B. H.; Kumaran, E. A. P.; McManigal, B.; Agarwal, R.; Akech, S.; Albertson, S.; Amuasi, J.; Andrews, J.; Aravkin, A.; Ashley, E.; Bailey, F.; Baker, S.; Basnyat, B.; Bekker, A.; Bender, R.; Bethou, A.; Bielicki, J.; Boonkasidecha, S.; Bukosia, J.; Carvalheiro, C.; Castañeda-Orjuela, C.; Chansamouth, V.; Chaurasia, S.; Chiurchiù, S.; Chowdhury, F.; Cook, A. J.; Cooper, B.; Cressey, T. R.; Criollo-Mora, E.; Cunningham, M.; Darboe, S.; Day, N. P. J.; De Luca, M.; Dokova, K.; Dramowski, A.; Dunachie, S. J.; Eckmanns, T.; Eibach, D.; Emami, A.; Feasey, N.; Fisher-Pearson, N.; Forrest, K.; Garrett, D.; Gastmeier, P.; Giref, A. Z.; Greer, R. C.; Gupta, V.; Haller, S.; Haselbeck, A.; Hay, S. I.; Holm, M.; Hopkins, S.; Iregbu, K. C.; Jacobs, J.; Jarovsky, D.; Javanmardi, F.; Khorana, M.; Kissoon, N.; Kobeissi, E.; Kostyanev, T.; Krapp, F.; Krumkamp, R.; Kumar, A.; Kyu, H. H.; Lim, C.; Limmathurotsakul, D.; Loftus, M. J.; Lunn, M.; Ma, J.; Mturi, N.; Munera-Huertas, T.; Musicha, P.; Mussi-Pinhata, M. M.; Nakamura, T.; Nanavati, R.; Nangia, S.; Newton, P.; Ngoun, C.; Novotney, A.; Nwakanma, D.; Obiero, C. W.; Olivas-Martinez, A.; Olliaro, P.; Ooko, E.; Ortiz-Brizuela, E.; Peleg, A. Y.; Perrone, C.; Plakkal, N.; Ponce-de-Leon, A.; Raad, M.; Ramdin, T.; Riddell, A.; Roberts, T.; Robotham, J. V.; Roca, A.; Rudd, K. E.; Russell, N.; Schnall, J.; Scott, J. A. G.; Shivamallappa, M.; Sifuentes-Osornio, J.; Steenkeste, N.; Stewardson, A. J.; Stoeva, T.; Tasak, N.; Thaiprakong, A.; Thwaites, G.; Turner, C.; Turner, P.; van Doorn, H. R.; Velaphi, S.; Vongpradith, A.; Vu, H.; Walsh, T.; Waner, S.; Wangrangsimakul, T.; Wozniak, T.; Zheng, P.; Sartorius, B.; Lopez, A. D.; Stergachis, A.; Moore, C.; Dolecek, C.; Naghavi, M. Global Burden of Bacterial Antimicrobial Resistance in 2019: A Systematic Analysis. *The Lancet* **2022**, 399 (10325), 629–655. [https://doi.org/10.1016/S0140-6736\(21\)02724-0](https://doi.org/10.1016/S0140-6736(21)02724-0).
- (3) Walesch, S.; Birkelbach, J.; Jézéquel, G.; Haeckl, F. P. J.; Hegemann, J. D.; Hesterkamp, T.; Hirsch, A. K. H.; Hammann, P.; Müller, R. Fighting Antibiotic Resistance—Strategies and (Pre)Clinical Developments to Find New Antibacterials. *EMBO Rep* **2023**, 24 (1). <https://doi.org/10.15252/embr.202256033>.
- (4) Miethke, M.; Pieroni, M.; Weber, T.; Brönstrup, M.; Hammann, P.; Halby, L.; Arimondo, P. B.; Glaser, P.; Aigle, B.; Bode, H. B.; Moreira, R.; Li, Y.; Luzhetskyy, A.; Medema, M. H.; Pernodet, J. L.; Stadler, M.; Tormo, J. R.; Genilloud, O.; Truman, A. W.; Weissman, K. J.; Takano, E.; Sabatini, S.; Stegmann, E.; Brötz-Oesterheld, H.; Wohlleben, W.; Seemann, M.; Empting, M.; Hirsch, A. K. H.; Loretz, B.; Lehr, C. M.; Titz, A.; Herrmann, J.; Jaeger, T.; Alt, S.; Hesterkamp, T.; Winterhalter, M.; Schiefer, A.; Pfarr, K.; Hoerauf, A.; Graz, H.; Graz, M.; Lindvall, M.; Ramurthy, S.; Karlén, A.; van Dongen, M.; Petkovic, H.; Keller, A.; Peyrane, F.; Donadio, S.; Fraisse, L.; Piddock, L. J. V.; Gilbert, I. H.; Moser, H. E.; Müller, R. Towards the Sustainable Discovery and Development of New Antibiotics. *Nat Rev Chem* **2021**, 5 (10), 726–749. <https://doi.org/10.1038/s41570-021-00313-1>.
- (5) Hunter, W. N. The Non-Mevalonate Pathway of Isoprenoid Precursor Biosynthesis. *J. Biol. Chem.* **2007**, 282 (30), 21573–21577. <https://doi.org/10.1074/jbc.R700005200>.
- (6) Allamand, A.; Piechowiak, T.; Lièvremon, D.; Rohmer, M.; Grosdemange-Billiard, C. The Multifaceted MEP Pathway: Towards New Therapeutic Perspectives. *Molecules* **2023**, 28 (1403). <https://doi.org/10.3390/molecules28031403>.
- (7) Masini, T.; Hirsch, A. K. H. Development of Inhibitors of the 2C-Methyl-D-Erythritol 4-Phosphate (MEP) Pathway Enzymes as Potential Anti-Infective Agents. *J Med Chem* **2014**, 57 (23), 9740–9763. <https://doi.org/10.1021/jm5010978>.
- (8) Hirsch, A. K. H.; Alphey, M. S.; Lauw, S.; Seet, M.; Barandun, L.; Eisenreich, W.; Rohdich, F.; Hunter, W. N.; Bacher, A.; Diederich, F. Inhibitors of the Kinase IspE: Structure-Activity Relationships and Co-Crystal Structure Analysis. *Org Biomol Chem* **2008**, 6 (15), 2719–2730. <https://doi.org/10.1039/b804375b>.
- (9) Ropponen, H.; Diamanti, E.; Johannsen, S.; Illarionov, B.; Hamid, R.; Jaki, M.; Sass, P.; Fischer, M. Exploring the Translational Gap of a Novel Class of Escherichia Coli IspE Inhibitors. *ChemMedChem* **2023**, e202300346 (18). <https://doi.org/10.1002/cmdc.202300346>.
- (10) Bosc, D.; Camberlein, V.; Gealageas, R.; Castillo-Aguilera, O.; Deprez, B.; Deprez-Poulain, R. Kinetic Target-Guided Synthesis: Reaching the Age of Maturity. *J Med Chem* **2020**, 63 (8), 3817–3833. <https://doi.org/10.1021/acs.jmedchem.9b01183>.
- (11) Bertozzi, C. *A Special Virtual Issue Celebrating the 2022 Nobel Prize in Chemistry for the Development of Click Chemistry and Bioorthogonal Chemistry*; American Chemical Society, 2023; Vol. 9. <https://doi.org/10.1021/acscentsci.2c01430>.
- (12) Camberlein, V.; Fléau, C.; Sierocki, P.; Li, L.; Gealageas, R.; Bosc, D.; Guillaume, V.; Warenghem, S.; Leroux, F.; Rosell, M.; Cheng, K.; Medve, L.; Prigent, M.; Decanter, M.; Piveteau, C.; Biela, A.; Eveque, M.; Dumont, J.; Mpakali, A.; Giastas, P.; Herledan, A.; Couturier, C.; Haupenthal, J.; Lesire, L.; Hirsch, A. K. H.; Deprez, B.

- Stratikos, E.; Bouvier, M.; Deprez-Poulain, R. Discovery of the First Selective Nanomolar Inhibitors of ERAP2 by Kinetic Target-Guided Synthesis. *Angew Chem Int Ed* **2022**, *61* (39). <https://doi.org/10.1002/anie.202203560>.
- (13) Lewis, W. G.; Green, L. G.; Grynszpan, F.; Radić, Z.; Carlier, P. R.; Taylor, P.; Finn, M. G.; Sharpless, K. B. Click Chemistry in Situ: Acetylcholinesterase as a Reaction Vessel for the Selective Assembly of a Femtomolar Inhibitor from an Array of Building Blocks. *Angew Chem Int Ed* **2002**, *41* (6), 1053–1057. [https://doi.org/10.1002/1521-3773\(20020315\)41:6<1053::AID-ANIE1053>3.0.CO;2-4](https://doi.org/10.1002/1521-3773(20020315)41:6<1053::AID-ANIE1053>3.0.CO;2-4).
- (14) Molęda, Z.; Zawadzka, A.; Czarnocki, Z.; Monjas, L.; Hirsch, A. K. H.; Budzianowski, A.; Maurin, J. K. “Clicking” Fragment Leads to Novel Dual-Binding Cholinesterase Inhibitors. *Bioorg Med Chem* **2021**, *42*, 116269. <https://doi.org/10.1016/j.bmc.2021.116269>.
- (15) Bhardwaj, A.; Kaur, J.; Wuest, M.; Wuest, F. In Situ Click Chemistry Generation of Cyclooxygenase-2 Inhibitors. *Nat Commun* **2017**, *8* (1), 1. <https://doi.org/10.1038/s41467-016-0009-6>.
- (16) Jin, X.; Daher, S. S.; Lee, M.; Buttaro, B.; Andrade, R. B. Ribosome-Templated Azide–Alkyne Cycloadditions Using Resistant Bacteria as Reaction Vessels: *In Cellulo* Click Chemistry. *ACS Med Chem Lett* **2018**, *9* (9), 907–911. <https://doi.org/10.1021/acsmedchemlett.8b00248>.
- (17) Braun-Cornejo, M.; Platteschorre, M.; de Vries, V.; Bravo, P.; Sonawane, V.; Hamed, M. M.; Hauptenthal, J.; Reiling, N.; Rottmann, M.; Piet, D.; Maas, P.; Diamanti, E.; Hirsch, A. K. H. A Positive Charge in an Antimalarial Compound Unlocks Broad-Spectrum Antibacterial Activity. *ChemRxiv* **2024**, 1–14. <https://doi.org/10.26434/chemrxiv-2024-rs2v8>. This content is a preprint and has not been peer-reviewed.
- (18) Alhayek, A.; Abdelsamie, A. S.; Schönauer, E.; Camberlein, V.; Hutterer, E.; Posselt, G.; Serwanja, J.; Blöchl, C.; Huber, C. G.; Hauptenthal, J.; Brandstetter, H.; Wessler, S.; Hirsch, A. K. H. Discovery and Characterization of Synthesized and FDA-Approved Inhibitors of Clostridial and Bacillary Collagenases. *J Med Chem* **2022**, *65* (19), 12933–12955. <https://doi.org/10.1021/acs.jmedchem.2c00785>.
- (19) Camberlein, V. Target-Guided Synthesis of Metalloenzymes Ligands with Therapeutic Applications. Ph.D. Thesis, Lille University, Lille, France, Saarland University, Saarbrücken, Germany, 2022. <http://www.theses.fr/2022ULILS004/document> (accessed 2024-05-16).
- (20) Christian, D.; W, H. R.; Jörg, H.; H, H. A. K.; Andreas, K.; Cansu, K.; Jelena, K.; Katrin, V.; Isabell, W.; Samir, Y.; Saad, A. A.; Christian, S.; Ravindra, J.; Alexander, K. Inhibitors Of *Pseudomonas Aeruginosa* Virulence Factor LasB, 2022. <https://lens.org/086-698-204-916-246>.
- (21) Lossouarn, A.; Renard, P. Y.; Sabot, C. Tailored Bioorthogonal and Bioconjugate Chemistry: A Source of Inspiration for Developing Kinetic Target-Guided Synthesis Strategies. *Bioconjug Chem* **2021**, *32* (1), 63–72. <https://doi.org/10.1021/acs.bioconjchem.0c00568>.
- (22) Hein, J. E.; Fokin, V. V. Copper-Catalyzed Azide-Alkyne Cycloaddition (CuAAC) and beyond: New Reactivity of Copper(I) Acetylides. *Chem Soc Rev* **2010**, *39* (4), 1302–1315. <https://doi.org/10.1039/b904091a>.
- (23) Haldón, E.; Besora, M.; Cano, I.; Cambeiro, X. C.; Pericàs, M. A.; Maseras, F.; Nicasio, M. C.; Pérez, P. J. Reaction of Alkynes and Azides: Not Triazoles through Copper-Acetylides but Oxazoles through Copper-Nitrene Intermediates. *Chem Eur J* **2014**, *20* (12), 3463–3474. <https://doi.org/10.1002/chem.201303737>.
- (24) Braun-Cornejo, M.; Ornago, C.; Sonawane, V.; Hauptenthal, J.; Kany, A. M.; Diamanti, E.; Jézéquel, G.; Reiling, N.; Blankenfeldt, W.; Maas, P.; Hirsch, A. K. H. Target-Directed Dynamic Combinatorial Chemistry Affords Binders of *Mycobacterium Tuberculosis* IspE. *ChemRxiv* **2024**. <https://doi.org/10.26434/chemrxiv-2024-dh07n>. This content is a preprint and has not been peer-reviewed.
- (25) Niesen, F. H.; Berglund, H.; Vedadi, M. The Use of Differential Scanning Fluorimetry to Detect Ligand Interactions That Promote Protein Stability. *Nat Protoc* **2007**, *2* (9), 2212–2221. <https://doi.org/10.1038/nprot.2007.321>.
- (26) Peruzzotti, C.; Borrelli, S.; Ventura, M.; Pantano, R.; Fumagalli, G.; Christodoulou, M. S.; Monticelli, D.; Luzzani, M.; Fallacara, A. L.; Tintori, C.; Botta, M.; Passarella, D. Probing the Binding Site of Abl Tyrosine Kinase Using in Situ Click Chemistry. *ACS Med Chem Lett* **2013**, *4* (2), 274–277. <https://doi.org/10.1021/ml300394w>.
- (27) Kassu, M.; Parvatkar, P. T.; Milanes, J.; Monaghan, N. P.; Kim, C.; Dowgiallo, M.; Zhao, Y.; Asakawa, A. H.; Huang, L.; Wagner, A.; Miller, B.; Carter, K.; Barrett, K. F.; Tillery, L. M.; Barrett, L. K.; Phan, I. Q.; Subramanian, S.; Myler, P. J.; Van Voorhis, W. C.; Leahy, J. W.; Rice, C. A.; Kyle, D. E.; Morris, J.; Manetsch, R. Shotgun Kinetic Target-Guided Synthesis Approach Enables the Discovery of Small-Molecule Inhibitors against Pathogenic Free-Living Amoeba Glucokinases. *ACS Infect Dis* **2023**, *9* (11), 2190–2201. <https://doi.org/10.1021/acscinfecdis.3c00284>.

5.1 Supporting Information

Exploring Protein-Templated and Biophysical Approaches for Fragment Discovery using IspE from Gram-Negative Bacteria

Maria Braun-Cornejo,^{1,2,3} Camilla Ornago,⁴ Rawia Hamid,^{2,3} Virgyl Camberlein,^{2,3} Boris Illarionov,⁵ Eleonora Diamanti,³ Wulf Blankenfeldt,⁴ Peter Maas,¹ and Anna K. Hirsch^{2,3*}

¹ Specs Research Laboratory, Specs Compound Handling, B.V., Bleiswijkseweg 55, 2712 PB, Zoetermeer, The Netherlands.

² Saarland University, Department of Pharmacy, Campus Building E8.1, 66123 Saarbrücken, Germany.

³ Helmholtz Institute for Pharmaceutical Research Saarland (HIPS) – Helmholtz Centre for Infection Research (HZI), Campus Building E8.1, 66123 Saarbrücken, Germany.

⁴ Department Structure and Function of Proteins, HZI, Inhoffenstrasse 7, 38124 Braunschweig, Germany.

⁵ Hamburg School of Food Science, Institute of Food Chemistry, Grindelallee 117, 20146 Hamburg, Germany

* Corresponding author: Anna.Hirsch@helmholtz-hips.de

Table of Contents

Supplementary Methods.....	112
General information.....	112
Chemicals.....	112
Procedure for KTGS experiments	112
General procedure for Synthesis	113
Characterisation of products.....	113
IspE expression and purification	116
<i>Ecl</i> IspE stability study <i>via</i> thermal shift assay	116
IspE binding study <i>via</i> thermal shift assay.....	116
<i>Mtb</i> IspE binding study <i>via</i> MicroScale Thermophoresis	117
IspE Inhibition assay	117
Supplementary Tables and Figures	118
<i>Ecl</i> IspE stability study <i>via</i> thermal shift assay	118
Compound selections.....	118
Alkyne library designed for KTGS experiment	118
Follow-up compounds of alkyne hits	130
NMR, HRMS, and LCMS spectra	167
Azides 2 and 4	167
Triazoles 19–22	171
Supplementary references	179

Supplementary Methods

General information

All reactions using oxygen- and/or moisture-sensitive materials were carried out in dry solvents (*vide infra*) under a nitrogen atmosphere using oven-dried glassware. The reaction progress was monitored on thin layer chromatography (TLC) on silica gel-coated aluminum (silica gel F254, SiliCycle) or by a liquid chromatography-mass spectrometry (LC-MS) system equipped with a Dionex UltiMate 3000 pump, autosampler, column compartment, detector, and ESI quadrupole MS (MSQ Plus or ISQ EC) from Thermo Fisher Scientific, Dreieich, Germany. Purification of the final products, when necessary, was performed using preparative HPLC (Dionex UltiMate 3000 UHPLC+ focused, Thermo Scientific) on a reversed-phase column (C18 column, 5 μ M, Macherey-Nagel, Germany). The solvents used for the chromatography were water (0.1% formic acid) and MeCN (0.1% formic acid). High-resolution mass (HRMS) of final products was determined by LCMS/MS using a Thermo Scientific Q Exactive Focus Orbitrap LC-MS/MS system. NMR spectra were recorded on an Agilent 400 MHz or a Bruker Avance Neo 500 MHz. Chemical shifts (δ) are reported in ppm relative to residual solvent signals. The following abbreviations are used to describe peak patterns when appropriate: s (singlet), d (doublet), t (triplet), q (quartet), quint (quintet), sex (sextet), sept (septuplet), m (multiplet), br (broad). Coupling constants (J) are reported in Hertz (Hz). The periodic progress and analysis of KTGS was monitored by HPLC-MS/MS (ThermoScientific Dionex Ultimate 3000 UHPLC System coupled to a ThermoScientific Q Exactive Focus with an electrospray ion source) using an Acquity Waters Column (BEH, C8 1.7 μ m, 2.1 \times 150 mm, Waters, Germany) at a flow rate of 0.250 mL/min with detection set at 210, 254, 290, and 310 nm, and the mass spectrum recorded in a positive mode in the range of 100–700 m/z. The solvent system was 0.1% formic acid in H₂O (Solvent-A) and 0.1% formic acid in MeCN (Solvent-B). The gradient program began with 5% of Solvent-B for 1 min and was then increased to 95% of Solvent-B over 17 min and held for 2 min, followed by a decrease of Solvent-B to 5% over 0.1 min, where it was held for 2 min.

Chemicals

All reagents and solvents were purchased from Sigma-Aldrich, Specs, Fluorochem, or Acros Organics, were reagent grade, and used without purification unless indicated otherwise. All reactions were conducted under nitrogen atmosphere using oven-dried glassware. Purifications by flash chromatography were done using silica gel (Screening Devices 60-200 μ m). All new compounds were fully characterised by ¹H and ¹³C NMR and HRMS techniques. The purity of the final products was determined by HPLC-MS and found to be > 95%.

Procedure for KTGS experiments

Blank KTGS preparation:

To a well of a 96-well plate, containing HEPES buffer (50 mM, pH 7.0), were added alkynes (100 μ M each, in DMSO), azide (250 μ M, in DMSO), and an additional amount of DMSO to reach a final concentration of 5% with 250 μ L of end-volume. The KTGS was allowed to mix on a plate shaker (200 rpm) at room temperature (r.t.) and was monitored via LCMS-MS after 5, 10, and 14 days. For analysis, 50 μ L of the corresponding well was mixed with 50 μ L acetonitrile, the mixture was centrifuged, and filtered before analysis.

Protein-templated (PT) KTGS preparation:

To a well of a 96-well plate, containing HEPES buffer (50 mM, pH 7.0), were added alkynes (100 μ M each, in DMSO), azide (250 μ M, in DMSO), and the protein IspE from *Escherichia coli* (EclspE, 25 μ M) with 250 μ L of end-volume. The KTGS was allowed to mix on a plate shaker (200 rpm) at r.t. and was monitored via LCMS-MS after 5, 10, and 14 days. For analysis, 50 μ L of the corresponding well was mixed with 50 μ L acetonitrile, the mixture was centrifuged, and filtered before analysis.

Positive KTGS control preparation using copper(I)-catalysed azide-alkyne cycloaddition (CuAAC):

To a well of a 96-well plate, containing tBuOH:H₂O (2:1), were added alkynes (100 μ M each, in DMSO), azide (700 μ M, in DMSO), sodium ascorbate aq. (NaAsc, 800 μ M), CuSO₄ aq. (8 mM) with 200 μ L of end-volume. The reaction mixture was allowed to mix on a plate shaker (200 rpm) at r.t. and was monitored via LCMS-MS after 5 days. For analysis, 50 μ L of the corresponding well was mixed with 50 μ L acetonitrile.

The composition of KTGS experiments is as below:

Entry	Blank		PT		Entry	CuAAC	
	amount	final conc.	amount	final conc.		amount	final conc.
HEPES	237.5 μ L	-	232.1 μ L	-	<i>t</i>BuOH:H₂O (2:1)	140.6 μ L	-
Alkyne cluster	10.5 μ L (2.4 mM)	100 μ M each alkyne	6 \times 1.5 μ L (9 μ L)	100 μ M each alkyne	Alkyne cluster	8.6 μ L (2.4 mM)	100 μ M each alkyne
Azide	2 μ L (31.3 mM)	250 μ M	2 μ L (31.3 mM)	250 μ M	Azide	2.8 μ L (50 mM)	700 μ M
DMSO	4.5 μ L	5%	4.5 μ L	5%	NaAsc	32 μ L (50 mM)	800 μ M
EclspE	0	-	5.4 μ L (1.16 mM)	25 μ M	CuSO₄	16 μ L (10 mM)	8 mM

Note: The 50mM HEPES buffer contains 150 mM NaCl and 4mM MgCl₂. Details on the alkyne library and clusters can be found in Table S2 (p.8).

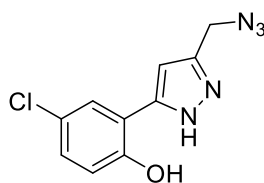
General procedure for Synthesis

Copper(I)-catalysed azide-alkyne cycloaddition (CuAAC) preparation (GP-1):

Alkyne **15** (1 eq.) and the respective azide (1 eq.) were dissolved in DCM (0.1 M), sodium ascorbate aq. (NaAsc, 20mol%) and CuSO₄ aq. (10mol%) were added to obtain a 1:1 mixture of DCM:H₂O. The reaction mixture was covered to avoid exposure to light and stirred vigorously for 24 h. The mixture was filtered with a phase separation filter and washed with diethyl ether (2 mL) to obtain the pure triazole products (72–94%).

Characterisation of products

2-(3-(azidomethyl)-1*H*-pyrazol-5-yl)-4-chlorophenol (**2**):



Compound **9** (58 mg, 0.20 mmol, 1 eq.) was suspended in DMF (2 mL), potassium iodide (3 mg, 0.02 mmol, 0.1 eq.), and sodium azide (16 mg, 0.24 mmol, 1.2 eq.) was added. The reaction mixture stirred for 1 h at r.t. and was quenched with water (20 mL), and extracted with EtOAc (3 x 30 mL). The combined organic layers were washed with brine, dried over anhydrous MgSO₄, filtered, and concentrated *in vacuo*, obtaining a yellow oil. The crude was purified by column

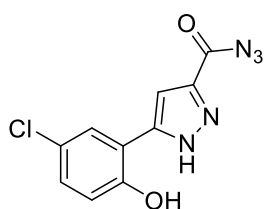
chromatography using a gradient of 30–50% EtOAc in petroleum ether (PE) as eluent to obtain compound **2** as off-white solid (33 mg, 0.13 mmol, 63%).

¹H NMR (500 MHz, CDCl₃) δ = 9.63 (br s, 2H), 7.50 (d, *J* = 2.5 Hz, 1H), 7.18 (dd, *J* = 8.8, 2.5 Hz, 1H), 6.97 (d, *J* = 8.8 Hz, 1H), 6.61 (s, 1H), 4.54 (s, 2H) ppm.

¹³C NMR (126 MHz, CDCl₃) δ = 154.2, 151.0, 138.9, 129.2, 126.1, 124.3, 118.4, 117.4, 101.5, 45.4 ppm.

HRMS (ESI⁺): *m/z* calcd. for C₁₀H₉ClN₅O⁺ ([*M*+*H*]⁺) 250.0490, measured 250.0495.

5-(5-chloro-2-hydroxyphenyl)-1*H*-pyrazole-3-carbonyl azide (**4**):



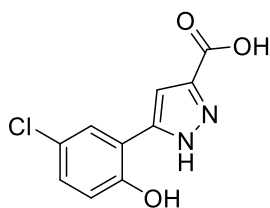
Compound **5** (640 mg, 2.7 mmol, 1 eq.) was suspended in dry toluene (15 mL), SOCl₂ (970 mL, 13.4 mmol, 5 eq.) and 5 drops of DMF were added. The reaction mixture was heated to reflux, and after 1.5 h allowed to cool to r.t. before concentrating under reduced pressure. The residue was resuspended in toluene (2 x 10 mL) and concentrated under reduced pressure. To the residue was added acetone (5mL) and sodium azide (262 mg, 4.0 mmol, 1.5 eq.) as solution in acetone:H₂O (2:1, 6 mL). The yellow reaction mixture turned brown

after 15 min and was quenched with ice-cold water (150 mL). The resulting precipitate was filtered and purified by column chromatography using a gradient of 10–15% EtOAc in cyclohexane as eluent to obtain compound **5** as orange solid (179 mg, 0.68 mmol, 25%).

¹H NMR (500 MHz, DMSO-*d*₆) δ = 13.86 (br s, 1H), 10.72 (br s, 1H), 7.79 (br s, 1H), 7.32 (s, 1H), 7.25 (br d, *J* = 8.3 Hz, 1H), 7.00 ppm (br d, *J* = 8.3 Hz, 1H).

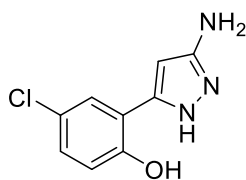
¹³C NMR (126 MHz, DMSO-*d*₆) δ = 167.8, 153.6, 144.4, 140.5, 129.8, 127.1, 123.5, 118.5, 117.0, 108.3 ppm.

HRMS (ESI⁺): *m/z* calcd. for C₁₀H₇ClN₅O₂⁺ ([*M*+*H*]⁺) 264.0283, measured 264.0275

5-(5-Chloro-2-hydroxyphenyl)-1H-pyrazole-3-carboxylic acid (**5**):

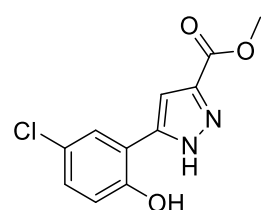
Compound **5** was synthesised according to the literature procedure.¹

¹H NMR (400 MHz, DMSO-*d*₆) δ = 10.57 (br s, 1H), 7.83 (br d, *J* = 2.1 Hz, 1H), 7.31 (br s, 1H), 7.22 (dd, *J* = 8.6, 2.1 Hz, 1H), 6.99 (d, *J* = 8.6 Hz, 1H) ppm.

2-(3-Amino-1H-pyrazol-5-yl)-4-chlorophenol (**6**):

Compound **4** (33 mg,) was suspended in acetic acid:H₂O (1:1, 5 mL) and heated to reflux for 1 h. The mixture was allowed to cool to r.t. NaOH aq. (2 M) was added until pH = 10 was reached. The mixture was extracted with EtOAc (3 x 30 mL) and the combined organic layers were washed with brine, dried over anhydrous MgSO₄, filtered, and concentrated to dryness *in vacuo*. Compound **4** was obtained as pale yellow powder (24 mg, 0.11 mmol, 91%) and used without further purification.

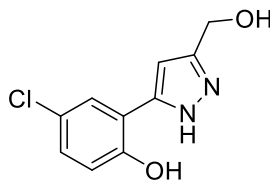
¹H NMR (500 MHz, DMSO-*d*₆) δ = 7.62 (d, *J* = 2.4 Hz, 1H), 7.19 (dd, *J* = 8.7, 2.4 Hz, 1H), 6.92 (d, *J* = 8.7 Hz, 1H), 5.92 (s, 1H), 5.43 (br s, 2H) ppm.

Methyl 5-(5-chloro-2-hydroxyphenyl)-1H-pyrazole-3-carboxylate (**7**):

Compound **5** (250 mg, 1.05 mmol, 1 eq.) was suspended in MeOH (10 mL), cooled in an ice-water bath and sulfuric acid (1.0 mL, 19 mmol, 18 eq.) was added dropwise. The reaction mixture was heated to reflux and after 2.5 h it was allowed to cool to r.t. and added to water (75 mL). The resulting precipitate was filtered and the water layer was extracted with EtOAc (3 x 50 mL). The precipitate was added to the combined organic layers and they

were washed with brine, dried over anhydrous MgSO₄, filtered, and concentrated to dryness *in vacuo*. Compound **7** was obtained as white solid (241 mg, 0.91 mmol, 91%) and used without further purification.

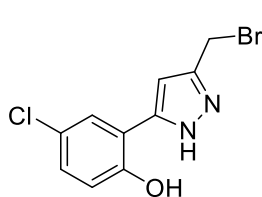
¹H NMR (500 MHz, DMSO-*d*₆) δ = 10.57 (br s, 1H), 7.83 (d, *J* = 2.6 Hz, 1H), 7.34 (s, 1H), 7.24 (dd, *J* = 8.7, 2.6 Hz, 1H), 6.99 (d, *J* = 8.7 Hz, 1H), 3.85 (s, 3H) ppm.

4-chloro-2-(3-(hydroxymethyl)-1H-pyrazol-5-yl)phenol (**8**):

Compound **7** (226 mg, 0.89 mmol, 1 eq.) was dissolved in THF (10 mL), cooled in an ice-water bath and lithium aluminium hydride (1.2 mL, 2.9 mmol, 3 eq., 2.4 M) was added dropwise. The reaction mixture stirred for 2 h at 0 °C and was quenched with Rochelle salt (100 mL, 2 M) and acidified with HCl (2 M). The mixture was extracted with DCM (3 x 100 mL) and the combined organic layers were washed with brine, dried over anhydrous MgSO₄, filtered, and

concentrated to dryness *in vacuo*. The resulting crude was purified by column chromatography using a gradient of 5–35% EtOAc in PE as eluent to obtain compound **8** as off-white solid (117 mg, 3.42 mmol, 58%).

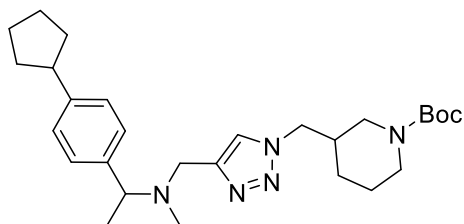
¹H NMR (500 MHz, DMSO-*d*₆) δ = 13.19 (br s, 1H), 11.10 (br s, 1H), 7.75 (br s, 1H), 7.18 (dd, *J* = 8.7, 2.6 Hz, 1H), 6.92 (d, *J* = 8.7 Hz, 1H), 6.81 (s, 1H), 5.41 (br s, 1H), 4.55 (br s, 2H) ppm.

2-(3-(bromomethyl)-1H-pyrazol-5-yl)-4-chlorophenol (**9**):

Compound **8** (115 mg, 0.51 mmol, 1 eq.) and triphenylphosphine (336 mg, 1.3 mmol, 2.5 eq.) were cooled in an ice-water bath, and carbon tetrabromide (0.10 mL, 1.0 mmol, 2 eq) and DCM (10 mL). After 30 min the ice-bath was removed and the reaction mixture stirred for 2 h at r.t. before it was concentrated under reduced pressure. The resulting residue was purified by column chromatography using a gradient of 40–70% EtOAc in PE as eluent to obtain compound **9** as yellow solid (62 mg, 0.22 mmol, 42%).

¹H NMR (500 MHz, CDCl₃) δ = 10.49 (br s, 1H), 10.07 (br s, 1H), 7.49 (d, *J* = 2.5 Hz, 1H), 7.18 (dd, *J* = 8.8, 2.5 Hz, 1H), 6.96 (d, *J* = 8.8 Hz, 1H), 6.68 (s, 1H), 4.56 (s, 2H) ppm.

tert-Butyl 3-((4-(((1-(4-cyclopentylphenyl)ethyl)(methyl)amino)methyl)-1*H*-1,2,3-triazol-1-yl)methyl)piperidine-1-carboxylate (**19**):



Compound **19** was prepared following GP-1, alkyne **15** (70 mg, 0.25 mmol) was reacted with *tert*-butyl 3-(azidomethyl)piperidine-1-carboxylate (61 mg, 0.25 mmol) to obtain **19** as off-white solid (87 mg, 0.18 mmol, 72%).

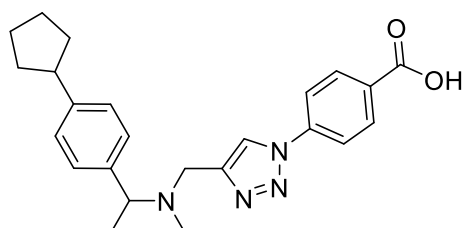
^1H NMR (400 MHz, CDCl_3) δ = 8.59 (br s, 1H), 7.50 (br s, 2H), 7.33 (br d, J = 7.8 Hz, 2H), 4.45 (br s, 1H), 4.22-4.36 (m, 2H), 4.09 (br s, 1H), 3.75 (br d, J = 10.9 Hz, 2H), 2.87-3.08 (m, 2H), 2.75 (br s, 1H), 2.44-2.64 (m, 3H), 2.02-2.19 (m, 3H), 1.89 (br d, J = 7.0 Hz,

3H), 1.77-1.85 (m, 2H), 1.63-1.75 (m, 4H), 1.51-1.62 (m, 2H), 1.39-1.44 (m, 9H), 1.15-1.28 (m, 1H) ppm.

^{13}C NMR (101 MHz, CDCl_3) δ = 154.6, 149.1, 136.9, 129.6, 129.1, 128.1, 79.7, 63.3, 53.1, 45.6, 36.5, 34.5, 30.6, 28.3, 27.9, 25.4, 24.9, 23.8, 17.1 ppm.

HRMS (ESI⁺): m/z calcd. for $\text{C}_{28}\text{H}_{44}\text{N}_5\text{O}_2^+$ ($[M+H]^+$) 482.3490, measured 482.3463.

4-(4-(((1-(4-Cyclopentylphenyl)ethyl)(methyl)amino)methyl)-1*H*-1,2,3-triazol-1-yl)benzoic acid (**20**):



Compound **20** was prepared following GP-1, alkyne **15** (45 mg, 0.16 mmol) was reacted with 4-azidobenzoic acid (26 mg, 0.16 mmol) to obtain **20** as light brown solid (56 mg, 0.14 mmol, 86%).

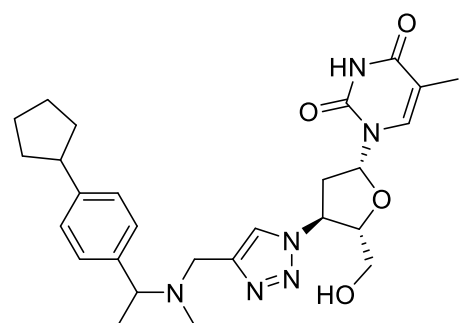
^1H NMR (400 MHz, CDCl_3) δ = 8.79 (br s, 2H), 8.05 (br s, 2H), 7.74 (br s, 2H), 7.52 (br s, 2H), 7.33 (br d, J = 6.3 Hz, 2H), 4.69 (br s, 1H), 4.35-4.52 (m, 1H), 4.06-4.35 (m, 1H), 3.78-3.83 (m, 1H), 3.76-3.84 (m, 1H), 3.01 (quin, J = 8.3 Hz, 1H), 2.68 (br s,

3H), 1.78-2.17 (m, 4H), 1.54-1.75 (m, 1H), 1.51 (br d, J = 6.7 Hz, 1H) ppm.

^{13}C NMR (101 MHz, CDCl_3) δ = 148.5, 139.1, 138.7, 131.6, 130.8, 129.6, 127.9, 127.6, 127.3, 125.0, 119.9, 45.6, 34.5, 25.5, 16.8 ppm.

HRMS (ESI⁺): m/z calcd. for $\text{C}_{24}\text{H}_{29}\text{N}_4\text{O}_2^+$ ($[M+H]^+$) 405.2285, measured 405.2261.

1-((2*R*,4*S*,5*S*)-4-(4-(((1-(4-cyclopentylphenyl)ethyl)(methyl)amino)methyl)-1*H*-1,2,3-triazol-1-yl)-5-(hydroxymethyl)tetrahydrofuran-2-yl)-5-methylpyrimidine-2,4(1*H*,3*H*)-dione (**21**):



Compound **21** was prepared following GP-1 with adaptations, alkyne **15** (72 mg, 0.26 mmol) was reacted with 1-((2*R*,4*S*,5*S*)-4-azido-5-(hydroxymethyl)tetrahydrofuran-2-yl)-5-methylpyrimidine-2,4(1*H*,3*H*)-dione (69 mg, 0.26 mmol). The mixture was extracted with DCM (3 x 3 mL) and the combined organic layers were washed with brine, dried over anhydrous MgSO_4 , filtered, and concentrated to dryness *in vacuo* to obtain **21** as off-white solid (124 mg, 0.24 mmol, 94%).

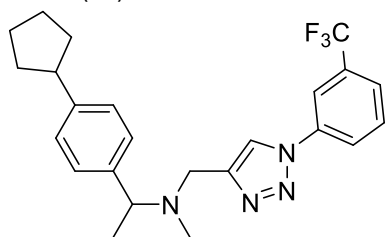
^1H NMR (400 MHz, CDCl_3) δ = 8.63 (br s, 1H), 7.65 (s, 1H), 7.51 (dd, J = 7.8, 2.7 Hz, 2H), 7.33 (br d, J = 7.8 Hz, 2H), 6.35 (t, J = 6.2 Hz, 1H), 5.59 (br s, 1H), 4.40 (br s, 1H), 4.14-4.33 (m, J = 6.2 Hz,

2H), 3.93-4.00 (m, 1H), 3.81-3.89 (m, 1H), 3.73 (q, J = 7.0 Hz, 1H), 2.96-3.08 (m, 2H), 2.82-2.93 (m, 1H), 2.58 (d, J = 2.7 Hz, 3H), 2.06-2.13 (m, 2H), 1.92 (s, 3H), 1.85 (br d, J = 7.0 Hz, 3H), 1.77-1.84 (m, 2H), 1.67-1.75 (m, 2H), 1.53-1.64 (m, 2H) ppm.

^{13}C NMR (101 MHz, CDCl_3) δ = 163.7, 150.3, 148.8, 137.2, 129.3, 128.1, 111.1, 87.2, 85.3, 67.1, 64.2, 61.2, 59.7, 45.6, 37.6, 34.5, 25.5, 17.2, 12.5 ppm.

HRMS (ESI⁺): m/z calcd. for $\text{C}_{27}\text{H}_{37}\text{N}_6\text{O}_4^+$ ($[M+H]^+$) 509.2871, measured 509.2839.

1-(4-cyclopentylphenyl)-N-methyl-N-((1-(3-(trifluoromethyl)phenyl)-1H-1,2,3-triazol-4-yl)methyl)ethan-1-amine (**22**):



Compound **22** was prepared following GP-1, alkyne **15** (47 mg, 0.17 mmol) was reacted with 1-azido-3-(trifluoromethyl)benzene (61 mg, 0.25 mmol) to obtain **22** as pale yellow solid (68 mg, 0.16 mmol, 94%).

$^1\text{H NMR}$ (400 MHz, CDCl_3) δ = 8.02 (s, 1H), 7.95-8.00 (m, 1H), 7.93 (s, 1H), 7.63-7.71 (m, 2H), 7.30 (d, J = 8.2 Hz, 2H), 7.21 (d, J = 8.2 Hz, 2H), 3.84 (d, J = 14.0 Hz, 1H), 3.61-3.70 (m, 2H), 2.91-3.05 (m, 1H), 2.28 (s, 3H), 1.99-2.11 (m, 2H), 1.74-1.85 (m, 2H), 1.63-1.72 (m, 2H), 1.53-1.63

(m, 2H), 1.45 (d, J = 6.8 Hz, 3H) ppm.

$^{13}\text{C NMR}$ (101 MHz, CDCl_3) δ = 147.6, 145.3, 140.6, 137.5, 132.2, 130.5, 127.5, 127.0, 125.1, 123.5, 122.0, 120.4, 117.3, 62.9, 49.6, 45.6, 38.9, 34.6, 25.5, 19.0 ppm.

HRMS (ESI⁺): m/z calcd. for $\text{C}_{24}\text{H}_{28}\text{F}_3\text{N}_4$ ⁺ ($[M+H]^+$) 429.2261, measured 429.2256.

IspE expression and purification

We transformed pET28a plasmids containing our construct into electrocompetent BL21 (DE3) *E. coli* cells. The transformed cells were subsequently cultured on LB-Agar supplemented with 25 $\mu\text{g}/\text{mL}$ kanamycin and allowed to incubate overnight at a temperature of 37 °C. We then transferred the selected colonies into LB medium supplemented with 25 $\mu\text{g}/\text{mL}$ kanamycin, at 37 °C until OD_{600} 0.3–0.6 for. We induced overexpression with 1 mM IPTG/18°C/180 RPM/overnight. The harvested cells were then disrupted before subsequently purifying the proteins. First, we performed affinity chromatography using HisTrap HP 5 mL, then removed Histag with TEV protease (1:20). The output from the reverse IMAC column was injected into a 7 mL loop of the ÄKTA pure system on an S200 SEC column. Peak fractions were combined and concentrated in the respective storage buffer for each protein. Finally, we performed SDS-PAGE gel electrophoresis to confirm the presence and purity of the purified protein at each purification step.

The expression and purification of the *Pseudomonas aeruginosa* (*Pa*) and *Aquifex aeolicus* (*Aa*) was performed as described.²

EclspE stability study via thermal shift assay

The stability of EclspE in different buffer conditions was studied by measuring its melting temperature (T_m) using thermal shift assay (TSA). EclspE incubated at r.t. at a final concentration of 0.2 mg/mL in HEPES or Tris buffer (50 mM with 150 mM NaCl and 4 mM MgCl_2) at pH = 7.0 or 8.0, with 5%,-or 10% DMSO, and samples were measured frequently over 14 days. The experiments were performed in a 96-well PCR plate (Thermoscientific). The final volume per well was 20 μL , consisting of 18 μL of EclspE sample (as mentioned above), and 2 μL of GloMelt dye (diluted 20x with H_2O). The plate was centrifuged for 1 minute at room temperature at 1200 rpm. The T_m of the protein was measured using a Real-time PCR machine (Step one plus, Applied Biosystem). The conditions of the experiment were adjusted using Step One 2.3 software. The starting temperature, the ending temperature and the heating rate were set as 21 °C, 95 °C and 0.5 °C / min, respectively. The melting curves were analysed using Protein Thermal Shift 1.3 software. EclspE was found to be most stable in HEPES buffer at pH = 7.0 and 5% DMSO (Table S1 and Figure S1).

IspE binding study via thermal shift assay

The shifts in T_m of PalspE induced by the compounds were determined via TSA. PalspE (2.5 μM) was incubated with 1 mM each compound for 30 min in 50 mM HEPES pH 7.5, 150 mM NaCl, 2 mM MgCl_2 , 10% glycerol. After that, SYPRO ORANGE fluorescent dye (Thermo Fisher) was added at a final concentration of 5X. Melting curves of each sample was measured increasing the temperature from 10 °C to 95 °C with an increase of 1 °C/30 sec and recording fluorescence of SYPRO ORANGE after every temperature increase using CFX96 real-time system-C1000 Thermal Cycler (Bio-Rad). T_m of each sample were calculated using CFX manager 2.0 software (Bio-Rad). Data analysis was performed using Excel and GraphPad 9.8.

AalspE TSA was performed adapting the same protocol: final protein concentration was increased to 5 μM and the buffer was changed to 20 mM Tris-HCl pH 8.5, 250 mM NaCl, 2 mM DTT.

To validate the TSA results and to determine whether the fluorescent dye could cause artifacts in the results, TSA was repeated with the compounds inducing a shift in T_m using Tycho 6.1 (Nanotemper, GmbH). To guarantee efficient protein detection, both PalspE and AalspE concentrations were increased to 30 μM . Buffers and compounds concentration remained unaltered.

For compound **18**, the dissociation constant (K_D) was measured using FoldAffinity,³ preparing twelve serial dilutions of the ligand starting from 1 mM and performing TSA with the protocol involving fluorescent dye described above. Melting curves of each serial dilutions were uploaded to FoldAffinity server for determination of K_D (<https://spc.embl-hamburg.de/app/foldAffinity>).

MtblspE binding study via MicroScale Thermophoresis

PalspE was labelled with Cy5 following the protocol indicated by NanoTemper in MicroScale Thermophoresis (MST) buffer (20 mM HEPES pH 7.5, 150 mM NaCl, 2 mM MgCl₂, 10% glycerol). Labelled *PalspE* was diluted to 400 nM in MST buffer and incubated 1:1 with 1 mM of each compound for 30 min. MST experiment was performed with a Monolith N.115 (Nanotemper Technologies, GmbH, Munich, Germany) using Standard Capillaries (Nanotemper Technologies, GmbH, Munich, Germany). Each binding event was evaluated at a final concentration of 200 nM *PalspE* and 500 μ M of each compound. All the measurements were performed in triplicates. Data analysis was automatically performed by Mololith NT.115 Control and Analysis software (Nanotemper Technologies, GmbH, Munich, Germany).

IspE Inhibition assay

Ec IspE for IspE assays was expressed, isolated and purified as previously described.⁴ All other enzymes and chemicals used in the assays were purchased from Sigma-Aldrich (Taufkirchen, Germany).

For testing of compounds in the *EcIspE* assay, CDP-ME (0.2 mM) in 100 mM Tris-HCl, pH 7.6, 0.02% NaN₃ (30 μ L) was added to a well of the 384-well microplate, preloaded either with DMSO or with test compound dissolved in DMSO (3 μ L). The reaction was started by addition of 100 mM Tris-HCl, pH 7.6, 10 mM MgCl₂, 60 mM KCl, 10 mM dithiothreitol, 0.02% NaN₃, 1 mM NADH, 2 mM phosphoenolpyruvate, 2 mM ATP, pyruvate kinase (1 U mL⁻¹), lactate dehydrogenase (1 U mL⁻¹) and *E. coli IspE* (0.05 U mL⁻¹) (27 μ L per microplate well). IC₅₀ values were measured at CDP-ME concentration 100 μ M. In order to find out if tested compounds are active vs auxiliary enzymes from the IspE assay, they were additionally tested in the pyruvate kinase assay. For this purpose, 1 mM ADP in 100 mM Tris-HCl, pH 7.6 (30 μ L) was added to a well of the 384-well microplate which had been preloaded with DMSO or with test compound solved in DMSO (3 μ L). The reaction was started by addition of 100 mM Tris-HCl, pH 7.6, 10 mM MgCl₂, 60 μ M KCl, 10 mM dithiothreitol, 0.02% NaN₃, 1 mM NADH, 2 mM phosphoenolpyruvate, pyruvate kinase (0.05 U mL⁻¹) and lactate dehydrogenase (0.05 U mL⁻¹) (27 μ L per microplate well). For both kind of assays the OD values in the microplate wells were monitored photometrically at 340 nm (room temperature) for 30 to 90 min in a plate reader (SpectraMax5, Molecular Dynamics, USA). Initial rate values were evaluated with a nonlinear regression method using the program Dynafit.⁵

The inhibition of *PalspE* was tested with KinaseGlo Plus (Promega GmbH) following manufacturer instructions in 384-well white plate (Corning, Glendale, Arizona USA) in a final volume of 25 μ L. The protein inhibition was measured either mixing all reaction components and initiating the enzymatic reaction by adding *PalspE* ("no incubation" samples), or incubating *PalspE* and each compound for 30 minutes before starting the reaction adding CDP-ME and ATP. *PalspE* kinase reaction was run for 45 minutes with 1 μ M *PalspE* in 100 mM Tris-HCl pH = 8.2, luminescence was recorded with a Spark Multimode plate reader (Tecan Trading AG, Switzerland). Data analysis was performed with GraphPad Prism 9.8 (GraphPad Software, Boston MA, USA).

Supplementary Tables and Figures

EclspE stability study via thermal shift assay

Table S1. Evaluation of buffer conditions over time for IspE from *Escherichia coli* via thermal shift assay, all buffers contained 150 mM NaCl and 4mM MgCl₂.

	HEPES 50mM				Tris 50mM			
	pH = 7.0		pH = 8.0		pH = 7.0		pH = 8.0	
DMSO	5%	10%	5%	10%	5%	10%	5%	10%
Entry	A	B	C	D	E	F	G	H
T _m day 0	50.0	50.0	49.8	50.3	49.5	49.5	50.5	51.0
T _m day 1	50.5	50.5	50.0	50.5	50.0	49.8	50.5	50.8
T _m day 2	50.3	50.5	50.0	50.3	50.0	50.0	50.5	50.5
T _m day 3	50.3	50.5	49.3	49.8	49.8	50.0	50.3	50.5
T _m day 7	49.8	50.5	49.0	47.5	--	50.0	49.3	46.5
Average T_m	50.2	50.4	49.6	49.7	49.8	49.9	50.2	49.9

Note: all values are in °C

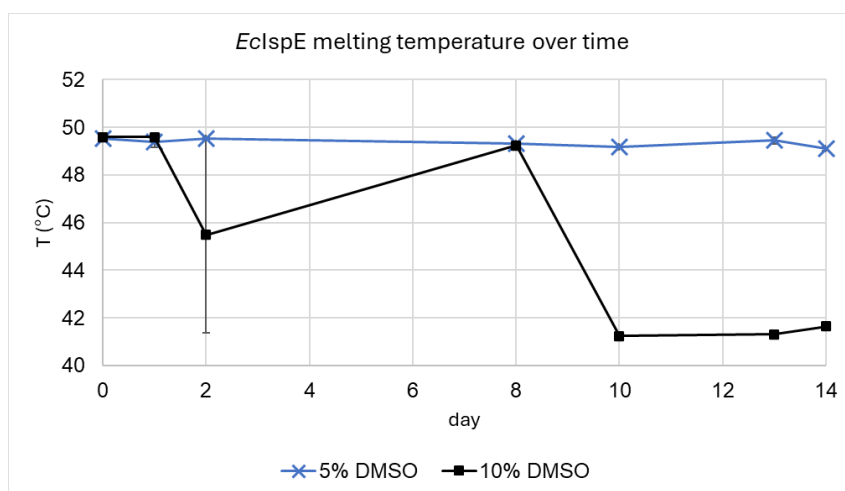
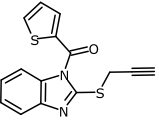
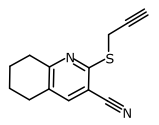


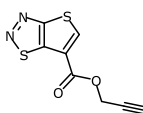
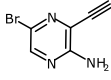
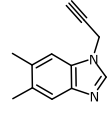
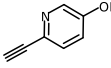
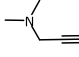
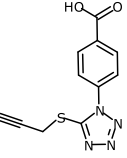
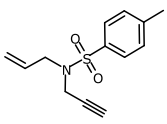
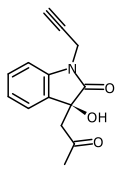
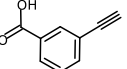
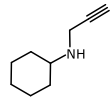
Figure S1. Melting temperature over fourteen days for IspE from *Escherichia coli* in pH 7.0, 50 mM HEPES buffer with 5%, and 10% DMSO.

Compound selections

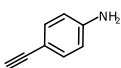
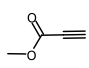
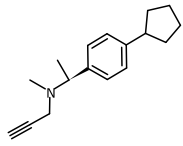
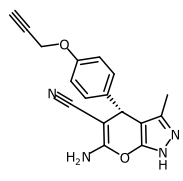
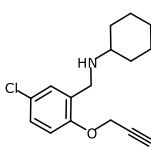
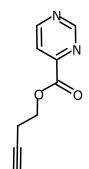
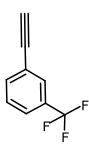
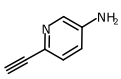

Alkyne library designed for KTGS experiment

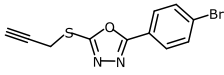
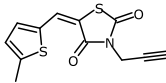
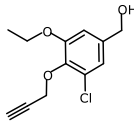
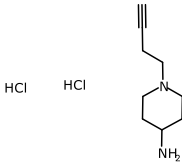
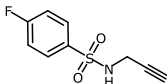
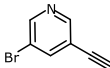
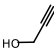
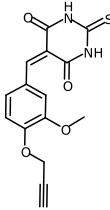
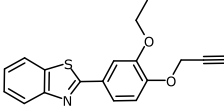
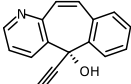
Table S2. Alkyne library consisting of 110 compounds divided into 16 clusters including chemical descriptors; molecular weight (MW), solubility (clogS), H-bond donor (HDon) / acceptor (HAcc), and shifts in melting temperature (ΔT_m) in IspE from *Aquifex aeolicus* (Aa) and *Pseudomonas aeruginosa* (Pa).

Compound	MW (g/mol)	Cluster	clogS	HAcc	HDon	ΔT_m AaIspE	ΔT_m PaIspE
 AF-399/37290004	298.39	01	-5.17	3	0	-26	1
 AG-690/12406102	228.32	01	-3.88	2	0	0	-2

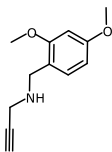
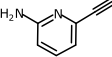
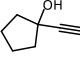
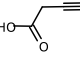
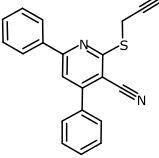
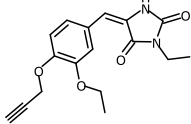
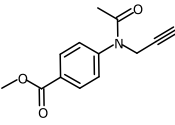
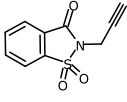
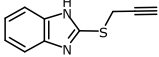
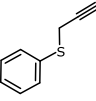
Compound	MW (g/mol)	Cluster	clogS	HAcc	HDon	ΔT_m AalspE	ΔT_m PalspE
 AP-836/41220090	224.26	01	-3.72	4	0	N/A	0
 CAS: 1209289-08-6	198.02	01	-0.68	3	1	3	N/A
 AS-871/43249232	184.24	01	-2.51	2	0	5	1
 CAS: 1346539-11-4	119.12	01	0.02	2	1	n.d.	n.d.
 CAS: 7223-38-3	83.13	01	-0.43	1	0	n.d.	n.d.
 AP-853/43445400	260.28	02	-3.10	6	1	-16	0
 AQ-917/42754681	249.33	02	-2.23	3	0	3	1
 AK-778/15234026	243.26	02	-2.67	4	1	0	0
 CAS: 10601-99-7	146.15	02	-1.06	2	1	n.d.	n.d.
 AE-641/30115033	137.23	02	-2.37	1	1	4	0

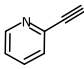
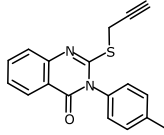
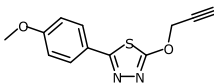
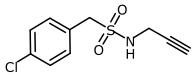
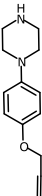
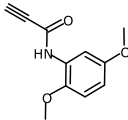
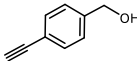
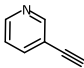
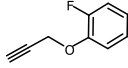
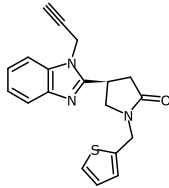
5. Chapter

Compound	MW (g/mol)	Cluster	clogS	HAcc	HDon	ΔT_m AalSpE	ΔT_m PalSpE
 CAS: 14235-81-5	117.15	02	-1.13	1	1	n.d.	n.d.
 CAS: 922-67-8	84.07	02	-0.91	2	0	n.d.	n.d.
 AE-641/30116040	241.38	03	-3.32	1	0	-12	1
 AN-988/41873727	306.32	03	-5.07	6	2	N/A	0
 AN-465/43491689	277.79	03	-4.44	2	1	0	1
 AC-907/34127013	176.18	03	-1.67	4	0	-6	0
 CAS: 705-28-2	170.13	03	-1.83	0	0	-1	0
 CAS: 1256824-94-8	118.14	03	-0.35	2	1	n.d.	n.d.
 CAS: 6746-94-7	66.10	03	-1.82	0	0	n.d.	n.d.

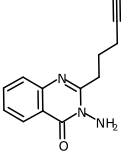
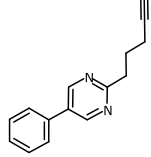
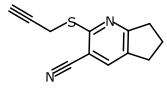
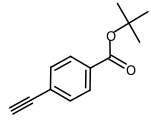
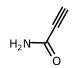
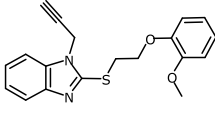
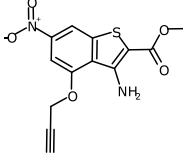
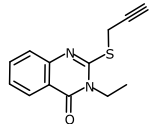
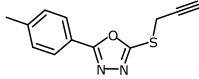
Compound	MW (g/mol)	Cluster	clogS	HAcc	HDon	ΔT_m AalspE	ΔT_m PalspE
 AP-853/41269940	295.16	04	-5.35	3	0	0	0
 AM-879/40861440	263.34	04	-3.88	3	0	-24	1
 AH-487/41801064	240.69	04	-3.20	3	1	1	0
 CAS: 1334148-24-1	225.16	04	-1.33	2	1	1	-1
 VIC-083	213.23	04	-2.11	3	1	2	-1
 AS-813/43501532	182.02	04	-1.09	1	0	2	1
 CAS: 107-19-7	56.06	04	-0.80	1	1	n.d.	n.d.
 AN-988/40840395	316.34	05	-3.15	6	2	-6	-8
 AN-698/42227207	309.39	05	-4.14	3	0	1	0
 AM-814/41093185	233.27	05	-3.46	2	1	2	0

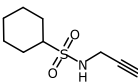
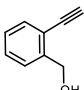
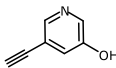
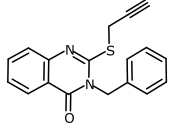
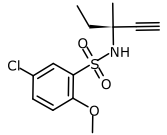
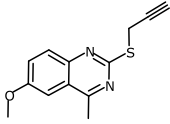
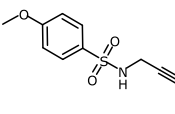
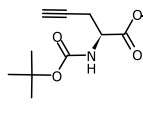
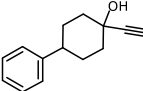
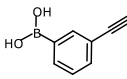
5. Chapter

Compound	MW (g/mol)	Cluster	clogS	HAcc	HDon	ΔT_m AalspE	ΔT_m PalspE
 AN-465/43479919	205.26	05	-2.15	3	1	0	1
 CAS: 173314-98-2	118.14	05	-0.88	2	1	n.d.	n.d.
 CAS: 17356-19-3	110.16	05	-1.91	1	1	-1	n.d.
 CAS: 2345-51-9	84.07	05	-1.05	2	1	n.d.	n.d.
 AG-690/12406103	326.42	06	-6.63	2	0	0	-7
 AN-648/42098633	314.34	06	-3.63	6	1	1	1
 AQ-917/42754702	231.25	06	-2.70	4	0	3	0
 VIC-121	221.24	06	-1.75	4	0	2	-1
 AF-399/13128002	188.25	06	-3.00	2	1	0	1
 CAS: 5651-88-7	148.23	06	-3.02	0	0	n.d.	n.d.

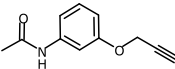
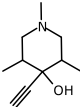
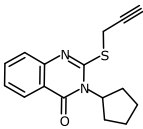
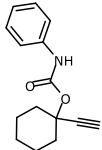
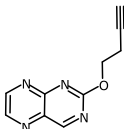
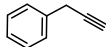

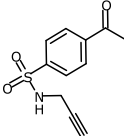
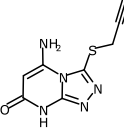
Compound	MW (g/mol)	Cluster	clogS	HAcc	HDon	ΔT_m AalspE	ΔT_m PalspE
 CAS: 1945-84-2	103.12	06	-0.28	1	0	n.d.	n.d.
 AG-690/12886057	306.39	07	-5.23	3	0	0	0
 AK-105/40836816	246.29	07	-2.78	4	0	0	0
 VIC-103	243.71	07	-3.86	3	1	2	-1
 AO-022/43513785	216.28	07	-2.23	3	1	N/A	0
 AB-337/25021050	205.21	07	-2.32	4	1	0	N/A
 CAS: 10602-04-7	132.16	07	-0.93	1	1	n.d.	n.d.
 CAS: 2510-23-8	103.12	07	-0.25	1	0	n.d.	n.d.
 VIC-CQ-009	150.15	08	-2.57	1	0	n.d.	n.d.
 AT-057/43468614	335.43	08	-2.53	4	0	1	N/A

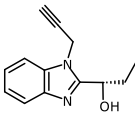
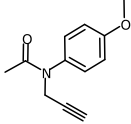
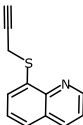
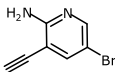
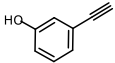
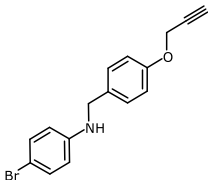
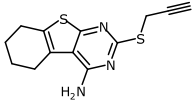
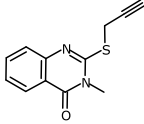
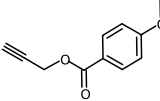
5. Chapter

Compound	MW (g/mol)	Cluster	clogS	HAcc	HDon	ΔT_m AalspE	ΔT_m PalspE
 AD-310/37069069	227.27	08	-3.03	4	1	1	0
 AC-907/34112061	222.29	08	-3.35	2	0	0	1
 AG-690/12403106	214.29	08	-3.61	2	0	0	-1
 CAS: 111291-97-5	202.25	08	-1.98	2	0	2	-1
 CAS: 7341-96-0	69.06	08	-0.86	2	1	n.d.	n.d.
 AT-057/43469431	338.43	09	-3.64	4	0	0	1
 AK-968/41922675	306.30	09	-4.28	6	1	23	48
 AJ-292/11720067	244.32	09	-3.34	3	0	0	0
 AP-853/41269939	230.29	09	-4.86	3	0	1	1

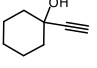
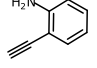
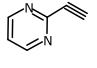
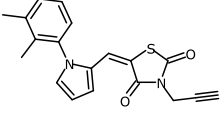
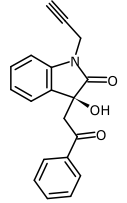
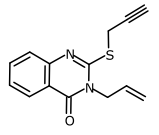
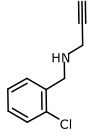
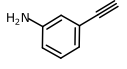
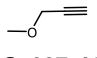
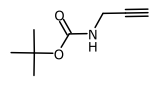
Compound	MW (g/mol)	Cluster	clogS	HAcc	HDon	ΔT_m AalspE	ΔT_m PalspE
 VIC-091	201.29	09	-2.87	3	1	N/A	-1
 CAS: 10602-08-1	132.16	09	-0.93	1	1	n.d.	n.d.
 CAS: 1207351-13-0	119.12	09	0.04	2	1	n.d.	n.d.
 AJ-292/11720072	306.39	10	-4.36	3	0	0	0
 AP-263/42610787	301.79	10	-3.30	4	1	1	0
 AJ-292/41686448	244.32	10	-3.67	3	0	N/A	0
 VIC-084	225.27	10	-1.81	4	1	2	-1
 CAS: 63039-46-3	212.22	10	-2.30	5	1	-35	-1
 AD-266/41884782	200.28	10	-3.42	1	1	0	1
 CAS: 1189127-05-6	145.95	10	1.67	2	2	n.d.	n.d.

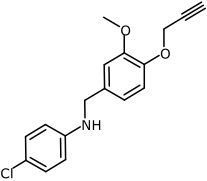
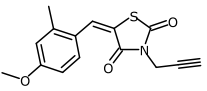
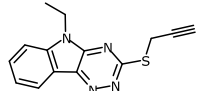
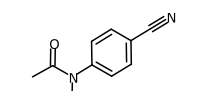
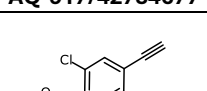
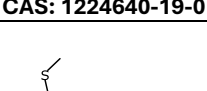
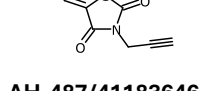
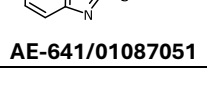
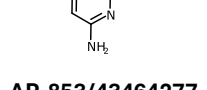
5. Chapter

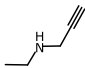
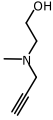
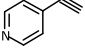
Compound	MW (g/mol)	Cluster	clogS	HAcc	HDon	ΔT_m AalspE	ΔT_m PalspE
 VIC-CQ-003	189.21	11	-2.60	3	1	2	-1
 AM-760/25031001	167.25	11	-1.12	2	1	9	0
 AJ-292/11720068	284.38	11	-4.34	3	0	0	1
 AD-266/40025804	243.31	11	-4.28	3	1	3	N/A
 AC-907/34112019	200.20	11	-2.45	5	0	0	-1
 CAS: 10147-11-2	116.16	11	-2.44	0	0	n.d.	n.d.
 CAS: 2450-71-7	91.54	11	-0.88	1	1	n.d.	n.d.
 VIC-199	237.28	12	-2.48	4	1	2	-2
 AP-906/41642052	221.24	12	-2.13	6	2	3	N/A

Compound	MW (g/mol)	Cluster	clogS	HAcc	HDon	ΔT_m AalspE	ΔT_m PalspE
 AS-871/43478633	214.27	12	-1.33	3	1	2	N/A
 AQ-917/42754701	203.24	12	-2.58	3	0	3	1
 AH-034/11964296	199.28	12	-3.73	1	0	0	0
 CAS: 205235	197.04	12	-1.69	2	1	2	-1
 CAS: 10401-11-3	118.14	12	-0.75	1	1	n.d.	n.d.
 AH-487/42308633	316.20	13	-4.48	2	1	0	0
 AF-399/40634560	275.40	13	-5.55	3	1	2	1
 AJ-292/11720066	230.29	13	-3.04	3	0	1	0
 AN-329/12136897	190.20	13	-2.40	3	0	N/A	0

5. Chapter

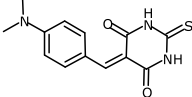
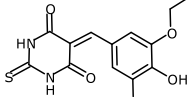
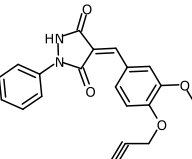
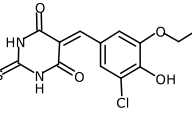
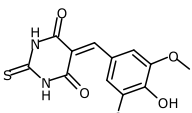
Compound	MW (g/mol)	Cluster	clogS	HAcc	HDon	ΔT_m AalspE	ΔT_m PalspE
 CAS: 78-27-3	124.18	13	-2.18	1	1	-1	n.d.
 CAS: 52670-38-9	117.15	13	-1.13	1	1	n.d.	n.d.
 CAS: 37972-24-0	104.11	13	0.67	2	0	n.d.	n.d.
 AH-487/41457720	336.41	14	-6.44	4	0	1	1
 AK-778/40897655	305.33	14	-4.06	4	1	1	0
 AJ-292/37095013	256.33	14	-3.55	3	0	-1	0
 AN-465/43370007	179.65	14	-2.85	1	1	N/A	1
 CAS: 54060-30-9	117.15	14	-1.13	1	1	n.d.	n.d.
 CAS: 627-41-8	70.09	14	-0.93	1	0	n.d.	n.d.
 CAS: 92136-39-5	155.20	15	-2.18	3	1	0	-2

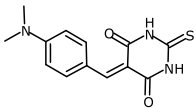
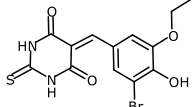
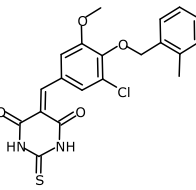
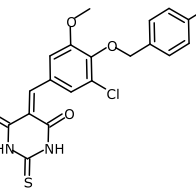
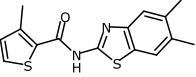
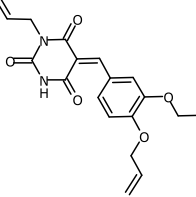
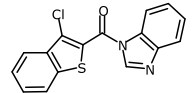
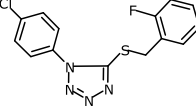
Compound	MW (g/mol)	Cluster	clogS	HAcc	HDon	ΔT_m AalspE	ΔT_m PalspE
 AH-487/42191483	301.77	15	-4.40	3	1	1	1
 AH-487/41449410	287.34	15	-3.77	4	0	N/A	1
 AG-205/12900028	268.34	15	-3.77	4	0	-1	1
 AQ-917/42754677	198.22	15	-3.33	3	0	2	0
 CAS: 1224640-19-0	194.62	15	-1.93	2	0	4	0
 AH-487/41183646	289.38	16	-4.26	3	0	1	1
 AE-641/01087051	205.31	16	-3.86	1	0	0	0
 AP-853/43464277	180.24	16	-2.99	4	2	2	0
 CAS: 13610-02-1	132.16	16	-2.26	1	0	n.d.	n.d.

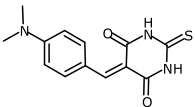
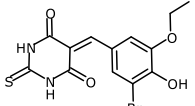
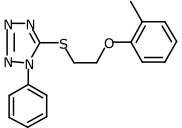
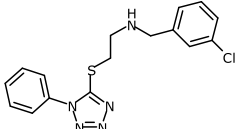
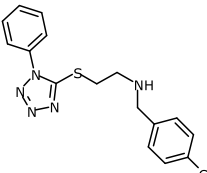
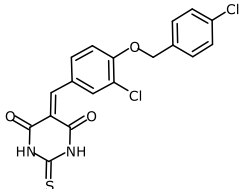
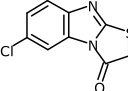
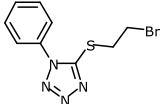
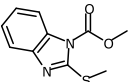
Compound	MW (g/mol)	Cluster	clogS	HAcc	HDon	ΔT_m AalspE	ΔT_m PalspE
HCl  CAS: 53227-33-1	119.59	16	-1.09	1	1	n.d.	n.d.
 CAS: 13105-72-1	113.16	16	-0.22	2	1	n.d.	n.d.
 CAS: 2510-22-7	103.12	16	-0.25	1	0	n.d.	n.d.

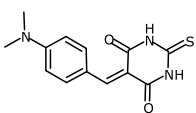
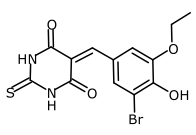
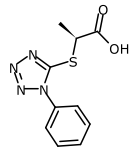
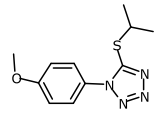
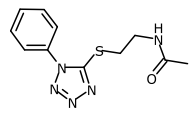
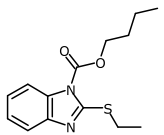
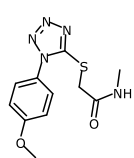
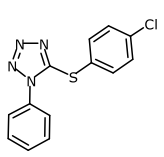
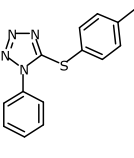
Follow-up compounds of alkyne hits

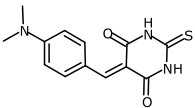
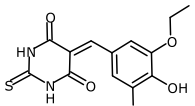
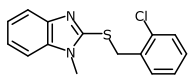
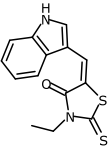
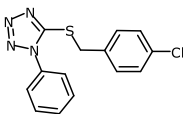
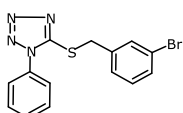
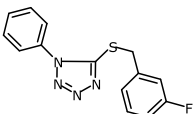
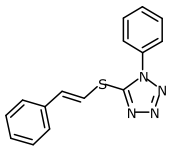
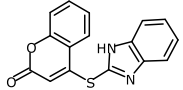
Table S3. Selection of 231 compounds from the Specs library to follow up the verified alkyne hits **11**, and **15–18**, including chemical descriptors; molecular weight (MW), solubility (clogS, clogP), number of H-bond donor (HDon) / acceptor (HAcc).

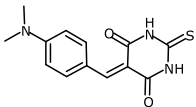
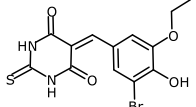
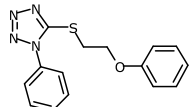
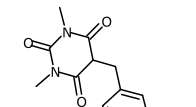
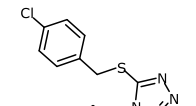
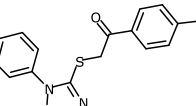
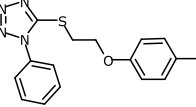
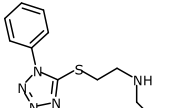
Compound	MW (g/mol)	clogS	clogP	HAcc	HDon
 AE-641/11700410	275.33	-2.52	0.66	5	2
 AG-690/36165057	371.21	-3.34	1.48	6	3
 AN-465/40742950	348.36	-3.55	1.23	6	1
 AK-968/12101155	326.76	-3.25	1.36	6	3
 AG-690/08630010	308.31	-2.23	0.28	7	3

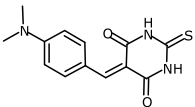
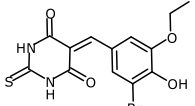
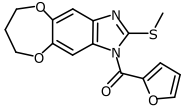
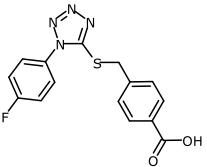
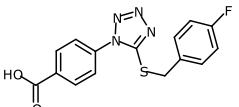
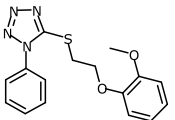
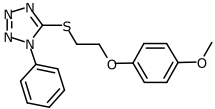
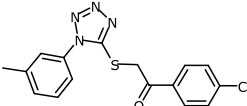
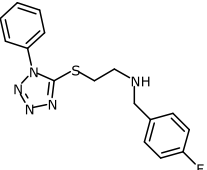
Compound	MW (g/mol)	clogS	clogP	HAcc	HDon
 AE-641/11700410	275.33	-2.52	0.66	5	2
 AG-690/36165057	371.21	-3.34	1.48	6	3
 AN-698/40677872	416.88	-4.93	3.00	6	2
 AN-698/40677882	420.85	-4.90	2.75	6	2
 AK-968/41171421	302.42	-5.14	4.51	3	1
 AM-879/12213021	356.38	-3.40	2.28	7	1
 AK-968/37005235	312.78	-6.07	4.67	3	0
 AN-465/15280027	320.78	-5.16	3.47	4	0

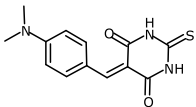
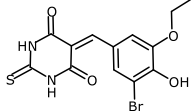
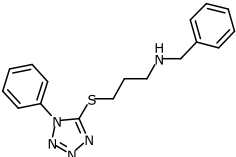
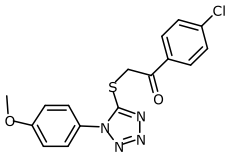
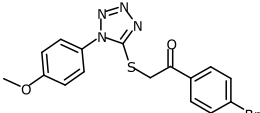
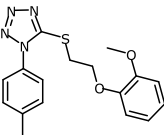
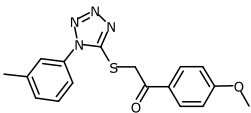
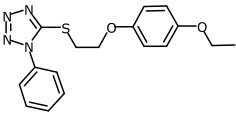
Compound	MW (g/mol)	clogS	clogP	HAcc	HDon
 AE-641/11700410	275.33	-2.52	0.66	5	2
 AG-690/36165057	371.21	-3.34	1.48	6	3
 AJ-145/12323002	312.40	-4.06	3.14	5	0
 AN-465/43369569	345.86	-4.31	2.83	5	1
 AN-465/43369690	345.86	-4.31	2.83	5	1
 AN-698/15136002	407.28	-5.30	3.33	5	2
 AP-381/41075628	224.67	-3.04	2.00	3	0
 AG-205/12014041	285.17	-3.31	2.13	4	0
 AI-204/31718012	222.27	-2.88	2.43	4	0

Compound	MW (g/mol)	clogS	clogP	HAcc	HDon
 AE-641/11700410	275.33	-2.52	0.66	5	2
 AG-690/36165057	371.21	-3.34	1.48	6	3
 AR-422/40159747	250.28	-2.44	0.90	6	1
 AN-648/15101113	250.33	-2.98	2.11	5	0
 AG-690/34448005	263.32	-2.53	0.86	6	1
 AG-205/32421007	278.38	-3.95	4.24	4	0
 AG-690/40819218	279.32	-2.25	0.38	7	1
 AI-204/31688045	288.76	-4.21	3.23	4	0
 AK-245/37100004	268.34	-3.81	2.97	4	0

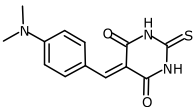
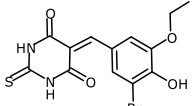
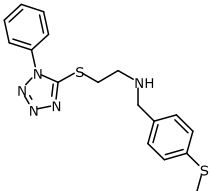
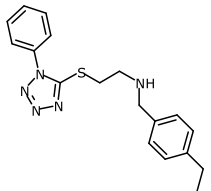
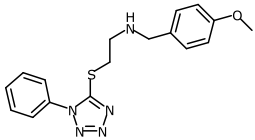
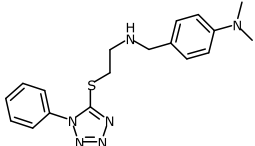
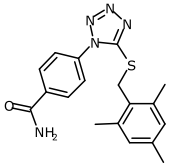
Compound	MW (g/mol)	clogS	clogP	HAcc	HDon
 AE-641/11700410	275.33	-2.52	0.66	5	2
 AG-690/36165057	371.21	-3.34	1.48	6	3
 AG-205/32456036	288.80	-4.42	4.20	2	0
 AG-690/33052023	288.39	-3.96	1.84	3	1
 AG-205/04509027	302.79	-4.85	3.37	4	0
 AG-205/36483037	347.24	-4.95	3.49	4	0
 AN-465/13570103	286.33	-4.43	2.86	4	0
 AN-967/15488233	280.35	-4.21	3.05	4	0
 AI-204/31718004	294.33	-2.81	3.37	4	1

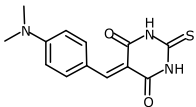
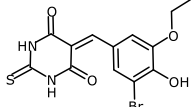
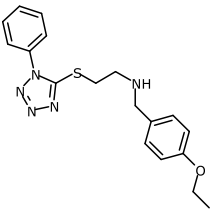
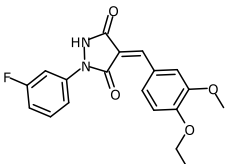
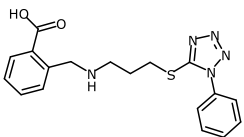
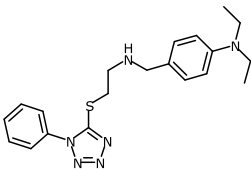
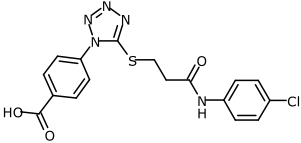
Compound	MW (g/mol)	clogS	clogP	HAcc	HDon
 AE-641/11700410	275.33	-2.52	0.66	5	2
 AG-690/36165057	371.21	-3.34	1.48	6	3
 AG-205/07685018	298.37	-3.71	2.79	5	0
 AG-670/33699004	290.27	-2.29	0.99	7	0
 AN-988/14610040	332.81	-4.87	3.30	5	0
 AI-204/31688060	314.34	-4.39	2.43	5	0
 AR-422/11668229	312.40	-4.06	3.14	5	0
 AN-465/43369536	311.41	-3.57	2.22	5	1

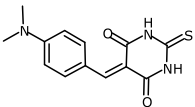
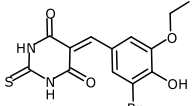
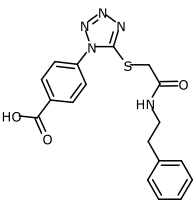
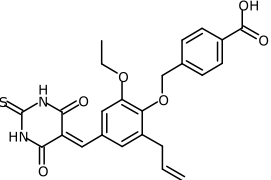
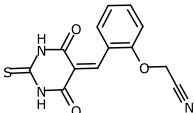
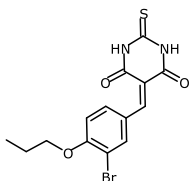
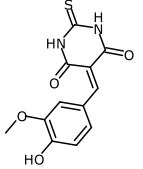
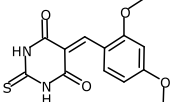
Compound	MW (g/mol)	clogS	clogP	HAcc	HDon
 AE-641/11700410	275.33	-2.52	0.66	5	2
 AG-690/36165057	371.21	-3.34	1.48	6	3
 AN-153/12400011	330.36	-4.73	3.37	6	0
 AN-465/42154560	330.34	-4.44	2.35	6	1
 AP-853/13113072	330.34	-4.44	2.35	6	1
 AG-690/11241075	328.40	-3.73	2.72	6	0
 AG-690/11668718	328.40	-3.73	2.72	6	0
 AF-399/14738025	344.83	-5.16	3.28	5	0
 AN-465/43369642	329.40	-3.89	2.32	5	1

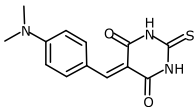
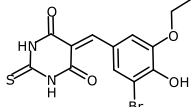
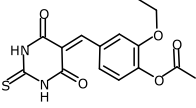
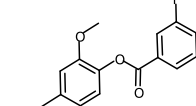
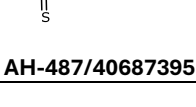
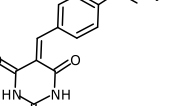
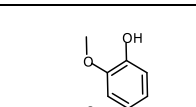
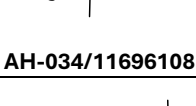
Compound	MW (g/mol)	clogS	clogP	HAcc	HDon
 AE-641/11700410	275.33	-2.52	0.66	5	2
 AG-690/36165057	371.21	-3.34	1.48	6	3
 AN-465/43369038	325.44	-3.84	2.67	5	1
 AN-648/15101053	360.82	-4.83	2.86	6	0
 AP-853/42936577	405.28	-4.93	2.98	6	0
 AG-690/11240025	342.42	-4.08	3.07	6	0
 AF-399/14738026	340.41	-4.44	2.60	6	0
 AG-690/11665299	342.42	-4.03	3.13	6	0

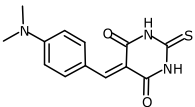
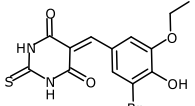
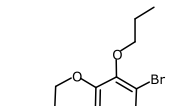
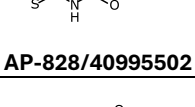
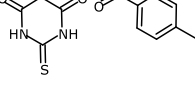
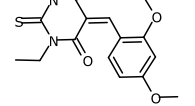
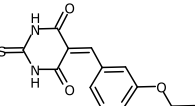
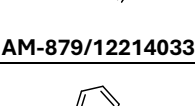
5. Chapter

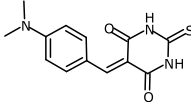
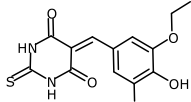
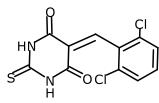
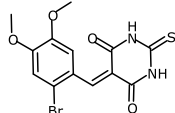
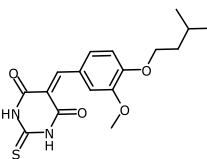
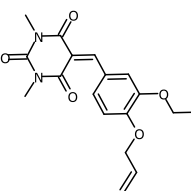
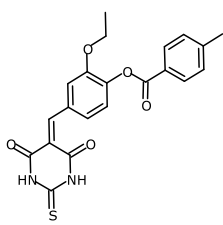
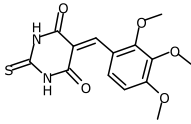
Compound	MW (g/mol)	clogS	clogP	HAcc	HDon
 AE-641/11700410	275.33	-2.52	0.66	5	2
 AG-690/36165057	371.21	-3.34	1.48	6	3
 AN-465/43369540	357.51	-4.42	2.70	5	1
 AN-465/43369894	339.47	-4.08	2.98	5	1
 AN-465/43369138	341.44	-3.59	2.15	6	1
 AN-465/43369764	354.48	-3.61	2.12	6	1
 AG-205/14141036	353.45	-5.23	2.88	6	1

Compound	MW (g/mol)	clogS	clogP	HAcc	HDon
 AE-641/11700410	275.33	-2.52	0.66	5	2
 AG-690/36165057	371.21	-3.34	1.48	6	3
 AN-465/43369811	355.47	-3.89	2.56	6	1
 AP-970/41848852	356.35	-3.54	1.71	6	1
 AN-465/43422191	369.45	-3.86	0.77	7	2
 AN-465/43369816	382.53	-4.21	2.93	6	1
 AP-853/43445410	403.85	-4.76	2.71	8	2

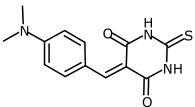
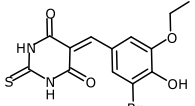
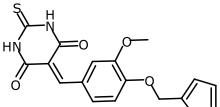
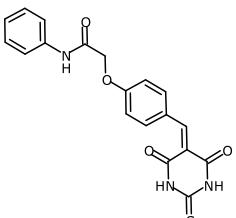
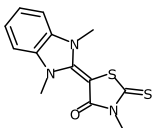
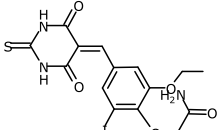
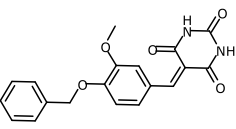
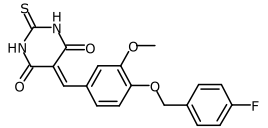
Compound	MW (g/mol)	clogS	clogP	HAcc	HDon
 AE-641/11700410	275.33	-2.52	0.66	5	2
 AG-690/36165057	371.21	-3.34	1.48	6	3
 AP-853/43445439	383.43	-3.68	1.79	8	2
 AH-487/41659850	466.51	-4.87	2.97	8	3
 AK-968/10818008	287.30	-2.95	0.35	6	2
 AN-465/40838743	369.24	-3.91	2.28	5	2
 AH-357/04328031	278.29	-2.21	0.35	6	3
 AE-848/30739042	292.31	-2.52	0.63	6	2

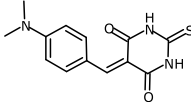
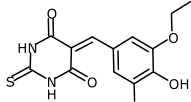
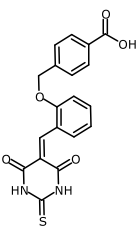
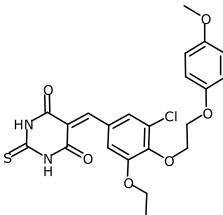
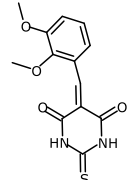
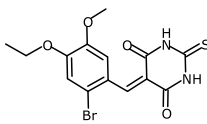
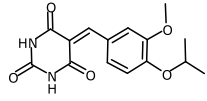
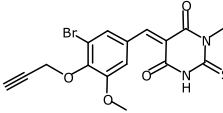
Compound	MW (g/mol)	clogS	clogP	HAcc	HDon
 AE-641/11700410	275.33	-2.52	0.66	5	2
 AG-690/36165057	371.21	-3.34	1.48	6	3
 AK-968/12342046	334.35	-3.11	1.09	7	2
 AH-487/40687395	400.39	-4.29	2.23	7	2
 AN-698/41107032	416.84	-4.71	2.73	7	2
 AH-034/11696108	292.31	-1.85	0.61	6	2
 AK-968/37055149	289.36	-2.82	1.07	5	2
 AK-968/12383312	322.34	-2.32	0.11	7	3

Compound	MW (g/mol)	clogS	clogP	HAcc	HDon
 AE-641/11700410	275.33	-2.52	0.66	5	2
 AG-690/36165057	371.21	-3.34	1.48	6	3
 AP-828/40995502	413.29	-4.23	2.62	6	2
 AN-698/15135005	396.42	-4.32	2.47	7	2
 AG-670/36765014	320.37	-2.46	1.29	6	1
 AM-879/12214033	332.38	-3.33	1.71	6	2
 AG-205/12378009	356.38	-4.14	2.22	5	2
 AO-299/41407232	396.47	-4.44	2.81	6	2

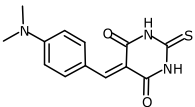
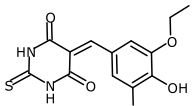
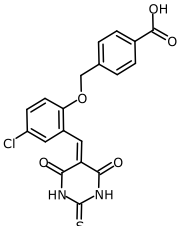
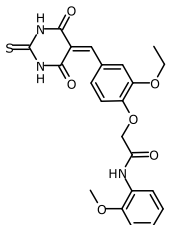
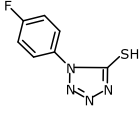
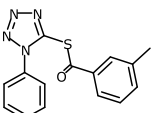
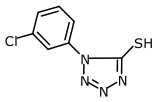
Compound	MW (g/mol)	clogS	clogP	HAcc	HDon
 AE-641/11700410	275.33	-2.52	0.66	5	2
 AG-690/36165057	371.21	-3.34	1.48	6	3
 AG-670/13121001	301.15	-3.96	1.98	4	2
 AG-690/11662088	371.21	-3.36	1.35	6	2
 AK-968/36977072	348.42	-3.52	2.16	6	2
 AM-879/12213027	344.37	-2.53	1.85	7	0
 AN-698/15136011	410.45	-4.62	2.88	7	2
 AG-690/08630011	322.34	-2.54	0.56	7	2

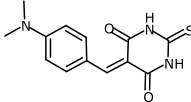
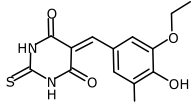
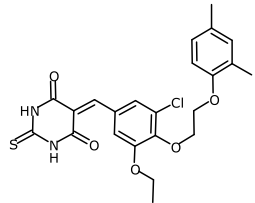
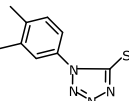
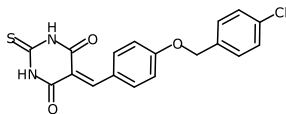
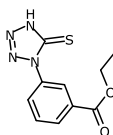
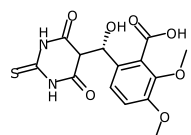
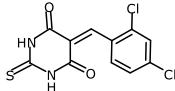
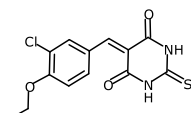
5. Chapter

Compound	MW (g/mol)	clogS	clogP	HAcc	HDon
 AE-641/11700410	275.33	-2.52	0.66	5	2
 AG-690/36165057	371.21	-3.34	1.48	6	3
 AP-970/41848875	374.44	-3.86	1.91	6	2
 AP-828/40845822	381.41	-3.78	1.49	7	3
 AG-690/11629236	291.40	-4.44	1.12	4	0
 AK-968/13025423	475.26	-3.69	0.20	8	3
 AG-690/36169052	352.35	-3.76	1.69	7	2
 AM-879/12129038	386.40	-4.16	2.15	6	2

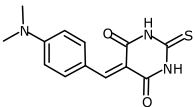
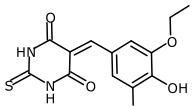
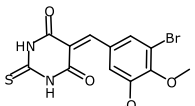
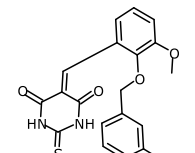
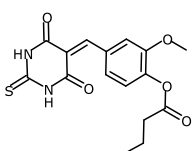
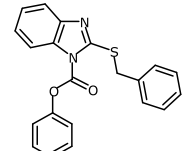
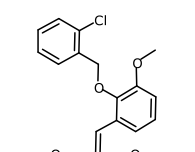
Compound	MW (g/mol)	clogS	clogP	HAcc	HDon
 AE-641/11700410	275.33	-2.52	0.66	5	2
 AG-690/36165057	371.21	-3.34	1.48	6	3
 AN-648/14910009	382.40	-3.84	1.60	7	3
 AN-758/15299041	476.94	-4.83	3.00	8	2
 AG-205/13166011	292.31	-2.52	0.63	6	2
 AG-205/12080003	385.24	-3.66	1.76	6	2
 AK-968/37055126	304.30	-3.12	1.03	7	2
 AH-487/41183754	409.26	-3.62	1.63	6	1

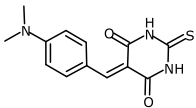
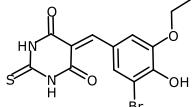
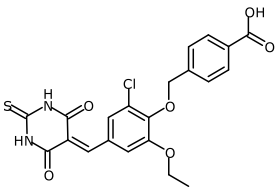
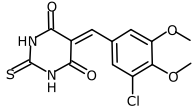
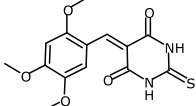
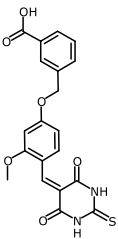
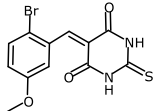
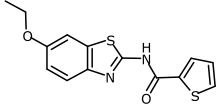
5. Chapter

Compound	MW (g/mol)	clogS	clogP	HAcc	HDon
 AE-641/11700410	275.33	-2.52	0.66	5	2
 AG-690/36165057	371.21	-3.34	1.48	6	3
 AH-487/41660486	416.84	-4.58	2.21	7	3
 AK-968/13025120	455.49	-4.12	1.76	9	3
 AN-465/13570097	196.21	-3.10	0.84	4	0
 AN-652/40801734	296.35	-4.69	2.49	5	0
 AN-465/13287018	212.66	-3.53	1.35	4	0

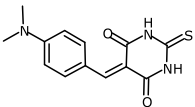
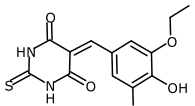
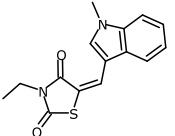
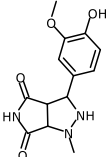
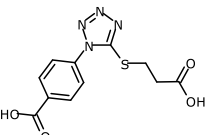
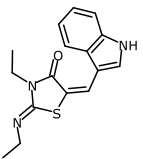
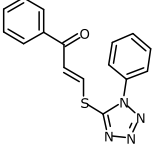
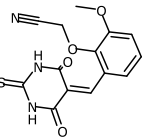
Compound	MW (g/mol)	clogS	clogP	HAcc	HDon
 AE-641/11700410	275.33	-2.52	0.66	5	2
 AG-690/36165057	371.21	-3.34	1.48	6	3
 AN-758/15299018	474.96	-5.50	3.75	7	2
 AN-988/14854001	206.27	-3.48	1.43	4	0
 AG-690/36983018	372.83	-4.57	2.72	5	2
 AG-690/33046023	250.28	-2.53	2.12	6	1
 AG-670/36457028	354.34	-1.89	-0.99	9	4
 AK-918/10656062	301.15	-3.96	1.98	4	2
 AN-988/14609010	310.76	-3.54	1.71	5	2

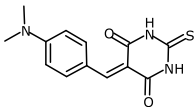
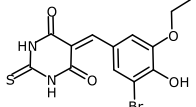
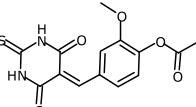
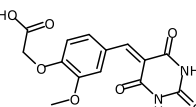
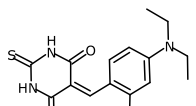
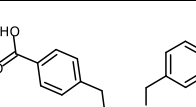
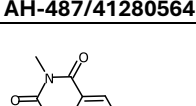
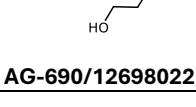
5. Chapter

Compound	MW (g/mol)	clogS	clogP	HAcc	HDon
 AE-641/11700410	275.33	-2.52	0.66	5	2
 AG-690/36165057	371.21	-3.34	1.48	6	3
 AK-968/11573124	371.21	-3.36	1.35	6	2
 AH-487/40686718	402.86	-4.58	2.65	6	2
 AN-465/15401020	348.38	-3.35	1.59	7	2
 AI-067/31573005	360.44	-5.79	5.43	4	0
 AH-487/40686452	402.86	-4.58	2.65	6	2

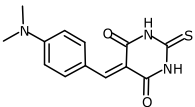
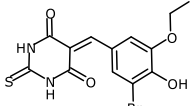
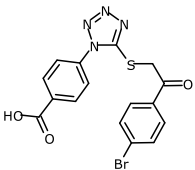
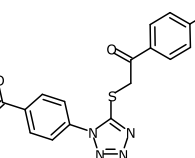
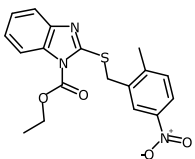
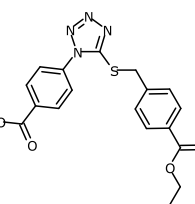
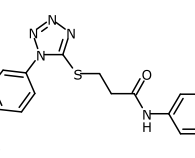
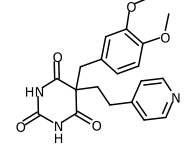
Compound	MW (g/mol)	clogS	clogP	HAcc	HDon
 AE-641/11700410	275.33	-2.52	0.66	5	2
 AG-690/36165057	371.21	-3.34	1.48	6	3
 AH-487/41663772	460.89	-4.90	2.54	8	3
 AK-968/12384394	326.76	-3.26	1.23	6	2
 AG-205/11611581	322.34	-2.54	0.56	7	2
 AH-487/40791466	412.42	-3.86	1.53	8	3
 AK-968/12686132	341.18	-3.34	1.42	5	2
 AH-034/06210039	304.39	-4.42	3.81	4	1

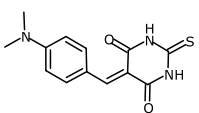
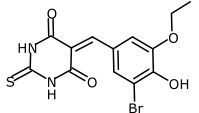
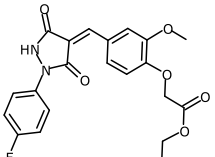
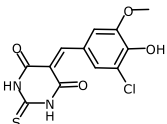
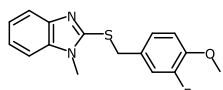
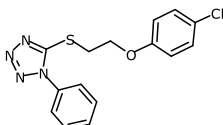
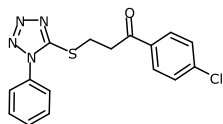
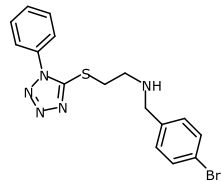
5. Chapter

Compound	MW (g/mol)	clogS	clogP	HAcc	HDon
 AE-641/11700410	275.33	-2.52	0.66	5	2
 AG-690/36165057	371.21	-3.34	1.48	6	3
 AH-487/41653788	286.35	-3.28	2.32	4	0
 AS-871/43476184	277.28	-0.97	-1.92	7	3
 AP-853/43445397	294.29	-2.52	0.44	8	2
 AG-205/40650150	299.40	-3.97	2.72	4	1
 AG-401/33922036	308.36	-4.30	2.49	5	0
 AG-670/12464047	317.32	-2.97	0.28	7	2

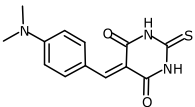
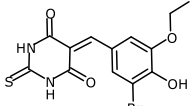
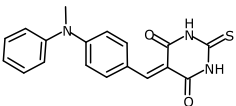
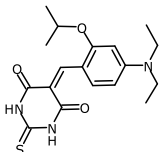
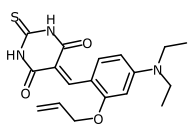
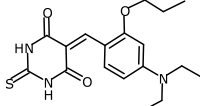
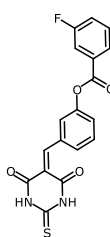
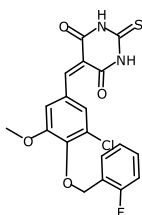
Compound	MW (g/mol)	clogS	clogP	HAcc	HDon
 AE-641/11700410	275.33	-2.52	0.66	5	2
 AG-690/36165057	371.21	-3.34	1.48	6	3
 AK-968/12117362	334.35	-3.08	1.14	7	2
 AK-968/11658795	320.26	-2.22	-0.60	9	3
 AH-487/36381059	333.41	-3.14	1.41	6	2
 AH-487/41280564	326.38	-3.95	2.50	6	1
 AG-690/12698022	334.33	-1.51	0.25	8	1
 AN-153/14988006	344.37	-5.10	3.94	5	0

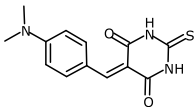
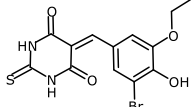
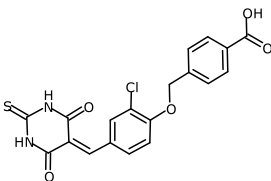
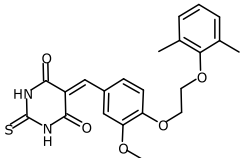
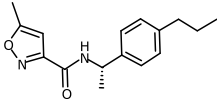
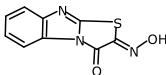
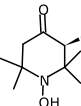
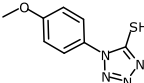
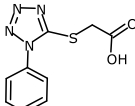
5. Chapter

Compound	MW (g/mol)	clogS	clogP	HAcc	HDon
 AE-641/11700410	275.33	-2.52	0.66	5	2
 AG-690/36165057	371.21	-3.34	1.48	6	3
 AP-853/43445414	419.26	-4.93	2.54	7	1
 AP-853/43416378	358.35	-4.41	1.91	7	1
 AI-067/31573003	371.42	-5.56	3.74	7	0
 AP-853/43445436	384.42	-4.57	2.57	8	1
 AP-853/43445411	448.30	-4.86	2.83	8	2
 AG-670/10567045	383.40	-3.13	1.46	8	2

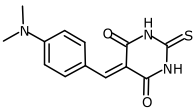
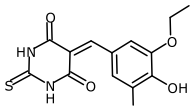
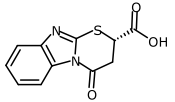
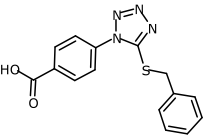
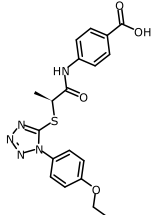
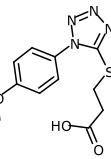
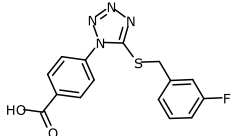
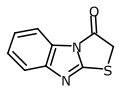
Compound	MW (g/mol)	clogS	clogP	HAcc	HDon
 AE-641/11700410	275.33	-2.52	0.66	5	2
 AG-690/36165057	371.21	-3.34	1.48	6	3
 AG-690/12242677	414.39	-3.44	1.27	8	1
 AK-968/12163589	312.73	-2.95	0.96	6	3
 AG-205/06496019	302.37	-4.02	3.63	3	0
 AG-690/12885306	332.81	-4.45	3.40	5	0
 AI-204/31688062	344.83	-5.09	3.39	5	0
 AN-465/43369639	390.31	-4.41	2.94	5	1

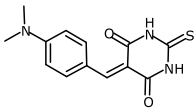
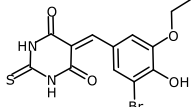
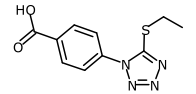
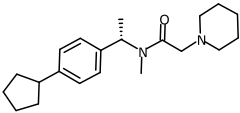
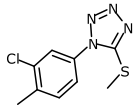
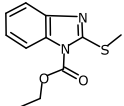
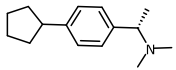
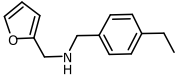
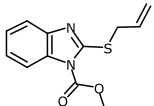
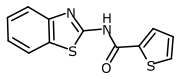
5. Chapter

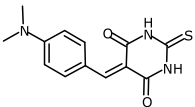
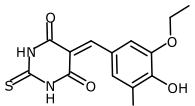
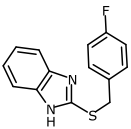
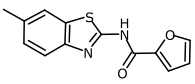
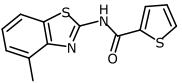
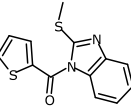
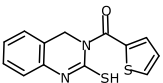
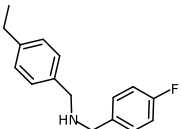
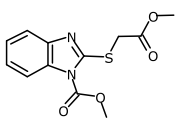
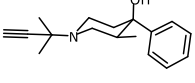
Compound	MW (g/mol)	clogS	clogP	HAcc	HDon
 AE-641/11700410	275.33	-2.52	0.66	5	2
 AG-690/36165057	371.21	-3.34	1.48	6	3
 AG-205/32459036	337.40	-4.54	1.32	5	2
 AG-690/12509031	361.47	-3.82	2.17	6	2
 AK-968/36977262	359.45	-3.65	2.08	6	2
 AG-690/12886013	361.47	-3.71	2.27	6	2
 AH-487/40686835	370.36	-4.27	2.30	6	2
 AH-487/40686553	420.85	-4.90	2.75	6	2

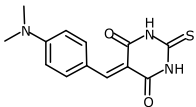
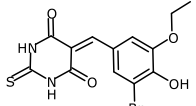
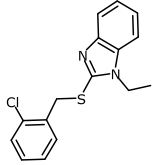
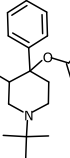
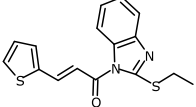
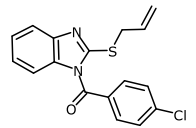
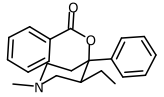
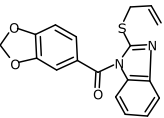
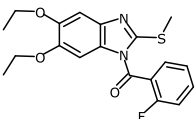
Compound	MW (g/mol)	clogS	clogP	HAcc	HDon
 AE-641/11700410	275.33	-2.52	0.66	5	2
 AG-690/36165057	371.21	-3.34	1.48	6	3
 AH-487/41660565	416.84	-4.58	2.21	7	3
 AO-299/41408834	426.49	-4.46	2.74	7	2
 AK-968/41025113	272.35	-3.28	2.88	4	1
 AG-205/13184093	219.22	-1.83	1.36	5	1
 AE-848/30744042	205.68	-1.86	0.91	3	1
 AA-504/33319034	208.25	-2.81	0.67	5	0
 AE-848/32010045	236.26	-2.24	0.50	6	1

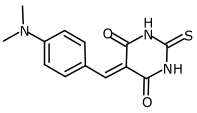
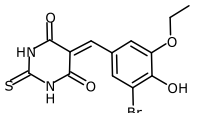
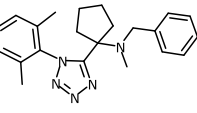
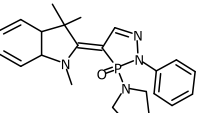
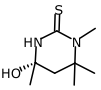
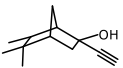
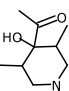
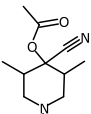
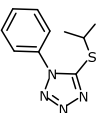
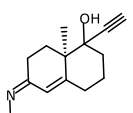
5. Chapter

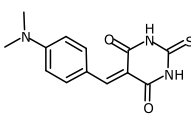
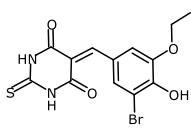
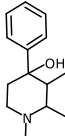
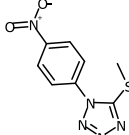
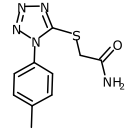
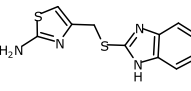
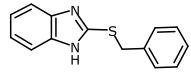
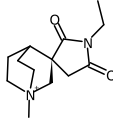
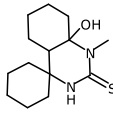
Compound	MW (g/mol)	clogS	clogP	HAcc	HDon
 AE-641/11700410	275.33	-2.52	0.66	5	2
 AG-690/36165057	371.21	-3.34	1.48	6	3
 AO-567/40646844	248.26	-2.25	1.13	5	1
 AG-205/13109132	312.35	-4.13	2.25	6	1
 AS-871/43478504	413.46	-4.27	2.39	9	2
 AG-690/40816740	280.31	-2.53	0.88	7	1
 AP-853/43445399	330.34	-4.44	2.35	6	1
 AH-357/03489045	190.23	-2.31	1.39	3	0

Compound	MW (g/mol)	clogS	clogP	HAcc	HDon
 AE-641/11700410	275.33	-2.52	0.66	5	2
 AG-690/36165057	371.21	-3.34	1.48	6	3
 AP-853/43416377	250.28	-2.78	1.26	6	1
 AE-641/30116043	328.50	-3.06	3.85	3	0
 AN-988/14854009	240.72	-3.61	2.23	4	0
 AN-970/40920741	236.29	-3.18	2.83	4	0
 AE-641/30116039	217.36	-2.70	3.36	1	0
 AP-505/42535604	215.30	-3.00	2.38	2	1
 AI-204/31718016	248.31	-3.32	3.19	4	0
 AH-034/11364278	260.34	-4.11	3.48	3	1

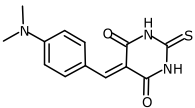
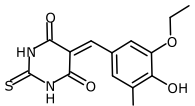
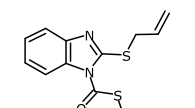
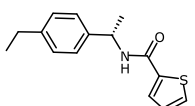
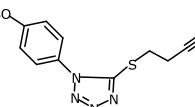
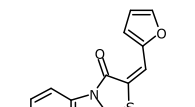
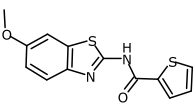
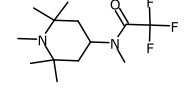
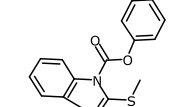
Compound	MW (g/mol)	clogS	clogP	HAcc	HDon
 AE-641/11700410	275.33	-2.52	0.66	5	2
 AG-690/36165057	371.21	-3.34	1.48	6	3
 AG-205/32244029	258.32	-4.34	3.56	2	1
 AG-205/08623001	258.30	-4.12	3.14	4	1
 AG-690/12887330	274.37	-4.45	3.82	3	1
 AS-871/42309115	274.37	-4.61	3.73	3	0
 AE-641/12195197	274.37	-4.10	2.42	3	0
 AN-465/42767184	243.32	-3.63	3.29	1	1
 AI-204/31718019	280.30	-2.71	2.07	6	0
 AG-205/12291035	257.38	-2.77	2.77	2	1

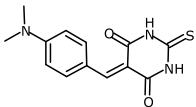
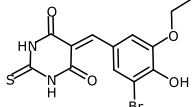
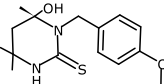
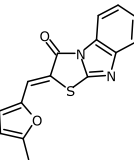
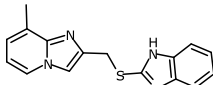
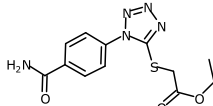
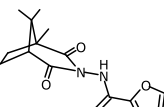
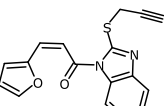
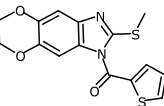
Compound	MW (g/mol)	clogS	clogP	HAcc	HDon
 AE-641/11700410	275.33	-2.52	0.66	5	2
 AG-690/36165057	371.21	-3.34	1.48	6	3
 AG-670/15096002	302.83	-4.43	4.46	2	0
 AG-205/36408033	289.42	-2.85	3.63	3	0
 AF-399/13907003	314.43	-4.31	4.28	3	0
 AI-204/31718014	328.82	-5.78	5.24	3	0
 AG-205/13058719	323.44	-3.50	4.38	3	0
 AF-399/37313009	338.39	-5.75	4.74	5	0
 AN-153/14989102	374.44	-5.55	4.64	5	0

Compound	MW (g/mol)	clogS	clogP	HAcc	HDon
 AE-641/11700410	275.33	-2.52	0.66	5	2
 AG-690/36165057	371.21	-3.34	1.48	6	3
 AG-667/12449013	361.49	-3.84	3.56	5	0
 AE-848/08812062	408.48	-4.89	4.09	5	0
 AG-219/36431015	188.29	-1.32	0.94	3	2
 AN-512/13208099	178.27	-2.82	1.89	1	1
 AG-690/33037037	185.27	-0.72	0.38	3	1
 AG-690/36704041	210.28	-1.35	0.71	4	0
 AG-205/33147055	220.30	-2.96	2.18	4	0
 AG-205/08595020	219.28	-3.07	2.19	3	2

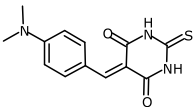
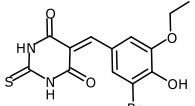
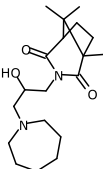
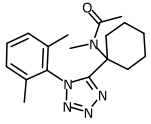
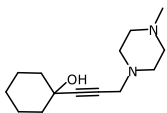
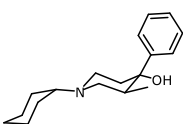
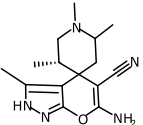
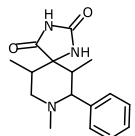
Compound	MW (g/mol)	clogS	clogP	HAcc	HDon
 AE-641/11700410	275.33	-2.52	0.66	5	2
 AG-690/36165057	371.21	-3.34	1.48	6	3
 AG-690/03048027	219.33	-2.03	2.32	2	1
 AL-291/13466002	237.24	-2.99	0.36	7	0
 AG-690/40699204	249.30	-2.66	0.44	6	1
 AG-205/33685051	262.36	-3.86	2.46	4	2
 AF-961/00501049	240.33	-4.03	3.46	2	1
 AE-641/01209028	237.32	-0.61	-2.76	4	0
 AG-690/36749002	268.42	-3.00	2.34	3	2

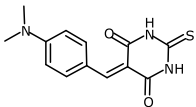
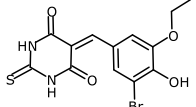
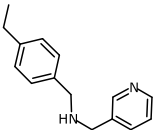
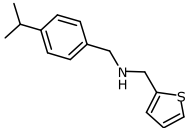
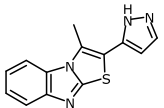
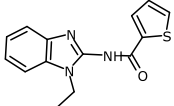
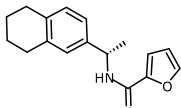
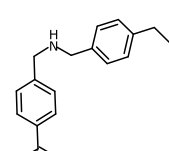
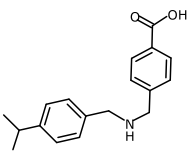
5. Chapter

Compound	MW (g/mol)	clogS	clogP	HAcc	HDon
 AE-641/11700410	275.33	-2.52	0.66	5	2
 AG-690/36165057	371.21	-3.34	1.48	6	3
 AI-204/31718018	278.40	-3.22	4.01	3	0
 AK-968/40708150	259.37	-3.53	3.43	2	1
 AN-648/15101031	261.31	-3.20	1.40	6	0
 AE-848/33856028	268.30	-3.82	2.69	4	0
 AH-034/04482058	290.37	-4.12	3.41	4	1
 AG-205/13058111	280.33	-1.99	2.15	3	0
 AG-205/40649782	284.34	-4.21	3.94	4	0

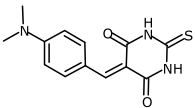
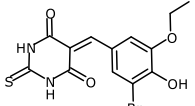
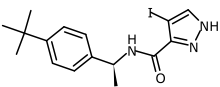
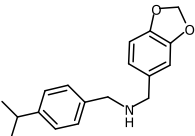
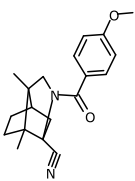
Compound	MW (g/mol)	clogS	clogP	HAcc	HDon
 AE-641/11700410	275.33	-2.52	0.66	5	2
 AG-690/36165057	371.21	-3.34	1.48	6	3
 AG-690/11665794	294.42	-2.66	2.29	4	2
 AG-690/12556010	282.32	-4.19	3.09	4	0
 AF-399/37112053	294.38	-5.67	2.80	4	1
 AG-205/13109364	307.33	-2.76	0.42	8	1
 AE-848/11734028	290.32	-2.88	0.31	6	1
 AF-399/37305042	308.36	-4.31	3.22	4	0
 AN-153/14988005	332.40	-4.79	3.71	5	0

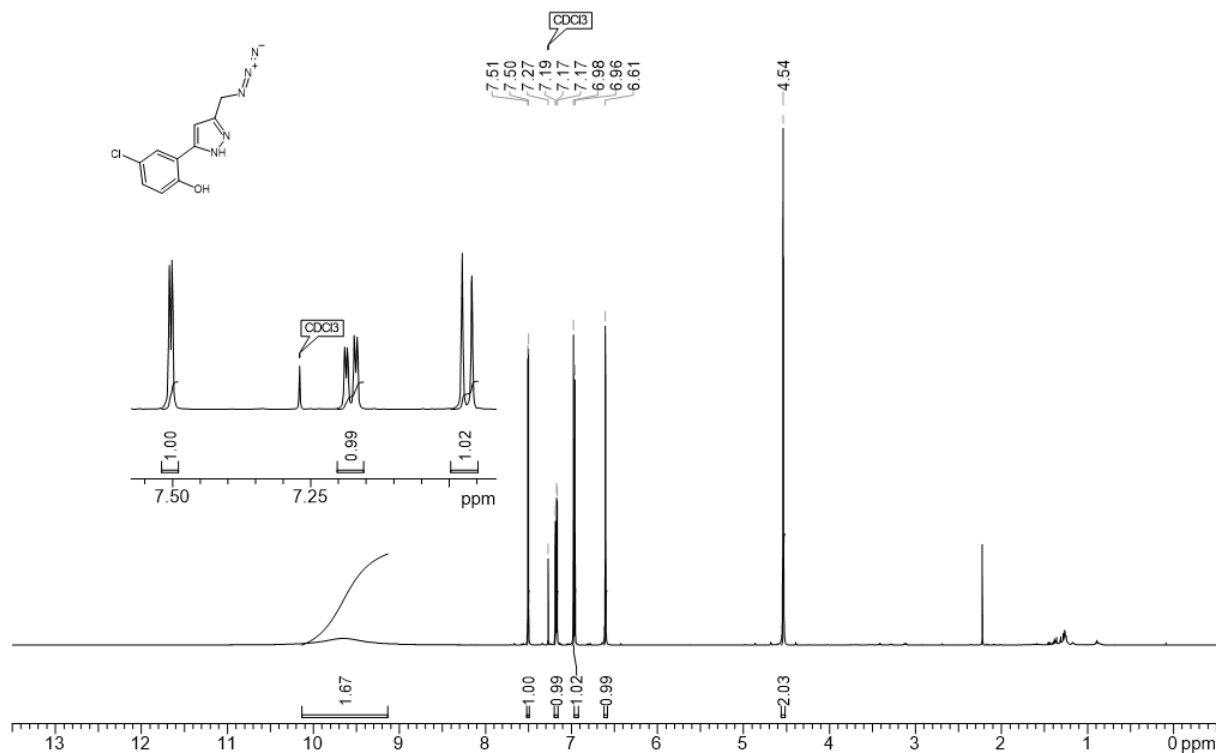
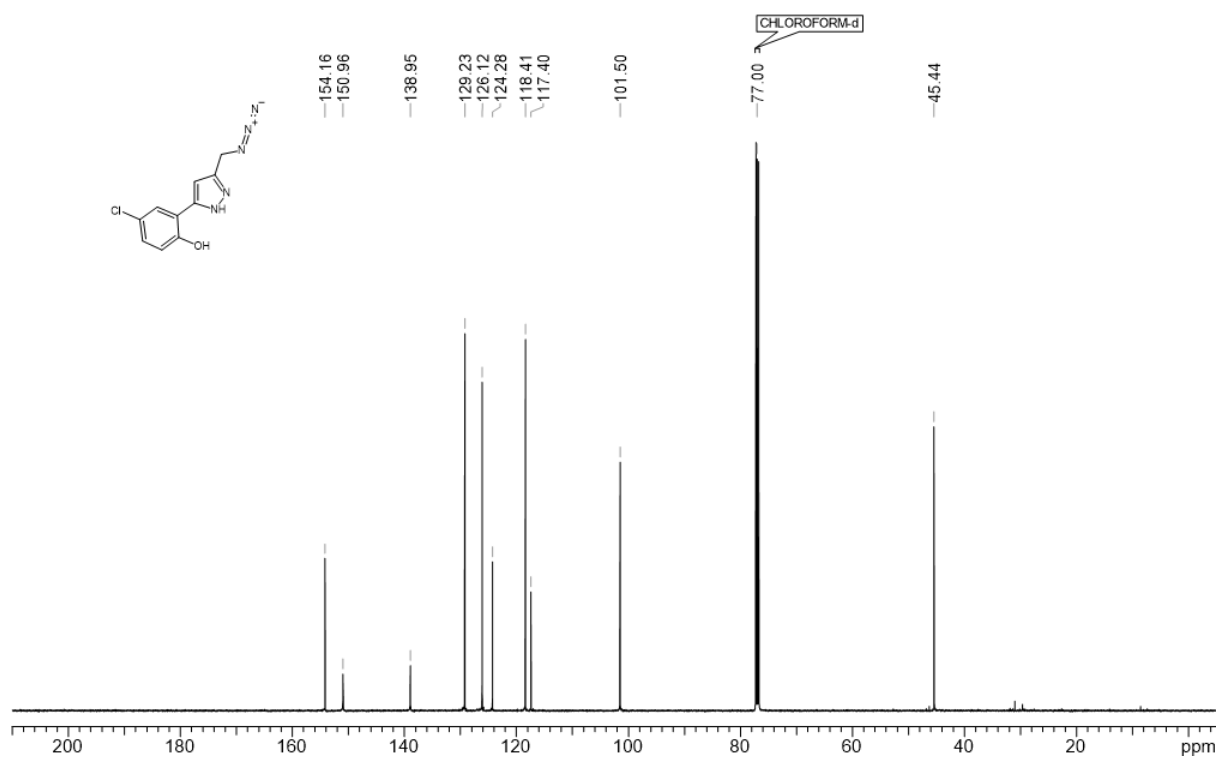
5. Chapter

Compound	MW (g/mol)	clogS	clogP	HAcc	HDon
 AE-641/11700410	275.33	-2.52	0.66	5	2
 AG-690/36165057	371.21	-3.34	1.48	6	3
 AE-848/34540023	336.47	-2.17	1.65	5	1
 AG-205/33685013	327.43	-3.06	2.54	6	0
 AG-205/11975048	236.36	-2.74	1.41	3	1
 AG-690/15435668	273.42	-3.23	3.55	2	1
 AK-777/37198001	287.37	-3.99	0.80	6	2
 AE-848/32962034	287.36	-2.17	1.24	5	2

Compound	MW (g/mol)	clogS	clogP	HAcc	HDon
 AE-641/11700410	275.33	-2.52	0.66	5	2
 AG-690/36165057	371.21	-3.34	1.48	6	3
 AN-465/41673597	226.32	-2.52	2.19	2	1
 AN-465/43369416	245.39	-3.70	3.49	1	1
 AS-938/43408245	254.32	-2.50	2.45	4	1
 AK-968/12342259	271.34	-3.29	3.03	4	1
 AN-153/42373973	269.34	-3.79	3.15	3	1
 AN-465/42886189	269.34	-3.33	1.29	3	2
 AN-465/43411669	283.37	-3.70	1.72	3	2

5. Chapter

Compound	MW (g/mol)	clogS	clogP	HAcc	HDon
 AE-641/11700410	275.33	-2.52	0.66	5	2
 AG-690/36165057	371.21	-3.34	1.48	6	3
 AK-968/41923855	397.26	-3.79	2.77	4	2
 AN-465/43369274	283.37	-4.40	3.73	3	1
 AF-399/42322379	310.40	-3.60	2.84	4	0

NMR, HRMS, and LCMS spectraAzides **2** and **4****Figure S2.** ^1H NMR spectrum of **2**.**Figure S3.** ^{13}C NMR spectrum of **2**.

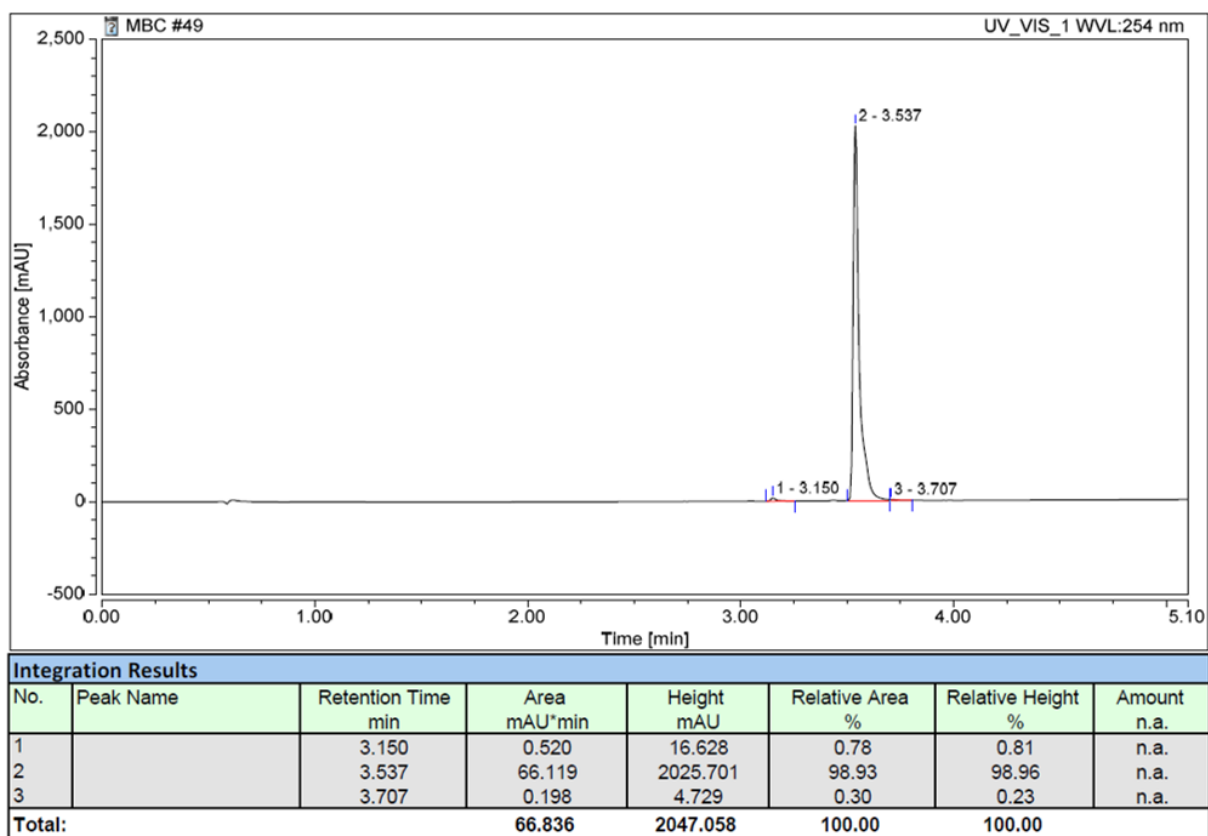


Figure S4. LCMS purity analysis of 2.

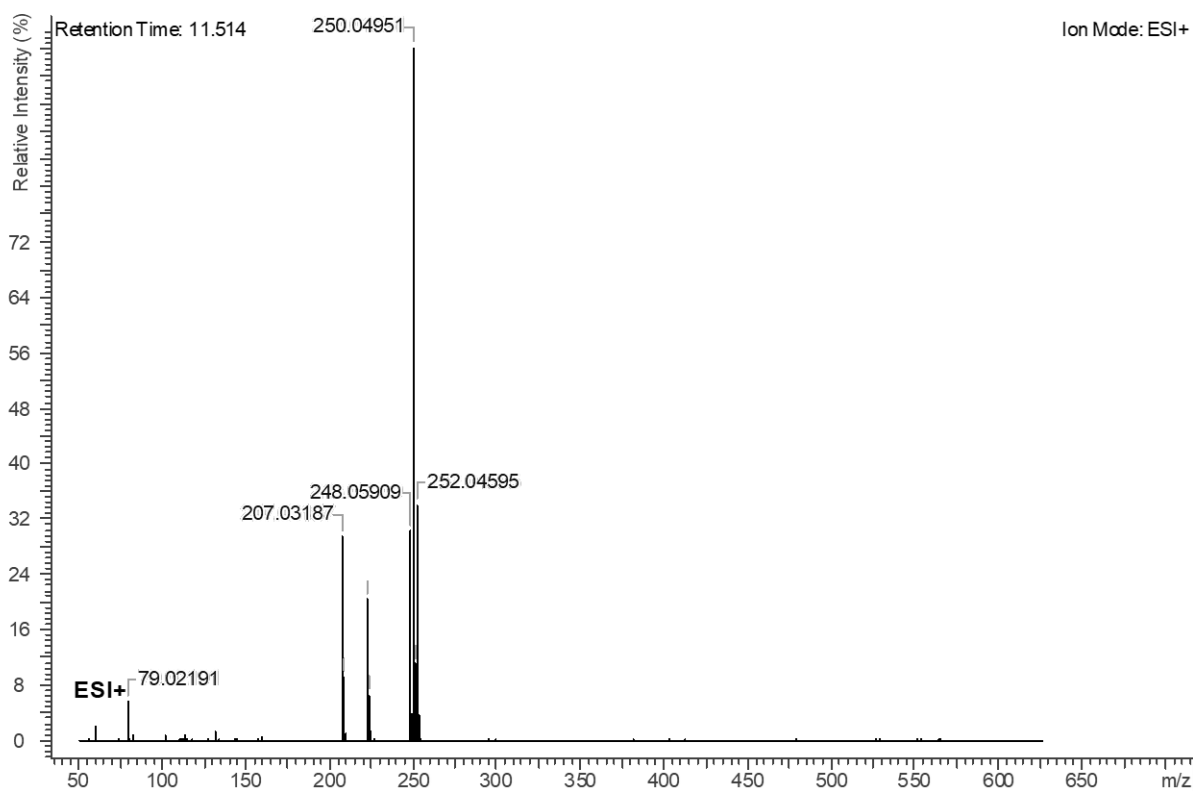


Figure S5. HRMS of 2.

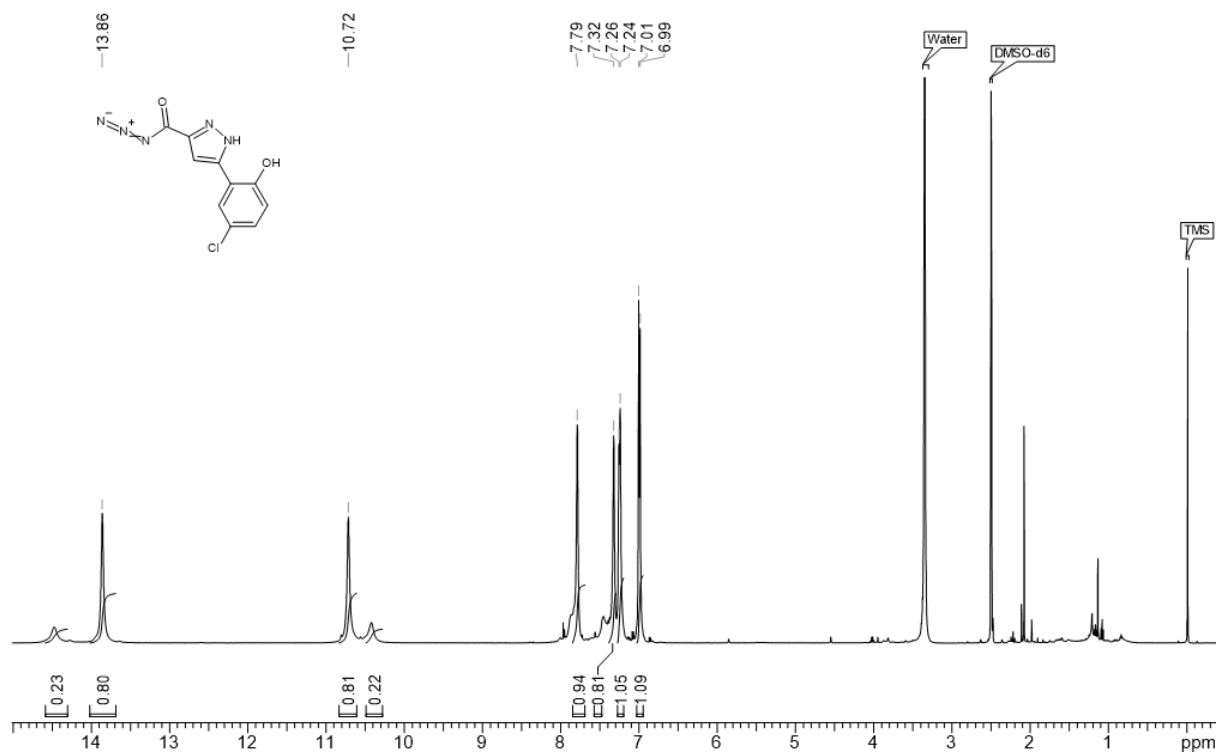


Figure S6. ¹H NMR spectrum of 4.

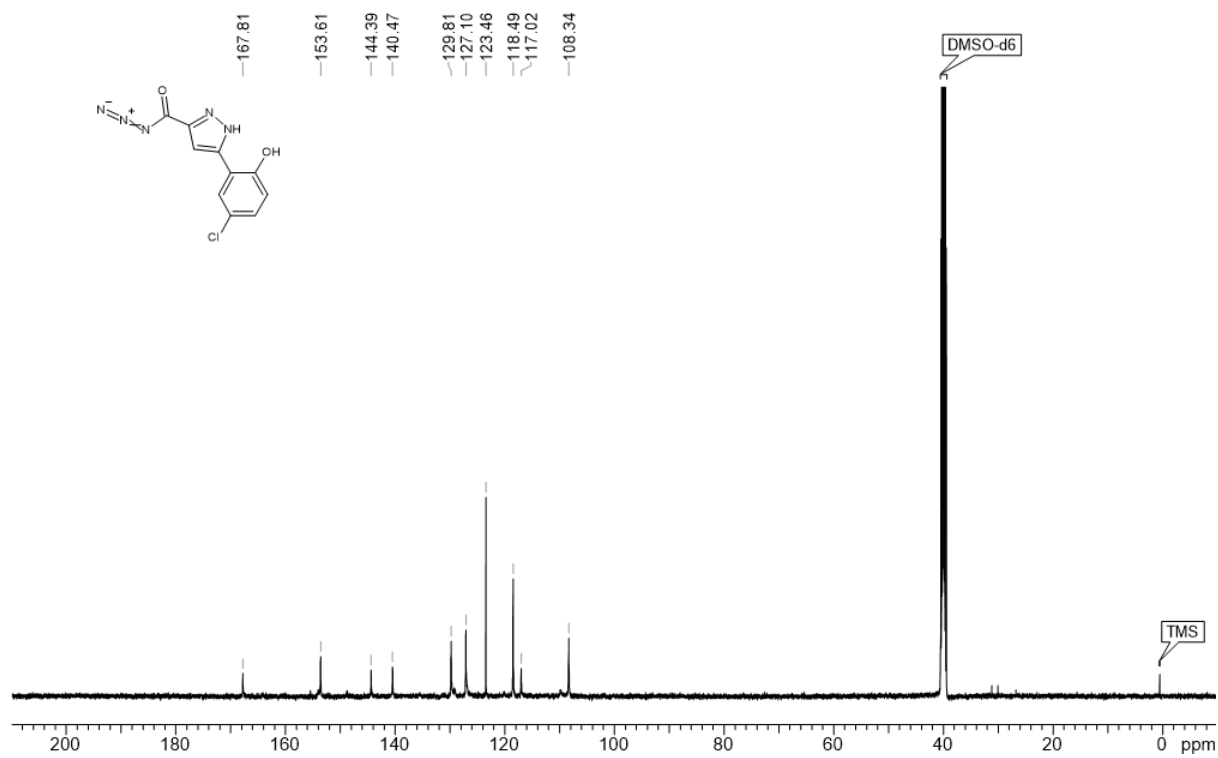


Figure S7. ¹³C NMR spectrum of 4.

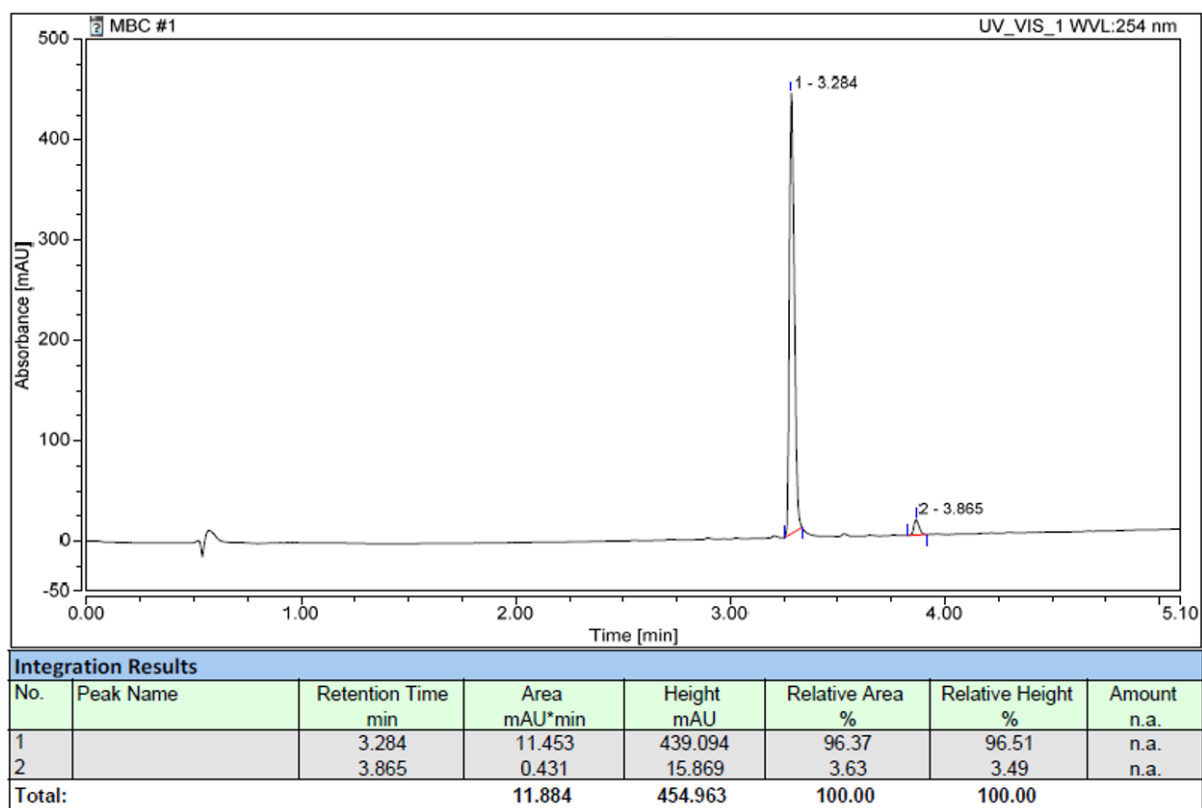


Figure S8. LCMS purity analysis of 4.

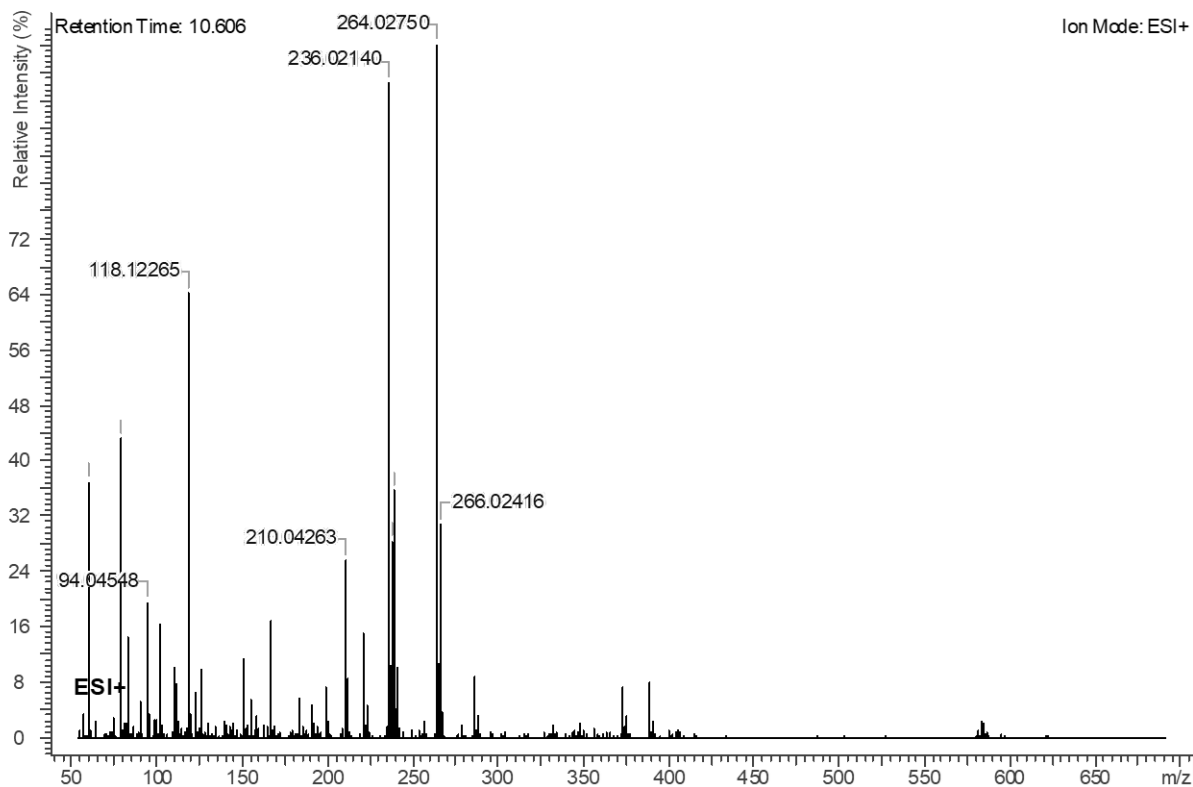


Figure S9. HRMS of 4.

Triazoles 19–22

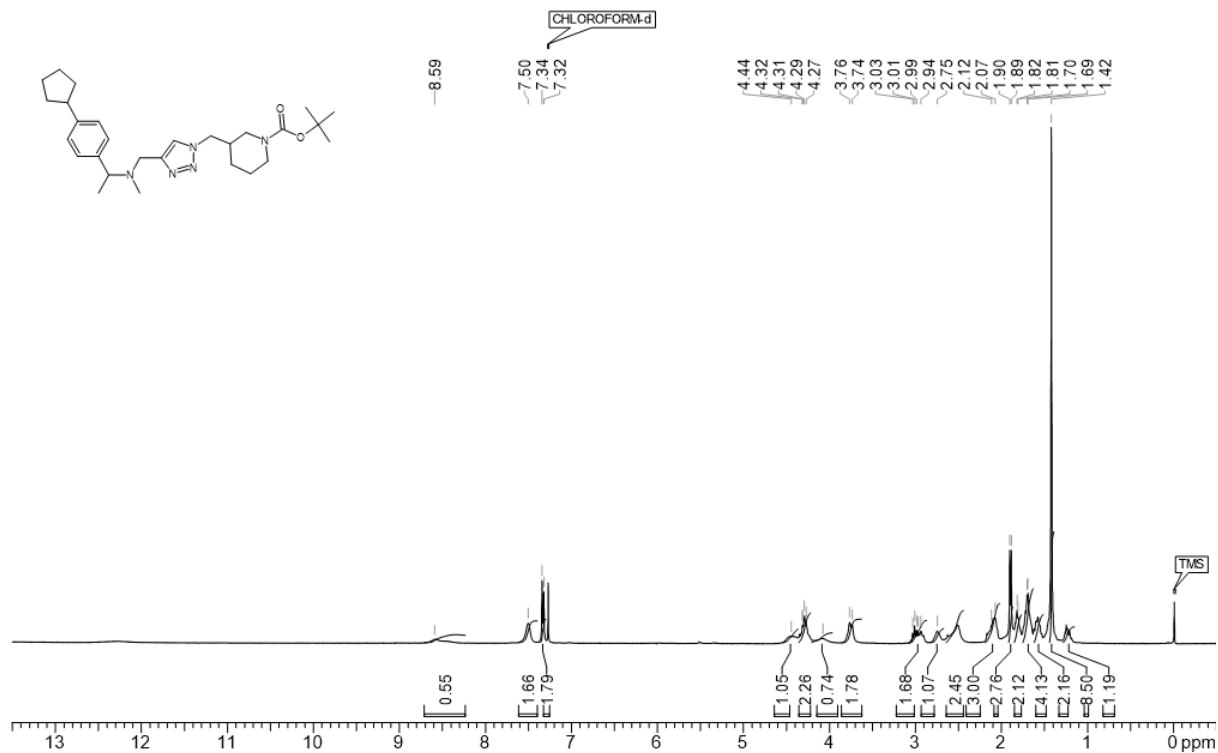


Figure S10. ^1H NMR spectrum of **19**.

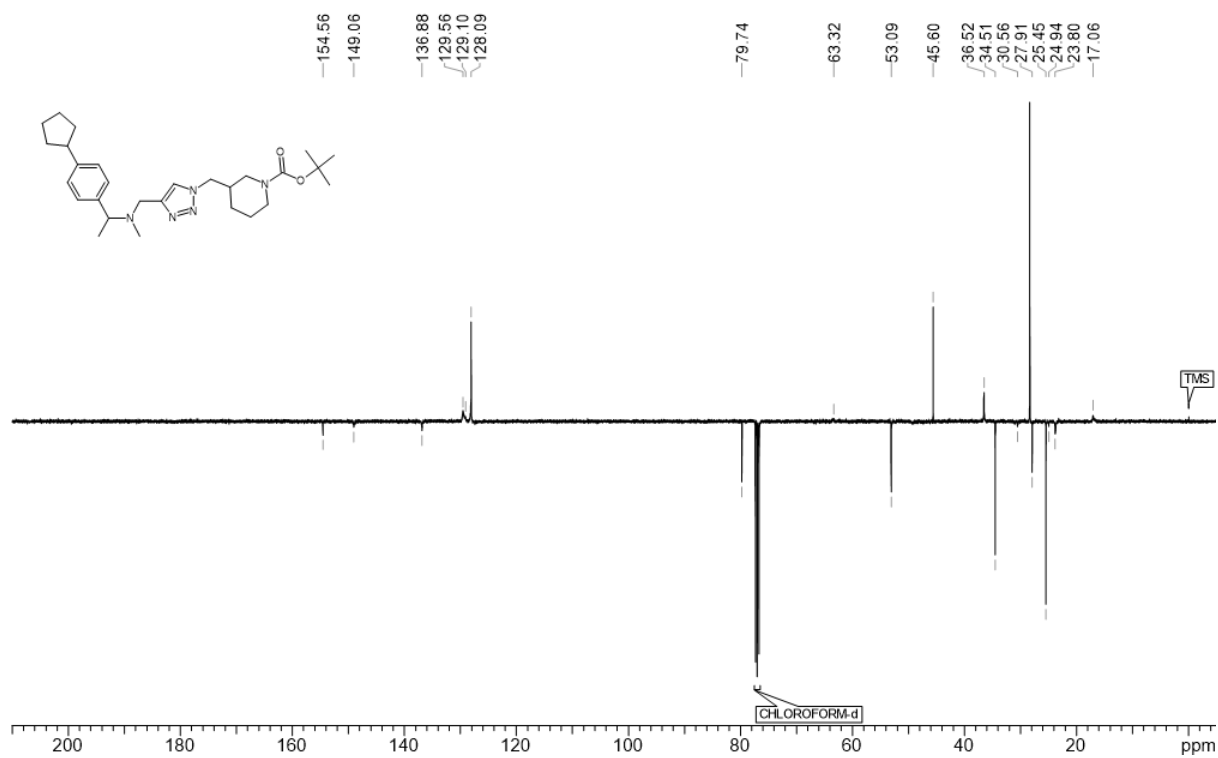


Figure S11. ^{13}C APT NMR spectrum of **19**.

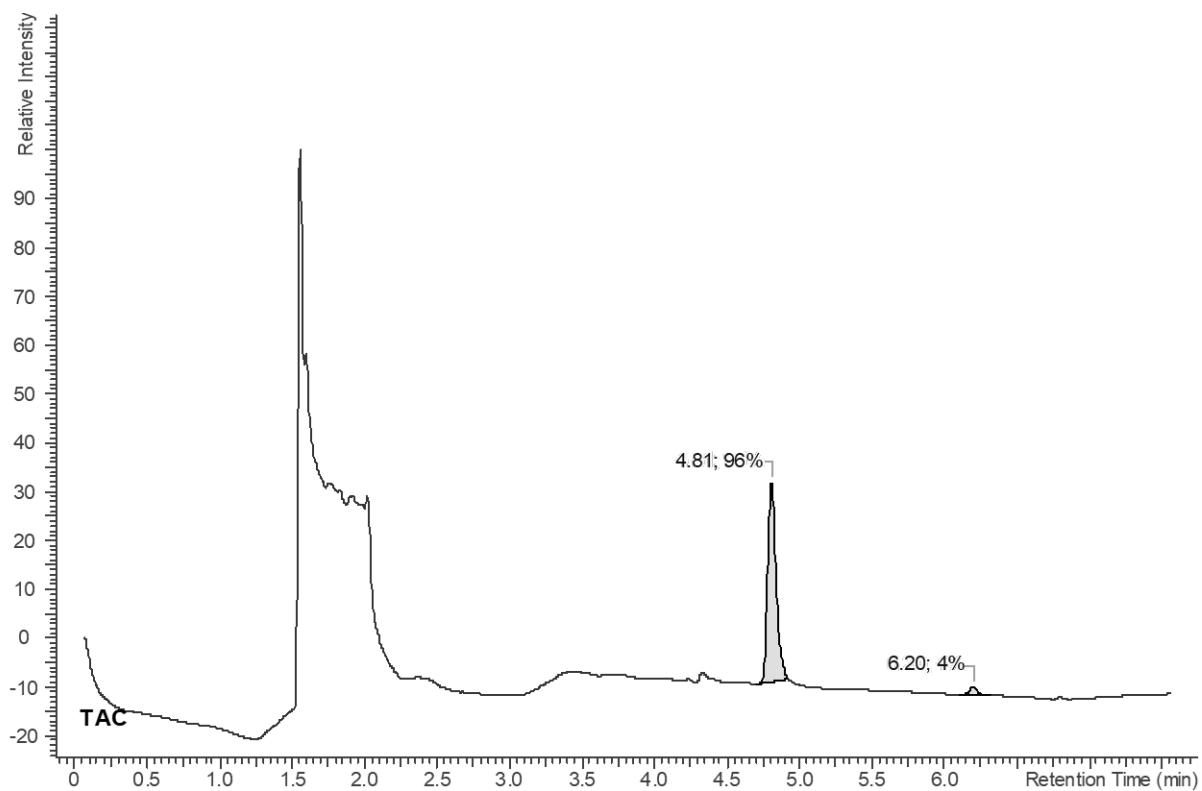


Figure S12. LCMS purity analysis of **19**.

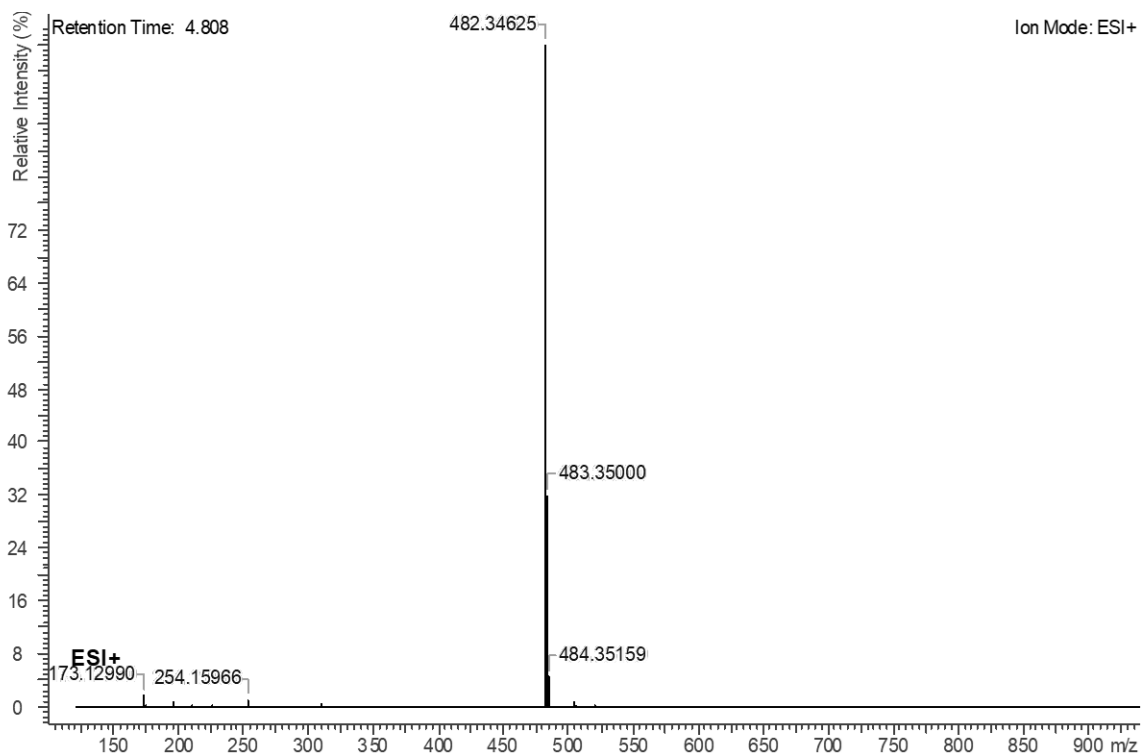
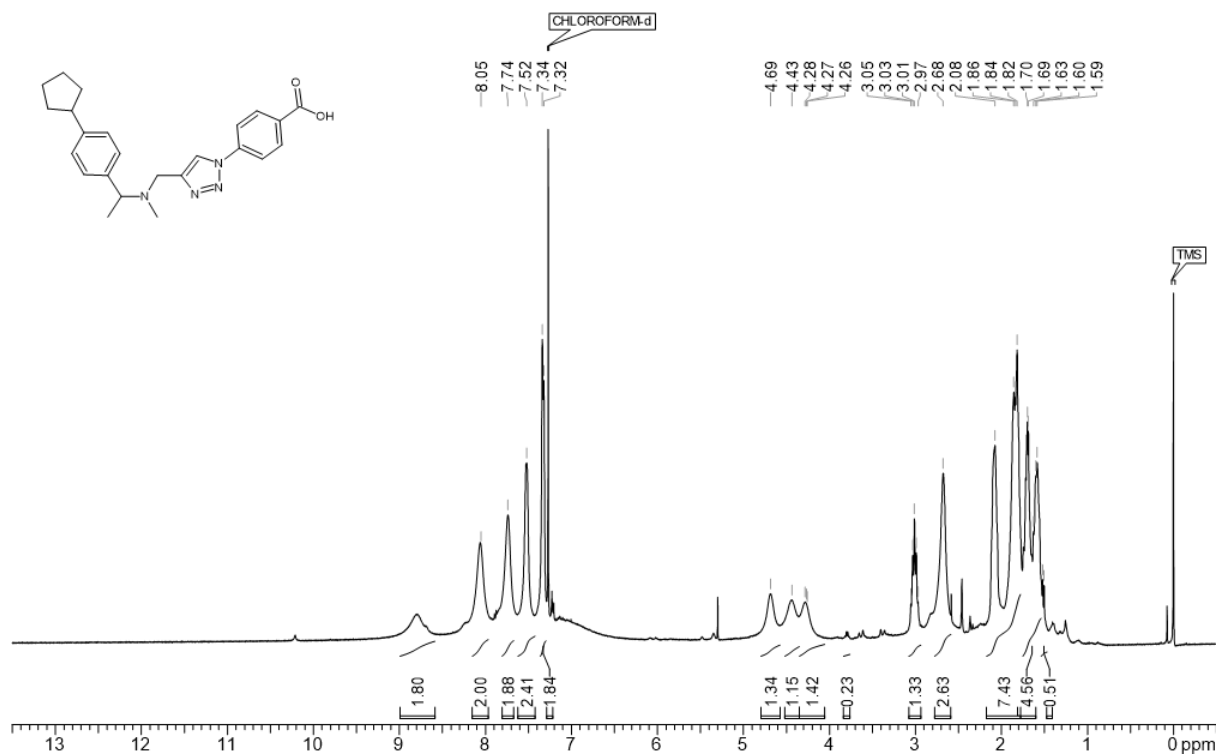
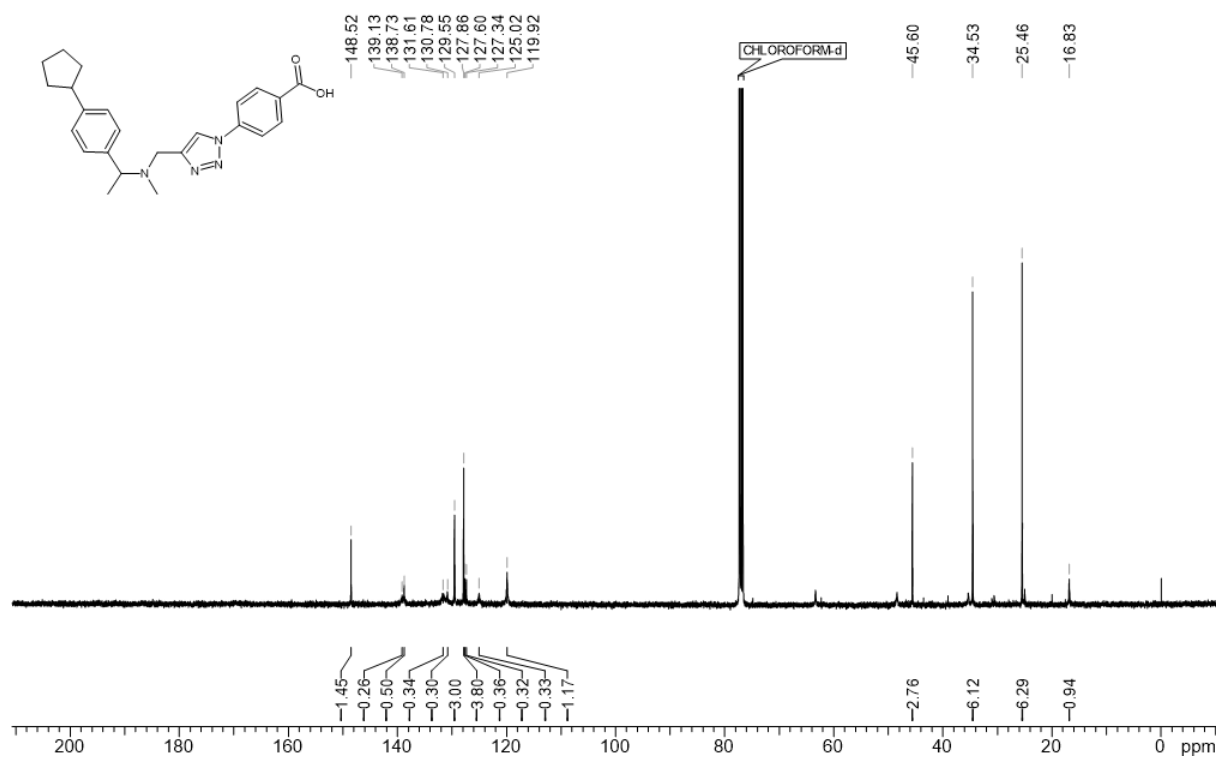


Figure S13. HRMS of **19**.

Figure S14. ¹H NMR spectrum of 20.Figure S15. ¹³C NMR spectrum of 20.

5. Chapter

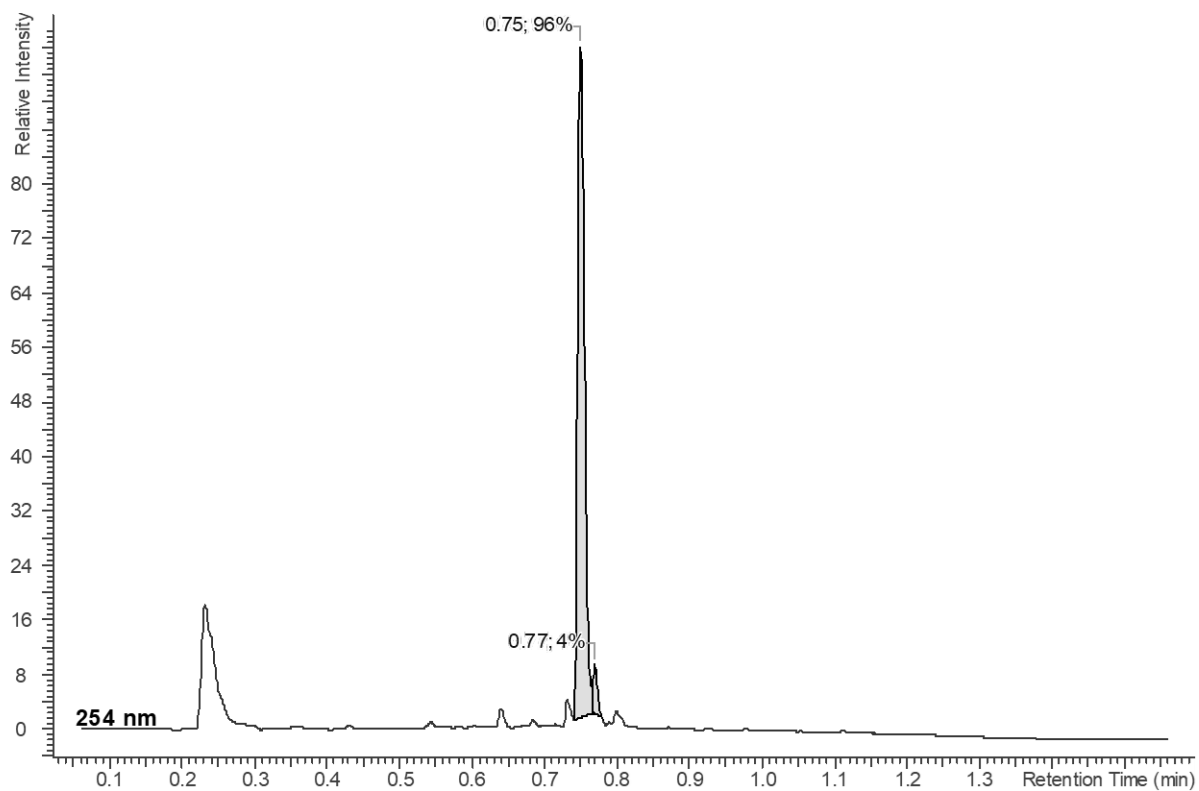


Figure S16. LCMS purity analysis of 20.

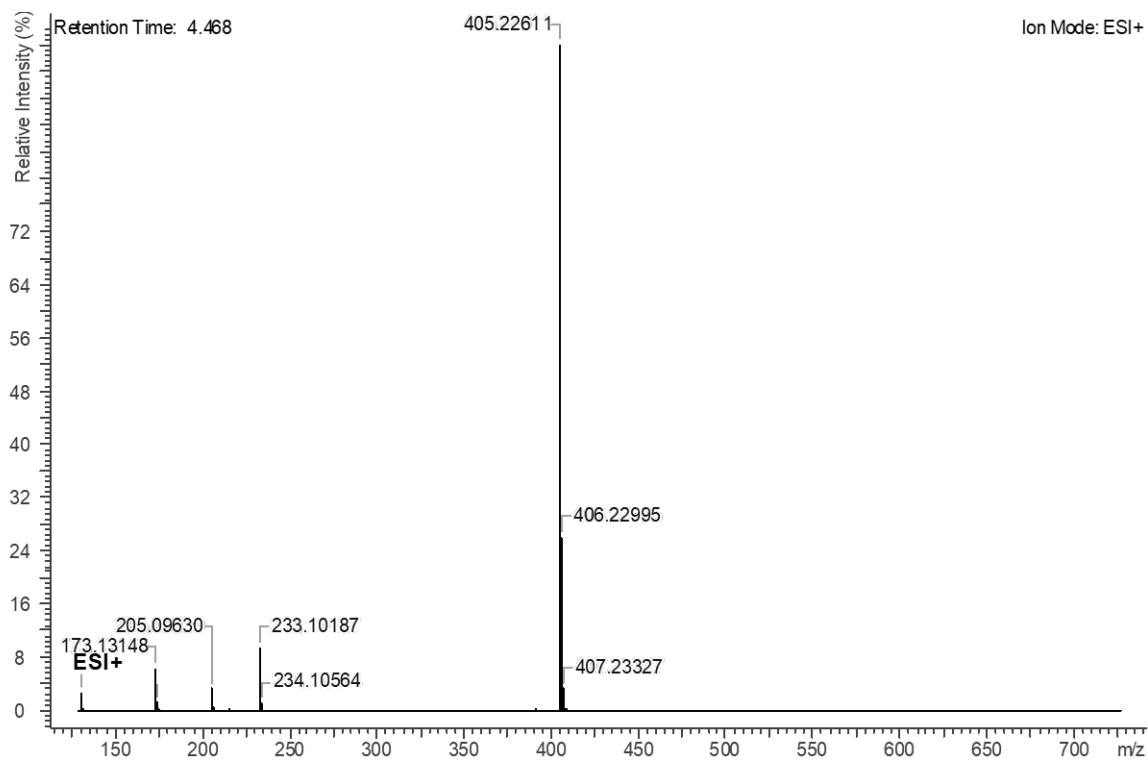


Figure S17. HRMS of 20.

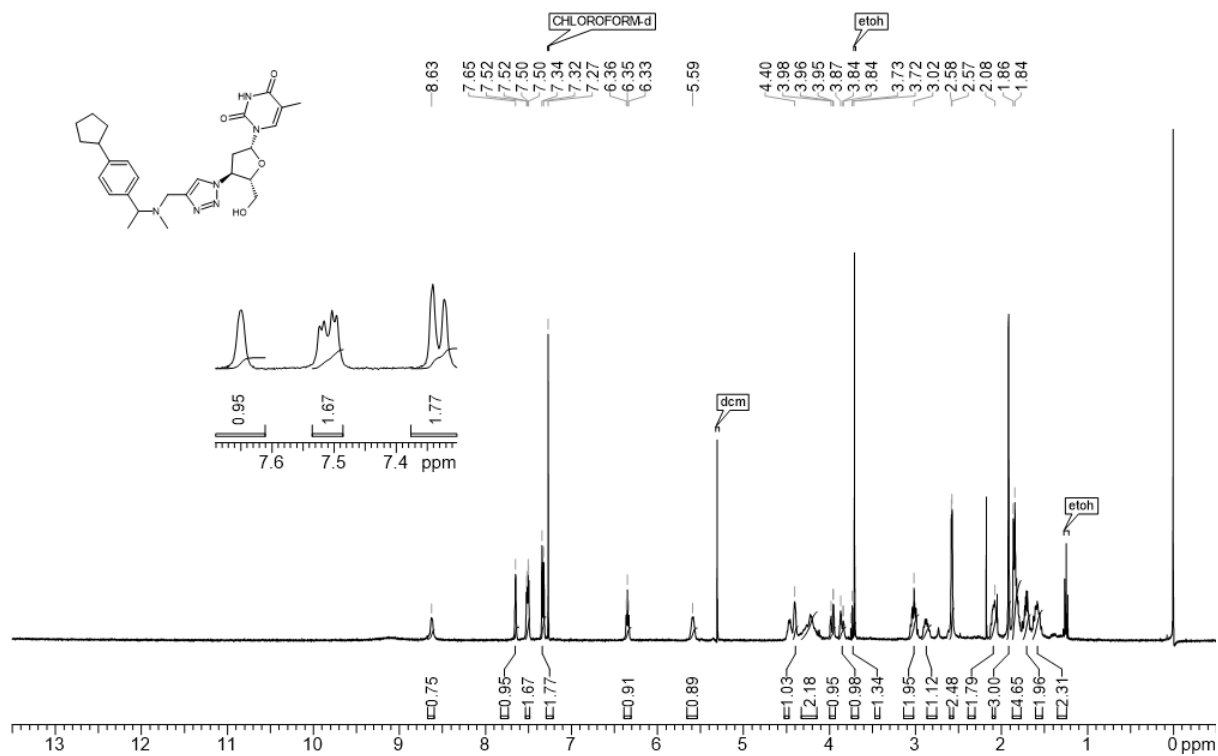


Figure S18. ^1H NMR spectrum of **21**.

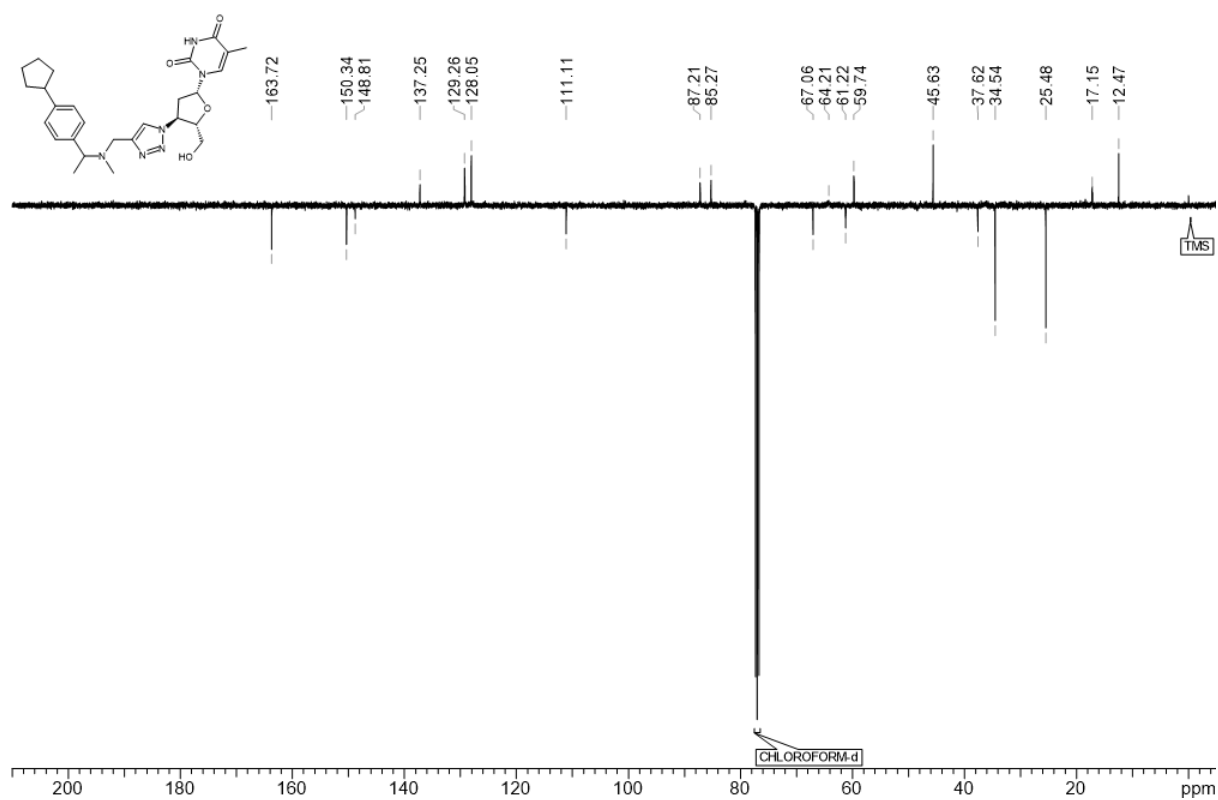


Figure S19. ^{13}C APT NMR spectrum of **21**.

5. Chapter

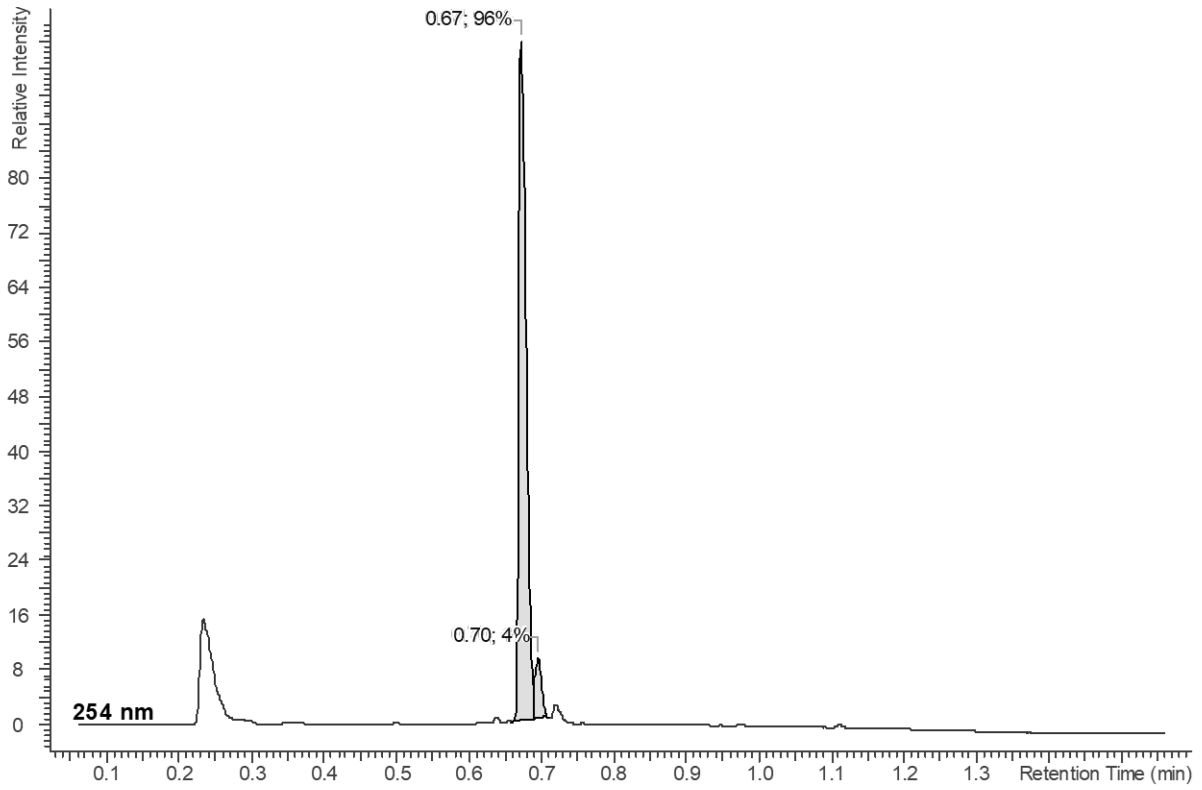


Figure S20. LCMS purity analysis of 21.

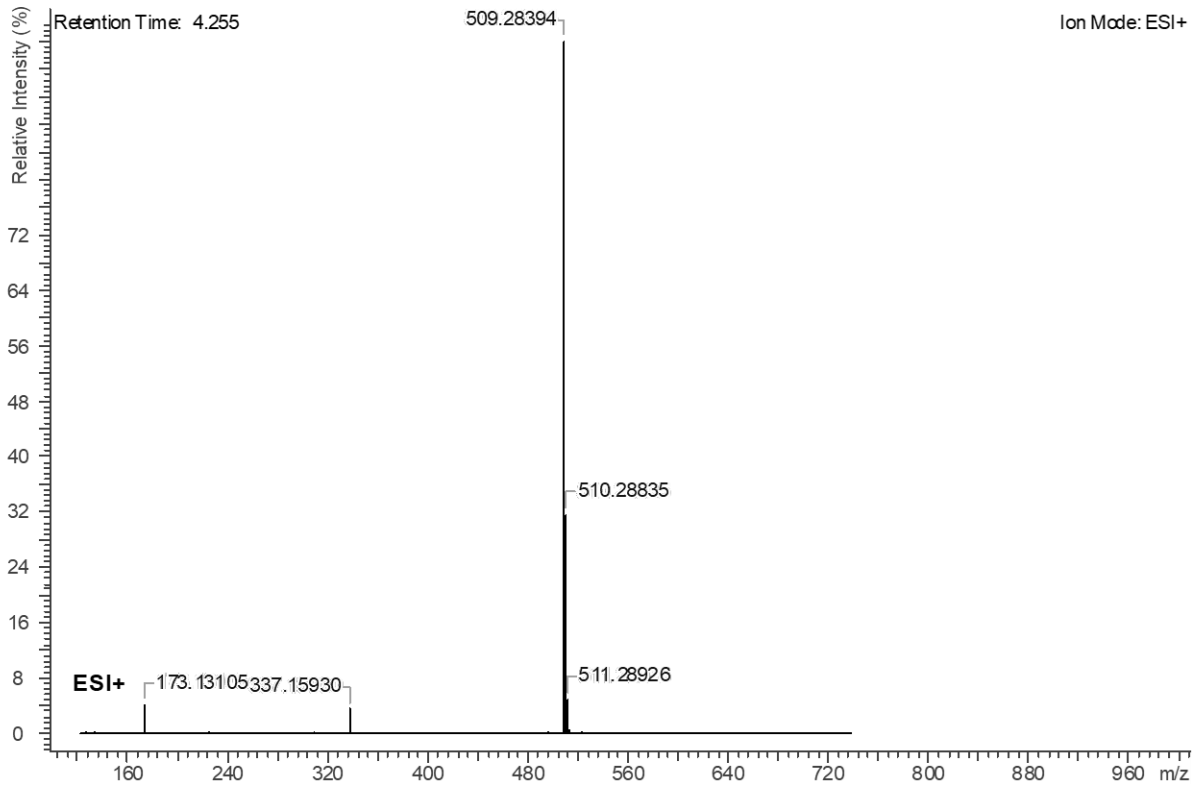
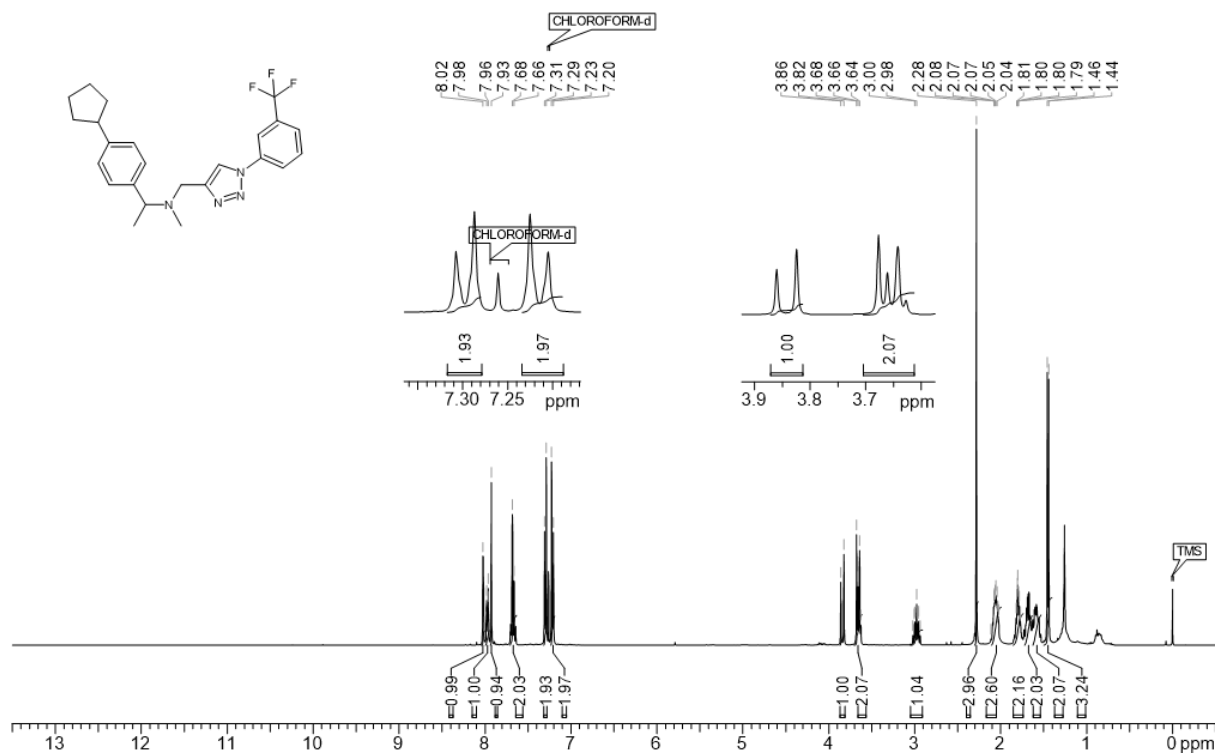
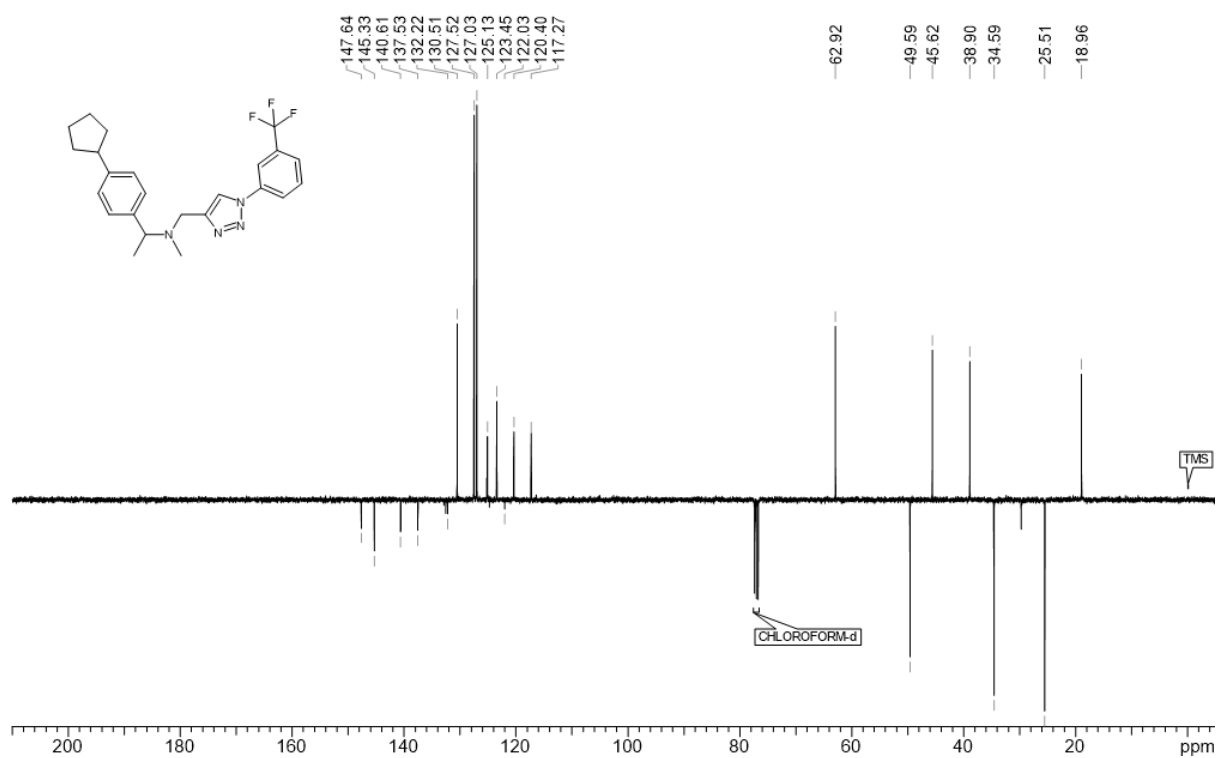


Figure S21. HRMS of 21.

Figure S22. ¹H NMR spectrum of 22.Figure S23. ¹³C APT NMR spectrum of 22.

5. Chapter

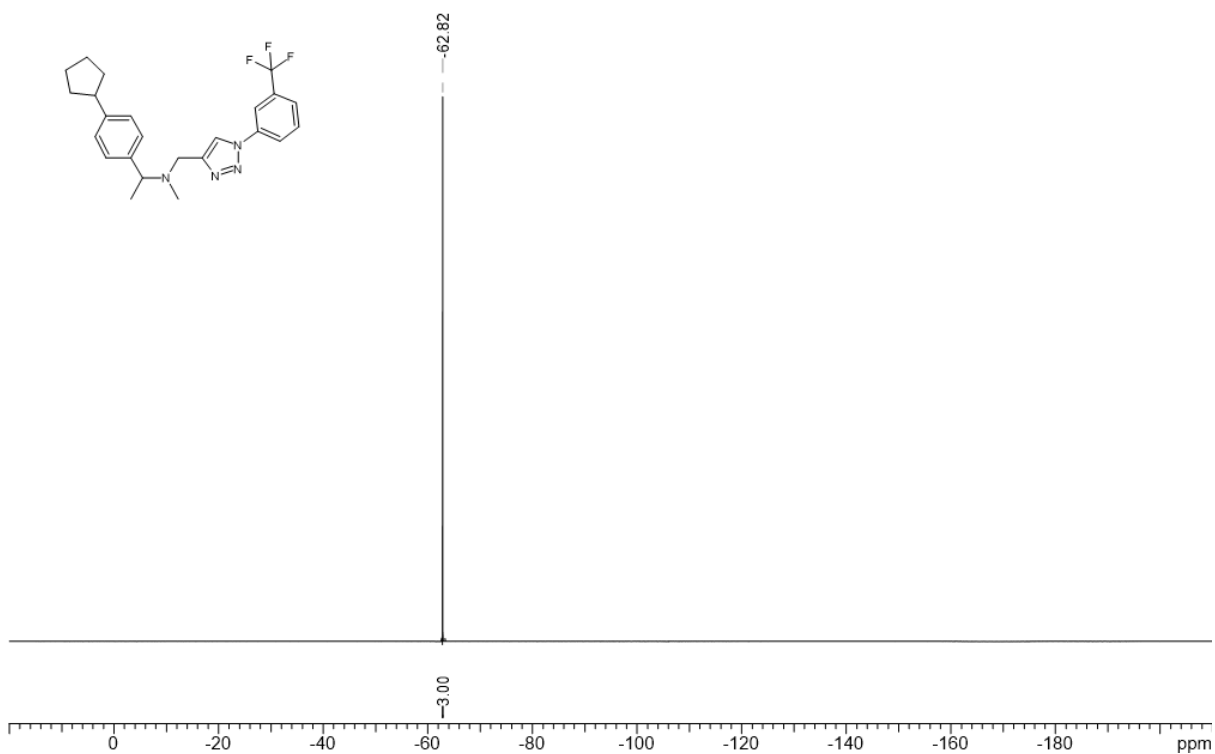


Figure S24. ¹⁹F NMR spectrum of 22.

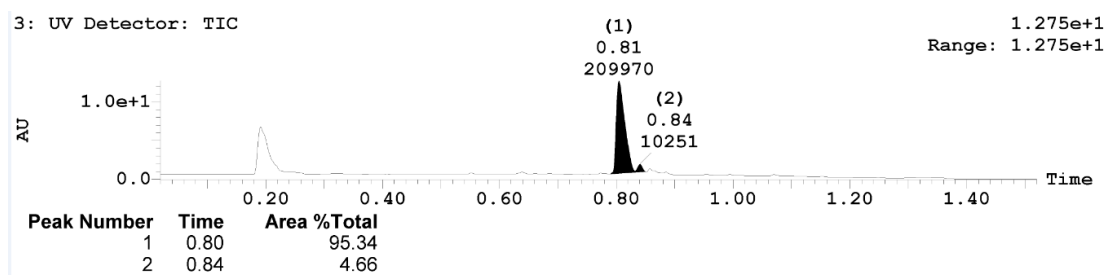


Figure S25. LCMS purity analysis of 22.

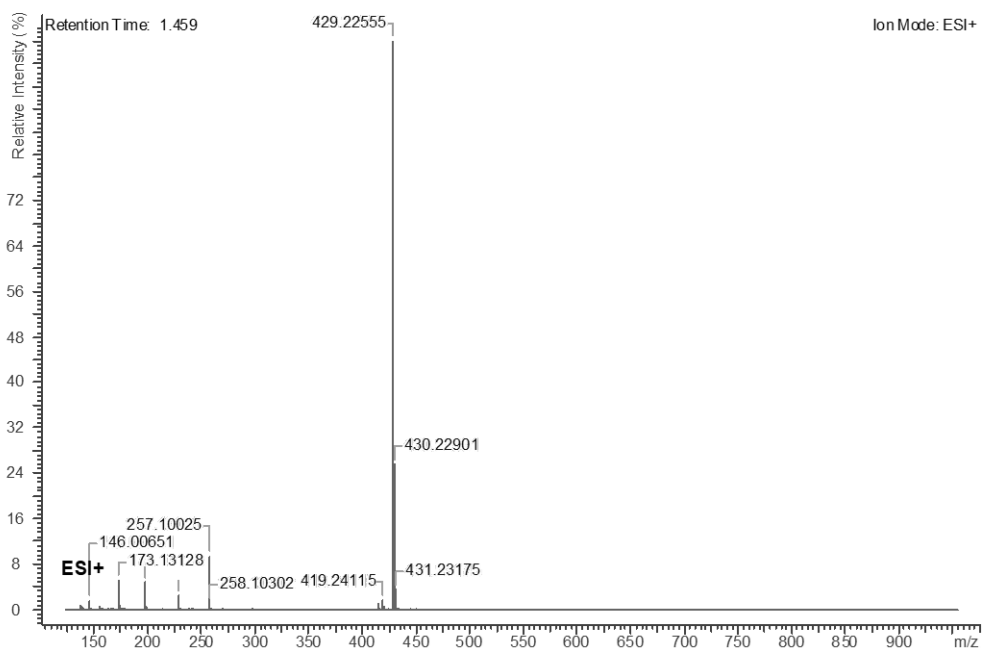


Figure S26. HRMS of 22.

Supplementary references

- (1) Varano, F.; Catarzi, D.; Colotta, V.; Cecchi, L.; Filacchioni, G.; Galli, A.; Costagli, C. Structure-Activity Relationship Studies of Novel Pyrazolo[1,5- c][1,3]Benzoxazines: Synthesis and Benzodiazepine Receptor Affinity. *Arch Pharm (Weinheim)* **1996**, 329 (12), 529–534. <https://doi.org/10.1002/ardp.19963291204>.
- (2) Ornago, C. *et al.* *Pseudomonas Aeruginosa* IspE Structure and In Solution Studies Reveal Monomeric Nature of the Kinase. **2024**, *Manuscript In Preparation*.
- (3) Niebling, S.; Burastero, O.; Bürgi, J.; Günther, C.; Defelipe, L. A.; Sander, S.; Gattkowsky, E.; Anjanappa, R.; Wilmanns, M.; Springer, S.; Tidow, H.; García-Alai, M. FoldAffinity: Binding Affinities from NDSF Experiments. *Sci Rep* **2021**, 11 (1), 9572. <https://doi.org/10.1038/s41598-021-88985-z>.
- (4) Illarionova, V.; Kaiser, J.; Ostrozhenkova, E.; Bacher, A.; Fischer, M.; Eisenreich, W.; Rohdich, F. Nonmevalonate Terpene Biosynthesis Enzymes as Antiinfective Drug Targets: Substrate Synthesis and High-Throughput Screening Methods. *J Org Chem* **2006**, 71 (23), 8824–8834. <https://doi.org/10.1021/jo061466o>.
- (5) Kuzmič, P. Program DYNAFIT for the Analysis of Enzyme Kinetic Data: Application to HIV Proteinase. *Anal Biochem* **1996**, 237 (2), 260–273. <https://doi.org/10.1006/abio.1996.0238>.
- (6) Alhayek, A.; Abdelsamie, A. S.; Schönauer, E.; Camberlein, V.; Hutterer, E.; Posselt, G.; Serwanja, J.; Blöchl, C.; Huber, C. G.; Haupenthal, J.; Brandstetter, H.; Wessler, S.; Hirsch, A. K. H. Discovery and Characterization of Synthesized and FDA-Approved Inhibitors of Clostridial and Bacillary Collagenases. *J Med Chem* **2022**, 65 (19), 12933–12955. <https://doi.org/10.1021/acs.jmedchem.2c00785>.
- (7) Camberlein, V. Target-Guided Synthesis of Metalloenzymes Ligands with Therapeutic Applications. Ph.D. Thesis, Lille University, Lille, France, Saarland University, Saarbrücken, Germany, 2022. <http://www.theses.fr/2022ULILS004/document> (accessed 2024-05-16).

Conclusions and Outlook

The development of novel antibiotics, particularly those effective against GNB is a major challenge in medicinal chemistry.¹ This difficulty arises not only from the need to identify and investigate entirely new chemical entities and targets with unprecedented mechanisms of action, but also from the complication of overcoming the barrier posed by the cell envelope in these bacteria. To address these challenges, this thesis presents a comprehensive investigation into the discovery of novel anti-infective compounds employing complementary strategies. First, we explored structural features that enhance GNB compound uptake and accumulation. Second, we employed the promising anti-infective target IspE in PT synthesis for the discovery of selective binders.

We developed a promising class of compounds with broad-spectrum anti-infective properties by strategically adding positively charged groups to antimalarial pyrazole-amide **1a**. This successful application of the eNTRY rules, not only yielded activity in GNB but also GPB, and *M. tuberculosis* while potentiating antimalarial properties. To achieve this, we incorporated amines, *N*-alkyl guanidines, and cyclised guanidine analogues through a methylene linker or piperazine to the phenyl ring of parent structure **1a**. We established a concise synthesis of *N*-Boc protected amine precursors (**B**-series) that were used as neutral control compounds. Simple Boc deprotection afforded the amine derivatives (**A**-series) which also served as intermediates to synthesise the *N*-alkyl guanidines (**G**-series), and cyclised guanidine analogues (**C**- & **D**-series). We verified the *P. falciparum* activity of the five series, establishing a good foundation to assess the eNTRY rules in our selection of pathogens. Our analysis of the SAR reveals that the aromatic ring is crucial for activity, with the trifluoromethyl substituent proving beneficial. These observations hold true across all pathogens except for *P. aeruginosa*, where the CF₃ substituent appears to be detrimental to activity.

In the **A**-series, one compound clearly stands out, with single-digit micromolar MIC₉₅ against *S. pneumoniae*, *S. aureus*, and *EcΔtolC*, **11A** is the most potent antibacterial amine derivative. It also is the top inhibitor of the **A**-series against *A. baumannii* (MIC₉₅ = 22 μM). The structure of **11A** comprises a piperazine and a CF₃ substituent, both in *meta* position of the phenyl ring with respect to the amide linkage. Inhibitor **11A** is the most potent antimalarial compound of the pyrazole-amide class (IC₅₀ = 0.05 μM), with analogue **12A**, whose structure solely differs in the placement of the piperazine, being in the same range (IC₅₀ = 0.06 μM). This compound is also the most potent *M. tuberculosis* inhibitor of the **A**-series (MIC₉₀ = 16 μM). Compared to **11A**, the inhibition profile of **12A** varies most regarding the GNB activity, indicating that the *meta*-piperazine substitution enhances GNB accumulation compared to the *ortho*-position. A major setback of this series is its cytotoxicity, the majority of amines exert a cytotoxic effect in HepG2 cells in the low micromolar range (CC₅₀ = 5–13 μM), including **11–12A**. This toxic liability is specific to the amine moiety, the vast majority of the remaining pyrazole-amides do not present toxicity concerns.

The guanidine derivatives (**C**-, **D**-, & **G**-series) are not only superior to the **A**-series in terms of cytotoxicity, but they also excel in potency against nearly every bacterial pathogen including *M. tuberculosis*, and GPB; *S. pneumoniae*, and *S. aureus*. Once again, the outlier being *P. aeruginosa*, which aligns with previous studies suggesting a more diverse membrane composition in this particular bacterium.² Nevertheless, five guanidines (**7D**, **6–7G**, **9–10G**) moderately inhibited the growth of *P. aeruginosa*, making them a promising motif to enhance broad-spectrum activity. The **C**-, and **G**-series contain the most potent antibacterial representatives of the pyrazole-amide class. The activity profile of **11A** and **12A** from the **A**-series has similarities to the **G**-series. Compound **11G** is more potent against GNB wild-types compared to **12G**, indicating that the phenyl scaffold in **11** is beneficial for accumulation in GNB. However, the roles are reversed when it comes to *M. tuberculosis*, **11G** presents a good inhibition (MIC₉₀ = 8 μM), but is surpassed by **12G** as the top inhibitor with an MIC₉₀ value of 4 μM. The **C**-series was designed to have a higher lipophilicity and a more drug-like structure compared to the **G**-derivatives, which came at a small cost in activity. In particular, the GNB wild-type potencies are lower in the **C**-derivatives, while the difference to

the **G**-analogues is smaller in *EcΔtolC* and GPB. Therefore, the imidazolidine motif of the **C**-series may be contributing to an increased efflux. Nevertheless, the **C**-series' antibacterial profile is promising and superior to the **A**-series, especially taking into consideration the toxicity. This type of guanidines, cyclised into five-membered rings had not been investigated in the context of enhancing bacterial accumulation before. The excellent anti-infective profile of the *N*-alkyl guanidinium derivatives encourages to pursue and investigate these motifs and derivatise them further. Our study provides strong support for the applicability of the eNTRY rules and for the first time indicates that these guidelines can aid in targeting pathogens beyond Gram-negative bacteria.

The convincing results of the pyrazole-amide study, motivated the introduction of ionisable nitrogen groups to an α -aryl β -aza reverse fosmidomycin class with the aim of improving antibacterial activity against *E. coli*. In this project, we explored various synthetic avenues to instal *N*-alkyl guanidines to this scaffold. Given the rather strict SAR and small size of fosmidomycin, this proved to be challenging.³ The first point of modification explored, was direct guanidinylation of the β -nitrogen of the structure. All our attempts were fruitless, indicating that the secondary amine was not nucleophilic enough and possibly too sterically hindered, rendering the parent structure inert to the tested guanidinylation conditions. This information opened the way to the successful late-stage guanidinylation of a primary amine installed on the α -phenyl substituent of the class. The synthesis of these α -derivatives could benefit from small adjustments to be fully optimised. The main issue we encountered was the partial debenzoylation of the phosphonate during a Boc deprotection step, leading to complications in the isolation and synthesis of subsequent products. Despite these issues, we obtained the final products **21** and **22**, containing *N*-alkyl guanidine and primary amine motifs, respectively. These compounds are currently undergoing biological evaluation to assess the activity against *E. coli* and affinity for DXR, the target of the class. The last point of modification we pursued was the underexplored γ -position. We successfully made use of the amino acid alanine to establish the synthetic route obtaining γ -methyl derivative **28**. This provided an effective pathway to install amine or guanidine motifs through amino acids lysine or arginine. To our disappointment, compound **28** degraded which precluded further investigations.

In addition to structural optimisation for GNB uptake, this thesis aimed at discovering hits for the anti-infective target IspE. For this purpose, we explored PT synthesis with two different homologues of the protein. IspE from *M. tuberculosis* was successfully used in hit-identification using tdDCC. In contrast, hit-expansion of the pyrazole-amide class using the *E. coli* homologue in KTGS did not lead to the identification of any hits. Both homologues were stable at room temperature for an extensive time period, which makes IspE a good candidate for PT synthesis.

The tdDCC experiment generated a total of 72 possible *N*-acylhydrazones by reacting three aldehydes with six hydrazides in four distinct DCLs. We investigated the influence of IspE on these dynamic libraries and identified eleven compounds that exhibited amplification. The accurate determination of the equilibrium time point is crucial for calculating the amplification factors of the library components. To optimise its analysis, we normalised the LCMS peak areas of the components and represented their change with respect to time, obtaining a clear visualisation, indicating an equilibrium time of 24 h in all libraries. The eleven selected tdDCC hits showed at least 50% increase in compound formation in presence of IspE, with the most amplified compound, **E1**, exceeding 1500%. Interestingly, this compound combines the two most frequently appearing building blocks in the hit structures, hydrazide **E** and aldehyde **1**. Unfortunately, the low solubility of these amplified hits significantly hindered biological evaluation, making their validation very difficult. To our disappointment, **E1** is particularly insoluble at 3.3 μ M in PBS with 5% DMSO and had to be excluded from IspE binding experiments. Three compounds (**C1**, **K1**, **E4**) showed consistent binding to *Mtb*IspE using MST and **K1** also induced a change in the melting temperature of *Mtb*IspE. This validated IspE binder also had a moderate inhibition effect on *E. coli* growth, making **K1** our most promising hit. Lastly, as the poor solubility of the compounds seriously impeded their validation, we decided to perform docking experiments to investigate possible binding modes of the hits and rationalise the structure-

amplification relationship. We found clear trends indicating that both motifs **E** and **1** preferentially bind in the CDP-ME substrate pocket. In the case of **E1**, fragment **E** maintained the positioning in the substrate binding site and fragment **1** fit into an unoccupied pocket. No other hit compounds showed binding poses interacting with that pocket of *MtblspE*, giving a possible explanation to the unmatched amplification of **E1**.

The initial hit-expansion strategy in the KTGS study involved the combination of tailored azides based on the pyrazole-amide class with a diverse alkyne library. However, a major obstacle was encountered given that the azides lacked affinity for IspE. This essentially transformed the experiment into a hit-discovery attempt exploring a limited chemical space, despite the use of 110 alkynes. An extensive analysis of the LCMS chromatogram and MS data revealed no triazole hits. We decided to shift the strategy and use the alkyne library in a fragment-based hit-discovery experiment. Using biophysical methods we identified five alkyne fragment hits that were followed up by selecting hundreds of analogues from the commercial Specs library. Ultimately, five compounds from two classes showed an inhibitory effect on IspE from *P. aeruginosa*. The pyrimidinedione class is particularly promising as the majority of inhibitors belong to this class, whereas the thiotetrazole class includes several binders but only one inhibitor. Additionally, one of the pyrimidinedione inhibitors is a full-size drug-like compound, indicating a good optimisation potential of this class.

With the groundwork laid in this thesis, promising avenues for further investigation into bacterial uptake and targeting the enzyme IspE emerge. The study on the pyrazole-amide class suggests that *N*-alkyl guanidines can unlock a broad-range of antibacterial activities. To better investigate the SUR, complementary to the inhibition of bacterial wild-types and *EcΔtolC*, testing the class in membrane-modified mutants of other species (or additional *E. coli* mutants) can be highly beneficial.^{2,4} Another crucial step is the currently ongoing target-identification of the pyrazole-amide class. The absence of the MEP-pathway in *S. aureus*,⁵ strongly suggests that IspE is not the target of the pyrazole-amides, or at least not the only target, given the potent antibacterial activity against *S. aureus*. Identification of the biological target would not only aid in the rationalisation of our current data and establish a clearer SAR and SUR, but also open the way to rational design approaches for hit optimisation. In the case that the biological target was compatible with KTGS, the attempt made with IspE could be worth repeating with the new target using the synthesised azides. In addition, based on the excellent results of the (cyclic) guanidine-containing pyrazole-amides, we encourage the exploration of diverse ionisable nitrogen functionalities to anti-infective hits, as we already initiated with fosmidomycin derivatives. We suggest amidine and imidazoline motifs as interesting groups to explore.

Our studies involving IspE resulted in the identification of new promising starting points to develop compounds targeting pathogenic homologues of the enzyme. In particular, one critical point of improvement for the hits from the tdDCC study is the solubility. Exchanging the hydrazone moiety for bioisosteres like oxazoles or amides could be a simple option worth exploring. The addition of charged groups, could also improve the solubility, while potentially enhancing antibacterial activity, if ionisable nitrogen functionalities are chosen. For this purpose it would be beneficial to guide the design by the elucidated binding modes from the docking experiment. For future PT synthesis endeavours, we recommend the use of highly soluble fragments, for example by including parameters like logS in the selection process. Hit-optimisation of the identified pyrimidinedione inhibitor class of *PalspE* can be promising. One interesting approach would be to screen a wider range of analogues. The Specs library contains thousands of suitable compounds that could be filtered with *in silico* screening for this purpose.

References

- (1) Stoorza, A. M.; Duerfeldt, A. S. Guiding the Way: Traditional Medicinal Chemistry Inspiration for Rational Gram-Negative Drug Design. *J Med Chem* **2024**, 67 (1), 65–80. <https://doi.org/10.1021/acs.jmedchem.3c01831>.
- (2) Hu, Z.; Leus, I. V.; Chandar, B.; Sherborne, B. S.; Avila, Q. P.; Rybenkov, V. V.; Zgurskaya, H. I.; Duerfeldt, A. S. Structure-Uptake Relationship Studies of Oxazolidinones in Gram-Negative ESKAPE Pathogens. *J Med Chem* **2022**, 65 (20), 14144–14179. <https://doi.org/10.1021/acs.jmedchem.2c01349>.

- (3) Knak, T.; Abdullaziz, M. A.; Höfmann, S.; Alves Avelar, L. A.; Klein, S.; Martin, M.; Fischer, M.; Tanaka, N.; Kurz, T. Over 40 Years of Fosmidomycin Drug Research: A Comprehensive Review and Future Opportunities. *Pharmaceuticals* **2022**, *15* (12). <https://doi.org/10.3390/ph15121553>.
- (4) Zgurskaya, H. I.; López, C. A.; Gnanakaran, S. Permeability Barrier of Gram-Negative Cell Envelopes and Approaches to Bypass It. *ACS Infect Dis* **2016**, *1* (11), 512–522. <https://doi.org/10.1021/acsinfecdis.5b00097>.
- (5) Matsumoto, Y.; Yasukawa, J.; Ishii, M.; Hayashi, Y.; Miyazaki, S.; Sekimizu, K. A Critical Role of Mevalonate for Peptidoglycan Synthesis in *Staphylococcus Aureus*. *Sci Rep* **2016**, *6* (1), 22894. <https://doi.org/10.1038/srep22894>.

Acknowledgements

I would like to start by expressing my gratitude to my primary supervisor, Peter Maas, your expertise and encouragement have been invaluable. I am deeply grateful for the support you provided and for always being there when I needed guidance. I am also very thankful to my academic supervisor Prof. Dr. Anna K. H. Hirsch for making this PhD possible, providing vital advice, and welcoming me in her group. My time at DDOP has profoundly shaped my PhD journey. I would also like to thank the members of my thesis committee, Prof. Dr. Andreas Speicher, Dr. Lukas Junk, who was in my committee for the first two years, and Dr. Matthias Engel. Your insightful feedback have greatly contributed to the improvement of my research.

My heartfelt thanks go to my key colleagues and collaborators, without your support this PhD would not have been possible. The Specs research team, Johan, Dennis, Nanda, and Tom, who supported me in many different ways, and the Specs beers will always be remembered. I am grateful to our dedicated students, Vincent and Mitchell, for their hard work and dedication in synthesising numerous pyrazoles. Your contributions have been crucial to the progress of my research. I would also like to acknowledge the support of the Specs office, especially Danielle, for always managing my urgent shipments efficiently.

To my MepAnti PhD colleagues, especially Camilla, Tony, Thibaut, Daan, Vidhisha, and Patricia, thank you for the great teamwork and banter. I am very happy to have been part of such a great consortium. I am also deeply thankful to the MepAnti project managers, Dr. Eleonora Diamanti and Dr. Mostafa Hamed, for their continuous guidance and support.

Special thanks to everyone at DDOP, and UGent for making me feel like I was part of your group from day one. In particular, Gwen, Rawia, Atanaz, Ioulia, Virgyl, and Yingwen, who were a critical support for me in Saarbrücken, inside and oftentimes outside of the lab. Chai, I could never have asked for a better desk neighbour, thanks for the encouragements. I am also very grateful to all the technicians and biologists for their hard work, and making my research possible.

This PhD journey has been enriched by the wonderful people I met during my time in the Netherlands, Germany, and Belgium. Your friendship and support have made this time memorable, I hope we will meet again.

I extend my deepest gratitude to all my friends and family who have supported me from afar. Your encouragement despite not always understanding the intricacies of my work, has been important. I hope we can spend more time together now.

Lastly, a special mention to Kraviz for providing great comfort throughout the writing phase.

